The Dissertation Committee for Erin Malia McMahon
certifies that this is the approved version of the following dissertation:

Gamma-ray bursts and their afterglows: toward a unified model

Committee:

Pawan Kumar, Supervisor

Edward L. Robinson

Don Winget

J. Craig Wheeler

Gennady Shvets

Gamma-ray bursts and their afterglows: toward a unified model

by

Erin Malia McMahon, B.S., M.A.

DISSERTATION

Presented to the Faculty of the Graduate School of

The University of Texas at Austin

in Partial Fulfillment

of the Requirements

for the Degree of

DOCTOR OF PHILOSOPHY

THE UNIVERSITY OF TEXAS AT AUSTIN

December 2007

To my love, Bo, and my beautiful son Damon.

Acknowledgments

First and foremost, my biggest thanks go to Bo – without him, this would not have been possible. He is a huge source of strength and support, and has taught me a great deal during the last 8 years.

I wish to thank Pawan Kumar for being the greatest possible thesis advisor. He is an amazing person, a caring friend, and always available to talk to, whether it be about astronomy, personal issues, or politics. He made it very easy for me to be a mom and a graduate student, allowing me over the last two years to have an extremely flexible schedule and not minding me doing most of my work from home.

Derek Wills also worked with me very much to create a TA that worked with my schedule. Thanks to Dan Jaffe and Athena Stacey, who helped me very much the semester that my son Damon was born.

Thanks to Shay Strong for being such a strong friend and fellow student, for teaching me how to paint, coffee breaks, babysitting, and her love and support. You're almost there! And thanks to Andrea Urban for all of her help with Damon too.

And last but not least, I thank my family for always believing in me, and for always being there to get me through the tough spots.

Gamma-ray bursts and their afterglows: toward a unified model

Publication No. _____

Erin Malia McMahon, Ph.D.
The University of Texas at Austin, 2007

Supervisor: Pawan Kumar

Although much progress has been made in our understanding of gamma-ray bursts (GRBs) and their afterglows in the last few decades, some critical questions remain unanswered. One of these questions regards the form in which energy is transported from the explosion to the site at which the gamma-rays are produced – i.e. is the energy carried in the kinetic energy of electrons and/or protons, or is much of it stored in a magnetic field? This dissertation documents a series of attempts to more clearly understand the nature of GRB outflows. First, we explore the possibility that the GRB is produced by an external shock, created when a baryonic outflow is decelerated by the surrounding medium. Next, emission from the external reverse shock is used to try to determine if the GRB ejecta is pair enriched. We then use data from several interesting, *Swift*-detected GRBs pin down the GRB emission radius, bulk Lorentz factor, magnetic field strength, and electron energy. We end by

describing our nearly model independent method of modeling the GRB radiation as a combination of synchrotron and synchrotron self-Compton. We find that the GRB is likely to be produced by the synchrotron self-Compton radiation mechanism and predict that the accompanying prompt optical emission should be very high. If bright optical radiation during the GRB is not found, we think that this is good evidence that the acceleration of electrons is taking place repeatedly on a short timescale, effectively ruling out shock-based acceleration models.

Table of Contents

List of Tables

List of Figures

Chapter 1

Introduction

Gamma-ray burst science in its infancy was restricted to chance observations of short bursts of gamma-rays at random positions in the sky. Many models were proposed, both galactic and extra-galactic, to describe these transient high energy events, but little could be learned from strictly gamma-ray observations to discriminate between opposing models. A revolution in our understanding of these objects began when longer wavelength emission following a burst, called the afterglow, was discovered in 1997. We have learned from afterglows that these events occur in distant galaxies and most likely signal the birth of stellar mass black holes. Although the general characteristics of the late time afterglow are now able to be explained in a fairly simple model, the process by which the gamma-rays are produced is still largely unknown – we are still unsure of the nature of the GRB outflow, i.e. whether the energy in the outflow is carried by baryons, leptons, and/or a magnetic field.

In this chapter, I will give the reader a little bit of background on GRB observations and burst characteristics.[1] I will also briefly introduce the

[1]The information in this chapter (and much more) has been reviewed in more detail by several authors (Piran 1999, 2005; Mészáros 2002, 2006; Woosley and Bloom 2006; Gehrels et al. 2007; Zhang 2007).

internal and external shock models – the currently popular interpretation of both the GRB and afterglow in the context of relativistic shocks – and give motivation for this dissertation project.

1.1 GRB observations and characteristics

GRBs were discovered in the late 1960's by the Vela satellites – US military satellites launched beginning in 1963 for the purpose of detecting violations of the Nuclear Test Ban Treaty (1963) (Mészáros 2002). By chance, these satellites detected bursts of gamma-rays that were not originating on Earth, but from other directions in the sky. The first announcement of the discovery of GRBs was made over thirty years ago by Klebesadel et al. (1973), and this was confirmed by Soviet Konus satellites by Mazets et al. (1974). The origins of these bursts remained largely a mystery for the next 25 years; there were many models of cosmological and galactic origin, but with sporadic observations only in the gamma-ray band, it was impossible to discriminate between models.

1.1.1 γ-ray characteristics

The launch of the Compton Gamma Ray Observatory (CGRO) in 1991 enabled the community to observe this high energy radiation more frequently, resulting in a significant improvement in our understanding of these events. The Burst And Transient Search Experiment (BATSE) instrument on board the CGRO detected 2704 bursts over its 9 year lifetime (Fishman and Meegan

1995), allowing for statistical studies of GRB properties. One of the most exciting results from this mission was the discovery of an isotropic distribution of BATSE detected GRBs in the sky. This alone was good evidence that GRBs occur at cosmological distances, but it did not completely rule out all galactic models.

GRBs are bursts of 25 keV to 1 MeV γ-rays that typically last from a tenth of a second to hundreds of seconds. BATSE found that there is a bimodal distribution of GRB durations (in log space) – there are so-called "short bursts" with durations less than ~ 2 seconds and "long bursts" with durations between ~ 2 and a few hundred seconds (Kouveliotou et al. 1993). This bimodal distribution peaks at 0.3 seconds and 30 seconds. It is generally thought that short and long bursts have separate progenitors.[2] GRB lightcurve morphology varies widely from burst to burst; at one extreme, we observe some bursts with smooth FRED-like (Fast Rise Exponential Decline) burst profiles, and at the other, we observe some with many pulses and millisecond variability. There are also many bursts with quiescent periods lasting hundreds of seconds.

GRB spectra are non-thermal (although see Ryde (2005) for evidence of a thermal component) and can be fit well by the empirical Band function (Band et al. 1993), which is a broken power law joined smoothly at the peak.

[2]From this point on, unless noted otherwise, the term GRB will be used to refer to long duration bursts.

The function describing the photon spectrum is

$$N_E(E) = A \begin{cases} E^{\alpha} \exp(\frac{E}{E_0}) & E < (\alpha - \beta) E_0 \\ [(\alpha - \beta) E_0]^{(\alpha - \beta)} E^{\beta} \exp(\beta - \alpha) & E > (\alpha - \beta) E_0 \end{cases} \quad (1.1)$$

where E is the photon energy, α is the low energy spectral slope, β is the high energy spectral slope, and $(\alpha - \beta) E_0$ is the break energy. The values for each fit parameter vary from burst to burst. Typically, $\alpha \sim -1$ (but ranges from -2 to 0) and $\beta \sim -2$. For some bursts, the spectrum can be fit by a single power law, with a spectral index of ~ -2. Most of the energy is released at the peak of the νf_ν spectrum, $E_p = (\alpha + 2) E_0$. E_p for most bursts is between 100 and 300 keV (Preece et al. 2000), and the distribution ranges from about 10 keV to several hundred keV. The fluence (flux integrated over the spectrum and duration of the burst) received in the 25 keV to 1 MeV band ranges from 10^{-7} to 10^{-4} erg cm^{-2}. The BeppoSAX satellite (discussed in the next subsection) discovered transient events that have very similar temporal structure to GRBs, but most of the energy in these bursts come out in the x-ray, below ~ 20 keV (Heise et al. 2001). These events are called X-ray Flashes (XRFs), and seem to have similar durations and peak flux to GRB emission in the x-ray.

1.1.2 The BeppoSAX and *Swift* afterglow revolutions

On February 28, 1997, the Dutch-Italian satellite BeppoSAX (Piro et al. 1995) detected transient emission in the x-rays at the position of a GRB (Costa et al. 1997). The detection of this x-ray afterglow enabled ~ 5 arc-minute accurate position measurements, and this information was passed on to ground-based observers who found the corresponding optical counterpart (Galama

et al. 1997; van Paradijs et al. 1997). On May 8 1997, the first spectrum of an optical afterglow was taken (Metzger et al. 1997); it unambiguously confirmed the cosmological distance of this burst, with its redshift being measured at $z = 0.85$. Subsequent GRB redshifts (pre-2005) averaged $z \sim 1$, from which we infer that the typical energy release from a GRB is $\sim 10^{52-55}$ ergs if the explosion is spherical.

The afterglow of 970508 was also detected in the radio (Frail et al. 1997). These observations allowed for the first direct detection of the expansion speed and size of the source. By observing the quenching of interstellar scintillation[3] in time, it was inferred that the source was expanding mildly relativistically and had a size of 10^{17} cm (Waxman et al. 1998). As the expansion speed two weeks following the explosion was mildly relativistic, higher speeds are implied prior to this time.

Prior to 2005, afterglow follow up observations typically commenced ~ 7 hours after the burst, and for a small number of cases optical observations began a few minutes following the GRB (Akerlof et al. 1999; Li et al. 2003a; Akerlof et al. 2003). In general, the afterglow flux in each wavelength band exhibited a power law dependence on both frequency and time, i.e. $f_\nu \propto \nu^{-\beta} t^{-\alpha}$. In the x-ray, β is typically ~ 0.9, and $\alpha \sim 1.4$ (Piran 2005). The optical light curve is typically a bit flatter, with $\alpha \sim 1$ and β is typically equal

[3]Scintillation causes large fluctuation in the intensity of radio emission. These fluctuations are caused by the scattering of light off of density irregularities in the interstellar gas in our Galaxy (Goodman 1997).

to or smaller than that measured in the x-ray. Occasionally a steepening is seen in the late-time optical afterglow light curve, near 1 day, to a t^{-2} decay. This steepening, called the jet-break, is naturally attributed to geometric beaming of the ejecta, thus reducing the energy budget by a factor of $100 - 1000$ (Rhoads 1999; Sari et al. 1999).[4] In two cases (GRBs 990123 and 021211), a bright optical flash occurred just at the end of the prompt emission (Akerlof et al. 1999; Li et al. 2003a), however there were many cases in which no optical flash was seen (Akerlof et al. 2000a; Kehoe et al. 2001). On March 29 2003, a very bright GRB was detected that happened to be very close, at $z = 0.168$. Optical spectra taken in a time sequence showed the emergence of a Type Ic supernova spectrum at late times (Matheson et al. 2003; Stanek et al. 2003). There have been several other nearby GRBs since that also show supernovae at late times (Malesani et al. 2004; Della Valle et al. 2003; Pian et al. 2006; Della Valle et al. 2006). This key piece of evidence shows that at least some GRBs are produced during the core collapse of massive stars at the end of their lives and signal the birth of a stellar mass compact object (black hole or neutron star).

The *Swift* satellite (Gehrels et al. 2004) was launched in November, 2004, with the purpose of closing the observational gap between the GRB and afterglow emission. *Swift* has three instruments: the Burst Alert Tele-

[4]It has been shown by numerical afterglow modeling that the jet kinetic energy (isotropic energy corrected for geometric beaming) for most bursts is clustered between $10^{50} - 10^{51}$ erg (Panaitescu and Kumar 2002). Also, the γ-ray energy released corrected for beaming also varies little from burst to burst (5×10^{51} erg) (Frail et al. 2001).

scope (BAT), a wide-field GRB detector, the X-ray Telescope (XRT), and the UV/Optical Telescope (UVOT), both narrow-field instruments that slew to the burst location within a few minutes of the burst trigger. The BAT has few arcminute position accuracy, enabling ground-based observatories to turn to the bursts within a few seconds after the burst trigger. On average, BAT detects a few bursts per week, and 90% of the detected GRBs have x-ray afterglow detections. 30% of the detected bursts were detected by the UVOT (Mészáros 2006) and 55% of bursts were detected in the optical by other observatories (Zhang 2007). The number of bursts with measured redshifts has now increased to over 100[5] and the average redshift of bursts detected with *Swift* is 2.3 (Gehrels et al. 2007). *Swift* has made a number of very interesting discoveries so far – we briefly discuss some highlights of the optical and x-ray observations.

Swift discovered that early x-ray light curves have a very interesting shape. All x-ray light curves show at least one component of the typical three component light curve (Chincarini et al. 2005; Nousek et al. 2006; O'Brien et al. 2006; Zhang et al. 2006): (1) a very steep decline ($3 \lesssim \alpha_1 \lesssim 5$, where $f_\nu \propto t^{-\alpha}$) that matches up to the end of the prompt GRB emission (Tagliaferri et al. 2005; Barthelmy et al. 2005), (2) a broad hump, or very slowly decaying segment ($0.2 \lesssim \alpha_2 \lesssim 0.8$), overtaking the rapidly decaying component (1), which breaks in to the final component, (3) the "normal" component, which decays in time

[5]Number as of July 1 2007. For updated list, see `http://www.mpe.mpg.de/~jcg/grbgen.html`.

as x-ray afterglows detected prior to the *Swift* launch ($1.1 \lesssim \alpha_3 \lesssim 1.7$). The time (since trigger) at which component (2) overtakes (1) ranges from about 300 s to 500 s, and the break from (2) to (3) occurs between 10^3 and 10^4 s after the burst. There is a spectral change when segment (2) overtakes (1), but none when segment (2) breaks to (3). The spectral index of segment (1), in most cases, is very similar to that of the GRB. For this reason, and the fact that the light curve of GRB emission extrapolated to the x-ray band matches up very well with the beginning of the x-ray afterglow, it is thought that segment (1) is the continuation of the prompt GRB emission and segment (2) is the beginning of the afterglow. Another interesting feature seen in about half of x-ray afterglows is high-amplitude flaring. These flares are seen out to 10^5 seconds from the burst, rise and fall very rapidly, and in some cases contain nearly as much energy as was emitted in the gamma-rays during the GRB itself (Burrows et al. 2005).

In some cases, the x-ray light curve breaks again to an even steeper decay ($2 \lesssim \alpha_4 \lesssim 4$) close to 1 day after the burst. It is possible that this is the jet-break, as seen in the x-ray – however there are many x-ray afterglows followed months after the burst in which no jet-breaks were seen (Willingale et al. 2006; Sato et al. 2007). Even in those cases in which a break is seen, the decay index following the break is inconsistent with the empirical jet-break relations found in optical light curves by Frail et al. (2001).

The optical afterglows of *Swift* GRBs are, in general, fainter than afterglows of GRBs detected previously with other instruments (Roming et al.

2006). In most cases the optical light curves are very similar to what was observed before *Swift* was launched. From during the burst to days after the burst, most optical afterglows fade as a single power law decaying as $\sim 1/t$, with no steep decline (as is seen in the x-ray) or optical flashes observed (Mundell et al. 2007; Yost et al. 2007). In a few cases optical flares have been observed contemporaneous with GRB pulses or x-ray flares, but it is far from the norm (Yost et al. 2007) – in most cases the smoothly decaying afterglow component dominates in the optical. No optical flashes consistent with what was seen in GRBs 990123 and 021211 have been observed.

In another interesting twist, two *Swift* optical afterglows following long, nearby ($z \sim 0.1$) GRBs were found to not exhibit the late-time rising indicative of an underlying supernova explosion (Gal-Yam et al. 2006; Watson et al. 2007). Upper limits for one of these bursts, GRB 060614, require that the accompanying supernova be at least 100 times fainter than any other GRB-associated supernova. It is unclear whether there was no underlying supernova or if much of the radioactive material that powers the supernova light curve fell back onto the compact remnant.

The quick, accurate position measurement of *Swift* has also enabled the discovery of x-ray, optical, and radio afterglow counterparts to short GRBs (Gehrels et al. 2005). Short bursts have similar afterglows to long bursts, even exhibiting x-ray flares, but seem to occur in nearby galaxies containing older populations of stars, or galaxies with smaller star formation rates than long GRB host galaxies (Nakar et al. 2006). This seems to indicate a different ex-

plosion mechanism than supernovae, which occur in hot, young stars. Another piece of evidence in favor of a different explosion mechanism is the apparent lack of supernova light in the late time optical afterglow (Hjorth et al. 2005; Soderberg et al. 2006).

Discoveries made by *Swift* have presented many new puzzles for us to decipher – in terms of the GRB itself, the afterglow, and the progenitor/explosion mechanism. There is still much evidence, however, that there is a simple late-time afterglow component that can be described by synchrotron radiation from shocked heated medium surrounding a relativistic decelerating outflow – called the external shock model. We now briefly discuss this external shock afterglow model, along with the currently popular model for GRBs themselves – internal shocks.

1.2 The internal/external shock model for GRBs and afterglows

Observations of contemporaneous supernovae with long GRBs make a pretty good argument that the energy of a GRB is associated with the energy released during the formation of a stellar mass compact object. It is far from clear whether this energy moves outward from the source in the form of kinetic energy of leptons and baryons or if a significant amount of energy is in a magnetic field advected from the source. The currently most popular model for GRB production, the internal shock model, assumes that the energy of the outflow is carried in the kinetic energy of baryons. The general idea

of the internal/external shock model is as follows: the GRB is produced by synchrotron emission in internal shocks formed when shells of material moving at varying speeds collide. After these shells collide, they merge and move outward from the source together as a single shell. This shell sweeps up the external medium, decelerates, and drives a relativistic forward shock into the external medium. The heated external medium emits synchrotron radiation to produce the afterglow. In the next two subsections we outline the basics of this model, since much of our investigation into the nature of the GRB outflow (discussed in the following chapters) disputes predictions of the internal shock model.

1.2.1 Prompt emission from internal shocks

Internal shocks are produced by internal collisions of shells ejected with variable Lorentz factors from an "inner engine" (Rees and Mészáros 1994; Paczynski and Xu 1994; Papathanassiou and Mészáros 1996; Mészáros and Rees 1997b; Sari and Piran 1997b). Shells with higher Lorentz factor will overtake slower ones ejected at earlier times, resulting in collisions, shock formation and dissipation of particle kinetic energy. The distance from the source at which the shells producing the emission collide is set by the burst variability timescale

$$R_{diss} \sim c\delta t\Gamma^2 \sim 3 \times 10^{14}\mathrm{cm}\,\delta t \left(\frac{\Gamma}{100}\right)^2 \tag{1.2}$$

where δt is the variability timescale and Γ is the bulk Lorentz factor of the outflow. Γ is on the order of 100 – a lower limit can be placed on it using

the requirement that the outflow be optically thin to electron scattering and the $\gamma\gamma \rightarrow e^+e^-$ process (Lithwick and Sari 2001). Rapid variability on millisecond timescales can be produced by internal shocks, as shown by numerical calculations (Kobayashi et al. 1999; Spada et al. 2000).

The relative Lorentz factor of colliding shells is small, of order a few, resulting in the formation of mildly relativistic shocks inside the shells. A magnetic field is thought to be produced by plasma instabilities behind the shock front (Medvedev and Loeb 1999), and there is probably some magnetic field that has been advected in the ejecta from the inner engine. In the presence of a magnetic field, relativistic electrons will emit synchrotron radiation (e.g. Rybicki and Lightman 1979). In mildly relativistic shocks ($\gamma_{sh} \sim 2$), the typical electron Lorentz factor will be on the order of the ratio of proton to electron masses, $\gamma_e \sim m_p/m_e \sim 1800$. These electrons will radiate at the typical (observer frame) synchrotron frequency

$$\nu_{sync} = \frac{qB\gamma_e^2\Gamma}{2\pi m_e c^2} \sim 300 \left(\frac{B}{10\mathrm{G}}\right) \left(\frac{\Gamma}{100}\right) \left(\frac{\gamma_e}{1800}\right)^2 \mathrm{keV}, \tag{1.3}$$

very close to the peak in the distribution of observed spectral peaks (Preece et al. 2000). Synchrotron self Compton (SSC) emission (the up-scattering of synchrotron photons on the synchrotron-emitting electrons) can also be produced, however it is typically assumed that the peak of the SSC emission will be at a factor of γ_e^2 higher than ν_{sync}, and therefore will not contribute to the emission observed in the 10 keV to 1 MeV energy range.

Although it seems that this model can easily produce GRBs with typi-

cal observed characteristics, there are two major outstanding issues that have yet to be resolved. First, it has been shown that efficiency for γ-ray production during the GRB is most likely higher, on average, than 50% (Panaitescu and Kumar 2002). Such high efficiency cannot be obtained by internal shocks (Panaitescu et al. 1999; Kumar 1999). The efficiency of colliding shells increases as the relative Lorentz factor between colliding shells increases, however the emission from these collisions peaks at an energy much larger than that observed. External shocks can convert bulk kinetic energy to radiation much more efficiently than internal shocks, however, an external shock cannot efficiently produce GRBs with short timescale variability (Sari and Piran 1997a). It is possible that external shocks can produce single-pulse GRBs – about 1 out of every 10 GRBs observed. The second problem with the internal shock model regards the reverse shock, discussed below.

1.2.2 Afterglow emission from an external shock

An external shock forms at the deceleration radius, R_d, when the material swept up by the relativistically expanding shell is comparable to the kinetic energy of the shell. Prior to this radius, the shell is not significantly decelerated, and coasts with approximately constant bulk Lorentz factor $\Gamma_0 \sim 100$. At R_d, the protons in the shell have the same Lorentz factor, γ_p, as the bulk Lorentz factor of the swept-up material, Γ_d:

$$\gamma_p = \Gamma_d = \left(\frac{\Gamma_0}{2}\right)^{1/2} \left(\frac{n_{ej}}{n}\right)^{1/4} \tag{1.4}$$

(Kumar and Panaitescu 2003) where n_{ej} is the comoving number density of the shell and n is the density of the surrounding medium, assumed here to be homogeneous (constant with distance from the progenitor). The energy deposited in the external medium at deceleration is:

$$E = \frac{8\pi}{3} R_d^3 \Gamma_d^2 n m_p c^2 = \frac{8\pi}{3} R_d^3 n m_p c^2 \frac{\Gamma_0}{2} \left(\frac{n_{ej}}{n}\right)^{1/2} \tag{1.5}$$

and the comoving ejecta proton number density is (assuming that the ejecta width is $\sim R/\Gamma_0$) is

$$n_{ej} = \frac{E}{4\pi R^3 m_p c^2}. \tag{1.6}$$

Using equations 1.4-1.6, we see the deceleration radius is

$$R_d = \left(\frac{9En}{4\pi m_p c^2 \Gamma_0^2}\right)^{1/3} = 10^{17}\mathrm{cm} \left(\frac{E}{10^{52}\mathrm{erg}}\right)^{1/3} \left(\frac{n}{1\mathrm{cm}^{-3}}\right)^{1/3} \left(\frac{\Gamma_0}{100}\right)^{-2/3}. \tag{1.7}$$

The deceleration time in the observer frame, t_d, is related to R_d by $t_d \sim R_d/\Gamma_d^2 c$ (within a factor of a few):

$$t_d \sim 300\mathrm{s} \left(\frac{E}{10^{52}\mathrm{erg}}\right)^{1/3} \left(\frac{n}{1\mathrm{cm}^{-3}}\right)^{1/3} \left(\frac{\Gamma_0}{100}\right)^{-8/3} \tag{1.8}$$

The Lorentz factor at deceleration is not much smaller than Γ_0, $\Gamma_d = \Gamma_0/\sqrt{6}$, where we have made use of equations 1.4, 1.6, and 1.7. After deceleration, the bulk Lorentz factor decreases as $\Gamma \propto R^{-3/2}$ for a fully adiabatic evolution and as $\Gamma \propto R^{-3}$ for a fully radiative evolution. The radius of the shell during adiabatic expansion decays with observer frame time as $R \propto t^{1/4}$ and during the radiative phase as $R \propto t^{1/7}$.

The forward shock propagates into the external medium, heating the material to relativistic temperatures. Synchrotron radiation generally fits the observed spectrum well (Paczynski and Rhoads 1993; Mészáros and Rees 1993b; Katz 1994), but inverse Compton losses also need to be taken into account (Mészáros et al. 1993, 1994). The magnetic field for synchrotron emission is again thought to be generated by plasma instabilities behind the forward shock, since the shock compression of the ambient magnetic field does not produce a strong enough magnetic field to explain the observed synchrotron emission. This emission is smooth, unlike the variable GRB emission. All temporal structure due to varying energy density in the shell will be smoothed out over a time scale $T_{ang} = R/2\Gamma^2 c$ due to the time delay of photons arriving to us from off-axis.

At deceleration, a mildly relativistic reverse shock is also launched into the ejecta from the explosion (Panaitescu and Mészáros 1998; Sari and Piran 1999; Kobayashi 2000), reheating the material. Since the reverse shock is mildly relativistic, this shock heating is predicted to produce synchrotron emission peaking at optical wavelengths. This process is thought to be the source of the early optical flashes observed for 021211 and 990123. The analysis for 990123 and 021211 suggests that if the optical flash is due to reverse shock emission, then the magnetic field in the ejecta was larger than that in the forward shock by a factor of ~ 10 (Kumar and Panaitescu 2003; Zhang et al. 2003) – perhaps suggesting a magnetic outflow, but it is far from proof. Reverse shock emission is predicted to occur in every burst; however, this

optical flash has not been seen in the *Swift* era (Roming et al. 2006), even though optical observations are consistently being performed during the GRB and shortly thereafter. This is the second major problem with the internal shock model – the predicted reverse shock emission has not been seen.

1.3 Determining the nature of GRB outflows

The internal/external shock model for GRB prompt and afterglow emissions is currently the most widely accepted model in the GRB community. The external shock model has been shown to explain the general characteristics of the late time afterglow in optical, x-ray and radio wavelengths fairly well (e.g. Panaitescu and Kumar 2002). However, as stated above, the internal shock model has a couple of major problems that have not been resolved – lower gamma-ray production efficiency than that inferred from afterglow modeling and non-detection of the optical flash presumably produced by the reverse shock. In light of these problems, we feel that it is prudent to explore the source of the prompt emission in great detail, to answer these main questions: How is the energy carried from the explosion – in protons, electron position pairs, or by magnetic field? What dissipation/emission processes are at work during the GRB?

In the next 5 chapters, we approach this question from a couple of different perspectives in an attempt to get to the bottom of this very important issue. In Chapter 2, we explore the possibility that the GRB and afterglow are both produced by one mechanism – an external shock. In Chapter 3, we

attempt to gain some insight about the GRB ejecta content using optical flash emission attributed to a reverse shock in the internal shock model. In Chapter 4, we use some exciting *Swift* gamma-ray, x-ray, and optical observations to constrain the emission mechanism of two GRBs. In Chapter 5, we estimate the distance from the GRB explosion at which the prompt GRB emission is produced for a sample of 10 bursts detected by *Swift*. Finally, in Chapter 6, we explain a unique method of modeling average prompt GRB spectral properties nearly model independently.

Chapter 2

An investigation of gamma-ray production in the external shock model for a sample of ten gamma-ray bursts

Multi-wavelength[1] afterglow data have enabled us to do broadband modeling of late-time afterglows. This broadband modeling results in the determination of burst energy, microphysical shock parameters, beaming angle, and environmental properties (surrounding density and stratification). Further improvements to our understanding of GRBs requires analysis/modeling of both the GRB and afterglow together, which we undertake here.

Here, we use parameters determined for 10 bursts by modeling their broadband afterglow emissions to extrapolate the radiation calculation back to the burst duration, with the goal of determining whether synchrotron emission from the forward shock can account for both the GRB prompt emission and the late-time afterglow. This is especially applicable for the $\sim$10% of bursts with a single pulse FRED (fast rise, exponential decline) GRB light-curve, where a single external shock is expected to produce the emission. This exercise is, however, carried out for all bursts in our sample, including those with

[1]Significant portions of this chapter have been previously published as McMahon et al. (2004).

moderately complex GRB light-curves.

Internal shocks were suggested as a mechanism for producing γ-ray emission because external shocks are not capable of producing rapid variability seen in many GRB light-curves, whereas variability arises naturally in internal shock models, reflecting fluctuations associated with the central engine (Rees and Mészáros 1994; Piran et al. 1993; Katz 1994). For GRB light-curves consisting of a single peak or just a few peaks, this rationale for internal shocks does not apply and such bursts could be produced in external shocks.

The determination of kinetic energy release in relativistic ejecta for ten bursts by modeling their broadband afterglow light-curves suggests that the efficiency for γ-ray production is typically in excess of 50% (Panaitescu and Kumar 2002). Such a high efficiency cannot be achieved in internal shocks; some published claims to the contrary (e.g. Beloborodov 2000) achieved high efficiency by colliding shells with very large relative Lorentz factor (hereafter LF), however in this case the emergent spectrum peaks at energies much larger than observed values. External shocks, on the other hand, can very efficiently convert bulk kinetic energy to radiation.

In addition to the problem of efficiency for the internal shock model we describe below other reasons for considering the external shock model for the generation of γ-ray emission for many of the ten bursts we consider in this paper (table 2.1 lists the ten bursts).

The 320-1090 keV light-curve for 990123 consisted of two broad peaks

of duration $\sim$ 10s each. Comparing this time scale with the deceleration time (t_d) of $\lesssim$50s – which is inferred from the peak of the prompt optical emission – suggests that γ-ray emission is produced within a factor 2 of the deceleration radius[2]. In the internal shock model for γ-ray production, the near equality of the radius where shells collide to produce γ-rays and the deceleration radius is a coincidence, whereas in the external shock model this is what one expects. It should be noted that the short time scale variability seen in 990123 (Fenimore et al. 1999) had an amplitude of $\sim$20% and could have arisen due to small scale turbulence in the shocked fluid. The observed low energy spectral index α for this burst was 0.4 ($f_\nu \propto \nu^{0.4}$) whereas in internal shock models we expect $\alpha \sim -0.5$ due to short cooling time for electrons or low cooling frequency (Ghisellini et al. 2000).

The light-curve for GRB 970508 was a FRED, 980519 was similar to a FRED, and 000301c light-curve was perhaps a FRED (Smith et al. 2002), however because of the low temporal resolution of the Ulysses observation (0.5 sec) we are unsure of it. One might expect these bursts to arise in an external shock. Two other bursts in our sample of ten – 980703 & 991208 – had light-curves consisting of two smooth peaks, and therefore are good candidates for a possible origin in an external shock. GRBs 990510 & 991216 light-curves had more fluctuations than the bursts mentioned above, however they each had two

[2]When the outermost γ-ray producing shell undergoes deceleration and is heated by the reverse shock it produces optical flash, and its radius increases as $\sim t^{1/4}$ for $t \gtrsim t_d/4$ (where t is the observer time). Therefore, the increase in the radius for a 5-fold increase in time is less than a factor 2.

broad peaks and a number of sub-pulses superimposed on them, and do not require internal shock to produce this modest variability. There are no light-curves available for the remaining two bursts in our sample, 000418 & 000926, which were both detected by the IPN (Interplanetary Network). It turns out that for all of these bursts, except 970508, the simplest theoretical model of synchrotron emission in the forward shock fails badly to explain their γ-ray emission (§2.1). Moreover, none of the possibilities we explore in the general framework of an external shock model seem to work satisfactorily.

In two GRBs (990123 and 021211), a bright, steeply falling off ($\sim t^{-2}$) early optical emission was observed. This has been explained by radiation from the reverse shock heated ejecta from the explosion. We have seen this emission from only these two bursts, while there are many cases for upper limits within a few hundred seconds after the GRB time and even a few bursts (e.g. 030418 and 021004) with early afterglow detections that do not exhibit the bright, steep optical decay. In this paper, we also estimate the reverse shock emission at deceleration for these ten bursts, and discuss possible reasons for numerous non-detections.

§2.1 outlines the afterglow fitting and describes our method for calculating the flux and the peak frequency during the GRB. A comparison between the theoretical calculation and γ-ray observations is also described in §2.1. Some alternate possibilities to explain the γ-ray observations such as inverse Compton in the forward or the reverse shocks, pair enriched ejecta, or high density clumps in the circum-stellar medium, are discussed in §2.2. In §2.3,

we discuss reverse shock optical emission at deceleration.

2.1 Afterglow to γ-ray Emission

The afterglow modeling is described in detail in Panaitescu and Kumar (2001) & Panaitescu and Kumar (2002). Briefly, we determine the collimated fireball dynamics by numerical integration of a simplified set of jet propagation equations, keeping track of radiative loss of energy due to synchrotron and inverse-Compton (IC) emissions. The synchrotron peak and cooling frequencies are calculated by assuming that a certain constant fraction of the thermal energy of the shocked fluid is imparted to electrons and magnetic field. The effect of IC loss including the proper Klein-Nishina cross-section is included in the calculation of the cooling frequency. The observed light-curves are calculated by integrating the emissivity over equal arrival time surface. All of the unknown parameters, which include jet opening angle, the total energy release in the explosion (which is is the sum of the kinetic energy given in Panaitescu and Kumar (2002) and the energy in γ-ray radiation), the fraction of energy in electrons (ε_{ef}), and the fraction in magnetic field (ε_{Bf}), are obtained by fitting the observed light-curves and the spectrum with the theoretically calculated curves by a χ^2 minimization. The parameter ε'_{ef}, which determines the minimum thermal Lorentz factor of electrons, is 0.1 for all bursts for which $p > 2$ (Panaitescu and Kumar 2002). Since the high energy spectral index during the burst gives $p > 2$ we set $\varepsilon'_{ef} = 0.1$ for all bursts in our calculations during the gamma-ray burst.

Using these parameters we estimate the frequency where the spectrum (νf_ν) peaks and the flux (f_ν) at this peak at deceleration (which we assume is half of the γ-ray burst duration). The results for ten bursts are summarized in Table 2.1 for a uniform circumburst density (wind circumburst medium had similar results, and for brevity are not listed here). The theoretical results are compared with the observed data for these bursts (see Table 2.1). Note that for six out of ten bursts in the table the peak frequency during the burst is within a factor of about 2 of the the observed value which we consider a reasonably good agreement. However, in four of these cases the theoretical peak flux is smaller than the observed value by an order of magnitude or more. For GRB 970508, which was a single peaked FRED burst, the fluxes are in good agreement. Therefore, for this burst the γ-ray emission could arise in an external shock; it is highly encouraging to see the forward shock model works so well to explain observations all the way from the γ-ray emission at 10s to radio at hundreds of days. However, for 000301C which was also likely a single pulse FRED, and 980703 & 991208 each of which contain two simple peaks in their γ-ray light-curve and are therefore good candidates for external shock mechanism for γ-ray production, the discrepancy between theory and observation is large.

To understand how sensitive the γ-ray emission is to errors in afterglow modeling and parameter determination, and to consider some possible solutions within the framework of the external shock model, we present an analytical derivation of the main results.

The forward shock synchrotron *injection* frequency, ν_{if}, and the flux at the peak of the F_ν spectrum are (Wijers and Galama 1999)

$$\nu_{if}(t) = \frac{0.98 q B \gamma_i^2 \Gamma}{2\pi m_e c(1+z)} \tag{2.1}$$

$$F_{pf}(t) = \frac{N_e P_{\nu_p} \Gamma (1+z)}{4\pi d_L^2} \tag{2.2}$$

where q & m_e are electron charge and mass, m_p is proton mass, $d_L = 2c\sqrt{1+z}[(1+z)^{1/2}-1]/H_0$ is the luminosity distance, $\gamma_i = \varepsilon'_{ef}(m_p/m_e)(\Gamma - 1)$ is the minimum thermal LF of electrons (the electron distribution for $\gamma > \gamma_i$ is assumed to be a power-law of index p, i.e.$dN_e/d\gamma \propto \gamma^{-p}$), $N_e = 4\pi A R^{3-s} m_p^{-1}/(3-s)$ is the total number of swept-up ISM electrons, $\rho_0 = AR^{-s}$ is the density of the medium just ahead of the shock, Γ is the bulk LF of shocked gas,

$$B = 4c\Gamma \left[2\pi \varepsilon_{Bf} A R^{-s}\right]^{1/2}, \quad R = (4-s)c\Gamma^2 t/(1+z), \tag{2.3}$$

t is the observer time, and

$$P_{\nu_p} = \frac{1.04 q^3 B}{m_e c^2} \tag{2.4}$$

is the power radiated per electron per unit frequency, in the shell comoving frame, at the peak of the synchrotron spectrum. The numerical factors of 1.04 in the above equation and 0.98 in equation (2.1) are taken from (Wijers and Galama 1999) for $p = 2$.

The synchrotron injection frequency and peak flux, at deceleration, for the particular cases of $s = 0$ & 2 are given below

$$\nu_{if}(t) = {\varepsilon'_{ef}}^2 \varepsilon_{Bf}^{\frac{1}{2}} \mathcal{E}_{52}^{\frac{1}{2}} (1+z)^{\frac{1}{2}} t_{d,1}^{-3/2} \times \begin{cases} 1.01 \times 10^4 \text{ keV} & \text{s} = 0 \\ 1.7 \times 10^4 \text{ keV} & \text{s} = 2 \end{cases} \tag{2.5}$$

$$F_{pf}(t) = \frac{\varepsilon_{Bf}^{\frac{1}{2}} \mathcal{E}_{52}^{\frac{1}{2}}}{\left[(1+z)^{1/2}-1\right]^2} \times \begin{cases} 1.8 \mathcal{E}_{52}^{\frac{1}{2}} n_0^{1/2} \text{ mJy} & \text{s} = 0 \\ \frac{4.2\times10^3 A_*}{[t_d/(1+z)]^{1/2}} \text{ mJy} & \text{s} = 2 \end{cases} \tag{2.6}$$

where $A_* = A/(5 \times 10^{11})$ g cm^{-1}, $\mathcal{E}$ is the isotropic equivalent of energy release in the explosion, t_d is the observer frame deceleration time in seconds, and an integer subscript n on a variable X, X_n, means $X/10^n$. In the derivation of the above equations we substituted for Γ using the equation $4\pi A R^{3-s} c^2(\Gamma^2-1)/(3-s) = \mathcal{E}/2$ at deceleration which states that half of the original kinetic energy of the explosion ($\mathcal{E}/2$) is deposited into swept-up ISM; the LF at deceleration is given by:

$$\Gamma_{d,2} = \begin{cases} 4.17 \left(\frac{\mathcal{E}_{52}}{n_0}\right)^{1/8} \left[\frac{(1+z)}{t_d}\right]^{3/8} & \text{s} = 0 \\ 0.74 \left[\frac{(1+z)\mathcal{E}_{52}}{A_* t_d}\right]^{1/4} & \text{s} = 2 \end{cases} \tag{2.7}$$

We next calculate the electron cooling frequency. For this we need the Compton Y parameter, defined as $Y \equiv \tau_T \int d\gamma_e \, \gamma_e^2 (dn_e/d\gamma_e)$, with τ_T being the column density of electrons times the Thomson cross-section. The Y-parameter is obtained by solving the equation describing the radiative loss of energy -

$$\frac{d}{dt'}\left[m_e c^2 \gamma_e \frac{dn_e}{d\gamma_e}\right] = -\frac{dn_e}{d\gamma_e}\frac{(1+Y)\sigma_T B^2 \gamma_e^2 c}{6\pi}, \tag{2.8}$$

where t' is the comoving time, B is the magnetic field which we assume is uniform, and σ_T is the Thomson scattering cross-section. Consider the comoving frame down-stream fluid velocity to be v. This relates t' and the comoving radial coordinate r' viz. $dr' = v\, dt'$. Changing the independent variable from t' to r' and integrating the above equation over the electron distribution we

find

$$\frac{d(\varepsilon_e U)}{dr'} = -\frac{(1+Y)\sigma_T B'^2 c n_e \overline{\gamma_e^2}}{6\pi v}, \tag{2.9}$$

where U is the thermal energy density of shocked fluid, and $\overline{\gamma_e^2}$ is the average γ_e^2. Integration of this equation over r' for a highly relativistic shock ($v \sim c$) and highly radiative fluid ($\nu_i \gg \nu_c$) we find

$$Y(1+Y) \approx \frac{\varepsilon_e}{4\varepsilon_B}. \tag{2.10}$$

The calculation of the cooling LF of electrons, γ_c, at deceleration, is straightforward and is given below; γ_c is the LF of electrons that lose their energy in a time available since crossing the shock front averaged over the population, given by $t_c \sim t_d/3^{(2-s)/2}$.

$$\gamma_c(t_d) = \frac{3\pi m_e c(1+z)}{2\sigma_T B'^2 t_c \Gamma_d (1+Y)} = \frac{3(1+z)^{1-s} m_e \Gamma_d^{2s-3}}{64\sigma_T \varepsilon_B A c (4ct_d)^s t_c (1+Y)} \tag{2.11}$$

This in turn is used to calculate the synchrotron frequency, in observer frame, corresponding to the LF γ_c, and is referred to as the cooling frequency (ν_c).

$$\nu_c(t_d) = \frac{qB'\gamma_c^2\Gamma_d}{2\pi m_e c(1+z)}$$

$$\text{or} \quad \nu_c(t_d) = \begin{cases} \frac{3.2}{(\mathcal{E}_{52}t_d(1+z)\varepsilon_B)^{1/2}\varepsilon_e n_0} & \text{eV} \quad \text{s} = 0 \\ 2.2\times10^{-7}\frac{(\mathcal{E}_{52}t_d)^{1/2}}{\varepsilon_B^{1/2}A_*^2\varepsilon_e(1+z)^{3/2}} & \text{eV} \quad \text{s} = 2 \end{cases} \tag{2.12}$$

where we have made use of equations (2.7), (2.10), and (2.11). We see that the cooling frequency at deceleration is typically much smaller than the synchrotron injection frequency (see eq. 2.5) and thus the peak of the νf_ν spectrum will generally be at ν_{if}. For the case where $\nu_{if} > \nu_c$, the flux at the peak

of the νf_ν spectrum is obtained by using equations (2.5), (2.6) & (2.12) and is given here

$$F_{\nu_p}(t_d) = \frac{(\mathcal{E}_{52} t_d)^{1/2}(1+z)^{-1/2}}{\varepsilon'_{ef}\varepsilon_{ef}^{1/2}\left[(1+z)^{1/2}-1\right]^2} \times \begin{cases} 6\times 10^{-4}\ \mathrm{mJy} & \mathrm{s}=0 \\ 3.5\times 10^{-4}\ \mathrm{mJy} & \mathrm{s}=2 \end{cases} \tag{2.13}$$

Note that the flux is independent of ε_B and the density of the ISM – the two parameters that have the largest error associated with them in afterglow modeling (Panaitescu and Kumar 2002). Using equations (2.5) and (2.13) we calculate the peak frequency and the flux during the γ-ray burst and the results are in good agreement with the numerical calculation result presented in table 2.1.

Table 2.1 shows that for all those bursts for which the observed and theoretical peak frequencies agree within a factor of two[3] (6 cases altogether), the theoretically calculated fluxes, with the exception of 970508, are too small by an order of magnitude compared to the observed fluxes.

We see from equation (2.13) that the flux at the peak of νf_ν depends only on $\mathcal{E}$, which is a very well determined parameter, and ε'_{ef} which is 0.1 for all the bursts with $p > 2$, and therefore there is no way to reconcile the difference between the observed flux and the theoretical expectation in the simplest version of the synchrotron emission in the external shock model. Any error in the parameter determination from afterglow modeling does not affect our calculation of the γ-ray flux. In other words, even if we consider ε_{Bf} and

[3]We have assumed that the peak frequency for 000301c was $\sim$ 500 keV, at the higher end of the peak frequency distribution, since it was a fairly short burst (8.4 seconds).

the ISM density n during the burst to take on values completely unrelated to what is determined from afterglow modeling the observed flux cannot be reconciled with the theoretical expectations in the forward shock model. This is a very robust result and effectively rules out synchrotron origin for γ-ray emission in the external shock model for these bursts.

In four cases, viz. 980519, 980703, 990123 & 000418, the theoretically calculated peak frequencies are much smaller than the observed value; these are the four cases with the smallest ε_{Bf} as determined by the afterglow modeling (see Table 2.1). Could a larger ε_{Bf} at early times, as in the case of 021211 (Kumar and Panaitescu 2003), explain the peak frequencies for these four cases? If ε_{Bf} were to be 0.5 during the burst for 980519 & 000418 we can explain the γ-ray emission for these GRBs. However, even if we set $\varepsilon_{Bf} = 1$ during the burst for 980703 & 990123 the synchrotron frequency falls short of the observed value. Could the gamma-ray burst in these cases arise as a result of inverse-Compton (IC) scattering of the synchrotron radiation in the forward or the reverse shock? We consider this possibility, and some others, in the next section. We also investigate whether the peak flux of the IC component might be able to match the observed flux for the other five bursts which have too small synchrotron flux.

Table 2.1. Forward Shock Emission at Deceleration For $s = 0$

Burst	$\mathcal{E}$ ($\times 10^{52}$ ergs)	ε_{Bf}	$\nu_p(t_d)$ (keV)	$\nu_{p,obs}$ (keV)	$f_{\nu_p}(t_d)$ (mJy)	$f_{\nu_p,obs}$ (mJy)	Refs.
970508	7.92	4.5×10^{-2}	98.4	100	0.51	0.6	2,4
980519[b]	99.8	3.5×10^{-5}	7.0	700	1.25	0.3	3,4
980703	0.40	3.0×10^{-3}	0.8	370	0.21	0.3	3
990123	277.5	9.9×10^{-4}	6.6	780	1.24	9.0	1,2,3,5
990510	55.5	5.0×10^{-3}	184.9	160	0.27	4.0	1,2,3
991208	11.9	3.8×10^{-2}	118.7	190	0.78	20.0	1,3,6
991216	100.0	6.2×10^{-3}	153.4	410	1.0	30.0	1,3
000301c	8.19	1.0×10^{-1}	541.6	500[a]	0.04	0.3	1,3,7
000418	8.05	1.6×10^{-2}	25.2	280	0.32	0.4	1,3
000926	39.7	8.1×10^{-2}	198.4	130	0.21	0.7	1

[a]No $\nu_{p,obs}$ available for this burst.

[b]Redshift not known for this burst, $z = 1$ used.

Note. — $\varepsilon'_{ef} = 0.1$, $\varepsilon_{ef} = 0.5$ for all bursts, n_0, θ_0 are equal to values found from afterglow modeling.

References. — (1) Mazets; (2) Amati et al. (2002); (3) Jimenez et al. (2001); (4) Nicastro et al. (1999); (5) Briggs et al. (1999); (6) Hurley et al. (2000); (7) Smith et al. (2002)

2.2 Gamma-rays in external shock: some alternate possibilities

We consider below (§2.2.1) a combination of synchrotron and inverse-Compton processes in the forward and reverse shocks to determine if this could explain the γ-ray emission properties for the nine "problem bursts" in our sample of ten discussed in the last section. In §2.2.2 we discuss if a collision between the GRB ejecta and a high density clump might be able to explain the large γ-ray flux for the five of the bursts in our sample, and in §2.2.3 we look into the effect of electron-positron pair loaded ejecta on γ-ray emission.

2.2.1 Inverse Compton in the external shock

We investigate the effect of IC in external shocks – forward as well as the reverse shock – to see if the observed γ-ray emission for the bursts in our sample could be explained by the IC process.

Consider the flux at the peak of the synchrotron radiation νf_ν spectrum, ν_p, to be f_{ν_p}. We consider inverse-Compton scattering by a population of electrons that could be distinct from the population that gives rise to the synchrotron radiation. For instance, the synchrotron emission could be produced in the reverse shock (RS) and the IC scattering in the FS. Let us take the minimum thermal LF of electrons in the IC-scattering region to be $\gamma_{min} = \min(\gamma_i, \gamma_c)$, the electron distribution to have a break at $\gamma_b = \max(\gamma_i, \gamma_c)$ such that for $\gamma > \gamma_b$ the electron distribution is proportional to γ^{-p-1}; γ_i & γ_c are the injection and cooling LFs for electrons. The peak of the IC radiation

(for νf_ν) is at

$$\nu_p^{IC} \sim \nu_p \gamma_b^2. \tag{2.14}$$

If the optical depth of the medium to Thomson scattering is τ_T, then the flux at the peak for the case where $\gamma_i \ll \gamma_c$ is

$$f_{\nu_p}^{IC} \sim \tau_T (\gamma_{min}/\gamma_b)^{p-1} f_{\nu_p}. \tag{2.15}$$

For $\gamma_c < \gamma_i$, there is a slightly different relationship. The optical depth at deceleration in the forward shock is given by

$$\tau_T = \frac{\sigma_T \mathcal{E}}{4\pi m_p c^2 \Gamma_0^2 R_d^2}, \tag{2.16}$$

where $R_d = (4-s)ct_d\Gamma_d^2/(1+z)$ is the deceleration radius, Γ_d is the LF at deceleration, and $\Gamma_0 \sim 1.5\Gamma_d$ is the initial LF of the ejecta (see eq. 2.19). Using equation (2.7) this can be rewritten as follows

$$\tau_T = \begin{cases} 3.9 \times 10^{-9} n_0^{3/4} \mathcal{E}_{52}^{1/4} [t_d/(1+z)]^{1/4} & \text{s} = 0 \\ 8.7 \times 10^{-4} A_*^{3/2} \mathcal{E}_{52}^{-1/2} [(1+z)/t_d]^{1/2} & \text{s} = 2 \end{cases} \tag{2.17}$$

We see that the optical depth for a uniform density ISM is very small, and therefore the inverse Compton flux due to scattering in the forward shock region, for $s = 0$, is likely to be too small to be observationally interesting.

The optical depth to Thomson scattering of the ejecta at deceleration can be obtained directly from equation (2.17) by recognizing that the mass of the ejecta is larger than the swept-up ISM mass by a factor Γ_d. Thus,

$$\tau_T = \begin{cases} 1.5 \times 10^{-6} n_0^{5/8} \mathcal{E}_{52}^{3/8} [t_d/(1+z)]^{-1/8} & \text{s} = 0 \\ 5.4 \times 10^{-2} A_*^{5/4} \mathcal{E}_{52}^{-1/4} [(1+z)/t_d]^{3/4} & \text{s} = 2 \end{cases} \tag{2.18}$$

2.2.1.1 Reverse Shock Break Frequencies and Peak Flux

To complete the calculation of inverse Compton scattering of synchrotron emission produced in the reverse shock (RS) region we provide below the synchrotron characteristic frequency and the flux from the RS (see Kumar and Panaitescu 2003, for details).

The thermal energy per proton in the RS at deceleration, e_p, can be calculated using the following pair of equations

$$e_p = \frac{1}{2}\left(\frac{\Gamma_d}{\Gamma_0} + \frac{\Gamma_0}{\Gamma_d}\right), \quad \frac{\Gamma_d}{\Gamma_0} = \left[1 + 2\left(\frac{n_0\Gamma_0^2}{n_{ej}}\right)^{1/2}\right]^{-1/2}. \tag{2.19}$$

which fits the results of numerical calculations to better than 8% in the Newtonian, relativistic and intermediate regimes; where n_{ej} is the comoving density of the ejecta, n_0 is the ISM density, and Γ_0 is the initial LF of the ejecta.

It can be shown that n_{ej}/n_0 at the time when the reverse shock arrives at the back end of the ejecta (which is approximately equal to the deceleration time for the ejecta) is $1.5\Gamma_0^2$ for a uniform density ISM and $3.5\Gamma_0^2$ for $s = 2$ medium. The reverse shock in this case is neither highly relativistic nor Newtonian. Using the above equation we find the thermal energy per proton in the RS in this case to be $0.13 m_p c^2$ ($0.067 m_p c^2$) for a $s = 0$ ($s = 2$) medium.

The injection frequency at deceleration for RS is smaller than the FS by a factor of $\Gamma_d^2/0.13^2$ for uniform ISM and is given below

$$\nu_{ir}\left(t_d\right) = \frac{0.07 q m_p^{5/2} \varepsilon_{Br}^{1/2} \varepsilon_{er}' n_0^{1/2} R_d^{-s/2} \Gamma_d^2}{\left(2\pi\right)^{1/2} m_e^3 (1+z)}. \tag{2.20}$$

This equation, and a similar one for $s = 2$, can be rewritten as

$$\nu_{ir}\left(t_d\right) = \varepsilon_{Br}^{1/2}\varepsilon_{er}^{\prime 2} \times \begin{cases} 37\, n_0^{1/4}\mathcal{E}_{52}^{1/4}(1+z)^{-1/4}t_d^{-3/4}\ \mathrm{eV} & \mathrm{s}=0 \\ 610\, A_*^{1/2}t_d^{-1}\ \mathrm{eV} & \mathrm{s}=2 \end{cases} \tag{2.21}$$

where we have used equation (2.7) to eliminate Γ_d. The cooling frequency in the reverse shock region, when $\nu_{ir} > \nu_{cr}$, is given by equation (6.2) with appropriate values of ε_B and $\varepsilon_e^{\prime}$ for the reverse shock. However, the reverse shock ν_{cr} is typically larger than ν_{ir} (see Table 2.2), so equation (2.10) is not a valid approximation for the Compton Y parameter any longer and we must also use an appropriately modified form version of equation (6.2).

The flux at the peak of the reverse shock f_ν spectrum at deceleration is larger than the peak flux from the FS by a factor Γ_d and can be written as

$$F_{pr}\left(t_d\right) = \frac{\left(3\varepsilon_{Br}A\right)^{1/2} q^3 \mathcal{E}(1+z)^{s/2}}{m_e m_p c^3 d_L^{\prime 2}\Gamma_d^{s-1}\left(4ct_d\right)^{s/2}\left[\left(3-s\right)\pi\right]^{1/2}} \tag{2.22}$$

or

$$F_{pr}\left(t_d\right) = \frac{\varepsilon_{Br}^{1/2}}{\left[(1+z)^{1/2}-1\right]^2} \times \begin{cases} 6.8\times 10^2 (1+z)^{3/8}\mathcal{E}_{52}^{9/8}n_0^{3/8}t_d^{-3/8}\ \mathrm{mJy} & \mathrm{s}=0 \\ 2.7\times 10^5 (1+z)^{3/4}\mathcal{E}_{52}^{3/4}A_*^{3/4}t_d^{-3/4}\ \mathrm{mJy} & \mathrm{s}=2 \end{cases} \tag{2.23}$$

The self-absorption frequency in the reverse shock region, ν_{Ar}, is often as large as the cooling and the injection frequencies, and therefore should be taken into consideration in the calculation of observed flux. The self-absorption and cooling frequencies and the Compton Y parameter need to be calculated together in a self-consistent way (as we do for all of our numerical calculations). However, when electron cooling is dominated by the inverse-Compton scattering and $\max\{\nu_{ir}, \nu_{cr}\} > \nu_{Ar}$, the calculation of self-absorption frequency is

considerably simplified and is given by Kumar and Panaitescu (2003)

$$\nu_{Ar}\left(t_d\right)\left(\frac{\nu_{ir}}{\nu_{Ar}}\right)^{\alpha/2} = \left(\frac{\varepsilon_{Br}}{\varepsilon'_{er}}\right)^{1/2} \times \begin{cases} 8.4\times10^{-2}\mathcal{E}_{52}^{3/8}n_0^{3/8}t_d^{-5/8}(1+z)^{-3/8}\ \mathrm{eV} & \mathrm{s}=0 \\ 49\,A_*^{3/4}t_d^{-1}\ \mathrm{eV} & \mathrm{s}=2 \end{cases} \quad (2.24)$$

where α depends on the ordering of ν_{ir}, ν_c and ν_{Ar}, and is equal to 1/3 if $\nu_c > \nu_{ir} > \nu_{Ar}$, and $-p/2$ when $\nu_c > \nu_{Ar} > \nu_{ir}$.

2.2.1.2 Inverse Compton results

The peak frequency and flux for the IC radiation is calculated as described in §2.2.1. The calculation of the synchrotron injection frequency is straightforward & is carried out as described in §2.1 for the FS and §2.2.1.1 for the RS. The synchrotron self-absorption frequency is typically small in the FS and is unimportant for IC calculation. However, in the RS the self-absorption can be larger than the cooling frequency and these frequencies must be calculated self-consistently; we calculate these frequencies numerically.

There are four cases of the IC scattering to consider: synchrotron in the FS and IC in either the FS or the RS, synchrotron in RS and IC in the RS or the FS. We have investigated these cases numerically, and we have explored the parameter space – $\mathcal{E}$, ε_{Br}, ε'_{er}, ε_{Bf}, ε'_{ef}, n – for each burst to determine if the observed γ-ray peak frequency and flux could be explained by the IC radiation, either for a uniform density circum-burst medium or a wind-like medium ($\rho \propto R^{-2}$). The results for each burst are described below.

For a uniform density ISM the synchrotron-IC mechanism in external

shock offers a vanishing parameter space that is consistent with the gamma-ray emission properties for GRB 990123. However, for a $s = 2$ medium we find some solutions where the synchrotron emission produced in the forward shock undergoes inverse-Compton scattering in the reverse-shock region. The density required for these solutions is $\sim 10^2$ times that normally associated with Wolf-Rayet star winds, and much greater than what is found from modeling of early and late time afterglow observations. Other parameters such as the energy in the explosion, micro-physics shock parameters in the forward and the reverse shock are roughly consistent with the afterglow observations. However, the low energy spectral index for the γ-ray spectrum (α) is -0.5 whereas the observed index is 0.4. Therefore, we do not have a fully self consistent solution for the gamma-ray emission properties for 990123 in the external shock model. This is surprising in the light of the arguments for external shock for this burst, and perhaps suggests that there may be some other mechanism producing the γ-ray photons that is completely different from the standard internal/external shocks model. In the next sub-section we explore if high density gas near the deceleration radius could explain the γ-ray emission.

In the case of 980519 there are IC solutions for $s = 2$ medium where the synchrotron radiation is produced in the forward shock & IC in the reverse-shock, and the parameter space consists of A_* in the range of 15 to 100 which is at least a factor of a few larger than the value of $A_* \sim 3.5$ determined from afterglow modeling. However, the IC solution requires $\varepsilon_B \sim 10^{-4}$ in the forward shock that is much smaller than the value of 0.1 we find for this burst

from the afterglow fitting when $s = 2$. The RS optical peak flux of $\sim$ 11th magnitude is perhaps not a problem for this solution.

For 980703 there are solutions found for $s = 0$. However, these solutions require $\mathcal{E} > 10^{55}$ erg and the RS optical flux is larger than 1 Jy, and therefore these are not acceptable solutions. The solutions we find for this burst with $s = 2$, which involve synchrotron in the FS and IC in the RS, require $A_* \gtrsim 5$ and other parameters are roughly consistent with the values we find from the afterglow modeling; the optical flux from the RS is $\sim$ 20 mJy. If we ignore the somewhat high density requirement, this burst could perhaps be produced as IC in the external shock.

For 990510 no solution is found that is in agreement with the observed properties of this burst. The same is true for 991208, 991216. To be precise, there are no solutions found when the density of the medium is taken to be uniform. However, for a pre-ejected wind medium there are regions in the multidimensional parameter space $(\mathcal{E}, A_*, \varepsilon_B, \varepsilon_e')$ that give gamma-ray flux and peak frequency in agreement with observations for these bursts where synchrotron emission is produced in the forward shock and the inverse-Compton scattering takes place in the reverse shock region. The problem is that for all of these "solutions" A_* is greater than about 10^2 which is larger than what we obtain from afterglow modeling by two orders of magnitude, and too large for winds from Wolf-Rayet stars. Moreover, the large ε_{Br} in the reverse shock for these solutions gives rise to optical R-band flux of about 10 Jy, or 6th magnitude, which is unlikely to have gone unnoticed. Therefore we do not consider

these solutions physically acceptable.

We find two different IC "solutions" for 000418 for a $s = 2$ circum-burst medium; one of which is synchrotron in the FS and IC in the RS, and the other is synchrotron in the RS and IC in the FS. The first scenario requires $A_* \gtrsim 25$ (which is larger by factor $\sim 10^2$ than determined from afterglow observations) and ε_{Bf} is between $\sim 10^{-5}$ and 2×10^{-4} which is smaller by two orders of magnitude than the value we find from afterglow modeling. The peak optical flux from the RS is between 20 mJy and 3 Jy; the lower flux value in this case certainly poses no difficulty with observations. The latter scenario requires $A_* \gtrsim 400$ and $\varepsilon_{Br} \sim 10^{-5}$ which are unlikely to be realized in nature.

There are also two solutions for 000301c with $s = 2$. For FS synchrotron & IC scattering in the RS, A_* is about an order of magnitude larger than that found by afterglow modeling, but the optical flux from RS is not a problem, being $\lesssim 0.5$ Jy. The magnetic field parameter in the forward shock required for the IC solution is, however, several orders of magnitude smaller compared with the value we find from afterglow modeling in a wind-like medium for this burst. This together with the required high density for the CBM makes this solution unacceptable. For the case of RS synchrotron & IC scattering in the FS, the allowed parameter space to explain the γ-ray observations require the energy to be a factor of 10 smaller than the observed value, and $A_* \gtrsim 100$. The magnetic field parameter is also 100 times smaller than the afterglow value, so we do not consider these solutions viable. For a uniform density medium the IC solution for 000301c requires $\mathcal{E} > 10^{55}$ which is more than two orders of

magnitude larger than the energy determined from either the γ-ray fluence or the afterglow emission. The situation for 000926 is a bit worse than 000301c.

We also note that the IC flux for 970508, in any of the four possible combinations, at the observed peak is too small to be a significant contributor to the observed flux.

2.2.2 Effect of density clumps in the ISM on gamma-ray flux

In this subsection we investigate whether a dense clump of gas in the circum-burst medium (CBM) might increase the flux in the γ-ray band and thereby explain flux observations at the peak of the νf_ν spectrum for some of the bursts in our sample.

Consider a dense clump of angular size greater than Γ_0^{-1}, and proton number density n; Γ_0 is the initial Lorentz factor (LF) of the ejecta which we assume does not decrease until it runs into the clump. For the calculation of radiation such a clump can be treated as a spherical object. We take the external density to be sufficiently high that the forward shock LF is less than Γ_0 and the reverse shock is relativistic; the parameter $\xi \equiv \Gamma_0^2 n/n_{ej} > 1$ determines the thermal LF of protons in the forward and the reverse shocks; n_{ej} is the density of the ejecta when it hits the clump. For large n the thermal LF of protons in the FS is $\gamma_{p,f} = \Gamma_0 \xi^{-1/4}/2^{1/2}$ and in the RS it is $\xi^{1/4}/2^{1/2}$.

The thermal energy density in these shock regions is $4nm_pc^2\gamma_{p,f}^2 \sim n\Gamma_0^2 m_p c^2 \xi^{-1/2}$, and therefore the magnetic field strength $B \propto (\varepsilon_{Bf} n)^{1/2}\Gamma_0 \xi^{-1/4}$. The synchrotron injection frequency in the forward shock is

$\nu_i \propto {\varepsilon'_{ef}}^2 (\varepsilon_{Bf} n)^{1/2} \Gamma_0^4 \xi^{-1}$.

The number of swept up protons at deceleration is obtained by equating the thermal energy of protons (in lab frame) with half the energy in the explosion i.e., $N_p m_p c^2 \gamma_{p,f}^2 = \mathcal{E}/2$ or $N_p = \mathcal{E}\xi^{1/2}/(m_p c^2 \Gamma_0^2)$.

Let us assume that the distance of the clump from the center of the explosion is R_c and the forward shock travels a distance of δR_c before the shocked material acquires half the energy of the explosion. Therefore, $N_p = 4\pi n R_c^3 \delta = \mathcal{E}\xi^{1/2}/(m_p c^2 \Gamma_0^2)$. The GRB duration (in the observer frame), if the γ-rays are produced due the ejecta colliding with the dense clump, is $t_\gamma \sim R_c/(c\gamma_{p,f}^2) \sim R_c \xi^{1/2}/(c\Gamma_0^2)$. Combining this with the equation for N_p we find: $n\Gamma_0^8 \sim \xi^2 \mathcal{E}/(4\pi m_p c^5 t_\gamma^3 \delta)$. Substituting this back into the equation for injection frequency we find $\nu_i \propto \varepsilon_{Bf}^{1/2} {\varepsilon'_{ef}}^2 \mathcal{E}^{1/2} t_\gamma^{-3/2} \delta^{-1/2}$.

The time scale in the lab frame for electrons to cool in the forward shock is $\sim \delta R_c/(c\gamma_{p,f})$, from which we calculate the cooling frequency to be $\nu_c \propto (n\varepsilon_{Bf})^{-3/2}(1+Y)^{-2}(\delta R_c)^{-2} \propto \varepsilon_{Bf}^{-3/2}(t_\gamma \mathcal{E})^{-1/2} n^{-1} \delta^{-3/2}(1+Y)^{-2}$.

The flux at the peak of the synchrotron spectrum is $f_p \propto \varepsilon_{Bf}^{1/2} n^{1/2} \mathcal{E}$. For $\nu_c < \nu_{if}$, expected for a high density clump, the Compton Y-parameter is $\sim (\varepsilon_{ef}/\varepsilon_{Bf})^{1/2}$, and the flux at the peak of νf_ν i.e. at ν_{if} is proportional to $\mathcal{E}^{1/2} t_\gamma^{1/2} \delta^{-1/2} \varepsilon_{ef}^{-1/2} {\varepsilon'_{ef}}^{-1}$. Note a weak dependence of the peak flux on $\delta \equiv \delta R_c/R_c$.

The distance δR_c the FS moves before the GRB ejecta is decelerated is obtained by calculating the density of the ejecta at R_c;

$n_{ej} \sim \mathcal{E}/[4\pi R_c^2 m_p c^2 \Gamma_0^2 \max(t_* c, R_c/\Gamma_0^2)]$, where t_* is the duration of the central engine in the lab frame. Using this expression and the definition of ξ we find that $\delta \sim \max(t_*/t_\gamma, \xi^{-1/2})$.

Since the peak flux is proportional to $\delta^{-1/2}$, a factor of ten increase in the flux requires $\xi \gtrsim 10^4$ or the clump density $n \sim n_{ej}(10^{-4}\Gamma_0^2)$. Therefore, for $\Gamma_0 \sim 10^2$, n is of order n_{ej} and we find that in order to explain the gamma-ray flux in the clump-ejecta collision the density of the clump needs to be similar to the ejecta as in the internal shock model! Very bright early afterglow will be produced in such a collision which might pose a problem for this scenario. We note that the increase in the flux is accompanied by an increase in the peak frequency, both of which are proportional to $\delta^{-1/2}$, but the latter quantity can be easily adjusted by a decrease in ε_{Bf} or ε_e' to match the observations.

2.2.3 Effect of $e^\pm$ pairs present in the ejecta

In this subsection we consider whether $e^\pm$ pairs present in the ejecta can make inverse-Compton radiation match the peak flux and frequency at deceleration. Pairs would soften the reverse shock spectrum, and the larger optical depth could increase IC flux at the peak. Adding $N_\pm$ pairs per proton to the ejecta increases the number of radiating particles in the reverse shock region thus lowering the energy per particle. This decreases ν_{ir} by a factor of $N_\pm^2$ while increasing the peak flux of the f_ν spectrum by a factor of $N_\pm$. The cooling frequency for the highly radiative regime is not affected, nor is it changed when the Compton-Y parameter is much less than one; it is, however,

affected when $\nu_{ir} < \nu_{cr}$ (more common in the reverse shock emission than $\nu_{ir} > \nu_{cr}$, see Table 2.2) and $Y > 1$, increasing it by a factor $N_{\pm}^{2(p-2)/(4-p)}$.

The flux at the cooling frequency, which is the peak of the reverse shock synchrotron νf_ν spectrum, is proportional to $N_{\pm}^{3(2-p)/(4-p)}$. We see that for $p = 2$ the cooling frequency and the peak flux are independent of $N_{\pm}$. The peak flux increases by a factor of $N_{\pm}^{3/5}$ for $p = 1.5$ (decreasing for $p > 2$). For inverse-Compton scattering of these reverse shock synchrotron photons by the ejecta, the IC peak, $\nu_{p,IC} = \gamma_c^2 \nu_c$, will increase by a factor of $N_{\pm}^{4(p-2)/(4-p)}$. We see again that $\nu_{p,IC}$ is not affected when $p = 2$, but can go up ($p > 2$) or down ($p < 2$) for other values. The IC flux at the peak changes by a factor of $N_{\pm}^{6(2-p)/(4-p)}$ (from its value without pairs present), which, similarly, does not change much for values of p around 2. The IC peak flux decreases for $p > 2$ and at most, can be increased by a factor of $\sim N_{\pm}$ when the electron distribution is very hard, i.e. $p \lesssim 1.5$.

It can be shown that the peak flux for synchrotron produced in the FS and IC in the RS decreases with $N_{\pm}$ for $p > 1.6$. The reverse process – synchrotron in the RS and IC in the FS – has also lower peak flux for $p > 2$. Thus, we find that pairs present in the ejecta are not likely to be able to account for the theoretical IC and observed γ-ray flux difference.

2.3 Early Afterglow Emission

It is generally believed that the steeply falling off early afterglow emission observed from GRBs 990123 and 021211 was produced by the reverse

shock heated ejecta from the explosion. This emission falls off roughly as $t^{-1.7}$ and flux falls below the forward shock emission level after about $10-20$ minutes. We use the equations in §2.2.1.1 to calculate the observed flux in the optical R-band at deceleration for this sample of 10 bursts. For the case of $\nu_{ir} < \nu_{cr} < \nu_R$, the flux at $\nu_R \sim 2$ eV, the R-band in observer frame, is given by

$$f_R(t_d) = \frac{\varepsilon_{Br}^{\frac{p}{4}} \varepsilon_{er}'^{\,p-1} \varepsilon_{er}^{-\frac{1}{2}}}{[(1+z)^{1/2}-1]^2} \times \begin{cases} 400 \times 3.3^{\frac{p-1}{2}} (1+z)^{\frac{2-p}{8}} \mathcal{E}_{52}^{\frac{p+6}{8}} n_0^{\frac{p-2}{8}} t_{d,1}^{-\frac{3p+2}{8}} \text{ mJy} & \text{s} = 0 \\ 584 \times 30^{\frac{p-1}{2}} \mathcal{E}_{52} A_*^{\frac{p-2}{4}} t_{d,1}^{-\frac{p}{2}} \text{ mJy} & \text{s} = 2 \end{cases} \quad (2.25)$$

Whereas for the case where $\nu_{ir} < \nu_R < \nu_{cr}$ the flux is

$$f_R(t_d) = \frac{\varepsilon_{Br}^{\frac{p+1}{4}} \varepsilon_{er}'^{\,p-1}}{[(1+z)^{1/2}-1]^2} \times \begin{cases} 290 \times 3.3^{\frac{p-1}{2}} (1+z)^{\frac{4-p}{8}} \mathcal{E}_{52}^{\frac{p+8}{8}} n_0^{\frac{p+2}{8}} t_{d,1}^{-\frac{3p}{8}} \text{ mJy} & \text{s} = 0 \\ 4.8\text{x}10^4 \times 30^{\frac{p-1}{2}} \mathcal{E}_{52}^{\frac{3}{4}} A_*^{\frac{p+2}{4}} t_{d,1}^{-\frac{2p+1}{4}} (1+z)^{-\frac{3}{4}} \text{ mJy} & \text{s} = 2 \end{cases} \quad (2.26)$$

In Table 2.2, we provide the theoretical estimations of the magnitude of the reverse shock emission for the ten bursts in our sample (for a homogeneous external medium and assuming the RS parameters to be same as the FS), to determine if these bursts would have had a bright optical flash. These results were obtained numerically using an accurate calculation of the cooling and the self-absorption frequencies, which can also be found in Table 2.2, and the flux is found to be consistent with the analytical estimate given above. Our fluxes are somewhat smaller than reported in Soderberg and Ramirez-Ruiz (2002). The difference is perhaps because the RS falls in a regime that is neither

Table 2.2. Predicted Reverse Shock Flux Using Afterglow Parameters for Homogeneous External Medium

Burst	R [a]	ν_{ir} (eV)	ν_{cr} (eV)	ν_{ar} (eV)
970508	9.8	1.0×10^{-2}	5.8	3.9×10^{-2}
980519[b]	17.1	3.8×10^{-4}	5.1×10^{5}	2.8×10^{-3}
980703	17.4	2.4×10^{-5}	6.0×10^{1}	2.0×10^{-3}
990123	14.4	5.3×10^{-4}	5.1×10^{4}	2.1×10^{-3}
990510	11.9	3.1×10^{-4}	3.2×10^{1}	1.2×10^{-2}
991208	8.8	1.0×10^{-2}	2.0×10^{-2}	1.0×10^{-1}
991216	8.5	1.7×10^{-4}	3.0×10^{-2}	7.0×10^{-2}
000301c	10.8	2.0×10^{-2}	7.0×10^{-3}	1.2×10^{-1}
000418	10.9	5.0×10^{-3}	7.9×10^{-1}	4.5×10^{-2}
000926	9.5	3.5×10^{-2}	1.5×10^{-1}	1.4×10^{-1}

[a]Reverse shock R-band magnitude at deceleration with parameters determined from afterglow modeling.

[b]Redshift not known for this burst, $z = 1$ used.

Newtonian nor relativistic where the usual asymptotic approximations are not very accurate, and one needs a more accurate calculation for this intermediate case (Nakar and Piran 2004, have made a similar point).

We see that for six of the ten bursts the optical flux is between 8.5 and 11-th magnitude, and the cooling frequency at deceleration is small (less than or of order the R-band frequency). With the cooling frequency either below or dropping below the optical rather quickly, and no electrons left in the RS capable of radiating in the optical band, we would not see the expected $\sim 1/t^2$ falloff, but a more rapid falloff of $\sim 1/t^3$ (Kumar and Panaitescu 2000). This falloff is fast, but even so, some of these bright optical transients could be seen for a few hundred seconds by rapid followup observations with a limiting magnitude of $R \sim 15$.

The remaining four have much fainter optical emission and large cooling frequency. The magnetic field parameter determined from afterglow modeling for these bursts is much lower than those with bright reverse shock emission. With the high cooling frequency (at least a factor of 10 above the observing band frequency of 2 eV), we expect this emission to exhibit t^{-2} falloff; however, this faint emission may be hidden by brighter forward shock afterglow emission.

For those bursts which are fit equally well in an $s = 2$ medium (970508, 000418, 991208, 000301c, 991216), the reverse shock flux at deceleration has been calculated using the afterglow parameters in Panaitescu and Kumar (2002). We find that the flux is typically a few times larger in the s=2 model than uniform ISM case discussed above.

According to table 2.2, the peak R magnitude for the reverse shock emission for 990123 is 14.4 (using the forward shock values for all parameters in the reverse shock) whereas the observed peak flux was $R = 8.9$ (Akerlof et al. 1999). This suggests, as has been pointed out by Zhang et al. (2003), that ε_B was larger in the RS by a factor of about 10^2 than in the FS. Since $\nu_c \propto \varepsilon_B^{-3/2}$, by making $\varepsilon_{Br} = 0.07$, the cooling frequency has been lowered from 51 keV to 100 eV. The R band is at about 2 eV, so the cooling frequency is still well above the optical at deceleration, allowing for the $\sim 1/t^2$ falloff that was observed.

Bursts with small optical flux at deceleration have small ε_B and/or ε_e' in the RS and their cooling frequency is generally high, allowing the optical emission falling off as $\sim 1/t^2$ to occur. If ε_B in the RS for these bursts were

larger than the FS, as found for 990123 (Zhang et al. 2003) & 021211 (Kumar and Panaitescu 2003), the flux will be boosted to levels comparable to that of the other brighter bursts.

Besides 990123 and 021211 there have been no observations of a bright and quickly fading early afterglow for any other bursts. There have been some early (time since onset of burst < 0.01 day or ~ 10 minutes) detections in the optical, for example 030329 and 021004, but the emission was not falling off as $\sim 1/t^2$. There have been about 18 bursts with upper limits published in the GCN Circulars (Barthelmy et al. 1995) and in the literature (e.g. Akerlof et al. 2000b; Kehoe et al. 2001), for emission between the GRB time and 0.01 day (9 of these bursts reported in the GCNs had later optical afterglow detections). Searching the GCN Circulars with the GRBlog website (Quimby et al. 2003), we find that the burst upper limits range from $R \sim 10$ for 030115 (Castro-Tirado et al. 2003) at early times to $R \sim 20$ for XRF 030723 (Smith et al. 2003) closer to 0.01 day. None of the bursts from the sample in this paper have upper limits available. However, if the bursts with available upper limits are representative of the total GRB population, then it is possible that the bursts in our sample would have had similar upper limits, i.e., roughly 14-15th magnitude at ~ 500s. So there is a disagreement between the theoretical expectation and the observational upper limit.

There are several possible resolutions for this apparent discrepancy. The small optical flux could be due to much smaller magnetic field in the RS compared with the FS; for 990123 and 021211, however, ε_B in the RS was

inferred to be larger than the FS, which perhaps might not be the common situation. Another possibility is that the deceleration time of GRB fireball is of order an hour instead of the burst duration of a few tens of seconds (assumed for the GRBs considered in this paper). Since the peak optical flux from RS is proportional to $\sim t_d^{-1}$ (see equations 2.25 & 2.26), the flux will be reduced by $\sim$3-5 magnitudes and therefore consistent with the observational upper limits of Kehoe et al. (2001). In this case the early light-curve should be rising, and subsequently turn over to a steep decay at the deceleration time. The most likely explanation for a typically faint optical flux in our view is related to the low cooling frequency in the RS. We see from the table 2.2 that cases with a bright optical flash have cooling frequency below the optical band at deceleration, in which case the light-curve should decline as $\sim t^{-3}$ and fade below the detection limit of 14-15 magnitude in a few hundred seconds.

The observational situation (whether bright reverse shock emission is typical or not) should become clearer when *Swift* is launched in September 2004.

2.4 Discussion

We have explored the possibility that prompt γ-ray emission for a selected sample of 10 long duration GRBs might arise in the external shocks. These bursts had good multi-wavelength afterglow data and temporal coverage which enabled Panaitescu and Kumar (2002) to determine their energy, jet opening angle, density of the surrounding medium, and microphysics pa-

rameters for the shock. We compared the observed peak flux and the peak frequency of the time averaged spectrum during the γ-ray burst with the theoretical extrapolation of the afterglow emission to the middle of the burst duration.

The motivation for considering external shocks for the generation of γ-ray emission for these 10 bursts is that most of these bursts are not highly variable, which is the primary reason for invoking internal shocks. Moreover, the efficiency for the production of γ-rays for these bursts is found to be very high – in excess of 50% – which is difficult to understand in the internal shock models. In the particular case of GRB 990123 the γ-ray pulse width was of the same order as the time when the prompt optical emission from the reverse shock peaked i.e. the deceleration time. This means that the radius where γ-rays were generated was roughly the same as the deceleration radius, thereby suggesting a forward shock origin for gamma-rays. Moreover, the low energy spectral slope α ($f_\nu \propto \nu^\alpha$) for 990123 was 0.4, an observation that is difficult to understand in the internal shock models which have generally very low cooling frequency and therefore have $\alpha = -0.5$.

We find that it is not possible that the forward shock synchrotron afterglow emission, extrapolated back to prompt GRB duration, can explain the flux and peak frequency of nine of these ten bursts; only in the case of 970508, which was a single pulse FRED burst, does the extrapolation of the afterglow match up with the γ-ray emission property. Moreover, it turns out that even when we take ε_{Bf} (the energy fraction in magnetic field) and ISM

density during the gamma-ray burst to be completely arbitrary, instead of the same as determined from afterglow modeling, we still cannot reconcile the gamma-ray observations with the theoretical calculations for seven of the ten bursts in our sample in the forward shock synchrotron emission model. The reason for this is that the forward shock is highly radiative at early times i.e., the cooling frequency during the gamma-ray burst is smaller than the synchrotron injection frequency, and therefore the flux at the peak of the νf_ν spectrum is independent of the density of the surrounding medium and ε_{Bf}, which happen to be the parameters with large uncertainty in afterglow modeling.

Two of the bursts in the sample, 980519 & 000418, can be understood as synchrotron emission in the forward shock provided that $\varepsilon_{Bf} \sim 1$ during the burst, a value that is larger by a factor$\sim 10^2$ than what we find during afterglow at $\sim$ 1day; it is unclear if this is a physically sensible solution.

We have also considered inverse-Compton scattering of synchrotron emission from reverse or forward shock off of material in the forward and reverse shock regions, and find that it is not possible to explain the γ-ray emission, except possibly for 980703, with a reasonable set of parameters. In particular, the only solutions we found are when the circum-burst medium is taken to have a wind like density profile with the density parameter about hundred times larger than the density of a typical Wolf-Rayet star wind and a few order of magnitude larger than the density determined from afterglow modeling.

Adding large density clumps to the external medium only increases the peak flux and frequency of νf_ν by a significant amount when the density of the clump and ejecta are similar when they collide to produce the γ-ray emission, in which case the early afterglow emission is extremely bright and hard to miss. Also, adding $e^{\pm}$ pairs to the ejecta decreases the inverse Compton flux, unless the electron distribution power law index is $\lesssim 2$, for any synchrotron-IC scattering scenario considered. Thus, neither of these two possibilities seem likely to explain the γ-ray emission properties of the bursts in our sample.

So, we are therefore forced to conclude that there must be another way to explain the GRB emission. The widely accepted internal shocks model might be the solution. However, considering the problem of efficiency, special cases of FREDs, and the problems for the internal shocks for 990123 discussed, we feel it is prudent to explore other possible mechanisms such as the conversion of Poynting flux to radiation.

As for the reverse shock emission, we find that at least 50% of these ten bursts have bright prompt optical flashes, 9-11th mag, provided that the shock parameters – the energy fraction in electrons and magnetic field – in the reverse shock are the same or larger than the value in the forward shock. However, five of these bursts have cooling frequencies below the optical band and therefore the RS flux will decline very steeply with time (roughly as t^{-3}) and could easily go undetected after a few deceleration times. Those bursts with dimmer early emission generally have high cooling frequencies, and are assumed to exhibit the expected $1/t^2$ fall off. Although they are dim, they

may still be detected.

If this sample of 10 bursts is representative of long duration GRBs then we expect very bright, rapidly fading ($\sim t^{-3}$), prompt optical flashes accompanying many γ-ray bursts. The RS emission is particularly bright just above the synchrotron self-absorption frequency of $\sim 10^{-1}$ eV where we expect the observed flux to be of order a Jansky, and declining rapidly with time since the cooling frequency is typically of the same order as the absorption frequency. It is also possible that the deceleration time is much longer than the GRB duration, which would reduce the predicted optical flux from the reverse shock. In this case we would expect to observe a dim, rising early optical afterglow light-curve, turning over to a steep descent (t^{-2} or t^{-3}) after the deceleration time.

These issues will be resolved in the *Swift* era when we will have excellent early time coverage in the optical band for a few hours for many bursts. Future measurements of the early afterglow should enable us to determine if bright optical emission from the reverse shock is common, and thus determine the nature of the explosion, i.e. whether the explosion is baryonic, leptonic, or Poynting-flux dominated.

Chapter 3

Using reverse shock emission to probe the electron-positron pair content of the ejecta from gamma-ray burst explosions

Since[1] the discovery of the bright optical flash from GRB 990123 (Akerlof et al. 1999), many authors have considered this early afterglow emission as being due to the reverse shock passing through baryonic ejecta from the explosion, as was predicted by Sari and Piran (1999). If this early emission is indeed caused by the reverse shock (hereafter RS) passing through the ejecta, then this emission provides direct information about the composition and magnetic field strength and orientation in the material ejected from the inner engine, giving us clues about the nature of the outflow and the inner engine itself. Early optical afterglow data from GRBs 990123 & 021211 have already been used to infer that the ejecta from these GRBs may have been fairly highly magnetized baryonic ejecta (Zhang et al. 2003; Fan et al. 2002; Kumar and Panaitescu 2003; McMahon et al. 2004).

Only the observations of GRBs 990123 & 021211 have exhibited this steeply falling off early optical emission, while other bursts observed in the

[1]Significant portions of this chapter have previously been published in McMahon et al. (2006).

optical so quickly following the burst have exhibited either rising emission (030418), shallower fall-off (021004), or no emission at all (Kehoe et al. 2001). There have also been some *Swift*-detected bursts recently that have not exhibited the steeply falling off emission expected from the RS (e.g. GRB 050319; Rykoff et al. 2005) or optical/IR emission varying on very short timescales, seemingly following the activity of the central engine (GRB 041219a; Blake et al. 2005; Vestrand et al. 2005).[2] There have also been some early optical upper limits from *Swift* of $V \sim 21$ magnitude within minutes after the burst (e.g. 050219a; Schady et al. 2005). This lack of observations of the optical flash begs the question: are GRBs 990123 and 021211 unique? What is the reason for the lack of optical flashes? These early upper limits on RS emission can provide information about the ejecta and help to answer these questions.

In the previous chapter (and also in McMahon et al. 2004, hereafter MKP04), we estimated the RS emission and break frequencies at deceleration for a baryonic outflow for 10 bursts with burst parameters determined from afterglow modeling (assuming deceleration time is on the order of the burst duration, as occurs in 990123). We determined that a possible reason for weak RS optical emission after deceleration for most bursts is due to a cooling frequency below the optical band at deceleration. Although the reverse shock emission is expected to be bright (R-mag $\sim$ 10) at deceleration, when the cooling frequency drops below the observing band, no more emission from the

[2]Note however, that the situation in GRB 041219a is not clear as the correlation reported in Vestrand et al. (2005) should have been enhanced with a further temporal division of the optical signal.

ejecta is observed, with the exception of off-axis emission which falls of very quickly, as $\sim 1/t^{(2+p/2)} \sim 1/t^3$ (Kumar and Panaitescu 2000). However, now that is is possible to quickly follow up GRBs with *Swift* UVOT, we are not seeing any bright optical flashes with this $1/t^3$ falloff. This suggests that the RS flux is suppressed for some reason.

In the calculation in MKP04, we assumed the ejecta was purely baryonic. This may not be the case. If many $e^{\pm}$ pairs are present in the ejecta (mixed with baryons), either ejected from the source or created by dissipation during the GRB, or if the magnetic field strength in the ejecta is very large (perhaps because the outflow was Poynting flux dominated), the RS emission could be suppressed significantly from the baryon dominated picture. Pair-enrichment of the ejecta causes reverse shock emission to be fainter than that expected from completely baryonic ejecta, and a very high ejecta magnetic field is likely to weaken the reverse shock as well; both scenarios provide alternate possibilities for suppression of reverse shock emission. It is useful then to determine the defining characteristics of reverse shock light curves and spectra for a baryonic, lepton-enriched, or highly magnetized ejecta, in order to distinguish between these possibilities when the *Swift* satellite and other robotic telescopes accumulate more multi-wavelength afterglow data at early times.

Pair enrichment of the ejecta has been looked at by Li et al. (2003b) and the case of highly magnetized ejecta has been investigated by Zhang and Kobayashi (2005). In this chapter, we take another look at pair-enrichment; we take into account that the reverse shock is mildly relativistic, and also

carry out a self consistent cooling and self absorption calculation, which is necessary, since the ejecta self absorption frequency can be on the order of or greater than the cooling frequency. Li et al. (2003b) predicted a bright IR flash with pair-enriched ejecta, as bright as that expected in the optical with strictly baryonic ejecta; we find that the optical/IR flux levels at deceleration have very little dependence on the number of pairs. Also, any change in spectral peak frequency or optical/IR flux at deceleration due to pair enrichment can also arise if the microphysics parameters in the ejecta are changed, thus creating a highly degenerate problem.

We first describe our model of reverse shock emission and the new physics we have added to the RS emission calculation (Section 3.1), then discuss our results (Section 3.2). In Section 3.3, we summarize the differences between baryonic and pair-enriched ejecta.

3.1 Description of the reverse shock model

Here, we briefly describe our RS model, then focus on the improvements we have made to the calculation of emission from the RS. For this calculation, we use the equations for the ejecta dynamics and RS emission described in Kumar and Panaitescu (2003) (KP03), Panaitescu and Kumar (2004) (PK04), and Nakar and Piran (2004) (NP04) and include synchrotron and inverse Compton cooling. We have added several new components to the calculation, namely (1) the effect of synchrotron & self inverse-Compton scattering on electron cooling & synchrotron self absorption frequencies, (2)

inverse Compton cooling of RS electrons by synchrotron flux of the forward shock (hereafter FS), (3) absorption of RS photons (particularly in the radio band) in the FS region as they traverse through the FS on their way to the observer, and (4) pair-enriched ejecta.

3.1.1 The Standard Model: dynamics & synchrotron emission in the RS

The ejecta dynamics are determined by assuming an initial Lorentz factor Γ_0, the burst duration in the observer frame t_{GRB}, number density of the external medium $n_0 = AR^{-s}$ where R is the radial distance from the center of the explosion, and isotropic equivalent energy $E_{52} = E/10^{52}$ergs. The Lorentz factor of the shocked ejecta with respect to the unshocked external medium is given by (PK04)

$$\Gamma = \Gamma_0 \left(1 + 2\Gamma_0 \left(n_0/n_{ej}\right)^{1/2}\right)^{-1/2} \tag{3.1}$$

where $n_{ej} = E/\left(4\pi m_p c^2 R^2 \Gamma_0^2 \Delta\right)$ is the comoving ejecta density and Δ is the lab frame ejecta width, taken to be $ct_{dur} + R/\left(2\Gamma_0^2\right)$, where t_{dur} is the host galaxy frame burst duration, $t_{GRB}/(1+z)$. When $\Delta \sim ct_{dur}$ at deceleration, we define this case to be the non spreading ejecta case (also called thick ejecta), whereas when $\Delta \sim R/\left(2\Gamma_0^2\right)$, we define this case to be the spreading ejecta case (also called thin ejecta).

When $\Gamma_0^2 n_0/n_{ej} \gg 1/4$ near shock crossing time (the time at which the RS reaches the rear of the ejecta shell), the RS is relativistic and the bulk Lorentz factor $\Gamma \propto R^{(s-2)/4}$ and the ejecta radius $R \propto t^{2/(4-s)}$ (t is time in

the observer frame), prior to deceleration time, for the case of non-spreading ejecta. In the case of spreading ejecta, $\Gamma_0^2 n_0/n_{ej} \sim 0.3$ for $s = 0$ and ~ 0.5 for $s = 2$ at shock crossing time, so the RS is mildly relativistic. The radial distance of the ejecta from the center of the explosion at the time when the RS reaches the back of the ejecta shell (the shock crossing radius) is given in Tables 3.1 and 3.2, as are the Lorentz factor and observer time at this radius. See Table 3.3 for the scalings of variables with observer time before deceleration, numerically determined for the mildly relativistic case.

The reverse shock speed with respect to the unshocked ejecta as measured in the lab frame is (KP03)

$$\beta_0 - \beta_{RS} = \frac{1.4}{\Gamma_0^2} \left(\frac{\Gamma_0^2 n_0}{n_{ej}} \right)^{1/2} \tag{3.2}$$

where β_{RS} is the reverse shock speed measured in the lab frame and β_0 is the outflow speed measured in the lab frame as well. The above equation is valid in all cases, from nonrelativistic to relativistic RS cases. It can be shown (PK04) that the radius at which the reverse shock has traversed the ejecta is within a factor of ~ 2 of the deceleration radius for both a wind and homogeneous external medium.

The rate at which the ejecta electrons are swept up by the RS is given by

$$\frac{dN_e}{dR} = \frac{1.4}{\Gamma_0} \left(\frac{n_0}{n_{ej}} \right)^{1/2} \frac{N_p}{\Delta} \tag{3.3}$$

where $N_p = E/\left(\Gamma_0 m_p c^2\right)$ is the total number of protons in the ejecta. For spreading ejecta, $N_e(R) \propto R^{3/2}$ for $s = 0$ and $R^{0.68}$ for $s = 2$ (determined

numerically) and for ejecta whose width is dominated by the GRB duration $N_e(R) \propto R^{(4-s)/2}$.

After deceleration (shock crossing time), the ejecta bulk Lorentz factor is assumed to evolve adiabatically following the Blandford-McKee solution, as described in PK04, as

$$\Gamma_{ej} \propto R^{-(3-s)/2} \left(R^{(2a-3)} \Delta'^{a} \right)^{-1.5(4-s)/(17-4s)}. \tag{3.4}$$

where a is the adiabatic index, set to 4/3 for relativistic ejecta and 5/3 for non-relativistic ejecta, and $\Delta' = \max(\Gamma_{ej} c t_{dur}, R/2\Gamma_{ej})$ is the comoving frame ejecta width. We take the ejecta expansion in the radial direction to be relativistic when the minimum electron thermal Lorentz factor in the ejecta $\gtrsim$10, and nonrelativistic when it is < 10.

Synchrotron radiation from the shocked electrons is calculated assuming a power law distribution of electron energy with index p, i.e. $dN_e/d\gamma \propto \gamma^{-p}$ for $\gamma > \gamma_{ir}$ (where γ_{ir} is the minimum electron thermal Lorentz factor averaged over all of the electrons as they cross the RS front), ε_{Br}, the fraction of energy in the magnetic field, and ε'_e, the minimum thermal energy given to the electrons; $\gamma_{ir} = \varepsilon'_e \langle e_p \rangle / m_e c^2$, where $e_p = m_p c^2 (\Gamma' - 1)$ is the minimum thermal energy per proton just behind the RS front, $\langle e_p \rangle \sim 0.5 e_p$, and

$$\Gamma' = \Gamma_0 \Gamma (1 - \beta_0 \beta) \simeq 0.5 \left(\frac{\Gamma}{\Gamma_0} + \frac{\Gamma_0}{\Gamma} \right) \tag{3.5}$$

is the relative Lorentz factor of the shocked and unshocked ejecta. Since $\Gamma' \lesssim 2$, we cannot approximate the evolution of γ_{ir} by assuming $\gamma_{ir} \propto \Gamma'$; we

numerically calculate the evolution for radii near the shock crossing radius, the results given in Table 3.3. The comoving magnetic field strength in the ejecta is given by $B' = \left[8\pi\varepsilon_{Br} n_{ej} \langle e_p \rangle (4\Gamma' + 3)\right]^{1/2}$.

We note that γ_{ir} can be less than 1, since $\gamma_{ir} m_e c^2$ is defined to be the minimum thermal energy for electrons. We take into account that some fraction of the electrons are nonrelativistic and emit cyclotron radiation. We remove these electrons from the electron column density used for our synchrotron calculation, i.e. $n_{col,r} = N_e(\gamma_{ir})^{p-1}/4\pi R^2$, and set the minimum thermal energy for electrons to be $m_e c^2$.

After deceleration, for adiabatically cooling electrons, $\gamma_{ir} \propto V'^{-(a_e-1)} \propto (R^2\Delta')^{-1/3}$, where V' is the comoving ejecta volume, and the ratio of specific heats is $a_e = 4/3$. The magnetic field is assumed to be predominantly transverse and frozen into the ejecta, decaying as $B' \propto (R\Delta')^{-1}$. When radiative cooling becomes less important than adiabatic cooling, the Lorentz factor of electrons cooling on a dynamical timescale, γ_{cr} (discussed in more detail below), evolves in the same manner as γ_{ir}.

The observer frame synchrotron injection frequency is calculated with

$$\nu_{ir} = \frac{0.98 q B' \gamma_{ir}^2 \Gamma}{2\pi m_e c (1+z)}, \tag{3.6}$$

where we use here and elsewhere the common notation of ν_x being the synchrotron frequency of an electron with a Lorentz factor γ_x. The synchrotron flux at the peak of the f_ν spectrum is given by

$$F_{pr} = \frac{N_e P_{\nu_p} \Gamma (1+z)}{4\pi d_L^2} \tag{3.7}$$

Table 3.1 Values of Parameters at Deceleration for $s = 0$

	$\Delta = ct_{dur}$	$\Delta = R_+/2\Gamma_0^2$
$R_+ =$	$\left[\frac{16t_{dur}}{5.6^2\pi m_p c}\frac{E}{A}\right]^{1/4}$	$\left[\frac{9}{7.9^2\pi m_p c^2}\frac{E}{A\Gamma_0^2}\right]^{1/3}$
$\Gamma_+ =$	$0.55\left(\frac{E}{n0m_pc^5\pi t_{dur}^3}\right)^{\frac{1}{8}}$	$0.69\Gamma_0$
$t_{obs,+} =$	$2.8t_{dur}$	$\left(\frac{1.1E}{n_0c^5m_p\pi\Gamma_0^8}\right)^{1/3}$
$\frac{\langle e_{p,+}\rangle}{m_pc^2} =$	$\Gamma_0\left(0.18n_0m_pc^5\pi t_{dur}^3E^{-1}\right)^{1/8}$	0.03
$\Gamma'_+ =$	$\left(0.91n_0m_pc^5\pi t_{dur}^3\Gamma_0E^{-1}\right)^{1/8}$	1.07
$B'_+ = \varepsilon_{Br,-1}^{1/2}\mathcal{L}_{ep}^{1/2}\times$	$21.5\left(n_0^3E_{52}t_{dur}^{-3}\right)^{1/8}$ G	$4.1n_0^{1/2}\Gamma_{0,2}$ G
$F_{p,+} = \frac{\varepsilon_{Br,-1}^{1/2}\mathcal{L}}{\mathcal{L}_{ep}^{1/2}(\sqrt{1+z}-1)^2}\times$	$791.0n_0^{1/4}E_{52}^{5/4}t_{dur}^{-3/4}\Gamma_{0,2}^{-1}$mJy	$26.1n_0^{1/2}E_{52}\Gamma_{0,2}$mJy
$\nu_{ir,+} = \frac{\varepsilon_{Br,-1}^{1/2}\varepsilon_{er,-1}'^2\mathcal{L}_{ep}^{5/2}}{\mathcal{L}^2(1+z)}\times$	$5.1\times10^{11}n_0^{1/2}\Gamma_{0,2}^2$Hz	$2.4\times10^{10}n_0^{1/2}\Gamma_{0,2}^2$Hz
$\nu_{cr,+} = \varepsilon_{Br,-1}^{3/2}(1+z)\mathcal{L}_{ep}^{3/2}\times$	$1.6\times10^{17}n_0^{-1}E_{52}^{-1/2}t_{dur}^{-1/2}$Hz	$2.2\times10^{16}\Gamma_{0,2}^{4/3}A^{-5/6}E_{52}^{-2/3}$Hz
$f_{\nu,R} = \varepsilon_{er,-1}'^{1.5}\varepsilon_{Br,-1}^{0.88}\mathcal{L}_{ep}^{1.38}\mathcal{L}^{-0.5}\times$	$12.9n_0^{0.63}E_{52}^{1.3}\Gamma_{0,2}^{0.5}t_{dur}^{-3/4}$	$0.043n_0^{0.88}\Gamma_{0,2}^{2.5}E_{52}$

$A_* = A/10^{35}$, $E_{52} = E/10^{52}$, $\Gamma_{0,2} = \Gamma_0/100$, $\varepsilon'_{er,-1} = \varepsilon'_{er}/0.1$ and $\varepsilon_{Br,-1} = \varepsilon_{Br}/0.1$. $f_{\nu,R}$ is the flux at deceleration in mJy in the R-band for $p = 2.5$ and $z = 1$, for which $(\nu_{ir}, \nu_{ar}) < \nu_R < \nu_{cr}$ is assumed. For full expression used in Figure 5, see Equation 3.19.

where $N_e \equiv N_e(R)$ is the number of electrons heated by the RS determined from Equation 3.3, $P_{\nu_p} = 1.04q^3B/m_ec^2$ is the comoving power radiated per electron per unit frequency at the peak of f_ν, and $d_L = 2c\sqrt{1+z}[(1+z)^{1/2} - 1]/H_0$ is the luminosity distance. We use $H_0 = 65$ km s^{-1} Mpc^{-1} and for simplicity $\Omega = 1$, $\Lambda = 0$. The factors of 0.98 in Equation 3.6 and 1.04 above for P_{ν_p} are from Wijers and Galama (1999) for the case of $p = 2$.

3.1.2 Inverse Compton cooling & synchrotron self absorption

We include the inverse Compton process to calculate electron cooling. The Compton Y parameter is obtained by solving the equation describing

Table 3.2 Values of Parameters at Deceleration for $s = 2$

	$\Delta = ct_{dur}$	$\Delta = R_+/2\Gamma_0^2$
$R_+ =$	$\left[\frac{4t_{dur}}{5.6^2\pi m_p c}\frac{E}{A}\right]^{1/2}$	$\left[\frac{1}{7.9^2\pi m_p c^2}\frac{E}{A\Gamma_0^2}\right]$
$\Gamma_+ =$	$0.51\left(\frac{E}{Am_pc^3\pi t_{dur}}\right)^{\frac{1}{4}}$	$0.83\Gamma_0$
$t_{obs,+} =$	$1.4t_{dur}$	$\frac{0.02E}{Am_pc^3\pi\Gamma_0^4}$
$\frac{\langle e_{p,+}\rangle}{m_pc^2} =$	$\Gamma_0\left(0.79Am_pc^3t_{dur}\pi E^{-1}\right)^{1/4}$	
$\Gamma'_+ =$	$\left(0.99Am_pc^3\pi t_{dur}\Gamma_0 E^{-1}\right)^{1/4}$	1.02
$B'_+ = \varepsilon_{Br,-1}^{1/2}\mathcal{L}_{ep}^{1/2}\times$	$2.2\times10^4\left(A_*^3E_{52}^{-1}t_{dur}^{-3}\right)^{1/4}$ G	$3.3\times10^5A_*^{3/2}\Gamma_{0,2}^3E_{52}^{-1}$ G
$F_{p,+} = \frac{\varepsilon_{Br,-1}^{1/2}\mathcal{L}}{\mathcal{L}_{ep}^{1/2}(\sqrt{1+z}-1)^2}\times$	$1.3\times10^5A_*^{1/2}E_{52}t_{dur}^{-1}\Gamma_{0,2}^{-1}$mJy	$2.6\times10^6A_*^{3/2}\Gamma_{0,2}^3$mJy
$\nu_{ir,+} = \frac{\varepsilon_{Br,-1}^{1/2}\varepsilon_{er,-1}'^2\mathcal{L}_{ep}^{5/2}}{\mathcal{L}^2(1+z)}\times$	$5.4\times10^{16}A_*\Gamma_{0,2}^2t_{dur}^{-1/2}E_{52}^{-1/2}$Hz	$2.6\times10^{14}A_*^{3/2}\Gamma_{0,2}^4E_{52}^{-1}$Hz
$\nu_{cr,+} = \varepsilon_{Br,-1}^{3/2}(1+z)\mathcal{L}_{ep}^{3/2}\times$	$3.6\times10^9E_{52}^{1/2}t_{dur}^{1/2}A_*^{-2}$Hz	$5.3\times10^8E_{52}A_*^{-5/2}\Gamma_{0,2}^{-2}$Hz
$f_{\nu,R} = \varepsilon_{er,-1}'^{1.5}\varepsilon_{Br,-1}^{0.88}\mathcal{L}_{ep}^{1.38}\mathcal{L}^{-0.5}\times$	$1.2\times10^7A_*^{1.3}\Gamma_{0,2}^{0.5}E_{52}^{0.63}t_{dur}^{-1.4}$	$4.6\times10^6A_*^{2.6}\Gamma_{0,2}^6E_{52}^{-0.75}$

See notes in Table 3.1.

Table 3.3 Scalings Before Deceleration

	$\Delta = ct_{dur}$ $s = 0$	$\Delta = ct_{dur}$ $s = 2$	$\Delta = R_+/2\Gamma_0^2$ $s = 0$	$\Delta = R_+/2\Gamma_0^2$ $s = 2$
R	$t^{1/2}$	t	$t^{0.67}$	$t^{0.88}$
Γ	$t^{-1/4}$	t^0	$t^{-0.17}$	$t^{-0.066}$
γ_{ir}	$t^{0.45}$	t^0	$t^{1.7}$	$t^{0.62}$
$f_{\nu,X}$	$t^{-0.18+0.19p}$	$t^{1-0.5p}$	$t^{1.5(p-1)}$	$t^{0.012+0.082p}$
$f_{\nu,R}$	$t^{0.29+0.19p}$	$t^{-0.5(p-1)}$	$t^{-0.86+1.5p}$	$t^{-0.56+0.082p}$

Values of exponents in this table are determined numerically for mildly relativistic spreading ejecta and determined analytically for relativistic non spreading ejecta, near, but prior to, deceleration time. t is time measured in the observer frame. For the non-relativistic case of $\Gamma_0^2 n_0/n_{ej} \ll 1/4$, $\Gamma \propto R^0$ and $R \propto t$. $f_{\nu,X}$ is the synchrotron flux for $\nu_{obs} > (\nu_{ir}, \nu_{cr}, \nu_{ar})$, and $f_{\nu,R}$ is the synchrotron flux for $(\nu_{ir}, \nu_{ar}) < \nu_{obs} < \nu_{cr}$. Scalings after deceleration can be found in e.g. PK04. Note: it is possible for $f_{\nu,X}$ to be decaying before deceleration because it peaks well before deceleration.

radiative loss of energy for a single electron with a Lorentz factor γ_e

$$\frac{d\left(\gamma_e m_e c^2\right)}{dt'} = -\frac{\sigma_T c B'^2 \gamma_e^2 \beta_e^2}{6\pi} \times \left[\frac{f'_{\nu'>\nu'_a}}{f'_{total}} + \frac{\tau_{es}\gamma_p^2\beta_p^2}{\nu'_p \sigma_T}\int d\nu' \frac{f\left(\nu'\right)\sigma_{KN}}{\left(1+\tau_{sa}\left(\nu'\right)\right)}\right] \quad (3.8)$$

where primes denote variables measured in the rest frame of the shocked fluid. The bracketed terms on the RHS are effectively $(1+Y)$; the first part, the fraction of energy emitted from one electron with Lorentz factor γ_c that is not absorbed by material in emitting region, is given by[3]

$$\frac{f'_{\nu'>\nu'_a}}{f'_{total}} = \begin{cases} \frac{\frac{3}{4}e^{-1}\left(1-x^{\frac{4}{3}}\right)+0.08\sqrt{\pi}+e^{-1}}{\frac{3}{4}e^{-1}\left(1-x^{\frac{4}{3}}\right)+0.08\sqrt{\pi}+e^{-1}\left(1+\frac{1}{3}x^{\frac{4}{3}}\right)} & \text{for } \nu'_c > \nu'_a \\ \frac{\frac{1}{2}\sqrt{\pi}\left[1-\mathrm{Erf}\left(\sqrt{x}\right)\right]-e^{-x}\sqrt{x}}{\frac{1}{4}\sqrt{\pi}\left[1-\mathrm{Erf}\left(\sqrt{x}\right)\right]-\frac{1}{2}e^{-x}\sqrt{x}\left(1-\frac{2}{3}x\right)} & \text{for } \nu'_c < \nu'_a \end{cases} . \quad (3.9)$$

where $x = \nu'_a/\nu'_c$ and Erf is the error function. This equation is necessary for calculating electron cooling, since ν'_c can be less than the self absorption frequency, ν'_a, in the RS.

The second part of the bracketed term in Equation 3.8 is equivalent to Y; τ_{es} is the Thomson optical depth to electron scattering, $\gamma_p = \min(\gamma_i, \gamma_c)$ and β_p is the corresponding velocity in units of c, $\nu'_p = \min(\nu'_i, \nu'_c)$, σ_{KN} is an approximation of the Klein-Nishina correction to the electron scattering cross section, $\tau_{sa}\left(\nu'\right)$ is the optical depth to synchrotron self absorption, and $f\left(\nu'\right)$ is the normalized set of broken power-laws describing the synchrotron spectrum (ie $f\left(\nu'_p\right) = 1$).

Both of the bracketed terms of the effective $(1+Y)$ (Equation 3.8) are dependent on ν'_c and ν'_a, and in turn, ν'_c is also dependent on $(1+Y)$, so

[3]This equation was incorrect in the originally published version of this chapter (McMahon et al. 2006); the equation shown here is now in the proper form.

the equations for the three variables must be solved simultaneously; this has been done for all numerical results in this chapter. It is, however, possible to semi-analytically estimate ν'_c when we assume that $Y \ll 1$ and IC does not contribute to the cooling calculation (see Table 3.1).

The comoving frame synchrotron self absorption frequency is calculated by equating the comoving synchrotron flux at ν'_a to flux from a black body in the Rayleigh-Jeans part of the spectrum, or

$$2kT\frac{\nu'^{\,2}_a}{c^2} = f'_\nu\left(\nu'_a\right) \tag{3.10}$$

where $kT = \max\left[\gamma_a, \min(\gamma_i, \gamma_c)\right] m_e c^2$. A frequent arrangement of the RS break frequencies at deceleration is $\nu'_i < \nu'_a < \nu'_c$; in this case,

$$\nu'_a = \left[\frac{f'_p}{2m_e}\nu_i'^{\frac{(p-1)}{2}}\left(\frac{qB'}{2\pi m_e c}\right)^{1/2}\right]^{\frac{2}{(4+p)}} \tag{3.11}$$

where $f'_p = N_e\sqrt{3}q^3B'/\left(4\pi R^2 m_e c^2\right)$ is the comoving flux at the peak of f'_ν.

The scalings of RS optical and X-ray flux with observer time just before deceleration for the four cases of $s = 0, 2$ and $\Delta = (ct_{dur}, R/2\Gamma_0^2)$ are shown in Table 3.3. Only synchrotron emission is included for these scalings (inverse Compton is also important in the X-ray), and $Y \ll 1$ is assumed (the scaling for $f_{\nu,R}$ is not affected, but $f_{\nu,X}$ may be).

After deceleration, if ejecta is in the radiative regime, we continue to calculate the RS cooling and synchrotron self absorption frequencies ν_{cr} and ν_{ar} and the effective $(1 + Y)$ by solving Equations 3.8 & 3.10 simultaneously, as done before deceleration. If adiabatic cooling is more efficient, γ_{cr} decays as

γ_{ir} (§ 3.1.1) and the self absorption frequency is solved for using Equation 3.10. After ν_{cr} falls below the observing band, the ejecta emission turns off, and the observed flux is due to off axis emission that decays approximately as $t^{-(4+p)/2}$ (Kumar and Panaitescu 2000).

3.1.3 Inverse Compton cooling by an external source

We have also allowed for external sources of flux to influence the cooling of electrons in the ejecta. In particular, we include synchrotron flux from the FS incident on the ejecta in our calculation of ν_{cr}. The external synchrotron flux in the shocked ejecta comoving frame is given by

$$f_{ex} = \frac{\tau_{es,ex} c {B'_{ex}}^2 \gamma_{e,ex}^2}{6\pi} \tag{3.12}$$

where the subscript "ex" denotes values from a source external to the cooling calculation being done (here, FS flux is the external flux incident on the RS ejecta), $\gamma_{e,ex}^2$ is the average electron thermal electron Lorentz factor squared in the forward shock. The equation for γ_c which includes the contribution of f_{ex} to the electron cooling is:

$$\gamma_c = \frac{1}{\chi_1 (1+Y) + \frac{\chi_2 f_{ex}}{\sigma_{KN,ex}}} \tag{3.13}$$

where

$$\chi_1 = \sigma_T B'^2 t' / \left(6\pi m_e c^2\right), \quad \chi_2 = \sigma_T t' / \left(m_e c^2\right),$$
$$\text{and} \quad \sigma_{KN,ex} = \left[h\nu_{p,ex}\gamma_c / \left(m_e c^2\right)\right]^{1+\alpha_{ex}}$$

is an approximation to the Klein-Nishina correction on the external flux, and $\nu_{p,ex}$ is the peak of the νf_ν spectrum in the FS; $\alpha_{ex} = -0.5$ if $\nu_{i,ex} > \nu_{c,ex}$,

and $(1-p)/2$ if $\nu_{i,ex} > \nu_{c,ex}$. We also allow for FS synchrotron self-Compton flux to influence RS cooling; however the high energy ($\gg m_e c^2$) of the FS synchrotron flux suppresses self-inverse Compton scattering, thus not significantly contributing to the RS cooling calculation. We do not consider the effect of RS emission on FS cooling; at most it is an order unity effect.

3.1.4 Absorption of RS photons in the FS material

We include the effect of absorption of RS photons in the FS material. For a selected observing band, ν_{obs}, the optical depth to absorption is

$$\tau_{abs,FS} = \begin{cases} \left(\frac{\nu_{obs}}{\nu_{af}}\right)^{\frac{5}{3}} & \nu_{obs} < \min(\nu_{cf}, \nu_{if}) \\ \left(\frac{\nu_{obs}}{\nu_{af}}\right)^{-\frac{p+4}{2}} & \nu_{obs} > \min(\nu_{cf}, \nu_{if}) \end{cases} \tag{3.14}$$

where ν_{af} is the observer frame FS synchrotron self absorption frequency. Before deceleration, the shocked ejecta and FS medium are moving together; however, after deceleration, these regions are moving at different Lorentz factors, and one must take care to use the appropriate value of ν_{af} when the RS photons are passing through the FS.

After calculating the RS emission as described above, the absorption in the FS is taken into account by reducing the RS flux by a factor of $\exp(-\tau_{abs,FS})$. This exponential cut off in flux can significantly reduce the RS emission, especially for observations at longer wavelengths, such as the radio.

3.1.5 Lepton-enriched ejecta

We include $e^{\pm}$ pairs in the calculation by simply adding a certain number of pairs per ejecta proton, $N_{\pm}$, to the calculation described above. We do not calculate the creation of these pairs; we make the assumption that a certain number of pairs per proton are present in the ejecta already, either being intrinsic from the source or being created by dissipative processes during the GRB, prior to the afterglow stage.

We change the radiation calculation described above by multiplying the column density of electrons by the number of ejecta pairs, $\mathcal{L} \equiv 1 + 2N_{\pm}$ (the 1 is for the electrons already accompanying the protons in the baryonic ejecta) and by dividing the minimum electron energy by the number of pairs (i.e.the new minimum thermal Lorentz factor is $\gamma_{ir}/\mathcal{L}$). The dynamics calculation is only altered when $N_{\pm} \gtrsim m_p/m_e$. To account for the presence of a high number of pairs, we alter the dynamics calculation by reducing the number of protons in the ejecta for a fixed burst energy by $\mathcal{L}_{ep} \equiv 1 + 2N_{\pm}m_e/m_p$ (see Table 3.1).

The RS minimum electron thermal Lorentz factor averaged over the entire lepton population at shock crossing is

$$\gamma_{ir,+} = \frac{\varepsilon'_{er} \langle e_{p,+} \rangle \mathcal{L}_{ep}}{m_e c^2 \mathcal{L}}. \tag{3.15}$$

Since the RS is only mildly relativistic in the spreading ejecta width case, the addition of pairs to the ejecta quickly drops γ_{ir} into the Newtonian regime. The already low injection frequency in the reverse shock can be reduced dramatically by even modest $\mathcal{L}$ (see Table 3.1). The injection frequency of course

cannot drop below the cyclotron frequency; we keep track of this in our numerical calculation.

The cooling frequency has very weak dependence on $N_{\pm}$ (there is dependence on $N_{\pm}$ through $\mathcal{L}_{ep}$, but this only makes a difference if $N_{\pm} \gtrsim 1000$). If $Y \gg 1$ and $\nu_{ir} < \nu_{cr}$, $\nu_{cr} \propto \mathcal{L}^{2(p_r-2)/(4-p_r)}$ (for $N_{\pm} \ll m_p/m_e$). The dependence of ν_{ar} on the pair content when $\nu_{ir} < \nu_{ar} < \nu_{cr}$ is $\nu_{ar} \propto \mathcal{L}^{(4-2p_r)/(4+p_r)}$ for $N_{\pm} \ll m_p/m_e$; ν_{ar} is also fairly insensitive to pair content.

3.2 Results

In this section, we describe the effects of IC cooling by flux generated in the RS and FS, absorption in the FS, and the effect of lepton-enriched ejecta on the RS emission, then determine if there are observable signatures of pair enriched ejecta. To ascertain the effect of each of these new additions to our calculation over the entire parameter space and a wide range of RS strengths for $s = 0, 2$, we randomly vary each parameter in the ranges: $50 \leq \Gamma_0 \leq 1000$, $1s \leq t_{GRB} \leq 100s$, $0.1 \leq E_{52} \leq 1000$, 10^{-3} cm$^{-3} \leq n_0 \leq 100$ cm^{-3} ($10^{-2} \leq A_* \leq 10$ for $s = 2$), $10^{-5} \leq \varepsilon_{Br} \leq 0.1$, $0.01 \leq \varepsilon_{ir} \leq 0.1$, $2.01 \leq p_r \leq 2.91$, and $1 \leq N_{\pm} \leq 1000$ for 1000 test cases (synthetic GRB afterglows). All of the parameters are assumed to have uniform distributions in log space with the exception of p_r, which is assumed to have a uniform distribution. The microphysics parameter ranges were chosen to be consistent with values found from late time afterglow modeling.

3.2.1 Inverse Compton & external cooling

In the left panel of Figure 3.1, the ratio of our numerical value of $\nu_{cr,+}$ to the analytical value given in Table 3.1 for 1000 test cases is plotted against ξ, the dimensionless RS strength parameter, at deceleration, for $s = 0$.[4] Each RS parameter is randomly varied in the ranges described above, except for $N_{\pm}$, which is set to 0. For each of the 1000 cases, the spreading condition is evaluated at deceleration, and the numerically calculated $\nu_{cr,+}$ is compared to the analytical value in the proper ejecta evolution case.

The numerically calculated value of $\nu_{cr,+}$, which includes the self consistent inverse Compton and synchrotron self absorption calculation as described in §3.1.2, is in general about a factor of 10 lower than the analytic value (not including IC losses) that is typically used over a wide range of RS strengths. For those cases where the numerical value is even smaller, the Compton Y parameter is rather large (these cases are more abundant for the non spreading case, with relativistic RS). For $s = 2$ (not shown in the figure), the analytical value of $\nu_{cr,+}$ can also be less than the numerical value of $\nu_{cr,+}$. This is because our cooling calculation has taken into account the fraction of the synchrotron flux that has been synchrotron self-absorbed, reducing the rate of energy loss for electrons; synchrotron self-absorption contributes more to the RS cooling

[4] $\xi = (l/\Delta)^{1/2}\Gamma_0^{-4/3}$, where $l = (3E/(4\pi n_0 m_p c^2))^{1/3}$; $\xi \ll 1$ is relativistic RS and $\xi \lesssim 1$ is the generic, mildly relativistic RS case. For $\xi \sim 2$, the ejecta is in the spreading regime with a mildly to non-relativistic RS (these points are bunched very closely together in the figures, since ξ is virtually constant over the dynamics parameter space for all spreading cases), whereas the non spreading ejecta case ranges from $\xi \ll 1$ to $\xi \lesssim 2$.

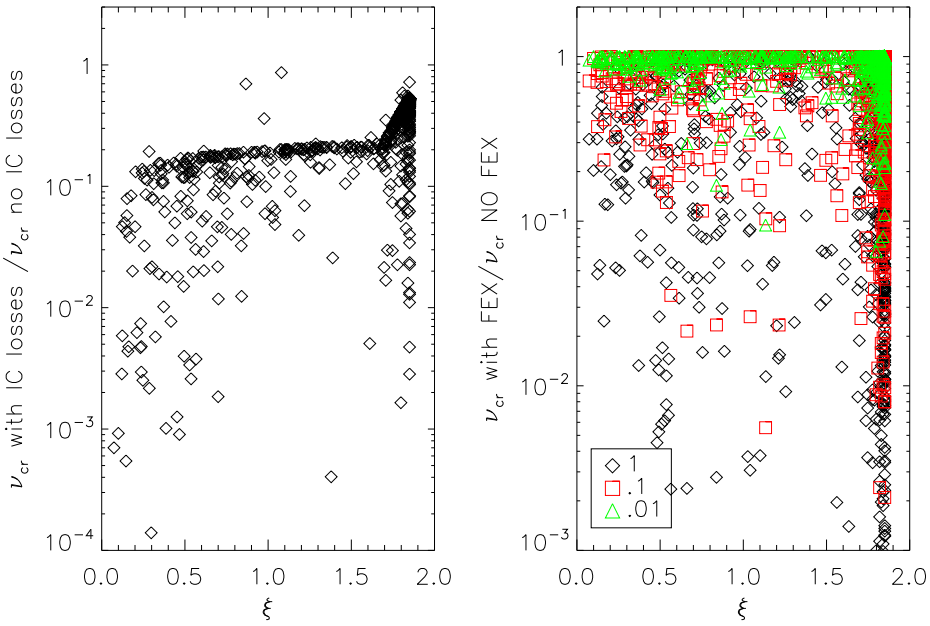

Figure 3.1 Left panel: Ratio at deceleration of numerically calculated ν_{cr} (with IC cooling) to analytic estimate given in Table 3.1 (not including IC cooling) for 1000 test cases in $s = 0$. The inclusion of IC cooling reduces ν_{cr} by a factor of roughly 10 over a wide range of RS strengths (ξ). Right panel: Ratio at deceleration of numerically calculated cooling frequency without external cooling included to numerical value with external cooling included, also for the $s = 0$ case. The legend gives the value of ε_{Bf} in comparison to the value of ε_{Br}, e.g. for the red squares, $\varepsilon_{Bf} = 0.1\varepsilon_{Br}$.

calculation in $s = 2$ than $s = 0$.

External flux influences the RS cooling calculation by decreasing ν_{cr}. If the FS radiation was produced with $\varepsilon_{Bf} \sim \varepsilon_{Br}$, the external flux can lower ν_{cr} via IC scattering by up to a few orders of magnitude for both $s = 0, 2$ cases. The effect of external flux IC cooling on the RS synchrotron flux near

deceleration in most cases is relatively small; the effect is greatest in the x-ray band, where $\nu_{obs} > (\nu_{ar}, \nu_{ir}, \nu_{cr})$, and flux here can be decreased by a factor of a few (IC flux is also an important contributing factor to the total light curve in the x-ray, and is not considered here). The more important effect of the external flux is to decrease the cooling frequency below the R band on a shorter time scale after deceleration, causing the light curve to fall off very steeply, as $\sim 1/t^3$, soon after deceleration. Overall, the effect of external flux on electron cooling makes RS synchrotron emission a little fainter at the peak of the light curve and fall off faster after deceleration, making the RS synchrotron emission more difficult to detect.

In the right panel of Figure 3.1, we show the effect of adding external cooling to our calculation. We plot the ratio of the numerically calculated $\nu_{cr,+}$ without external cooling to $\nu_{cr,+}$ including external cooling from the FS. We let $p_f = p_r$, $\varepsilon_{if} = \varepsilon_{ir}$, and try three cases of $\varepsilon_{Bf} = (1, 0.1, 0.01)\varepsilon_{Br}$. With external cooling included, ν_{cr} in either the spreading or non spreading case can be reduced by up to 3-4 orders of magnitude! This is true over a wide range of RS strengths, and also for $s = 2$. The effect is strongest when $\varepsilon_{Bf} = \varepsilon_{Br}$ and weakest when $\varepsilon_{Bf} = 0.01\varepsilon_{Br}$.

3.2.2 Effect of absorption in FS

Absorption of RS synchrotron photons in the FS is most important in the radio, as the FS self absorption frequency lies in this band. In a large part of the parameter space, the low frequency ($\sim$4 GHz) RS flux can be completely

absorbed; in a another run of 1000 different RS cases (varying the parameters as described above, and setting FS ε_{if}, ε_{Bf}, and p_f equal to RS values), we find that in approximately 15% of 1000 test cases, the RS radio (8.5 GHz) flux is completely absorbed by the FS material. In approximately 40% of the test cases, $\tau_{abs,FS} > 1$ (including those cases where the RS radio flux is completely absorbed), meaning that the RS radio flux was decreased by at least a factor of 3. If we set $\varepsilon_{Bf} = \varepsilon_{Br}/100$, we find that 12% of 1000 test cases are completely absorbed in the FS, and in 23% of the cases, $\tau_{abs,FS} > 1$. Absorption in the FS may turn out to be a contributing factor to the difficulty in observing RS flux in the radio.

3.2.3 RS emission with pair-enriched ejecta

Adding a certain number of pairs per proton to the ejecta adds another parameter to the RS flux calculation, bringing the total number of parameters in the RS to four, viz. ε_{ir}, ε_{Br}, p_r, and $N_{\pm}$.[5] We need four independent measurements of the RS emission to constrain these four parameters. Flux in the optical & X-ray at early times, spectral index and radio flux at ~ 0.1 day are four quantities that can be observed with the current generation of instruments.

For $\nu_{obs} > (\nu_{ir}, \nu_{cr}, \nu_{ar})$ (x-ray) with $Y \ll 1$ or $\nu_{ir} < \nu_{ar} < \nu_{obs} < \nu_{cr}$ (optical) for any Y, the observed flux at deceleration has a dependence on $N_{\pm}$

[5]FS microphysics parameters and the energy in the explosion, external density, and initial jet opening angle can be determined, as has been done in the past, by late-time FS light curve fitting when the RS makes a small contribution to the total flux.

of

$$f_\nu \propto \frac{\mathcal{L}^{(2-p_r)}}{\mathcal{L}_{ep}^{5(2-p_r)/4}}. \tag{3.16}$$

For $p_r \sim 2$, this flux depends very weakly on the number of pairs in the ejecta. For $p_r > 2$, the x-ray and optical flux are decreased from the $N_\pm = 0$ case as $N_\pm$ is increased (for $N_\pm \ll m_p/m_e$), but the shape of the light curve does not change (i.e. no breaks are introduced by reducing the injection frequency below the low value at which it already sits in the absence pairs in the ejecta).

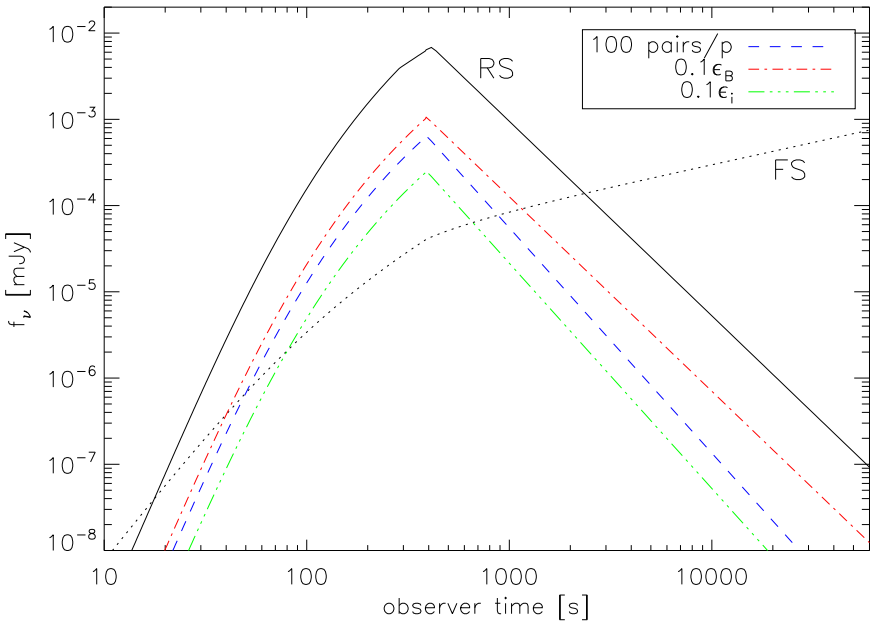

Figure 3.2 Radio (8.5 GHz) light curve for $s = 0$ with the input parameters $E_{52} = 3$, $\Gamma_0 = 160$, $t_{GRB} = 4$ s, $n_0 = 1.6 \times 10^{-3}$ cm^{-3}, $\varepsilon_{Br} = \varepsilon_{Bf} = 4 \times 10^{-5}$, $\varepsilon_{ir} = \varepsilon_{if} = 0.09$, $p_r = p_f = 2.5$, $N_\pm = 0$, and $z = 1$. External cooling and absorption in the FS are not included in this calculation. The solid line represents the RS light curve with the above parameters and the FS emission is shown by the dotted line. The three colored lines alter the parameters in the calculation as detailed in the legend.

In the radio, the observer flux for $\nu_{obs} < \nu_{ir} < \nu_{ar} < \nu_{cr}$ is proportional to $\mathcal{L}^{-1}\mathcal{L}_{ep}$. The flux in the radio is the most greatly affected by the addition of pairs to the calculation, so the best possible place to look for a signature of pair-enriched ejecta is in the radio wavelengths. In Figure 3.2, we plot an example of RS and FS radio light curves (8.5 GHz) without pairs (for burst parameters see figure caption) compared to three cases: (1) adding 100 pairs/p to the ejecta, (2) decreasing ε_{Br} by a factor of 10, and (3) decreasing ε_{ir} by a factor of 10. All three of these actions produce very similar RS radio light curves; the situation is highly degenerate, and it would be difficult to distinguish the effect of pairs in the ejecta on the emission from a variation in the microphysics parameters in the RS.

1000 RS test cases (parameters varied over ranges described above with no external cooling or absorption in the FS) show that the peak frequency of f_ν, at $\max\{\nu_{ar}, \min(\nu_{ir}, \nu_{cr})\}$, at deceleration also has very little, if any, dependence on the number of pairs in the ejecta for $s = 0, 2$. This is also true if external cooling is included in the calculation. This is in contradiction to the conclusion that Li et al. (2003b) came to; this is because, over a large portion of the parameter space, the peak of the spectrum in both the baryonic and pair-enriched cases is at ν_{ar}, and ν_{ar} has little dependence on the number of pairs in the ejecta.

Thus, we conclude there is no single wavelength light curve signature that depends only on the pair content of the ejecta, and not on the microphysics parameters in the RS as well.

3.2.4 Using optical and radio observations to determine pair content

The best way to discriminate between baryonic and pair-enriched ejecta is by comparing flux at low frequencies (radio band) and the optical band. NP04 suggested a particular combination of the ratio of observed RS optical and radio fluxes at the peak of each respective light curve and the ratio of the observer times at which these peaks occur as a way of determining if the radiation is from the reverse shock. We use a similar combination to decide whether the ejecta is pair enriched.

The parameter we use to determine the pair-enrichment (χ) is slightly different than that in NP04 (note the difference in exponents on the ratio of observer times),

$$\chi \equiv \left(\frac{F_*}{F_0}\right)\left(\frac{t_*}{t_0}\right)^k = \left(\frac{\nu_{\rm optical}}{\nu_{\rm radio}}\right)^{\frac{(p_r-1)}{2}} \sim 1000 \tag{3.17}$$

where

$$k \equiv \begin{cases} \frac{5(p_r-1)}{6} + \frac{9}{8} & s = 0 \\ (p_r - 1) + \frac{5}{6} & s = 2 \end{cases} \tag{3.18}$$

and are determined analytically using decay indices after deceleration of $\nu_{ir} \propto t^{-5/3}$ and $F_{pr} \propto t^{-9/8}$ for $s = 0$ and $\nu_{ir} \propto t^{-2}$ and $F_{pr} \propto t^{-5/4}$ for $s = 2$ (assuming spreading ejecta evolution for both cases). As in NP04, t_0 is the observer time peak of the optical RS emission, t_* is the observer time peak of the radio RS emission (the peak is produced when ν_{ar} falls below the radio), and F_0 & F_* are the observed fluxes at these two points. The shell width at

deceleration in both shell evolution cases is $\sim R_+/\Gamma_+^2$ which is $\ll R$,[6] so time delay between photons arising from the front and back ends of the shell has small effect on the observed flux.

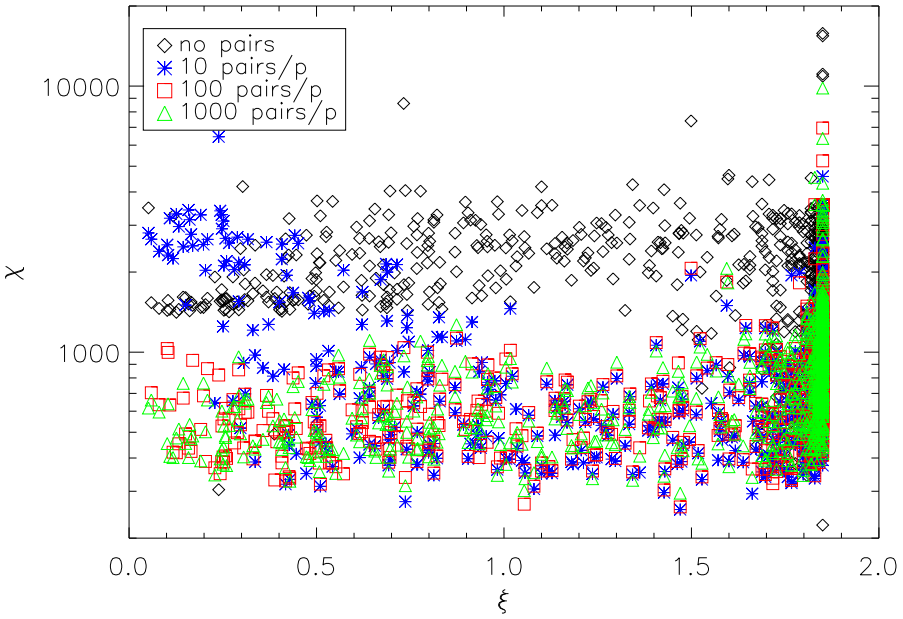

Figure 3.3 χ for $p_r = 2.5$ and $s = 0$ for 1000 test RS numerical light curves, excluding absorption of RS photons in the FS and external cooling. We randomly vary all RS parameters but p_r and $N_\pm$; other values of p_r give qualitatively similar results when adding leptons to baryonic ejecta, however χ for the reference purely baryonic case is higher for higher p_r and vice versa. $s = 2$ has qualitatively similar results which are discussed in §3.2.4. The scatter in each case is caused for the most part by the variation in dynamics parameters. There are some points with very low χ cut off of the bottom of the plot; these are caused when $\nu_{ar} > \nu_{cr}$, and ν_{ar} tracks ν_{cr} in time (which evolves more quickly, leading to smaller t_*).

[6]This is true in the non spreading case because of causality–the distance traveled by the shock front in the shell comoving frame is of order R_+/Γ_+, which is R_+/Γ_+^2 in the lab frame

We plot χ in Figure 3.3 versus the dimensionless RS strength parameter, ξ, in a run of 1000 RS cases as described in § 3.2, except that p_r is held fixed at 2.5 and $N_\pm$ is held constant for each case. External cooling and absorption in the FS were turned off. For $N_\pm = 0$, the value for χ can be larger or smaller by a factor of a few from 1000 for a constant value of $p_r \sim 2.5$, and is fairly constant over a large range of reverse shock strengths. There are a few points which are cut off the bottom of the plot with abnormally low χ–these points are caused by ν_{cr} falling below ν_{ar}. When this happens, ν_{ar} tracks ν_{cr} (since there are no electrons radiating above ν_{cr} after the RS reaches the rear of the shell), which evolves more quickly than ν_{ar} does when $\nu_{ar} < \nu_{cr}$, making t_* and F_* smaller. This scenario is easily detected by checking the decay of the radio light curve after the peak; if the decay is steep, like $\sim 1/t^3$, the abnormally low value of χ is due to ν_{cr} falling below the radio band with ν_{ar}.

When pairs are added to the ejecta, we find that for $N_\pm \gtrsim 100$, the value of χ has dropped by a factor of about 5 for the parameter space with $\xi \lesssim 1.6$ (ultra-relativistic to mildly relativistic RS). For $N_\pm = 10$, the value for χ ranges from ~ 3000 when the RS is relativistic ($\xi \ll 1$) to ~ 200 when the RS is mildly to non relativistic, making it difficult to distinguish between baryonic and pair enriched ejecta. Compared with the range of χ for baryonic ejecta (greater or less than 2000 by a factor of about 2), the drop in χ by a factor of 5 for $N_\pm \gtrsim 100$ could possibly be used as a tool to distinguish the pair content of the ejecta. So, if observations are available for a burst at the peak of the R band and radio RS emission, and p_r is able to be determined from spectra, we

can calculate χ and determine if $N_{\pm}\gtrsim 100$ (it is not possible to determine the exact number of pairs per proton, but only if $N_{\pm}\gtrsim 100$). It will be extremely difficult to tell if the ejecta has a pair content of $N_{\pm}\lesssim 100$.

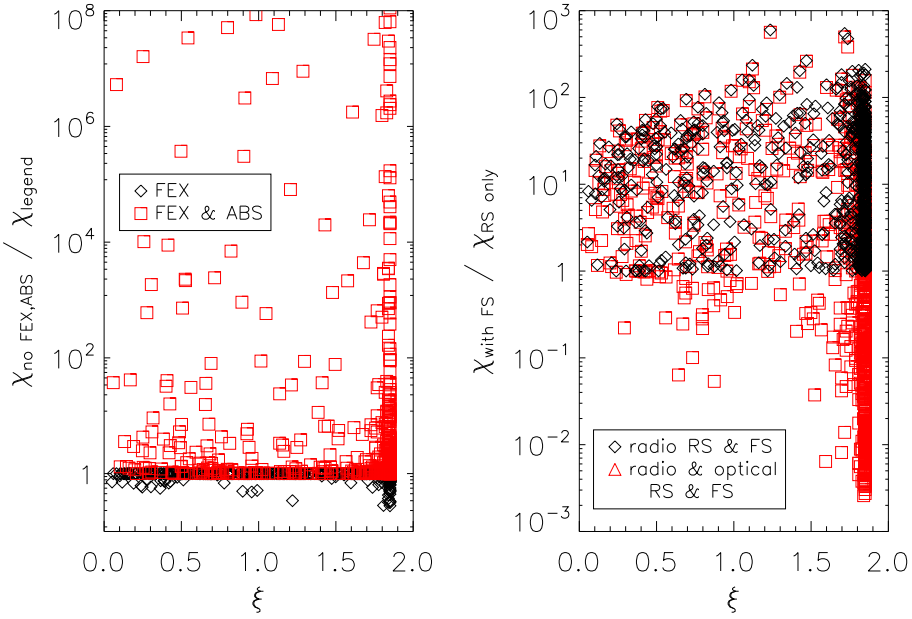

Figure 3.4 Left panel: Ratio of χ (no pairs) without external flux or absorption in the FS to χ with external flux and absorption in the FS plotted against the value of ξ at deceleration. Note that the ratio including absorption can go to arbitrarily high numbers, since radio flux can be completely absorbed ($\chi = 0$ with absorption in FS in these cases); some of these points have been cut off the plot. Right panel: Ratio of χ calculated including contributions of FS in just the radio and in both the radio and optical band to χ calculated without FS contribution, plotted against ξ at deceleration.

In Figure 3.4, in the left panel, χ is shown including the effect of adding external cooling and FS absorption to the purely baryonic ejecta case. We repeat the calculation of 1000 test cases with $p_r = 2.5$ and $N_{\pm} = 0$, and we

set $p_f = p_r$, and vary ε_{if} and ε_{Bf} in the same ranges as the corresponding RS parameters. The inclusion of external cooling in the calculation does not affect χ much. The value of χ is increased at most by a factor of a few from the calculation without external cooling included, and still lies within the scatter for the baryonic case shown in Figure 3.3.

Including absorption in the FS, however, will invalidate Equation 3.17, since we assumed in deriving it that the RS radio flux at the light curve peak is equal to the flux at the peak of the RS spectrum at t_*. This decrease in F_* by a large factor also decreases χ by the the same factor (χ in this case could be $\lesssim$1). In §3.2.2, we found that absorption in the FS can be a large effect for much of the parameter space at 8.5 GHz. Absorption in the FS for observer frequencies less than $\sim$ 10 GHz may indeed make it more difficult to accurately determine the pair content of the ejecta. However, at higher frequencies, $\sim$ 100 GHz, FS absorption is less important and one can calculate χ at these frequencies to determine $N_\pm$ (note that χ will be a factor of a few smaller at higher radio frequencies for the purely baryonic case).

To determine if χ for $s = 2$ has similar properties to the $s = 0$ case, we carry out a numerical simulation of 1000 RS test cases for $s = 2$ identical to that done for $s = 0$ (without external cooling or absorption), finding qualitatively similar results as the $s = 0$ case. With $N_\pm \lesssim 100$, the pair content is difficult to determine, but for $N_\pm \gtrsim 100$, the value of χ is about a factor of 5 lower than in the baryonic case. In the purely baryonic case, $\chi \sim 3000$ for $s = 2$ and this value ranges between a factor of 3 higher and lower. The spread

of χ values here is larger because the range of $n_0 = AR^{-s}$ for $s = 2$ is larger than the range of n_0 chosen for the $s = 0$ case.

Up to this point, we have not considered the contaminating effect of the FS emission to the optical or radio RS emission at the RS light curve peaks. It may be most difficult to distinguish RS from FS flux in observed radio light curves, so we calculate the value of χ with the FS radio flux included. In the right panel of Figure 3.4, we've plotted the ratio of χ calculated (for $s = 0$) with the FS radio flux contribution to χ without FS flux at the time which the RS radio light curve peaks. Again, for 1000 test cases, we set $p_f = p_r$, set $N_\pm = 0$, and vary ε_{if} and ε_{Bf} in the same ranges as the corresponding RS parameters. We find that the value of χ can increase by a factor of up to 100 from the RS only case, outside of the scatter in χ. In 60% of the 1000 test cases, the FS radio contribution was greater than the RS radio contribution at the RS radio peak. For $s = 2$, this occurs in 83% of the 1000 test cases. One needs to separate the contribution of the RS and FS to the radio flux using late time data in order to use this tool reliably to determine the ejecta pair content.

If the RS radio peak was observed, but the light curve has significant FS contribution, it may be possible to separate the contribution of FS from the RS radio flux by continued monitoring of the radio band for a period of a week or so, when the FS radio LC peaks. This information can be used to determine the contribution of the FS to the radio flux at the time of the RS peak, and χ due to the RS alone. If the radio flux is dominated by the FS

contribution during the RS peak and the RS peak is not observed, then this tool cannot be used to determine ejecta pair content.

We also find that the optical RS peak may be as difficult to observe as the radio peak due to FS contamination, in agreement with the conclusion drawn in NP04. In the right panel of Figure 3.4, we also show the ratio of χ with FS contribution (both radio and optical) to χ with only RS flux. The inclusion of FS optical flux at deceleration increases the scatter in χ even more; χ with FS flux ranges from being 100 times smaller to 100 times larger larger than χ with RS flux only. For the $s = 0$ case, the FS optical flux at deceleration is brighter than the RS optical flux 70% of 1000 test cases; in the $s = 2$ case, this occurred in only 30% of 1000 test cases. This is another difficulty in calculating χ for observed light curves. However, as in the radio, if an RS optical peak is observed, the FS contribution may be able to be removed if the optical light curve is followed for long enough after deceleration to determine the FS contribution to the total observed flux. We note that the fact that the FS optical emission is larger than the RS optical emission at deceleration in $\sim$70% of test cases for $s = 0$ may explain the lack of optical flashes and rapidly declining light curves at detected early times.

Scintillation in the radio may also be a problem for observing the RS radio peak due to the high level of variability that this process introduces into the observed radio light curve, as was observed in GRB 970508 (Frail et al. 1997; Taylor et al. 1997). The fluctuations are more pronounced at early times, when the RS radio light curve is expected to peak, because the source

size is smaller. One can reduce fluctuations from scintillation by observing at frequencies higher than 8.5 GHz. Observations made at frequencies near 50 GHz and even in the millimeter range (250 GHz) may be more suitable for determining χ and $N_{\pm}$ because of the insensitivity to scintillation at these frequencies. The effect of absorption in the FS is also smaller for these higher energy radio photons ($\tau_{abs,FS} > 1$ for a much smaller parameter space), and the RS light curve peaks at earlier times at these frequencies when the FS light curve may not be as bright. With current technology, radio observations on the timescales necessary for calculating χ of few minutes/hours to days after the burst are feasible at around 8.5 GHz. At higher frequencies like the sub-millimeter, recent observations are typically being done $\sim$ 0.1 to 1 day post-burst (Smith et al. 2005); the timescale for the sub-millimeter light curve peak is from a few minutes to a few hours after the burst (up to about 0.1 day).

Other things that may limit the usefulness of χ as a tool for estimating $N_{\pm}$ include sparseness of sampling of the radio light curve near the RS and FS peaks and breaks in the electron energy distribution between the optical and radio. The sparseness of radio data points near the RS and FS light curve peaks may introduce an error into the determination of χ of a factor of a few. Panaitescu and Kumar (2002) have found evidence in late-time afterglow modeling of a break in the electron energy distribution between the radio and the optical; one must be careful to choose the correct value of p_r (value of p_r between ν_{ir} and the optical band) for the calculation of χ.

In summary, it is possible to use optical and radio flux and observer times at the respective peaks of the light curves to determine pair content if the number of pairs/proton is $\gtrsim$100. There are many factors, however, that one must take into account when using this tool. The contributions to the optical and radio flux from the RS and FS must be separated, which may be difficult and requires good time coverage from $\sim$ 1 minute to hours in the optical and $\sim$ 1 hour to days in the radio. In the radio band, below 10 GHz, absorption in the FS and interstellar scintillation pose problems, and in order to avoid these issues, one should use observations at a higher frequency than $\sim$ 100 GHz.

3.2.5 Constraining parameters with available observations and upper limits

In Figure 3.5, we plot the comparison of our numerically calculated R band flux at deceleration with the full analytical expression given in the last row of Table 3.1 ($p = 2.5$ and $z = 1$). The full expressions for the R band flux at deceleration (in cgs units) for each of the four cases are as follows:

$$f_{\nu,R} = \frac{\sigma_T \varepsilon_{ir}^{p_r-1} \varepsilon_{Br}^{\frac{(p_r+1)}{4}} \mathcal{L}_{ep}^{\frac{(5p_r-7)}{4}} \mathcal{L}^{2-p_r} (1+z)^{\frac{(1-p_r)}{2}}}{H_0^2 \left(\sqrt{1+z}-1\right)^2} \times$$

$$\begin{cases} \frac{0.018\left(5.2\times10^{16}\right)^{\frac{(1-p_r)}{2}} m_p^{\frac{(5p_r-8)}{4}} n_0^{\frac{p_r}{4}} \Gamma_0^{p_r-2} E_{52}^{\frac{5}{4}}}{m_e^{\frac{(3p_r-5)}{2}} q^{\frac{(3-p_r)}{2}} \pi^{\frac{(6+p_r)}{4}} c^{\frac{9}{4}} t_{dur}^{\frac{3}{4}}} & s=0 \quad ct_{dur} \\ \frac{0.086\left(5.8\times10^{14}\right)^{\frac{(1-p_r)}{2}} A_*^{\frac{p_r}{2}} \Gamma_0^{p_r-2} E_{52}^{\frac{(5-p_r)}{4}} m_p^{\frac{(3p_r-4)}{2}}}{m_e^{\frac{(3p_r-5)}{2}} q^{\frac{(3-p_r)}{2}} \pi^{\frac{3}{2}} c^{\frac{(9-p_r)}{4}} t_{dur}^{\frac{(3+p_r)}{4}}} & s=2 \quad ct_{dur} \\ \frac{0.03\left(1.1\times10^{18}\right)^{\frac{(1-p_r)}{2}} n_0^{\frac{(p_r+1)}{4}} \Gamma_0^{p_r} E_{52} m_p^{\frac{(5p_r-7)}{4}}}{m_e^{\frac{(3p_r-5)}{2}} \pi^{\frac{(5+p_r)}{4}} q^{\frac{(3-p_r)}{2}} c} & s=0 \quad \frac{R}{2\Gamma_0^2} \\ \frac{4.06\left(7.7\times10^{16}\right)^{\frac{(1-p_r)}{2}} c^{p_r} A_*^{\frac{3(1+p_r)}{4}} \Gamma_0^{1+2p_r} m_p^{\frac{(7p_r-5)}{4}}}{m_e^{\frac{(3p_r-5)}{2}} \pi^{\frac{(3-p_r)}{4}} q^{\frac{(3-p_r)}{2}} E_{52}^{\frac{(p_r-1)}{2}}} & s=2 \quad \frac{R}{2\Gamma_0^2} \end{cases}$$

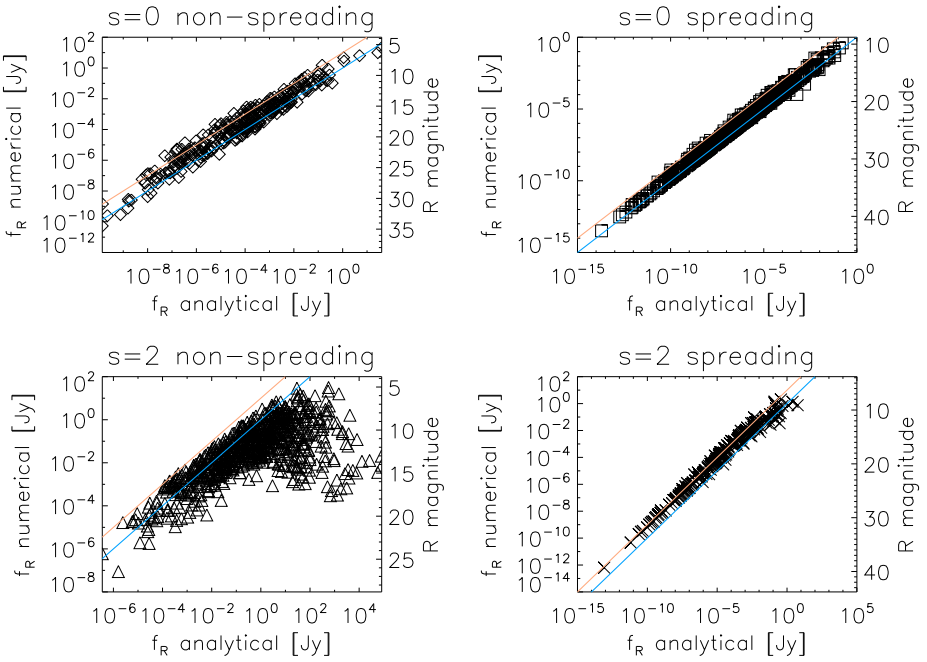

Figure 3.5 Comparison of 1000 test cases of numerically calculated R-band flux at deceleration with analytical expression for each case of $s = 0, 2$ spreading/non-spreading. All parameters, including $N_{\pm}$, are varied. The full analytical expressions assume $(\nu_{ir}, \nu_{ar}) < \nu_{obs} < \nu_{cr}$ and are given in the last row of Table 3.1 for the case of $p = 2.5$, $z = 1$ and in Equation 3.19 for the general case. A linear relationship (blue line) and f_R analytical =10 times f_R numerical (orange line) are shown on each panel for a guide.

The numerical calculation does not include external cooling or absorption in the FS (the latter is unimportant for the R band, but the former could decrease the flux by a factor of ~ 2), and all parameters are varied, including $N_{\pm}$. The analytical expressions assume $(\nu_{ir}, \nu_{ar}) < \nu_{obs} < \nu_{cr}$ and include pairs. For each case of $s = 0$ or $s = 2$, we ran 1000 test cases, and separated these 1000 cases into two sets determined by their ejecta width at deceleration. The blue

line shown on each plot shows a linear relationship for a guide, and the orange line shows the relationship if the numerical flux were 10 times the analytically calculated flux.

In all four cases, the scatter around the linear relationship is due to the estimations made for Γ_{ej} and more importantly γ_{ir} in the analytical expression. γ_{ir} is more difficult to estimate in the non spreading case, since the range of RS strengths ranges from ultra-relativistic to Newtonian. Since we use a mildly relativistic RS estimate for the analytical expression, the analytical expression underestimates the ultra-relativistic RS flux and overestimates the Newtonian RS flux. Likewise, in the spreading case, we made an estimate of γ_{ir} being mildly relativistic; all spreading cases are mildly relativistic to Newtonian, so the scatter around a linear relationship is much smaller than for non spreading ejecta. There is still a small bit of scatter due to the value of γ_{ir} that we chose (see Table 3.1), and the analytical value is typically within a factor of a few to 10.

The analytical expression given in Table 3.1 is a good estimation of the R band flux at deceleration for both spreading cases. It is less useful for the non spreading cases; in the $s = 2$ non-spreading case, the ordering of break frequencies assumed in the analytical expression is often not applicable, and the linear relationship does not hold over the entire parameter space explored– this occurs in the top right hand corner of the plot for this case. The cooling frequency is typically lower in $s = 2$ compared to $s = 0$, and drops below the other two break frequencies frequently in this calculation.

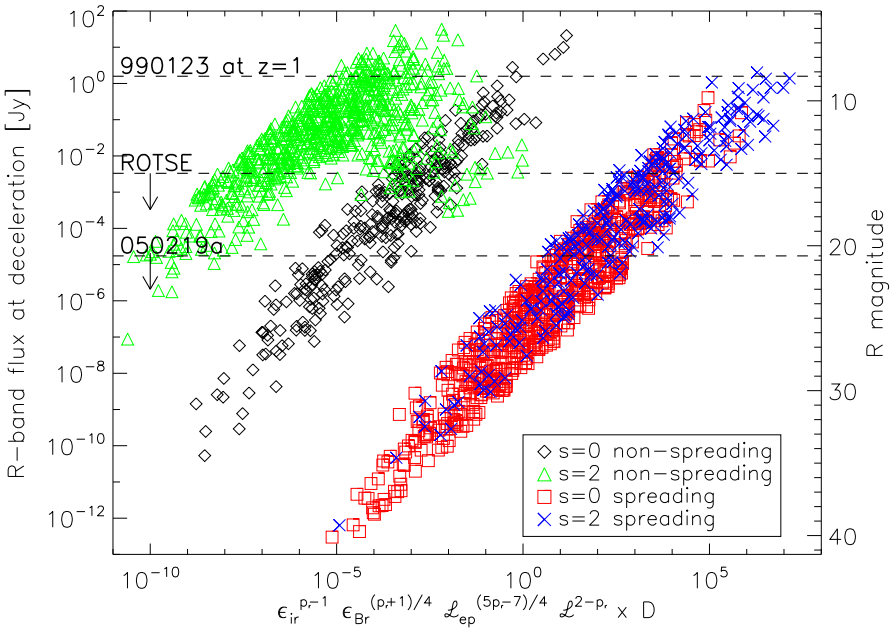

Figure 3.6 Observer frame RS flux in the R-band at deceleration assuming $z = 1$ and including pairs (no external cooling or absorption in the FS) plotted against the parameter dependences in the expression for flux in the R band at deceleration (without constants). All parameters are varied. The variable D in the expression on the x-axis contains all of the dynamics parameters and is different for each of the four cases shown: $D = n_0^{p_r/4}\Gamma_0^{p_r-2}E_{52}^{5/4}t_{dur}^{-3/4}$ for $s = 0$ non-spreading, $A_*^{p_r/2}\Gamma_0^{p_r-2}E_{52}^{(5-p_r)/4}\ t_{dur}^{-(3+p_r)/4}$ for $s = 2$ non-spreading, $n_0^{(p_r+1)/4}\Gamma_0^{p_r}E_{52}$ for $s = 0$ spreading, and $A_*^{3(1+p_r)/4}\Gamma_0^{1+2p_r}E_{52}^{(1-p_r)/2}$ for $s = 2$ spreading. The three dashed lines denote the observed R band flux at deceleration for GRB 990123 shifted to $z = 1$, observed upper limits reported in Kehoe et al. (2001) from the ROTSE telescope, and the V-band upper limit reported by Swift UVOT for GRB 050219a (Schady et al. 2005), shown for comparison to expected theoretical R band flux from the RS. Note that 990123 was an exceptional burst–a very small fraction of the parameter space produces optical flashes this bright.

In Figure 3.6, we have done the same calculation as described above for Figure 3.5, only here we have plotted the numerical observer frame R band

flux against only the parameter dependences from the analytical expression for R band flux. For example, for $s = 0$, $\Delta = R_+/(2\Gamma_0^2)$, we have plotted numerically calculated RS flux f_ν against the analytical combination of parameters $\varepsilon_{ir}^{p_r-1}\varepsilon_{Br}^{(p_r+1)/4}\mathcal{L}^{2-p_r}n_0^{(p_r+1)/4}\Gamma_0^{p_r}E_{52}$. The scatter (width) of the spreading regions on this plot are mainly due to the variation of p_r, while the scatter of the non spreading regions is due to p_r and the dynamics parameters. The $s = 2$ non spreading case is again not quite linear, for reasons discussed above for Figure 3.5.

This plot can be used as a tool to constrain the burst parameters using observed R-band flux or upper limits at or near deceleration using the more accurate results of the numerical calculation. Also, this plot can be used to view the ranges of expected R-band flux at deceleration if the early afterglow is caused by the RS with baryonic or pair enriched ejecta. Lines are drawn onto the plot to compare to the early afterglow detection of GRB 990123 at the peak (scaled from $z = 1.61$ to $z = 1$) and upper limits from ROTSE and *Swift*.

We find that optical flash emission from GRB 990123 falls at the very bright end of the distribution of RS R band flux at deceleration for all 4 cases shown in Figure 3.6. There are a great many synthetic bursts in our calculation, especially in the case of $s = 0$, spreading ejecta, with intrinsically low R band RS flux levels for burst parameters consistent with those found from afterglow modeling. This may indeed be the reason that the growing number of GRBs with rapid follow up do not show a bright optical flash.

As an example of how to use Figure 3.6 to constrain burst parameters with optical data or upper limits near deceleration, we look at the case of GRB 050219a. GRB050219a was a 23.6 s long *Swift*-detected burst of with a fluence of $(5.2 \pm 0.4) \times 10^{-6}$ erg cm^{-2} and was detected in the x-ray by XRT (Romano et al. 2005). An optical upper limit from *Swift* of $V = 20.7$ was found 96 s after the burst (Schady et al. 2005). We find that the upper limit for this burst falls near the bottom of the distribution of the non-spreading cases (although the distribution can be extended to lower values of $f_{\nu,R}$ using even lower limits for the ranges on n_0/A_* and ε_{Br}) but is in the middle of the distribution for the two spreading cases. It seems that RS flux fainter than this upper limit is fairly typical in the case of spreading ejecta.

Using Figure 3.6, we can make constraints on the burst parameters of 050219a (assuming that the upper limit of $V = 20.7$ applies at deceleration for this burst and there was no extinction). In the $s = 2$ cases, we can make fairly severe constraints on ε_{Br} and A_*. For example, using the plot for the $s = 2$ non spreading case, if we assume $z = 1$ (although see Berger et al. 2005 for the redshift distribution for *Swift* GRBs so far) and $p_r \sim 2.2$ we find (see Table 3.1)

$$\varepsilon_{ir}^{1.2} \varepsilon_{Br}^{0.8} \mathcal{L}_{ep} \mathcal{L}^{-0.2} A_*^{1.1} \Gamma_0^{0.2} E_{52}^{1.8} t_{dur}^{-1.3} \lesssim 1.2 \times 10^{-8}. \tag{3.19}$$

Using the observed burst duration and using the assumption $z = 1$, $t_{dur} = 11.8$ s, and estimating E_{52} from the fluence, we set $E_{52} \sim 2$. We set $\varepsilon_{ir} = 0.1$, a typical value, as indicated from afterglow modeling (Panaitescu and Kumar

2002). Inserting these values and setting $\Gamma_0 = 100\Gamma_{0,2}$, we have

$$\varepsilon_{Br}^{0.8}\mathcal{L}^{-0.2}A_*^{1.1}\Gamma_{0,2}^{0.2} \lesssim 5.3 \times 10^{-7}. \tag{3.20}$$

Since the dependence of this relation on the number of pairs and $\Gamma_{0,2}$ is small, we can say that within a factor of a few, $A_*^{1.1}\varepsilon_{Br}^{0.8}\lesssim 5.3 \times 10^{-7}$, implying very small values for A_* and/or ε_{Br}.

If we set $\varepsilon_{Br} \sim 10^{-5}$, on the lower end of the distribution of values found from afterglow modeling (Panaitescu and Kumar 2002), $A_*\lesssim 10^{-2}$. Also, if we choose to make ε_{ir} smaller for this burst than the typical value we have chosen, say $\varepsilon_{ir} \sim 0.01$, then if $A_* \sim 1$, $\varepsilon_{Br}\lesssim 10^{-7}$, still a rather low value.

If we try the $s = 2$ spreading case, we find similarly severe requirements for A_* and ε_{Br}. The expression for the spreading case, however, is much more sensitive to $\Gamma_{0,2}$, so the limits on A_* and ε_{Br} are not as robust as in the non spreading case above. For $A_* \sim 1$ and $\Gamma_{0,2} \sim 1$, $\varepsilon_{Br}\lesssim 10^{-9}$. If we require $\varepsilon_{Br} \sim 10^{-5}$, then $A_* \sim 0.1$. In summary, for the $s = 2$ density profile to apply, with either spreading or non spreading ejecta, the upper limit at 96 s requires low values of A_* or ε_{Br} near deceleration. For the $s = 0$ cases, using the typical values above ($\varepsilon_{ir} \sim 0.1$), we find the optical upper limit at 96 s to be less constraining on n_0 and ε_{Br}.

3.3 Discussion

In this chapter, we have calculated RS emission from purely baryonic and pair-enriched ejecta. We take into account the mildly relativistic nature

of the RS (we allow for the full range of RS speeds, from Newtonian to ultra-relativistic), and self consistently calculate synchrotron self absorption and inverse Compton cooling in the ejecta. Additionally, we have allowed for the ejecta to be cooled by FS synchrotron flux incident on the ejecta and for the low-energy RS photons to be absorbed in the FS material as they move outward from the source.

We find that the flux in the R band at deceleration depends very weakly on the ejecta pair content. The RS radio emission is affected by ejecta pairs the most, however the shape of the radio light curve is not affected. The effect of pairs on any single wavelength light curve (a reduction in the flux with increasing number of pairs per proton) can be replicated by varying the shock microphysics parameters in the RS; it is a degenerate problem. It is impossible to determine the pair content of the ejecta from a single wavelength light curve.

It may be possible to determine if $N_{\pm} \gtrsim 100$ by using observations of the RS optical and radio light curve peaks. By calculating χ (see Equation 3.17) using observations, one may be able to determine if $N_{\pm} \gtrsim 100$; one cannot determine the precise number of pairs per proton with χ, but whether there are a significant number of pairs present in the ejecta. The value of χ for purely baryonic ejecta is fairly constant (for a given value of p_r) over a wide range of RS strengths; effects that may increase the spread in χ (reducing the effectiveness of χ as a tool for determining ejecta pair content) include absorption of radio RS photons in the FS, contribution of the FS emission to the RS flux at the light curve peaks, and scintillation in the radio light curve. External

(FS synchrotron) flux incident on the ejecta has little effect on the value of χ. By using radio observations at higher frequencies, e.g. at 50 GHz or 250 GHZ (mm), effects of scintillation and FS contribution to radio emission can be reduced, and χ, and therefore the pair content of the ejecta, can be more accurately determined.

Li et al. (2003b) have also looked at the emission from pair enriched ejecta; we agree that it is possible for a large number of pairs to be present in the ejecta and that the resulting R band flux is largely insensitive to the number of pairs in the ejecta, however we come to different conclusions regarding the resulting ejecta emission. Li et al. (2003b) predict a strong flash in the IR band; we find that the peak frequency of the RS is largely unaffected by the pair content of the ejecta. Indeed, the injection frequency is reduced greatly by even a modest number of pairs, however we find that in the most frequent arrangement of frequencies, the peak of f_ν is at ν_{ar}, which is not affected by pairs much at all. Most of the difference between our calculations result from the treatment of RS strength; we have taken into account the mildly relativistic nature of the reverse shock, where Li et al. (2003b) have approximated the RS as being highly relativistic. Another contributing factor to the difference in our results is the more careful and self consistent calculation of synchrotron cooling and self absorption frequencies that we have done here.

In conclusion, RS emission from pair-enriched ejecta looks very similar to that from purely baryonic ejecta. The most promising tool to determine if GRB ejecta is pair-enriched, by the measurement of the parameter χ defined in

Equation 3.17, depends greatly on well sampled observations near the peak of the light curves in the optical and the radio; if the optical flash is seen quickly after the burst with *Swift* or other ground based telescopes, radio follow up in frequency bands between 50 GHz and 250 GHz (mm) from 15 minutes to ~ 1 day should provide some information about the pair enrichment of the ejecta.

Chapter 4

A unified analysis of the prompt gamma-ray and x-ray emissions from two *Swift*-detected gamma-ray bursts

The[1] successful launch of the *Swift* satellite in November 2004 filled a crucial gap in the gamma-ray burst data at early times – between a minute to a few hours – that existed in prior GRB missions. This has led to a number of very interesting discoveries regarding emission from GRBs on time scales of minutes following a burst. One of these discoveries is that the very early X-ray lightcurve (LC) of many bursts falls off very rapidly: $f_x \propto t^{-3}$ (Tagliaferri et al. 2005; Goad et al. 2006; Burrows et al. 2005; Chincarini et al. 2005). This phase of rapid fall off lasts for about 5 minutes, and is followed by the usual $f_x \propto t^{-1}$ behavior. In most cases, no change to the spectral slope is seen accompanying the change to the lightcurve. In this chapter, we discuss two bursts exhibiting such behavior, GRBs 050126 and 050219A. We provide an argument that the γ-rays and the early X-rays (for the first $\sim$5 minutes) have a common source, and we determine the physical properties of the source.

[1]Significant portions of this chapter were previously published in Kumar et al. (2006).

4.1 Modeling prompt γ-ray emission

We start with some very general physical considerations and describe a model with as few assumptions as possible to try to understand the γ-ray and X-ray emissions together.

We do not assume that γ-rays are produced in the internal shock or external shock or any other of a number of different models that have been suggested. We determine the properties of the γ-ray source from the data and use it to decide which of the proposed models, if any, work. The only assumption that we make is that γ-rays are generated by synchrotron or inverse-Compton (IC) mechanisms – an assumption that is supported by their non-thermal spectrum and also indirectly by the excellent overall agreement between models based on synchrotron & IC emission and multiwavelength afterglow data for a large number of GRBs (Piran 2005; Mészáros and Rees 1997b; Panaitescu and Kumar 2002; Granot et al. 1999).

The two bursts considered here have γ-ray light curves dominated by a single peak and small fluctuations and therefore much of the γ-ray flux is likely produced in a single source localized in space. In such a case the synchrotron and IC emissions from the object are completely determined if we know the magnetic field strength (B), the optical thickness of the object to Thomson scattering (τ_e), the speed of the object toward the observer (Lorentz factor – Γ), the total number of radiating particles assuming isotropic source (N), and the minimum energy for radiating particles, $\gamma_i m_e c^2$, (m_e is electron mass & c is the speed of light). The particle energy distribution above γ_i, at the acceleration

region where particles have not suffered appreciable loss of energy, is assumed to be a power-law function with index p. The energy distribution of particles for the entire population, however, is not a single power law function due to the loss of energy via radiative processes. We determine this modified distribution numerically by carrying out a self-consistent calculation of synchrotron cooling and self-absorption frequencies as described in Panaitescu and Mészáros (2000) and McMahon et al. (2006).

The average energy per particle, at the acceleration site, in the co-moving frame of the source is $\varepsilon = \gamma_i m_e c^2 (p-1)/(p-2)$, and therefore $N \approx E_{iso}/(\varepsilon\Gamma)$; where E_{iso} is the isotropic equivalent of energy in γ-rays. The index p is determined by the observed spectral index; we take $p = 2.4$ when the spectrum above the peak is not known – results reported here have been checked for dependence on p, and found qualitatively to be insensitive to p.

So we are left with four unknown parameters viz., B, τ_e, Γ and γ_i. The observational constraints on these parameters are: the γ-ray flux at the peak of the observed light curve, the frequency at which the spectrum peaks, the duration of the burst, the spectral index below the peak, and the optical flux limit (when available). The last two constraints are not independent and typically provide a limit on synchrotron cooling and/or injection frequencies.

The optical depth, τ_e, and N determine the distance of the γ-ray source from the center of the explosion: $r = \sqrt{N\sigma_T/4\pi\tau_e}$; and the burst duration $t_{GRB} \approx r/2\Gamma^2 c$. The parameters we use describe the state of the γ-ray produc-

ing source at the time of the peak of the observed lightcurve. The observed peak flux is the synchrotron or inverse-Compton flux in the appropriate observer energy band which is determined from B, N (the total number of electrons/positrons in the source), τ_e, γ_i and Γ; the details of the calculation is described in Chapter 6. By searching the parameter space (B, τ_e, Γ, γ_i) for emission properties consistent with those observed for each burst we can decide among various GRB models. As we shall see, we are led to more or less a unique solution: γ-rays are generated via synchrotron-self-IC (SSC) in a source with typical electron energy less than $10^3 m_e c^2$ and with properties that favor the external reverse-shock or internal shocks. Moreover, the γ-ray source we thus find also accounts for the steeply decaying early X-ray afterglow in a natural way, as off axis flux from the γ-ray emitting material or flux from the adiabatically cooling source.

These rapidly falling X-ray LCs are significantly steeper than any early optical LCs observed to date; the steepest optical LC fall off observed is t^{-2} and is believed to be synchrotron radiation from the RS heated GRB ejecta (see Piran 2005 for a review). Tagliaferri et al. (2005) suggested a number of different possibilities for the rapid fall of the X-ray LC. One possible explanation for the rapidly decaying X-ray LC is off-axis emission (Kumar and Panaitescu 2000). This is the radiation arriving at the observer that was emitted from the source at an angle with respect to the observer line of sight that is greater than Γ^{-1}. The off-axis flux decays as $t^{-2+\beta}$, where β is the spectral index, and the bolometric fluence scales with time as t^{-2}.

Modeling results for GRBs 050126 and 050219A are discussed below.

4.1.1 GRB 050126

GRB 050126 was 25s long with a fluence in 15-350 keV band of $1.7 \pm 0.3 \times 10^{-6}$ erg cm^{-2}, and redshift 1.29 (Tagliaferri et al. 2005). The average spectral index β ($f_\nu \propto \nu^\beta$) during the burst was -0.34 ± 0.14 and during the X-ray afterglow, the spectral index was $\beta = -1.35 \pm 0.3$ and the LC fell off as $t^{-2.52^{+0.5}_{-0.2}}$. We describe the results for γ-ray and X-ray emissions below.

4.1.1.1 Gamma-ray generation via the synchrotron process

Figure 4.1 shows the parameter space allowed – for a source radiating via the synchrotron process – to explain the observed γ-ray data for 050126. In particular we show the allowed range for γ_i, B, Γ_1 (the lower limit to the Lorentz factor of unshocked shell which produced the γ-ray photons when it was shock heated – we will refer to it as shell 1), and the upper limit to the Lorentz factor of the shell or the medium that shell 1 collided with (Γ_2).[2] These quantities are plotted against the radius, r, at which γ-rays are generated, to determine which GRB model could be described by the four parameter solution

[2] $\Gamma_1 = \Gamma\Gamma_{sh}(1+vv_{sh})$ is the LF of the inner unshocked shell; where $\Gamma_{sh} = (p-1)\gamma_i m_e/(p-2)m_p$ is the minimum LF of the shock front wrt the unshocked shell – this assumes that electrons have the same energy as protons (Γ_{sh} will be larger if electrons have lower energy) – and Γ is the LF of the shocked material as seen by a lab frame observer. Γ_2 is the LF of the unshocked outer shell/medium and is given by: $\Gamma\Gamma_{sh}(1 - vv_{sh})$. The calculations of Γ_1 and Γ_2 are valid when the γ-ray producing shell/medium is the inner and the outer shell respectively, and they are also valid for most internal shell collision situations where the shock front speed in the two shells is about the same.

space.

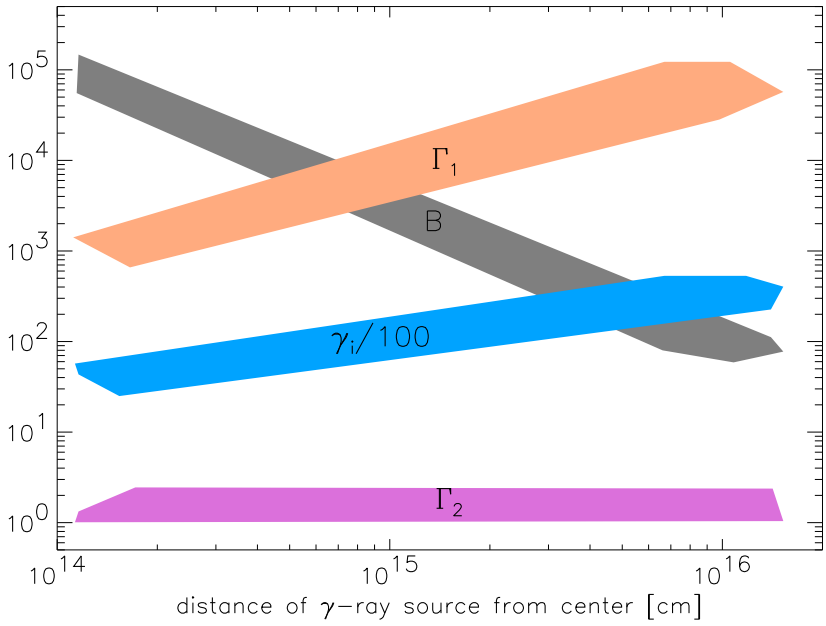

Figure 4.1 The parameter space for the synchrotron radiation solution to GRB 050126. The x-axis is the radial distance of the γ-ray source from the center of explosion. Shown in the figure is the minimum energy of electrons divided by the rest mass (γ_i) at the location where these particles are accelerated in the source, i.e., where radiative losses are unimportant. Also shown are the comoving magnetic field (B) in Gauss, the Lorentz factor (LF) of the unshocked shells/medium – Γ_1 & Γ_2. For these calculations we took $E_{iso} = 10^{52}$ erg, $p = 2.4$, $z = 1.29$, and the flux at 150keV at the peak of the γ-ray LC (7s) to be 0.2mJy. We use a factor of 2 tolerance in all of the observational data such as γ-ray flux, burst duration etc. in constructing the acceptable solution parameter space.

The solutions we find have $\gamma_i > 3000$, and a high magnetic field strength is needed to explain the γ-ray emission for this burst if it were to arise due to synchrotron emission. The synchrotron cooling frequency is found to be less

than a few eV which is in part due to the constraint that the low energy spectral index is -0.34±0.14 (so all of the solutions are in highly radiative cooling regime). The radius where the observed γ-rays could have been generated varies from the typical internal shock radius of $\sim 10^{14}$ cm to the external shock radius of $\sim 10^{16}$cm; the lower limit to the radius is due to our choice of $\tau_e < 0.1$ in order to avoid excessive Compton scattering — for $\tau_e = 1$ the minimum r is a factor 2 smaller. In the case of internal shocks we find that the Lorentz factor of the two colliding shells must satisfy the condition $\Gamma_1 \gtrsim 10^3$ and $\Gamma_2 \lesssim 3$ (see fig. 4.1), which seems an unrealistic requirement for any central engine to meet, and in any case this situation would not be that different from the interaction of GRB ejecta with the ISM where $\Gamma_2 = 1$. Note that the time interval between the ejection of the two shells (with $\Gamma_1 = 10^3$ and $\Gamma_2 = 2$) is larger than 500s for the internal shock radius of $r \sim 10^{14}$cm while the duration of this burst was 25s – this is another problem for this solution. Furthermore, the fact that the GRB LC was a FRED (fast rise, exponential decline) means that internal shocks are not required to generate the γ-ray emission.

The allowed parameter space contains an external forward-shock solution as well ($r \sim 10^{16}$cm; $\Gamma_2 = 1$). This solution, however, requires $\Gamma > 10^4$ (figure 4.1) which makes the already acute problem of baryonic loading much worse. Moreover, the deceleration radius for this large Γ, for a typical GRB-circumstellar medium density of ~ 10 cm^{-3}, is less than 10^{16}cm – the distance at which the γ-ray source according to our solution is located. Therefore, we conclude that γ-rays from 050126 are unlikely to have been produced via the

synchrotron process in internal or external shocks.

4.1.1.2 Gamma-ray production via the inverse-Compton process

Figure 4.2 shows the allowed parameter space for synchrotron-self-IC solutions. The entire solution space consists of mildly relativistic shocks with $2 < \gamma_i < 1000$, and the Lorentz factor (LF) of the source is between 20 & 300. Mildly relativistic shocks arise naturally in internal collisions (with the ratio of LFs for colliding shells of order a few) and the external reverse-shock (RS). A good fraction of the allowed parameter space has electron cooling time, due to radiative losses, of order the dynamical time or less, and the synchrotron cooling frequency is of order a few eV. The magnetic field strength is about 50 Gauss (which corresponds to $\varepsilon_B \sim 0.1$) & Compton Y $\sim$ 1 for the part of parameter space corresponding to reverse-shocks, whereas B is between 1 and 10^3 gauss and $1 \lesssim Y \lesssim 10^4$ for internal shocks. The IC γ-ray lightcurve falls off very rapidly for both the internal and the reverse shock emission as does the observed LC (Kobayashi et al. 2007). Therefore, γ-rays from GRB050126 could have been produced via SSC in either internal or external shocks, and we don't see any reason to prefer one solution over the other for this burst.

4.1.1.3 X-ray afterglow

Is it possible that the early X-ray afterglow was produced by the same source as the GRB IC photons? The IC cooling frequency, $\nu_c^{IC} \sim \nu_c \gamma_c^2$, at the GRB LC peak (7s) is typically of order a few hundred keV for the allowed

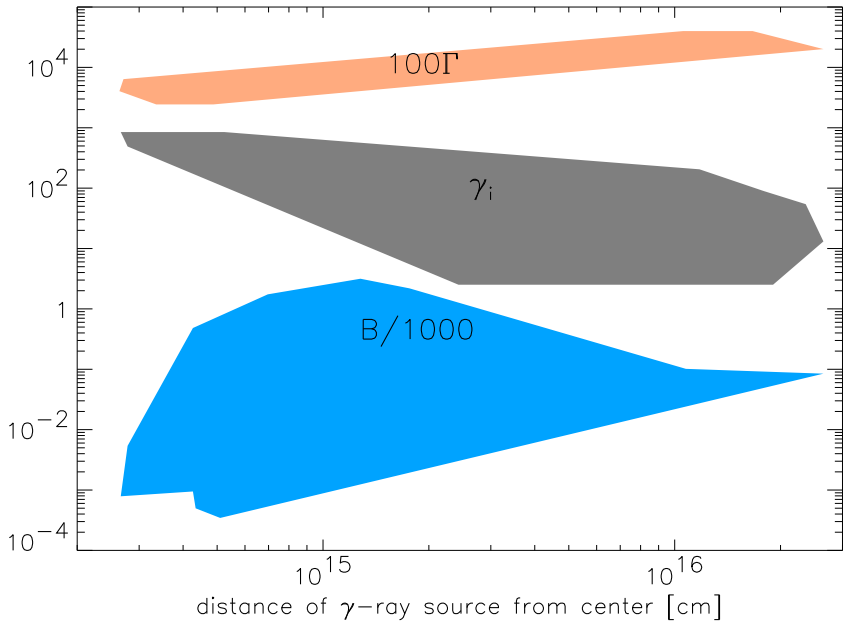

Figure 4.2 The parameter space for synchrotron-self-inverse-Compton solution to GRB050126. Shown in the figure are allowed range for γ_i, Γ (the Lorentz factor of γ-ray source), and B (the comoving magnetic field strength in Gauss). See figure 4.1 caption for some relevant details about the calculation.

parameter space for this burst. Since ν_c^{IC} shifts to lower energies due to adiabatic cooling, as $\sim t^{-2}$, at 100s it will have dropped to $\sim$1 keV. In this case the flux in the XRT band at 100s from $\theta \lesssim \Gamma^{-1}$ part of the source will be very small, and will rapidly drop to zero on a short time scale. The early X-ray LC could be explained by this adiabatically cooling γ-ray source provided that $\nu_c^{IC} \gtrsim 10$ MeV at 7 s, which is somewhat outside of the parameter space we find for this burst.

Could photons detected by the XRT in 0.2-10 keV band at $t > 100$s

be off-axis photons (Kumar and Panaitescu 2000) that originate at the source at an angle w.r.t. the line of sight $> \Gamma^{-1}$? The flux at 10 keV at the peak of the GRB 050126 lightcurve was 0.54±0.08mJy. This gives the flux[3] at 100s due to off axis emission of 1.1±.15μJy, in rough agreement with the XRT measurement of 2.8±1.2μJy. The X-ray light-curve between 100s and 425s declined as $t^{-2.52^{+0.5}_{-0.22}}$. This decline is also consistent with that expected of off-axis emission; $\beta = 1.26 \pm 0.22$ during this period would give rise to off-axis LC decaying as $t^{-3.26\pm0.22}$. The spectral peak for the off-axis emission from a uniform jet decreases with time as $1/t$, and so the peak at 100s is at $\sim$ 10keV. The peak frequency decreases more rapidly when electron energy and/or magnetic field is smaller at higher θ. In this case the spectral peak will be below 10 keV, and β in the XRT band, for $t >$ 100s, smaller than during the GRB. We note that a decrease of γ_i and B would not lead to a decrease in the flux in the XRT band so long as these changes are accompanied with an increase in the number of radiating particles as might be expected, for instance, when Γ decreases with θ but the energy per unit solid angle is roughly constant. The angular structure of the ejecta can be constrained by the difference between the observed spectral peak at 100s and during the burst.

[3]The off-axis flux falls off as $t^{-2+\beta}$, see Kumar and Panaitescu (2000), where β is the spectral index, i.e. $f_\nu \propto \nu^{-\beta}$.

4.1.2 GRB 050219A

GRB 050219A was 23.6s long with fluence in the BAT 15-350 keV band of $5.2 \pm 0.4 \times 10^{-6}$ erg cm^{-2}. The average spectral index β during the burst was 0.75 ± 0.30 ($f_\nu \propto \nu^{0.75\pm0.30}$), and the peak of the spectrum was at 90±9 keV (Tagliaferri et al. 2005). During the X-ray afterglow, the spectral index was $\beta = -1.1 \pm 0.2$ and the X-ray LC declined as $t^{-3.15\pm0.22}$. We describe below the mechanism for γ-ray, X-ray, and optical emissions.

4.1.2.1 Gamma-ray production

The positive β during the GRB, although consistent with the synchrotron spectrum of $\nu^{1/3}$ to within 1.5σ, rules out the synchrotron process for the generation of γ-rays for 050219A. The reason is that the magnetic field required to produce synchrotron peak frequency of 90keV is sufficiently strong that electrons lose their energy on a time scale much less than the duration of the burst (23s), and in this case the spectrum below 90 keV would be $\sim \nu^{-1/2}$. [4] This is in conflict with the observed spectrum and rules out the synchrotron process for γ-ray generation.

The inverse-Compton process on the other hand provides a very natural way of explaining the observed spectrum and other properties. The spectrum

[4] A synchrotron frequency of 90 keV implies that $B\gamma_i^2\Gamma = 10^{13}$ and the electron cooling LF is $\gamma_c/\gamma_i \sim 10^{-17}\gamma_i^3\Gamma/t_{GRB}(1+Y)$; the Compton parameter $Y \sim \tau_e\gamma_i\gamma_c$, and therefore, $(\gamma_c/\gamma_i)^2 \sim 10^{-17}\gamma_i\Gamma/(\tau_e t_{GRB})$, where t_{GRB} is the burst duration in the host galaxy rest frame. Since $\tau_e > 10^{-8}$and $t_{GRB} \sim 10$s, and $\gamma_i < 10^3\Gamma$, we see that $\gamma_c/\gamma_i < 1$ unless $\Gamma > 3000$ which is highly unlikely.

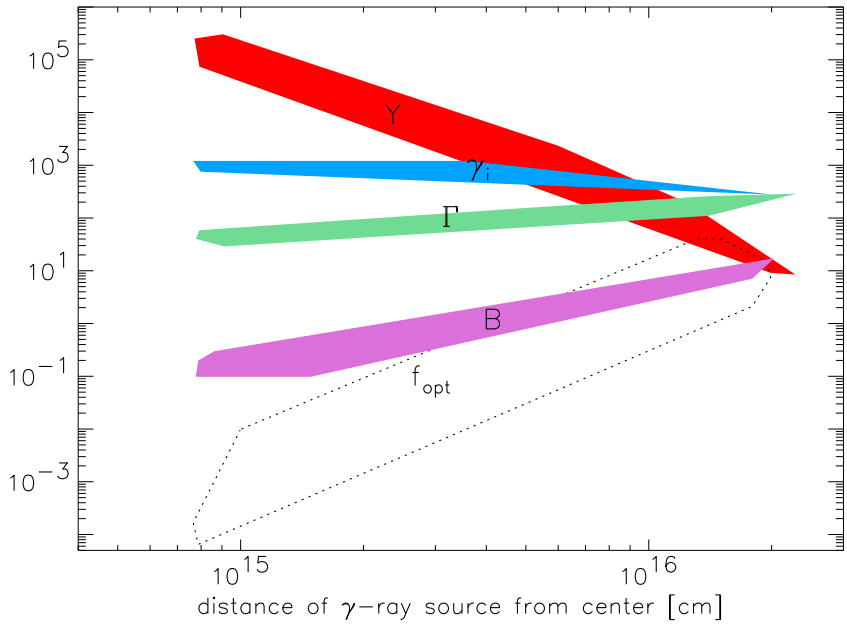

Figure 4.3 The parameter space for the synchrotron-self-inverse-Compton solution to GRB050219A. Shown in the figure are allowed range of γ_i, Γ (the Lorentz factor of γ-ray source), Compton Y parameter, B (the comoving magnetic field strength in Gauss), and the predicted optical flux at 100s for these solutions (assuming burst redshift of 1 and no extinction). The solutions with $r < 4 \times 10^{15}$cm have $Y \gtrsim 10^4$ and are physically unacceptable since the energy in the 2nd Compton scattering will be of order 10^{54}erg which is too large to obtain from a stellar mass object. Therefore, the only viable solution for the γ-ray emission is IC in the external reverse-shock. We took $E_{iso} = 10^{53}$ erg, $p = 2.9$, $z = 1$, the peak of the spectrum at 90keV, and the flux at the peak of the γ-ray LC (15s) at 90keV to be 1.2mJy. We applied the condition that $\nu_a^{IC} \equiv \nu_a \times \min(\gamma_i, \gamma_c)^2 \sim$90 keV; this automatically ensures that $\beta = 0.75 \pm 0.3$ as observed. We use a factor of 2 tolerance in all of the observational data such as γ-ray flux, burst duration, the peak frequency etc. in constructing the acceptable solution parameter space.

produced by inverse Compton scattering of a self-absorbed synchrotron radiation is $f_\nu \propto \nu$ for $\nu < \nu_a \times \min(\gamma_i, \gamma_c)^2 \equiv \nu_a^{IC}$; where ν_a is the synchrotron

self-absorption frequency. For $\min(\gamma_i, \gamma_c) \sim 300$ and $\nu_a \sim 1$eV, the peak of the IC spectrum at ν_a^{IC} is close to the observed value of 90±9 keV. These parameters arise naturally in an external reverse-shock.

Figure 4.3 shows the allowed parameter space for SSC solution for GRB 050219A, assuming $z = 1$. The range of γ_i for the allowed solutions is 200–1500 which is typical for the external reverse-shock and for internal shocks, but not the external forward-shock. The magnetic field B is between 0.1 and 20 Gauss. This is highly sub-equipartition ($\varepsilon_B \lesssim 10^{-3}$), and therefore for 050219A we can rule out the possibility that the γ-ray burst was produced as a result of dissipation of magnetic field or that much of the energy of the explosion was carried outward by the magnetic field.

The Compton Y is rather large – of order 10–100 for external shock ($r \sim 10^{16}$cm), and larger than 10^4 for internal shock radius of $r \sim 10^{14}$–10^{15}cm (fig. 4.3). One might suspect that the large Y renders these solutions unphysical since the energy in the 2nd Compton scattering, which produces >100 GeV photons, will far exceed the γ-ray energy. However, for low optical depth systems with $\Gamma \gg 1$ the radius of the system increases by about a factor 2 in the time it takes photons to traverse the shell. Therefore, the optical depth for the 2nd scattering is smaller than the 1st by a factor 4, and the electron thermal energy has decreased due to adiabatic expansion during this period by a factor of about 4 for RS (shell thickness for RS increases as $r^{7/2}$), and a factor 2 for internal shocks. Thus, the effective Y for the 2nd Compton scattering is smaller than the 1st scattering Compton-Y by a factor

of about 64 for the RS and 16 for internal shocks. For this reason $Y \sim 100$ for the external shock is quite acceptable, as the total energy requirement is of order 10^{51} erg. However, $Y > 10^4$ for internal shocks (see fig. 4.3) would require the total energy in the explosion to be $\sim 10^3$ times larger than energy in the γ-ray band and that is highly unlikely considering that $E_\gamma \sim 10^{51}$ erg. Therefore, the only viable solution for the γ-ray production for 050219A is inverse-Compton in the external reverse-shock heated ejecta.

4.1.2.2 X-ray afterglow

There are two mechanisms that can explain the X-ray observations for this burst. One of these is the off-axis emission. The flux at the peak of γ-ray LC (15s) at 10keV was $\sim 300\mu$Jy. Using this and $\nu^{0.75\pm0.3}$, we find the flux at 100s, due to the off-axis emission mechanism ($f_\nu \propto t^{-2+\beta=-1.25\pm0.3}$), to be $\sim 29 \pm 7\mu$Jy, which is consistent with the observed XRT flux ($25 \pm 9\mu$Jy at 10 keV at 100s). The LC decay according to the off-axis emission after the spectral peak falls through the XRT band is $t^{-2+\beta}$, where $\beta = -1.1 \pm 0.2$ is the spectral index for $t > 100$s, and this is consistent with the observed decay of $t^{-3.15\pm0.22}$. The difference between the X-ray afterglow and γ-ray spectra can be understood in the same way as discussed for 050126, i.e. the peak of f_ν during the GRB (90keV) is well below 10keV at 100s if γ_i and B decrease with θ slightly and this changes the spectrum from $\sim \nu^{0.7}$ to $\sim \nu^{-1}$.[5]

[5]Angular variation is almost unavoidable, because in the absence of it the early X-ray LC would have declined as $t^{-1.25}$ due to the off axis emission.

The second possibility is that we continue to see radiation from within Γ^{-1} angle of the adiabatically cooling γ-ray source. We find that for a large part of the allowed parameter space for γ-ray solution $\nu_c^{IC} \gtrsim 1$MeV, and therefore we expect to receive emission in the 0.2-10 keV band for a period of about 5 minutes, during which time the flux decline will be $\sim t^{-2.8}$, which is consistent with the observed decay.[6] We note that the discontinuity in the BAT and XRT lightcurves for this burst could be due to an underestimation of the spectral evolution in 20-50s time interval where the BAT signal was low. A discontinuous jump can also arise in the off-axis model as a result of a rapid increase in jet energy for θ between γ^{-1} and $2\gamma^{-1}$.

Both of these solutions suggest a common source for the γ-ray burst and early X-rays.

4.1.2.3 Optical observations

The optical flux at 100s from the γ-ray source is shown in figure 4.3. For the RS solution the flux is about 1 mJy whereas the observed UVOT upper limit at 96s is 0.02mJy (Schady et al. 2005). The much smaller optical flux could be due to absorption in the host galaxy. The total hydrogen column density for this burst was[1] $2.2 \pm 0.6 \times 10^{21}$ cm^{-2}, in excess of the galactic

[6]The IC frequencies for an adiabatically cooling ejecta shift with time as t^{-2}, so the 90 keV peak at 15s would have shifted to 2 keV at 100s. During the time when this peak is above the XRT band of 10keV, the IC flux from the RS decreases very weakly with time ($\sim t^{-0.4}$), and subsequently, the flux decreases as $t^{-2.8}$. The cross-over is expected at about 45s. Thus, the flux from the RS at 100s at 10 keV is expected to be about $18 \pm 4\mu$Jy which is consistent with the XRT flux of $25 \pm 9\mu$Jy. The spectrum at 100s will be as expected of IC above ν_a^{IC}, i.e. roughly ν^{-1}.

value, which for a burst at $z \sim 1$ could give $\sim$7mag of optical extinction, more than sufficient to bring the optical flux below the observed upper limit.[7] Alternatively, if the RS occurs at $r \lesssim 10^{16}$ cm the optical flux would be roughly consistent with the observed upper limit (see fig. 4.3). However, in this case $Y \sim 300$, and the energy in the 2nd Compton scattered, photons, at 100 GeV, will be almost an order of magnitude larger than the energy in γ-rays.

4.2 Conclusion

We find that the prompt γ-ray and early (first few minutes) X-ray emissions for GRBs 050126 and 050219A are consistent with being produced by the same source. In the case of 050126, the emission is inverse Compton radiation from either internal shocks or external-reverse shock, and in the case of 050219A, the photons are produced by inverse Compton in the external-reverse shock. The late time X-ray ($t \gtrsim$5min) is produced, as usual, in the forward shock.

These results can be applied to the class of gamma-ray bursts with consist of a simple, i.e. not highly variable, lightcurve. For instance, our conclusion that γ-rays were generated via the inverse-Compton process for GRB 050219A is valid for all those GRBs which, like GRB 050219A, have a positive low energy spectral index for the prompt gamma-ray emission ($f_\nu \propto \nu^\beta$

[7] Galactic correlation between N_H and extinction might not apply to GRBs due to possible dust destruction by GRB emission (Galama and Wijers 2001). It is therefore difficult to say with confidence the amount of extinction for this burst in the V-band.

with $\beta > 1$). The allowed values for parameters – B, Γ & γ_i – for the source of γ-rays for any GRB consisting of a single peak in the γ-ray lightcurve should be similar to that shown in figures 4.1 and 4.3 for 050126 & 050219A.

Chapter 5

Estimation of the gamma-ray burst source radius using steeply decaying x-ray afterglows

The[1] x-ray flux of a large fraction of the bursts detected by *Swift* exhibits a rapid decline with time, as $\sim t^{-2}$ or faster, for about 10 minutes (Tagliaferri et al. 2005; Nousek et al. 2006; O'Brien et al. 2006) after trigger. This is often followed by a slowly declining light curve (LC), with the flux falling-off as $\sim t^{-1/2}$ for a few hours. The extrapolation of the fast declining x-ray LC backward in time matches the LC during the burst, which suggests that the early x-ray and late γ-ray emissions are produced by the same source (O'Brien et al. 2006).

The fastest decline of the LC from a relativistic source moving at Lorentz factor Γ_0 and of angular size $\theta_j > \Gamma_0^{-1}$ arises when the source switches-off quickly due to, for instance, a rapid adiabatic cooling at the end of the ejecta heating episode. In this case, the observed flux declines as $t^{-2-\beta}$ (Kumar and Panaitescu 2000), where β is the spectral index of the burst emission, i.e. $f_\nu \propto \nu^{-\beta}$. The observed decline rate of the early x-ray LC is often at this theoretical limit (O'Brien et al. 2006), therefore the γ-ray source must have

[1]Significant portions of this chapter were previously published in Kumar et al. (2007).

a finite, short life and, consequently, must be distinct from the much longer lived afterglow source.

In this chapter we determine some properties of the γ-ray source and its distance from the center of the explosion using the early time data obtained by instruments aboard the *Swift* satellite.

5.1 Gamma-ray source distance

The early x-ray light curve can be used to determine the distance of the γ-ray source (R_γ) from the central explosion, as suggested by Lazzati and Begelman (2006) and Lyutikov (2006). However, instead of using the unknown GRB jet angle to determine R_γ, as done in previous works, we determine the source radius in terms of the forward shock radius, which has a very weak dependence on the only unknown parameter: the density of the circumstellar medium. In order to exploit this method, we analyze the γ-ray, x-ray and optical data within the first 10 minutes for ten *Swift* bursts for which we can establish that the steeply falling off portion of the LC is the large-angle emission.

Some conditions need to be satisfied by the rapidly falling-off early x-ray afterglow LC to be identified with the large-angle emission from the γ-ray source. These conditions are: (i) the temporal decay index (α) of the x-ray LC during the steep decline phase should be equal to $2 + \beta$; (ii) the spectral index β during early x-ray afterglow should be the same as at the end of the gamma-ray burst; (iii) the x-ray afterglow flux extrapolated to the end of the

prompt γ-ray emission should be same as the γ-ray flux at the end of the burst extrapolated to the x-ray band. We apply an additional condition: $t_2/t_1 > 3$, where t_1 & t_2 are the beginning and end of the steep x-ray decline phase, to ensure that we have a sufficiently long baseline for an accurate determination of α (i.e. this index will not be too sensitive to the uncertainty in the origin of time).

Ten bursts detected by *Swift* between January 2005 and May 2006 meet these four conditions. Four of these bursts have a single-peaked LC or are FRED (fast rise, exponential decline) shaped; the remaining six bursts contain multiple peaks. The relevant properties for these 10 GRBs are listed in Table 5.1.

Table 5.1 GRB sample

GRB	FRED?	α	β_γ	β_x	z	$E_{iso,52}$	T_{90}	t_2	V	t_{opt}
050315	yes	4.3±0.36	1.2±0.09	1.6±0.25	1.95	8.9	96	400	>18.5	140
050713b	yes	3.1±0.32	0.53±0.15	0.70±0.11		23	120	720	>19.5	190
050714b	no	4.8±1.2	1.7±0.41	1.7±0.41		3.0	70	550	>18.7	170
050814	yes	3.0±0.17	0.98±0.19	1.1±0.08	5.3	67	65	1300	>18.7	210
050819	no	3.0±0.40	1.6±0.21	1.2±0.23		2.2	36	900	>18.1	130
051016a	no	2.93±1.03	0.95±0.16	1.2±0.73		4.5	22	530	>20.3	210
060108	yes	2.3±0.31	0.94±0.11	0.98±0.25	2.03	1.1	14	360	>19.1	190
060211a	no	3.7±0.36	0.83±0.08	0.99±0.08		7.7	126	1000	>18	250
060219	no	2.7±0.75	1.7±0.28	2.15±1.06		2.2	62	540	>18.6	220
060223a	no	3.82±4.84	0.77±0.08	0.90±0.23	4.41	13	11	85	17.8	190

α is the decay index of the fast falling early XRT emission, β_γ is the BAT spectral index averaged over the duration of the burst, β_x is XRT spectral index at the beginning of the steep decline phase, z is the burst redshift (set to 2.5, the median z for *Swift* bursts, for those without a measured z), $E_{iso,52}$ is the isotropic equivalent energy released in the BAT band (15-150 keV) in 10^{52} erg, T_{90} is the burst duration in seconds ($t_1 \sim T_{90}$ in most cases), t_2 is the time when the steep decline of the x-ray LC ends, measured from t_0 as defined in O'Brien et al. (2006), V is the UVOT magnitude measured at time t_{opt} (in seconds) from the GRB peak.

Consider a γ-ray source moving at Γ_0, that turns off at radius R_γ. After the turn-off, the observed x-ray flux comes from regions of the γ-ray source that move at an angle θ larger than Γ_0^{-1} with respect to the line of sight (Kumar and Panaitescu 2000) – this will be referred to as the large-angle emission or **LAE**. The LAE arrives at an observer time $t = (1+z)R_\gamma\theta^2/2c$ and has a specific intensity smaller than that for $\theta = 0$ by factor $(1+\theta^2\Gamma_0^2)^3$. The LAE starts at t_1, the end of the prompt phase, and dominates the LC until some time t_2 when emission from the forward shock overtakes the rapidly decreasing flux from the γ-ray source. Thus, the source turn-off radius is $R_\gamma = 2ct_1\Gamma_0^2/(1+z)$.

The 0.3–10 keV fluence of the early rapidly declining x-ray LC, starting from the end of the GRB prompt emission to time t_2, is greater than $\sim 15\%$ of the GRB fluence for most of the bursts (Table 5.2). Therefore, the source for the steep x-ray LC is not some minor pulse in the explosion but is responsible for producing a good fraction of the prompt γ-ray energy, for both FRED and non-FRED bursts. For this reason, t_1 appearing in the above equation for R_γ should be roughly equal to the burst duration, t_γ, otherwise the fluence during the LAE would be much less than the observed value.

The radius (R_{FS}) and the LF (Γ_{FS}) of the shock front in the CSM are related by $R_{FS}(t_2) \approx 2ct_2\Gamma_{FS}^2(t_2)/(1+z)$. Since the energy of the LAE source is a significant fraction of the total GRB energy, it must have provided a good part of the kinetic energy deposited in the CSM, thus the LF of the LAE source, Γ_0, should be larger than Γ_{FS}. Given that $R_{FS}(t_2)/R_\gamma = [\Gamma_{FS}(t_2)/\Gamma_0]^2(t_2/t_\gamma)$, $\Gamma_0 > \Gamma_{FS}(t_2)$ implies that $R_{FS}(t_2)/R_\gamma < t_2/t_\gamma$. For the ten bursts in our

Table 5.2 Calculated quantities

GRB	LAE fluence[(a)]	optical flux ratio[(b)]	$\Gamma_{FS}(t_2)$	$R_{FS}(t_2)^{(c)}$	$R_\gamma^{(c)}$
050315	0.08	2.1×10^4	84	5.8	1.4
050713b	0.08	1.8×10^2	82	8.2	1.4
050714b	0.8	7.2×10^4	70	4.6	0.59
050814	0.17	9.2×10^2	93	11	0.53
050819	0.66	5.0×10^2	55	4.8	0.19
051016a	0.47	4.9×10^2	75	5.0	0.21
060108	0.29	1.9×10^1	69	3.4	0.13
060211a	0.23	2.9×10^2	63	6.7	0.86
060219	0.4	2.8×10^4	67	4.2	0.48
060223a	0.17		200	3.8	0.49

The first optical data for GRB 060223a was obtained at 187s after the BAT trigger whereas the steep decline of the x-ray LC ended at 85s ($t_2 = 85$s). The extrapolation of the x-ray flux at 85s to the optical band gives a V-mag of 16.3 whereas the observed flux at 187s was 17.8 mag. For all other bursts UVOT measurements were between t_1 and t_2.

[(a)] Ratio of fluence from the end of GRB to time t_2 in 0.3-10 keV band and the fluence in 15-150 keV band during the burst. [(b)] Ratio of the expected to observed optical flux (or upper limit) at the time of UVOT observation. The expected flux is the extrapolation of the x-ray flux to the optical band using the XRT spectral index. [(c)] In units of 10^{16} cm.

sample, t_2/t_γ is between 5 and 25; the average value of t_2/t_γ is 14.0 for the four FREDs and 13.5 for the six non-FREDs. If the deceleration time for CSM shock, t_d, is less than t_2 (as expected because the x-ray flux is decreasing monotonically) then the initial LF of the CSM shock, $\sim \Gamma_0$, is larger than the LF at deceleration by a factor 2, and $R_{FS}(t_d)/R_\gamma$ is smaller than t_2/t_γ by a factor ~ 4. Therefore, we conclude that γ-rays are produced within a factor ~ 4 of the deceleration radius, on the average, for our sample of bursts.

We now calculate $R_{FS}(t_2)$ and estimate R_γ. The forward shock radius at time t_2 can be calculated from the dynamics of adiabatic blast-waves, which yields $R_{FS}(t_2) = [3ct_2E_{iso}/2\pi m_pc^2(1+z)n_0]^{1/4}$, where E_{iso} is the isotropic equivalent of energy in the FS and n_0 is the mean density of the CSM within a sphere of radius $R_{FS}(t_2)$. The former is obtained from the GRB fluence and the CSM density (or an upper limit for n_0) is calculated from the x-ray and optical flux at t_2. For the bursts in our sample, we find $n_0 \lesssim 10\,\mathrm{cm}^{-3}$ provided that x-rays are produced via the synchrotron process (no conditions were imposed on microphysics parameters ε_e and ε_B in this calculation); the constraint on n_0 is weaker if x-rays are produced via the synchrotron-self-Compton process.[2] From the GRB fluence and assuming $n_0 = 10\,\mathrm{cm}^{-3}$, we calculate the forward shock radii $R_{FS}(t_2)$ and LFs, $\Gamma_{FS}(t_2) = [R_{FS}(t_2)(1+z)/2ct_2]^{1/2}$, given in Table 5.2. From $R_{FS}(t_2)$, we calculate the lower bound on the γ-ray source distance

[2]If the density of the CSM is set by the mass loss from the GRB progenitor star then this small mean density of ~ 10 cm^{-3} along the jet axis, within the radius $R_{FS}(t_2) \sim 5\times10^{16}$cm, means that the mass loss rate divided by the wind speed from the progenitor star in the polar region, in the last ~ 100 year of its life, was smaller than typical Wolf-Rayet stars by at least a factor of a few 10s.

from the center of explosion and find it to be between 10^{15} and 10^{16}cm. Note that R_{FS} and Γ_{FS} have a very weak dependence on E_{iso} and n_0 and therefore any error in E_{iso} or n_0 has small effect on these quantities.

5.2 Gamma-ray generation models

5.2.1 Forward-Shock

Although we find that the burst and early afterglow data are not incompatible with $R_\gamma \sim R_{FS}(t_2)$, the forward shock (FS) model for γ-ray generation can be ruled out because the γ-ray production mechanism is short-lived and because the FS produces too much optical flux (see below). Furthermore, Ramirez-Ruiz and Granot (2006) have pointed out that the the relations between the spectral peak, flux and burst duration expected if γ-rays are produced in the forward shock are not satisfied by the GRB prompt emission.

All ten bursts in our sample have deep optical upper limits or detections a few minutes after the burst – typically at the beginning of the steeply declining x-ray LC – provided by the UV-optical telescope aboard *Swift*. From the x-ray flux and spectrum at the time of the optical observations, we estimate the expected flux in the optical band and find it to exceed the observed value or upper limit by two orders of magnitude or more (Table 5.2). A large extinction in the optical can be ruled out because late time optical data show it to be less than a factor 2. Moreover, in those cases with optical detections, the optical spectrum is consistent with $f_\nu \propto \nu^{-1}$, similar to the spectrum in the x-ray band. Thus, the deep optical upper limits set by UVOT require

that the spectrum of the x-ray/γ-ray source turns over at lower energies and becomes steeper than $f_\nu \propto \nu^{1/3}$, i.e. that the optical band often lies below the synchrotron self-absorption frequency (ν_a) of the early x-ray/γ-ray emission. It also implies that the optical flux detected at early times must come from a different source.

A straightforward calculation of forward shock emission shows that, if the x-ray emission at time t_1 is produced via the synchrotron process, then $\nu_a \ll 2$ eV. This result holds even when we allow for an external medium enriched with up to 10^3 $e^{\pm}$ pairs per proton. Therefore, the forward shock model does not satisfy the $\nu_a > 2$ eV requirement needed to reconcile the optical and x-ray data at early times. If x-rays arise from synchrotron-self-Compton process then the spectrum below 0.3 keV can be as steep as $f_\nu \propto \nu$, however, the optical flux associated with the underlying synchrotron radiation exceeds the observed limit.

5.2.2 Internal Shocks

We now consider the internal shock model for prompt γ-ray generation. According to this model, fluctuations in the LF of the relativistic outflow lead to collisions between faster and slower ejecta, producing internal shocks and γ-ray radiation. No relationship is expected, in general, between where these collisions take place and the deceleration radius, whereas we find the average $R_{FS}(t_d)/R_\gamma \lesssim 4$. We also found that the average value of $R_{FS}(t_2)/R_\gamma$ is the same for bursts with multiple γ-ray light curve spikes and for FRED bursts.

This suggests that gamma-rays are produced at a radius that is not set by the variability time scale of the central engine, contrary to what is expected in the internal shock model.

The GRB ejecta should consist of baryonic material and/or $e^{\pm}$ in order to undergo internal shocks. The interaction of such ejecta with the CSM launches a reverse shock moving into the ejecta, heating it and producing synchrotron radiation that peaks in the optical band (Panaitescu and Mészáros 1998) and declines with time as t^{-2} (Sari and Piran 1999). It is widely believed that such an emission from shocked ejecta was seen for GRBs 990123 and 021211.

In Figure 5.1, we show the early optical light curve for these two bursts resulting after subtracting the extrapolation of the late time optical emission, which arises in the forward shock. This extrapolation is justified because the optical light curves for many *Swift* bursts display a single power-law decline from ~ 300 s to hours (Panaitescu et al. 2006; Fan and Piran 2006). We find that, after subtracting the forward shock contribution, the early light curves of GRBs 990123 and 021211 decline as $f_{opt} \propto t^{-2.5}$. This decline is steeper than expected for the reverse-shock optical emission and is similar to that of the early x-ray LCs. Therefore, it is likely that the steeply falling early optical emissions of these bursts are produced via the same mechanism as the early x-ray, i.e. the LAE from the γ-ray source (Panaitescu et al. 2006). This interpretation is also supported by the observations that for both these bursts the prompt emission spectrum below the peak is $f_{\nu} \propto \nu^{1/3}$.

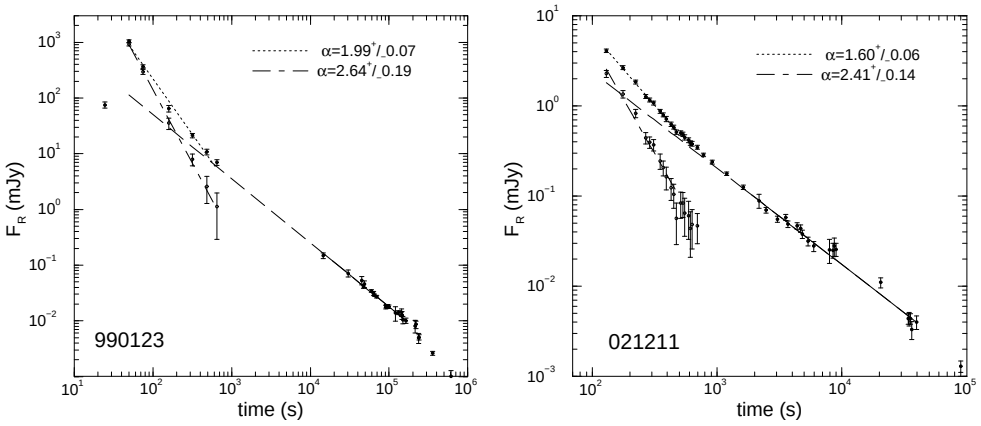

Figure 5.1 Left panel: Power-law fits to the early and late optical afterglow of GRB 990123. Dotted line shows a power-law fit to the ROTSE data at $50 - 10^3$ s after trigger, solid line is the power-law fit ($\alpha = 1.15 \pm 0.07$) to the forward-shock emission at $10^4 - 10^5$ s, which is back-extrapolated (dashed line) to the epoch of the ROTSE measurements. Dot-dashed line shows the fit to the ROTSE emission with the forward-shock subtracted – the residual flux declines as $t^{-2.64\pm0.19}$. Right panel: Power-law fits to the early and late optical afterglow of GRB 021211. Dotted line shows the fit to the KAIT data at 100–500 s, solid line is the fit ($\alpha = 1.07\pm0.04$) to the forward-shock emission at $10^3 - 4\times10^4$ s, which is back-extrapolated (dashed line) to the epoch of the early KAIT measurements. Dot-dashed line shows the fit to the KAIT emission with the forward-shock subtracted – the residual flux decays as $t^{-2.41\pm0.14}$.

Furthermore, a good fraction of *Swift* bursts have been followed in the optical starting at a few minutes after the burst and most of these have either weak optical flux or very stringent upper limit on the flux (Roming et al. 2006). Therefore, we lack evidence for the expected reverse-shock emission from a baryonic/leptonic ejecta. There are various possibilities to account for a dim reverse-shock emission including the obvious one that there is no reverse shock because the baryonic/leptonic component in GRB outflows is small and the bulk of the explosion energy is carried outward by magnetic fields.

5.2.3 Modeling GRB prompt emission

We can obtain further insights regarding γ-ray sources by modeling the average properties of the prompt emission in our set of GRBs. The basic procedure is to calculate the synchrotron and IC radiations for a relativistic, shock heated medium and compare this to the average burst spectrum and variability timescale. This synchrotron and IC radiation is completely described by five parameters: B, τ_e, Γ_0, N_e, and γ_i, which are respectively, magnetic field strength, optical depth of the source to Thompson scattering, the LF of the source, the total number of shocked electrons, and the lowest LF of electrons in the source comoving frame just behind the shock front; the electron distribution just behind the shock front is a power-law function of index p which is constrained by the observed high energy spectra. The distribution in the source as a whole has a more complicated shape due to radiative losses which we calculate using the five parameters. We determine which part of the 5D parameter space produces radiation matching the observed low energy spectral index, peak energy, flux at the peak, and average pulse duration of the GRBs in our sample. The solutions we find apply to any relativistic-shock heated medium – internal or external shocks.

We first attempt to describe the prompt emission of these 10 bursts with synchrotron radiation. The low energy (20-150 keV) spectral index for 6 of the 10 bursts is $0.5 < \beta_\gamma < 1$, and therefore the synchrotron cooling frequency (ν_c) should be larger than about 150 keV and the injection frequency ν_i below 20 keV. This constraint along with peak flux of 0.2 mJy and pulse duration of 10s

produces a 5D solution space with $\Gamma_0 > 600$ and $R_\gamma = (N_e \sigma_T / 4\pi\tau_e)^{1/2} \gtrsim 10^{17}$ cm (Figure 5.2). This is in contradiction to what we found using the steep x-ray light curve decay – $R_\gamma \lesssim 10^{16}$cm and bulk LF of < 100 (Table 5.2). This discrepancy suggests that synchrotron radiation from a relativistically shock heated medium (internal or external shocks) cannot describe the prompt γ-ray emission properties of the GRBs in our sample. For the remaining four GRBs, $1.2 < \beta_\gamma < 1.8$ and both ν_i and ν_c should be below 20 keV. The synchrotron solutions for this case for the most part are very similar to the previous synchrotron case. There are a few intriguing solutions consistent with the R_γ and Γ_0 found in the LAE calculation, but the prompt optical flux is very bright, and can also be ruled out. Therefore, we rule out synchrotron emission in shock heated medium as the mechanism for GRB prompt emission.[3]

Is it possible that the γ-rays were produced via synchrotron-self-Compton (SSC) process in a relativistic shock? We perform the 5D parameter space search for SSC radiation for both of the β_γ cases described above and find that (for either β_γ) the source radius R_γ and Γ_0 for the allowed 5D parameter space are consistent with the values we obtained for our sample in Table 5.2 (see Figure 5.2). The problem, however, is that the prompt optical flux with SSC is many orders of magnitude larger than the observational upper limits (Figure 5.2). It is very unlikely that this large flux has gone undetected because of dust extinction or bursts going off at very high redshifts (Roming

[3]Three assumptions were made in these calculations: electron pitch angle distribution is uniform; electrons are not continuously energized as they move downstream from the shock front; and B does not vary by a large factor across the source.

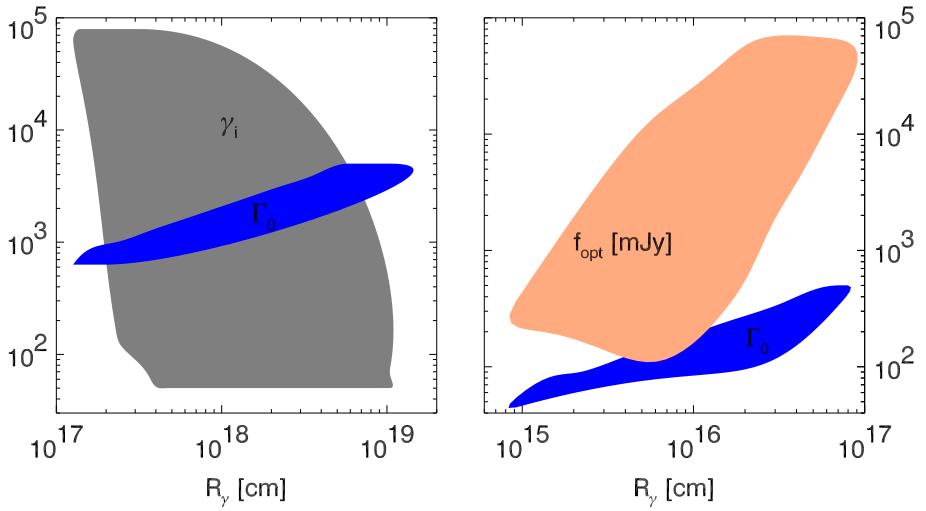

Figure 5.2 Left panel: the allowed range of value for R_γ, Γ_0 (the LF of the γ-ray source – blue band) and γ_i, the minimum LF of shocked electrons close to the shock front, for the case when the prompt GRB emission is produced via the synchrotron process. These results were obtained for a GRB pulse duration of 10 s, the flux at 100 keV of 0.2 mJy, cooling frequency (ν_c) greater than 150 keV and the synchrotron frequency ν_m corresponding to γ_i less than 20 keV, so that the spectrum in the BAT band corresponds to $f_\nu \propto \nu^{-(p-1)/2}$. For a GRB pulse duration of 1 s the minimum R_γ decreases by a factor of ~ 4 and the minimum Γ_0 increases by a factor of ~ 2. The allowed parameter space for synchrotron solution is found to be not very sensitive to the peak flux, ν_c and ν_m. The allowed range for R_γ & Γ_0 is very similar for the γ-ray fluxes measured for the 10 bursts in our sample, including the $\nu_m < \nu_c < 20$ keV (i.e. $f_\nu \propto \nu^{-p/2}$) case. For $\nu_c < \nu_m < 20$ keV, there are solutions consistent with the parameters shown in Table 5.2, but they lead to a too bright optical flux. The large range allowed for γ_i encompasses internal and external shock 'solutions'. Right panel: The allowed range of values for R_γ and Γ_0 in the case when the burst emission is synchrotron self-Compton case and for the same burst parameters as for the left panel. Also shown is the optical flux (in mJy) for the SSC solutions. 1mJy corresponds to an R-magnitude of 16.2; the upper limits on the optical flux for most GRBs in our sample is $\lesssim$0.1 mJy.

et al. 2006). Therefore, we conclude that GRB prompt emission is not due to the SSC process in relativistic shocks either. This means that synchrotron or SSC from any shock model has problems describing the γ-ray emission in any of the bursts in our sample – and that internal & external shocks can be ruled out as possible γ-ray emission mechanisms.

We have described a few problems with the external and internal shock models and, more generally, for any model based on shock physics. These together with the lack of evidence for baryonic outflow – no firm detection of reverse-shock emission in GRBs – suggests that GRB prompt emission is produced by some very different process. It either involves a very different kind of shock physics than we see during GRB afterglows, which seems unlikely, or γ-ray generation does not involve shocks, such as, for instance, would be the case when magnetic field transports the energy in GRB outflows and its dissipation produces the radiation we see cf. Usov (1992, 1994), Thompson (1994), Katz (1997), Mészáros and Rees (1997a), Wheeler et al. (2000, 2002), Vlahakis and Königl (2001); Spruit et al. (2001), and Lyutikov and Blandford (2003). The Poynting model has some attractive features such as high radiative efficiency, no reverse shock, large radius for γ-ray source (Lyutikov and Blandford 2003), and low baryon loading comes for free. The Poynting outflow, however, might have difficulty explaining the observed variability of GRB prompt light curve (personal communication, Piran).

5.3 Summary

The early x-ray data show that the gamma-ray source is short lived and turns off at a distance of $\sim 5 \times 10^{15}$ cm from the central explosion – which is found to be within a factor of ~ 10 of the forward shock radius at early times for all ten bursts in our sample. We have presented arguments that the prompt γ-ray emission is unlikely to be produced in the external or internal shocks or any mechanism based on shock heating of electrons. In their electromagnetic model, Lyutikov & Blandford (2003) find that γ-rays are generated at a distance of $\sim 3 \times 10^{16}$ cm from the central explosion, which is comparable to the value that we find. This could just be a coincidence but, considering the problems with shock based models, the lack of reverse-shock optical detection, and very high efficiency for γ-ray generation, we find the Poynting outflow model for GRBs to be an attractive possibility.

Chapter 6

A general method for modeling prompt gamma-ray burst emission

The[1] goal of this chapter is to provide a nearly model independent way of modeling the prompt γ-ray emission with synchrotron or synchrotron-self-Compton (SSC) processes. We determine the basic properties of the γ-ray source from the data, and then determine how these can be interpreted in currently popular models such as the internal/external shock model.

In the next section we provide the basic idea and details of the technique we use to model γ-ray emission (the idea in its early form can be found in Chapter 4), and in §6.2 & §6.3 we describe the synchrotron and SSC results, respectively.

6.1 Modeling γ-ray emission: basic idea and technical formalism

The starting point for our modeling of the prompt γ-ray emission in GRBs is the assumption that the radiation is produced via the synchrotron or

[1]Significant portions of this chapter were submitted for publication in MNRAS on June 27, 2007.

synchrotron-self-Compton processes[2] in a source moving relativistically outward from the inner engine. Figure 6.1 provides a cartoon description of our model. For a simple GRB light-curve (LC) consisting of a single peak we determine the average source properties corresponding to the time when the observed light curve peaks, and for a multi-peak GRB LC our calculation applies to individual pulses or spikes in the lightcurve.

The source property can be uniquely described by the following set of 5 parameters: the magnetic field strength (B) in Gauss, the number of radiating particles (N) i.e., electrons and positrons, the optical depth of the source to Thomson scattering (τ), the Lorentz factor of the source with respect to the rest frame of the GRB host galaxy (Γ), and the minimum electron energy[3] γ_i at the location where particles are accelerated (all the variables we use in this chapter are defined in table 6.1 for easy reference). In addition, the particle distribution above γ_i is taken to be a power-law function: $dn/d\gamma \propto \gamma^{-p}$. Particles cool as a result of radiative losses and with time, or as they travel away from the acceleration site, and the distribution function becomes steeper than the index p at some energy where radiative losses become important. We calculate the modified distribution self-consistently as discussed below. We constrain this 5D parameter space with at least 4 observed quantities – the νf_ν peak frequency ν_γ, the spectral index below ν_γ, the flux f_γ at ν_γ,

[2]Mechanisms such as the inverse-Compton scattering of "photospheric" emission from a hot fireball (cf. Lazzati et al. 2000; Broderick 2005) are not modeled by the approach we have adopted. And if it were to turn out that the GRB prompt emission is produced by such a mechanism then the work presented here is of little relevance.

[3]The electron energy is $\gamma_i m_e c^2$, however, for convenience we suppress the factor $m_e c^2$.

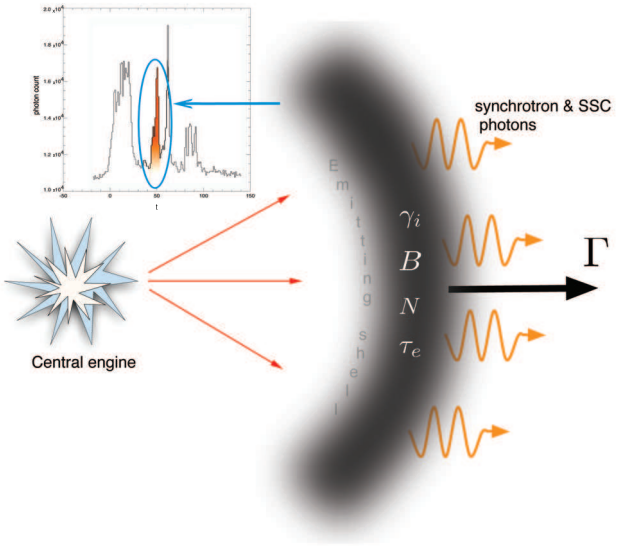

Figure 6.1 A schematic representation of our model. Assuming that radiation is synchrotron and inverse Compton, the γ-ray source properties can be described by five parameters $(\gamma_i, \Gamma, B, N, \tau)$ that determine the observed flux at one instance in time. We take this time to be the peak of a pulse in a GRB lightcurve. All of the calculations presented in this work apply to one single pulse in a typical GRB prompt lightcurve, as shown in the top left corner.

the duration of a single pulse in a GRB LC t_γ; p, the power law index, is constrained by the high energy spectral index, for $\nu > \nu_\gamma$.

A relativistic moving source of finite angular size θ_j (as seen by an observer at the center of explosion) can be treated as spherically symmetric as long as $\Gamma^{-1} < \theta_j$. The angular size determined from afterglow modeling suggests that θ_j is larger than about two degrees for all bursts for which we have good data (Frail et al. 2001; Panaitescu and Kumar 2001) and a number of lines of argument and evidence suggests that Γ is greater than about 100

Table 6.1 Definition of variables

γ_i	minimum electron LF in source comoving frame
Γ	bulk LF of the source
B	magnetic field strength, in Gauss, in source comoving frame
τ	optical depth to Thomson scattering
N	number of radiating electrons(isotropic equivalent)
α	The spectral index below the peak of νf_ν i.e. $f_\nu \propto \nu^\alpha$
γ_a	LF of electrons emitting synchrotron at ν_a
γ_c	LF of electrons emitting synchrotron at ν_c
Γ_{sh}	LF of the shocked gas wrt the unshocked gas
ν_γ	observed peak frequency of GRB νf_ν spectrum ($\nu_{\gamma_5} \equiv \nu_\gamma/10^5$eV)
ν_i	synchrotron injection frequency in observer frame ($\nu_{i_5} \equiv \nu_i/10^5$ eV)
ν_c	synchrotron cooling frequency in observer frame ($\nu_{c_5} \equiv \nu_c/10^5$ eV)
ν_a	synchrotron self absorption frequency in observer frame
ν_a^{ic}	SSC self absorption frequency, below which the f_ν^{ic} spectral index is +1
A_*	external medium wind parameter, $n = (A/m_p)r^{-2}$; $A_* \equiv A/5 \times 10^{11}$g cm^{-1}
$d_{L_{28}}$	luminosity distance in units of 10^{28} cm
$E_\pm$	kinetic energy of electrons and positrons (lab frame; isotropic equivalent)
E_B	energy in magnetic field (lab frame; isotropic equivalent)
E_{53}	isotropic equivalent of outflow energy in units of 10^{53} ergs
$f_{B/ke}$	$E_B/E_\pm$ – ratio of magnetic to $e^\pm$ energy
f_R	synchrotron prompt optical flux (in R band, at 2 eV)
f_x	synchrotron prompt x-ray flux, at 1 keV
f_γ	observed flux (in mJy) at ν_γ
f_{ν_p}	synchrotron flux at peak – $\min(\nu_i, \nu_c)$
n_0	density of circum-burst medium
n_e	comoving electron density in unshocked shell
p	power law index of electron energy distribution
R_γ	distance from center-of-explosion at which the radiation is produced
R_d	deceleration radius
t_γ	duration of one pulse in GRB light-curve (observer frame)
t_a	the time available for electrons to cool before being re-accelerated
Y	Compton parameter
z	redshift
η_i	γ_i/γ_c
η_a	γ_a/γ_i

(Piran 1992; Lithwick and Sari 2001). Therefore, we can treat the source for prompt γ-ray emission as spherically symmetric, and the numerical values we quote in this chapter are all isotropic equivalent quantities; for instance N is the total number of radiating particles in the source assuming the source to be spherically symmetric.

The synchrotron injection frequency, ν_i, corresponding to electron minimum energy γ_i, is

$$\nu_i = \frac{qB\gamma_i^2\Gamma}{2\pi m_e c(1+z)}, \tag{6.1}$$

(e.g. Rybicki and Lightman 1979; Wijers and Galama 1999), where q is electron charge, m_e the electron mass, c the speed of light, and z is the burst redshift. The synchrotron cooling frequency, ν_c, the characteristic frequency at which electrons cooling on a time scale t_a (observer frame) radiate, is

$$\nu_c = \frac{18\pi q m_e c(1+z)}{\sigma_T^2 B^3 \Gamma t_a^2 (1+Y)^2}. \tag{6.2}$$

where σ_T is the Thomson scattering cross-section, and Y the Compton parameter.

For most of the calculations in this work we assume that electrons are accelerated only once, and the time scale for acceleration is taken to be much less than the duration of a pulse in the GRB light-curve (t_γ). One time acceleration is, for instance, believed to apply to shocks where electrons are accelerated at the shock front and not while they travel downstream; the picture is likely very different in magnetic reconnection/dissipation. To capture some of the effects of multiple-times particle acceleration in time period of

a pulse duration in GRB LC we introduce a time scale, t_a, which is the average time in between two successive episodes of particle acceleration or the time available for electrons to cool in between acceleration; for one shot acceleration $t_a = t_\gamma$, and in the opposite limit of continuous acceleration $t_a = 0$ when the rate of energy gain is balanced by radiative loss rate. The electron distribution function resulting from the acceleration process is taken to be $dn/d\gamma_e \propto \gamma_e^{-p}$. The distribution function in the source as a whole is different due to the radiative cooling of electrons with time. The electron distribution function averaged over the source is described by two characteristic energies viz. γ_i and γ_c; $\gamma_c m_e c^2$ is the energy of electrons that cool on time scale t_a. The electron distribution for $\gamma_e > \max(\gamma_i, \gamma_c)$ is proportional to γ_e^{-p-1}, and the distribution between γ_c and γ_i (for $\gamma_c < \gamma_i$) is proportional to γ_e^{-2}. Electrons cool via synchrotron and inverse-Compton losses. The rate of loss of energy is affected by the synchrotron self-absorption frequency ν_a — electrons with characteristic synchrotron frequency below ν_a lose energy only via the inverse-Compton scattering process. We calculate γ_c and ν_a by solving a coupled set of equations as described in McMahon et al. (2006).

The synchrotron flux at the peak of the f_ν spectrum, at $\min[\nu_i, \nu_c]$, is given by

$$f_{\nu_p} = \frac{\sqrt{3} q^3 B N \Gamma}{4\pi d_L^2 m_e c^2}, \tag{6.3}$$

where d_L is the luminosity distance to the source. The effect of synchrotron self absorption is not included in the above expression for f_{ν_p}, and therefore the observed flux, in general, would be different from f_{ν_p}. The flux at other

frequencies are calculated as described in Sari et al. (1998).

The inverse-Compton flux (in observer frame) at frequency ν, $f^{ic}(\nu)$, is calculated using the following equation (c.f. Rybicki and Lightman 1979)

$$f^{ic}(\nu) = \frac{3}{4}\sigma_T \delta r \int \frac{d\nu_s}{\nu_s}\frac{\nu}{\nu_s} f(\nu_s) \int_{\gamma_1}^{\infty} d\gamma_e \frac{dn}{\gamma_e^2 d\gamma_e} F\left(\frac{\nu}{4\gamma_e^2 \nu_s}\right), \tag{6.4}$$

where $f(\nu_s)$ is the synchrotron flux per unit frequency in the observer frame, δr is the radial extent of the source (comoving frame) which is related to the optical depth τ (one of the five parameters we use to characterize the source), the function $F(x)$ is

$$F(x) = 2x \ln x + x + 1 - 2x^2, \qquad \text{for } 0 < x < 1, \tag{6.5}$$

and γ_1 is the minimum LF for electron distribution. We include the Klein-Nishina correction to the above expression when $\nu_s \gamma_e / \Gamma > m_e c^2$.

The expression for the Compton Y parameter is

$$Y = \sigma_T \int dr' \int d\gamma_e \gamma_e^2 \frac{dn_e}{d\gamma_e} = \frac{4}{3}\tau \left(\frac{p-1}{p-2}\right) \gamma_i^2 \xi \tag{6.6}$$

where the r'-integral is over the comoving radial width of the source and ξ is

$$\xi \equiv \left(\frac{p-1}{p-2}\right) \times \begin{cases} (\nu_c/\nu_i)^{\frac{1}{2}} & \gamma_c \ll \gamma_i \quad p > 2 \\ (\nu_c/\nu_i)^{3-p} (3-p)^{-1} & \gamma_i \ll \gamma_c \quad 2 < p < 3 \\ (p-3)^{-1} & \gamma_i \ll \gamma_c \quad p > 3 \\ p\,(p-1)^{-1} & \gamma_i \sim \gamma_c \quad p > 2. \end{cases} \tag{6.7}$$

In our 5D parameter space search, we limit the Compton Y-parameter for a synchrotron solution to be less than 10 and for an inverse-Compton solution $Y \lesssim 100$. The rationale for the constraint on the Y-parameter is that we want

an efficiency of $\gtrsim$10% in the γ-ray energy band of $\sim$ 10–400 keV; observations suggest this efficiency for a typical long duration burst from a comparison of energy in the γ-ray radiation and the kinetic energy of the ejecta determined from the afterglow observations (Panaitescu and Kumar 2002).

We can calculate the distance of the source from the center of explosion with 2 of the 5 parameters, N and τ:

$$R_\gamma = \left(\frac{N\sigma_T}{4\pi\tau}\right)^{1/2}. \tag{6.8}$$

The time duration of a pulse in GRB LC, in observer frame at redshift z, is

$$t_\gamma \approx \frac{R_\gamma(1+z)}{4c\Gamma^2}. \tag{6.9}$$

The total energy in the source consists of the kinetic energy of electrons and positrons ($E_\pm$) and the magnetic field (E_B):

$$E_\pm = N(p-1)\gamma_i m_e c^2\Gamma/(p-2), \qquad E_B = R_\gamma^3 B^2/6. \tag{6.10}$$

Note that $(p-1)\gamma_i m_e c^2/(p-2)$ is the average energy per electron/positron in the source comoving frame at the acceleration site, and in the calculation of E_B we took the comoving radial thickness of the source to be R_γ/Γ which is roughly what one expects for a causally connected source where particle random speed is close to the speed of light.

We do not make any assumptions regarding the energy in protons since protons do not contribute to the observed γ-ray radiation. This has the effect that the parameter space we determine is larger than it would be if protons

carried a substantial amount of energy since the energy available to $e^{\pm}$ would be smaller than the upper limit of 10^{55} erg (isotropic equivalent) we impose in our search for solutions in the 5D parameter space.

For a γ-ray source that arises from shock heated gas, the minimum electron energy behind the shock front, γ_i (one of the five parameters we use), can be related to the Lorentz factor of the shocked gas wrt the unshocked gas, Γ_{sh}. The minimum Γ_{sh} needed to produce γ_i is

$$\Gamma_{sh} = \left[\frac{m_e(p-1)}{m_p(p-2)}\right] 2\gamma_i, \tag{6.11}$$

where m_p (m_e) is proton (electron) mass. The factor 2 in the above expression is for the case where there is an energy equipartition between electrons and protons and there are no $e^{\pm}$ pairs in the plasma; Γ_{sh} will be larger if there are pairs or if electrons have less energy than protons.[4]

For a given set of 5 parameters, we calculate the synchrotron and SSC spectra. We determine the properties of the γ-ray source for a GRB by finding the region in the 5-D parameter space that satisfies the following set of observational constraints: 1) the frequency at the peak of the νf_ν spectrum (ν_γ); 2) the peak flux at ν_γ; 3) the spectral index above ν_γ – which constrains electron

[4]If there are "cold" protons and electrons in the shocked gas, i.e. only a fraction of particles in the shocked gas are accelerated, and electrons have more than $m_p c^2 \Gamma_{sh}$ energy, we would in that case overestimate Γ_{sh}. However, in this work we do not consider that there is a cold component to the γ-ray source since such a component would not radiate and affect observations and the solutions in the 5-D parameter space. Therefore, such a cold component, if present, would have little effect on all of the major results in this work; the only quantity affected by the cold component is the value for Γ_{sh} which is a peripheral quantity and not part of the central flow of the logic in this chapter.

index p – and the index below ν_γ; 4) the burst duration – for a GRB with a single pulse in the LC – or the duration of an individual pulse (t_γ) for GRBs with complicated LC; 5) optical and x-ray prompt flux or limit if available. The flux at a given observer time reflects the property of the source averaged over equal-arrival-time volume, therefore, the observed peak flux depends on the evolution of the source and this introduces uncertainty in the flux calculation by a factor of about two. For this reason we only require the theoretical flux to match the observed value to within a factor of ~ 2.

We now use this technique to find the 5D solution space and source property for GRBs produced via synchrotron (§3) and SSC (§4).

6.2 Synchrotron solutions

We consider in this section the parameter space of solutions when the observed γ-rays are produced via the synchrotron process.[5] First, we determine approximate solutions by analytically solving a system of equations for our 5 parameters $(\gamma_i, \Gamma, B, N, \tau)$ for the generic synchrotron case. The solutions for each parameter are expressed in terms of the Compton Y parameter and three observed quantities: the frequency ν_γ where νf_ν peaks, the γ-ray flux at this frequency (f_γ; in mJy), and the duration of a pulse in GRB LC (t_γ); Y

[5]It has been suggested that another radiation process, called jitter, might be responsible for γ-ray generation for those bursts that have low energy spectrum $f_\nu \propto \nu$ (Medvedev 2000). We show in appendix **B** that whenever jitter radiation dominates the observed flux to produce a $f_\nu \propto \nu$ spectrum the Compton-Y parameter is extremely large – $Y \gtrsim 10^6$ – and most of the energy of the explosion comes out in ~ 100 GeV SSC photons.

is a convenient and useful parameter because its value is expected to lie in a limited range, e.g. $Y \lesssim 1$ for the synchrotron solutions & $1 \lesssim Y \lesssim 10$ for the SSC process. Having the general synchrotron solutions in hand, we then apply the analytical results to the low energy spectral index cases of $\alpha = 1/3$, $\alpha = -1/2$ and $\alpha = -(p-1)/2$, compare the analytical and numerical results, and draw conclusions as to the process by which γ-rays are generated in GRBs; the spectral index α is defined by $f_\nu \propto \nu^\alpha$ for $\nu < \nu_\gamma$.

The 5 equations that we solve are those for the observer frame synchrotron injection frequency ν_i (6.1), the cooling frequency ν_c (6.2), the pulse duration (t_γ) (6.8 & 6.9), synchrotron flux f_{ν_p} in mJy at $\nu_p \equiv \min(\nu_i, \nu_c)$ (6.3), and the Compton Y parameter (6.6):

$$\nu_{i_5} = 1.1 \times 10^{-13} B \gamma_i^2 \Gamma (1+z)^{-1} \tag{6.12}$$

$$\nu_{c_5} = 6.6 \times 10^4 (1+z) B^{-3} \Gamma^{-1} t_a^{-2} (1+Y)^{-2} \tag{6.13}$$

$$\tau \approx 1.5 \times 10^8 N_{55} (1+z)^2 \Gamma^{-4} t_\gamma^{-2} \tag{6.14}$$

$$f_{\nu_p} = 110 B \Gamma N_{55} d_{L28}^{-2} (1+z)\,\mathrm{mJy} \tag{6.15}$$

where $\nu_{i_5} \equiv \nu_i / 10^5 \mathrm{eV}$, $\nu_{c_5} \equiv \nu_c / 10^5 \mathrm{eV}$, and $N_{55} \equiv N / 10^{55}$.

To solve Equations 6.12-6.15 & 6.6, we first eliminate N_{55} from equation (6.15) using equation (6.14), then eliminate τ using equation (6.6) to find

$$B \Gamma^5 \gamma_i^{-2} \approx 1.9 \times 10^6 f_{\nu_p} d_{L28}^2 (1+z) t_\gamma^{-2} Y^{-1} \xi. \tag{6.16}$$

Next, combining (6.16) & (6.12) we get

$$\gamma_i^{-4}\Gamma^4 \approx 2.1\times 10^{-7}\nu_{i_5}^{-1} f_{\nu_p} d_{L_{28}}^2 Y^{-1}\xi t_\gamma^{-2}. \tag{6.17}$$

Multiplying equations (6.12) and (6.13) together, we have

$$B\gamma_i^{-1} \approx 8.5\times 10^{-5} t_a^{-1}\nu_{c_5}^{-\frac{1}{2}}\nu_{i_5}^{-\frac{1}{2}}(1+Y)^{-1}. \tag{6.18}$$

We can eliminate γ_i from equations (6.17) and (6.18) by dividing equation (6.17) by (6.18) to the fourth power:

$$\Gamma^4 B^{-4} \approx 4.0\times 10^{9}\nu_{i_5}\nu_{c_5}^2 f_{\nu_p} d_{L_{28}}^2 Y^{-1}(1+Y)^4\xi t_a^4 t_\gamma^{-2} \tag{6.19}$$

And finally, if we multiply equation (6.19) by the fourth power of (6.16) and divide by the square of (6.17) we find the solution for Γ to be

$$\Gamma \approx 10^3\nu_{i_5}^{\frac{3}{16}}\nu_{c_5}^{\frac{1}{8}} f_{\nu_p}^{\frac{3}{16}} t_\gamma^{-\frac{3}{8}} t_a^{\frac{1}{4}} Y^{-\frac{3}{16}}(1+Y)^{\frac{1}{4}}\xi^{\frac{3}{16}} d_{L_{28}}^{\frac{3}{8}}(1+z)^{\frac{1}{4}}. \tag{6.20}$$

Using Γ, we can solve for γ_i, B, and τ:

$$\gamma_i \approx 4.7\times 10^4\nu_{i_5}^{\frac{7}{16}}\nu_{c_5}^{\frac{1}{8}} f_{\nu_p}^{-\frac{1}{16}} t_\gamma^{\frac{1}{8}} t_a^{\frac{1}{4}} Y^{\frac{1}{16}}(1+Y)^{\frac{1}{4}}\xi^{-\frac{1}{16}} d_{L_{28}}^{-\frac{1}{8}}(1+z)^{\frac{1}{4}} \tag{6.21}$$

$$B \approx 4.0\nu_{i_5}^{-\frac{1}{16}}\nu_{c_5}^{-\frac{3}{8}} f_{\nu_p}^{-\frac{1}{16}} t_\gamma^{\frac{1}{8}} t_a^{-\frac{3}{4}} Y^{\frac{1}{16}}(1+Y)^{-\frac{3}{4}}\xi^{-\frac{1}{16}} d_{L_{28}}^{-\frac{1}{8}}(1+z)^{\frac{1}{4}}\ \text{Gauss} \tag{6.22}$$

$$\tau \approx 3.3\times 10^{-10}\nu_{i_5}^{-\frac{7}{8}}\nu_{c_5}^{-\frac{1}{4}} f_{\nu_p}^{\frac{1}{8}} t_\gamma^{-\frac{1}{4}} t_a^{-\frac{1}{2}} Y^{\frac{7}{8}}(1+Y)^{-\frac{1}{2}}\xi^{-\frac{7}{8}} d_{L_{28}}^{\frac{1}{4}}(1+z)^{-\frac{1}{2}}. \tag{6.23}$$

Equations (6.20)–(6.23) provide approximate solutions for $(\gamma_i, \Gamma, B, N, \tau)$ when the synchrotron process produces the observed γ-ray radiation; more accurate solutions for these parameters are obtained by numerical calculations and the

results are shown in Figures 6.2–6.8. These general solutions can be used to investigate different cases of low energy spectral indices (α) by adopting appropriate values for ν_{i_5} and ν_{c_5}. The full dependences on these two frequencies are not completely shown here – each case of α has a different functional dependence on ξ, and ξ is a function of ν_i and ν_c.

Note that f_{ν_p} is not the observed flux at ν_γ, the peak of γ-ray spectrum, but is the flux at $\min(\nu_i, \nu_c) \equiv \nu_p$, and the effect of synchrotron-self-absorption, if any, at ν_p has been ignored. Since the dependence of the parameters Γ, γ_i etc. on f_{ν_p} is very weak (eqs. 6.20–6.23), we do not worry about the difference between f_{ν_p} & f_γ at this point, even though f_{ν_p} can be much greater than f_γ (the flux at the peak frequency $\nu_\gamma = \max[\nu_i, \nu_c]$).

Using the parameter solutions, we can derive the distance of the γ-ray source from the center of explosion (R_γ), the LF of the shock front (Γ_{sh}) if electrons are accelerated in a relativistic shock, and the energy in the magnetic field and electrons. The radius $R_\gamma = 2c\Gamma^2 t_\gamma (1+z)^{-1}$ is found to be

$$R_\gamma \approx 6.0 \times 10^{16} \nu_{i_5}^{\frac{3}{8}} \nu_{c_5}^{\frac{1}{4}} f_{\nu_p}^{\frac{3}{8}} t_\gamma^{\frac{1}{4}} t_a^{\frac{1}{2}} Y^{-\frac{3}{8}} (1+Y)^{\frac{1}{2}} \xi^{\frac{3}{8}} d_{L_{28}}^{\frac{3}{4}} (1+z)^{-\frac{1}{2}} \text{ cm} \qquad (6.24)$$

and should be compared to the deceleration radius (R_d) of the GRB outflow in both a homogeneous external medium with particle number density n_0, and a wind external medium where the particle number density is given by $(A/m_p)r^{-2}$ (these are two special cases of a power law density stratification –

the density varying as r^{-s} – corresponding to $s = 0$ & $s = 2$)

$$R_d = \begin{cases} 1.2 \times 10^{17} E_{53}^{\frac{1}{3}} n_0^{-\frac{1}{3}} \Gamma_2^{-\frac{2}{3}} \quad \text{cm} \quad s = 0 \\ \\ 1.8 \times 10^{15} E_{53} A_*^{-1} \Gamma_2^{-2} \quad \text{cm} \quad s = 2 \end{cases} \tag{6.25}$$

where E_{53} is the isotropic equivalent energy in GRB-ejecta in units of 10^{53} ergs, $\Gamma_2 = \Gamma/100$, and $A_* = A/(5 \times 10^{11} \text{g cm}^{-1})$. Substituting in the solution for Γ, we find R_d to be

$$R_d \approx \begin{cases} 2.6 \times 10^{16} E_{53}^{\frac{1}{3}} n_0^{-\frac{1}{3}} \nu_{i_5}^{-\frac{1}{8}} \nu_{c_5}^{-\frac{1}{12}} f_{\nu_p}^{-\frac{1}{8}} t_\gamma^{\frac{1}{4}} t_a^{-\frac{1}{6}} Y^{\frac{1}{8}} (1+Y)^{-\frac{1}{6}} \xi^{-\frac{1}{8}} d_{L_{28}}^{-\frac{1}{4}} (1+z)^{-\frac{1}{6}} \text{cm} \\ \quad s = 0 \\ \\ 1.8 \times 10^{13} E_{53} A_*^{-1} \nu_{i_5}^{-\frac{3}{8}} \nu_{c_5}^{-\frac{1}{4}} f_{\nu_p}^{-\frac{3}{8}} t_\gamma^{\frac{3}{4}} t_a^{-\frac{1}{2}} Y^{\frac{3}{8}} (1+Y)^{-\frac{1}{2}} \xi^{-\frac{3}{8}} d_{L_{28}}^{-\frac{3}{4}} (1+z)^{\frac{1}{2}} \text{cm} \\ \quad s = 2 \end{cases} \tag{6.26}$$

The LF of the shocked fluid wrt to the unshocked material, given by equation (6.11), is

$$\Gamma_{sh} \approx 26\, \varepsilon_e^{-1} \left(\frac{p-1}{p-2} \right) \nu_{i_5}^{\frac{7}{16}} \nu_{c_5}^{\frac{1}{8}} f_{\nu_p}^{-\frac{1}{16}} t_\gamma^{\frac{1}{8}} t_a^{\frac{1}{4}} Y^{\frac{1}{16}} (1+Y)^{\frac{1}{4}} \xi^{-\frac{1}{16}} d_{L_{28}}^{-\frac{1}{8}} (1+z)^{\frac{1}{4}}, \tag{6.27}$$

where ε_e is the ratio of energy in electrons and the total thermal energy in the γ-ray source.

The magnetic and $e^\pm$ energies, given by equation (6.10), are found to be

$$E_B \approx 1.9 \times 10^{51}\, \nu_{i_5} f_{\nu_p} t_\gamma Y^{-1} \xi d_{L_{28}}^2 (1+z)^{-1} \text{ ergs} \tag{6.28}$$

and

$$E_\pm \approx 8.5 \times 10^{50} \left(\frac{p-1}{p-2} \right) \nu_{i_5}^{\frac{1}{2}} \nu_{c_5}^{\frac{1}{2}} f_{\nu_p} t_a (1+Y) d_{L_{28}}^2 (1+z)^{-1} \text{ ergs.} \tag{6.29}$$

Since the dependence of the above two quantities on f_{ν_p} is linear, we should replace f_{ν_p} with f_γ, the flux observed at ν_γ. This will be done in the following sections, since the expression for f_γ depends on α.

We now apply the results obtained in this section to each possible synchrotron low energy spectral index α.

6.2.1 Synchrotron solutions when the low energy spectrum is $\nu^{-\frac{(p-1)}{2}}$

We use equation (6.7) to eliminate ξ from the analytical solutions given by equations 6.20–6.23 for the $\gamma_i \ll \gamma_c$ & $2 < p < 3$ case, and substitute $\nu_{\gamma_5} = \nu_{c_5}$ & $f_{\nu_p} = f_\gamma(\nu_{\gamma_5}/\nu_{i_5})^{\frac{(p-1)}{2}}$, to find that synchrotron solutions for $\alpha = -\frac{(p-1)}{2}$ are:

$$\Gamma \approx 10^3 \nu_{\gamma_5}^{\frac{19-3p}{32}} f_\gamma^{\frac{3}{16}} t_\gamma^{-\frac{3}{8}} \nu_{i_5}^{\frac{3p-9}{32}} t_a^{\frac{1}{4}} Y^{-\frac{3}{16}} (1+Y)^{\frac{1}{4}} (1+z)^{\frac{1}{4}} d_{L_{28}}^{\frac{3}{8}} A_{1p}^{\frac{3}{16}} \quad (6.30)$$

$$\gamma_i \approx 4.7 \times 10^4 \nu_{\gamma_5}^{\frac{p-1}{32}} f_\gamma^{-\frac{1}{16}} t_\gamma^{\frac{1}{8}} \nu_{i_5}^{\frac{19-p}{32}} t_a^{\frac{1}{4}} Y^{\frac{1}{16}} (1+Y)^{\frac{1}{4}} (1+z)^{\frac{1}{4}} d_{L_{28}}^{-\frac{1}{8}} A_{1p}^{-\frac{1}{16}} \quad (6.31)$$

$$B \approx 4.0 \nu_{\gamma_5}^{\frac{p-17}{32}} f_\gamma^{-\frac{1}{16}} t_\gamma^{\frac{1}{8}} \nu_{i_5}^{\frac{3-p}{32}} t_a^{-\frac{3}{4}} Y^{\frac{1}{16}} (1+Y)^{-\frac{3}{4}} (1+z)^{\frac{1}{4}} d_{L_{28}}^{-\frac{1}{8}} A_{1p}^{-\frac{1}{16}} \text{ Gauss} \quad (6.32)$$

$$\tau \approx 3.3 \times 10^{-10} \nu_{\gamma_5}^{\frac{15p-47}{16}} f_\gamma^{\frac{1}{8}} t_\gamma^{-\frac{1}{4}} \nu_{i_5}^{\frac{29-15p}{16}} t_a^{-\frac{1}{2}} Y^{\frac{7}{8}} (1+Y)^{-\frac{1}{2}} (1+z)^{-\frac{1}{2}} d_{L_{28}}^{\frac{1}{4}} A_{1p}^{-\frac{7}{8}} \quad (6.33)$$

where

$$A_{1p} \equiv \frac{(p-1)}{(p-2)\,(3-p)}, \quad (6.34)$$

and we should emphasize that t_γ is **not** the burst duration – it is the width of a single spike in the GRB prompt-lightcurve.

For a typical long duration GRB with $f_\gamma = 1$mJy, $\nu_\gamma = 100$keV, $t_\gamma = 0.1$s, $z = 1$, $d_{L_{28}} = 2$, and $t_a \sim t_\gamma$ – henceforth we will refer to a GRB with these observed parameters as *GRB-♮* – the 5-parameters of the γ-ray source $(\gamma_i, \Gamma, B, N, \tau)$ are obtained from equations 6.30–6.33 and are given by

$$\Gamma \gtrsim 3.2 \times 10^3 Y^{-\frac{3}{16}} (1+Y)^{\frac{1}{4}} \tag{6.35}$$

$$\gamma_i \lesssim 6.0 \times 10^3 Y^{\frac{1}{16}} (1+Y)^{\frac{1}{4}} \tag{6.36}$$

$$B \lesssim 16 Y^{\frac{1}{16}} (1+Y)^{-\frac{3}{4}} \text{ Gauss} \tag{6.37}$$

$$\tau \gtrsim 4.7 \times 10^{-9} Y^{\frac{7}{8}} (1+Y)^{-\frac{1}{2}}. \tag{6.38}$$

In deriving these inequalities we took $p = 2.5$, $\nu_c = \nu_\gamma = 100$ keV, and $\nu_{i_5} < 0.1$.

The dependence of Γ, γ_i, B & τ on Y is weak, so the coefficients in above expressions are reasonable estimates for the γ-ray source basic physical parameters for *GRB-♮*. We see that the γ-ray source LF, Γ, is required to be rather large – $\Gamma \gtrsim 3 \times 10^3$ – if the radiation is to be produced via the synchrotron process. This large Γ is not consistent with afterglow modeling, which gives a value of a few hundred or less (Panaitescu and Kumar 2002). Furthermore, as shown below, the distance of γ-ray source from the center of explosion turns out to be larger than the deceleration radius for this large Γ value, unless n_0 is very small. This suggests that the synchrotron solution is internally inconsistent; after the deceleration radius Γ is a function of N, γ_i and n_0 and is no longer

an independent parameter as considered in these derivations. The possibility that $R_\gamma > R_d$ is also ruled out by early x-ray and optical afterglow data that show that γ-rays precede the declining afterglow flux that is produced by a decelerating forward shock.

The distance of the γ-ray source from the center of explosion, $R_\gamma \approx 2ct_\gamma\Gamma^2/(1+z)$, is calculated using eq. (6.30), and is given by

$$R_\gamma \approx 6.0\times10^{16}\quad \nu_{\gamma_5}^{\frac{19-3p}{16}} f_\gamma^{\frac{3}{8}} t_\gamma^{\frac{1}{4}} \nu_{i_5}^{\frac{3p-9}{16}} t_a^{\frac{1}{2}} Y^{-\frac{3}{8}}(1+Y)^{\frac{1}{2}}(1+z)^{-\frac{1}{2}} d_{L_{28}}^{\frac{3}{4}} A_{1p}^{\frac{3}{8}} \text{ cm} \quad (6.39)$$

or $R_\gamma \sim 3\times10^{16}\, Y^{-\frac{3}{8}}(1+Y)^{\frac{1}{2}}$ cm for *GRB-♮*.

We now compare these analytical estimates to the numerically computed solution space for synchrotron radiation. A numerical search of the allowed region of the 5-D parameter space that satisfies the observational constraints (ν_γ, f_γ & t_γ; the same constraints that we used in the derivation of analytical expressions), confirms that for synchrotron solutions $R_\gamma \gtrsim 10^{16}$cm, $\Gamma \gtrsim 10^3$, and $10 \lesssim \gamma_i \lesssim 10^4$ (see fig. 6.2). We have considered a wide range of values of peak frequency (ν_γ), γ-ray flux at the peak, and pulse duration, to see if we can find some viable synchrotron solutions for any GRBs with $\alpha = -(p-1)/2$. These solutions are shown in Figure 6.2. We find that by decreasing any of the observable parameters R_γ decreases, but the dependence is weak in agreement with the scaling given in equation (6.39). Furthermore, a decrease in t_γ reduces Γ as expected from equation (6.30), but even for $t_\gamma = 10$ ms, Γ is still $\gtrsim 10^3$.

We next calculate the deceleration radius and compare it with R_γ to

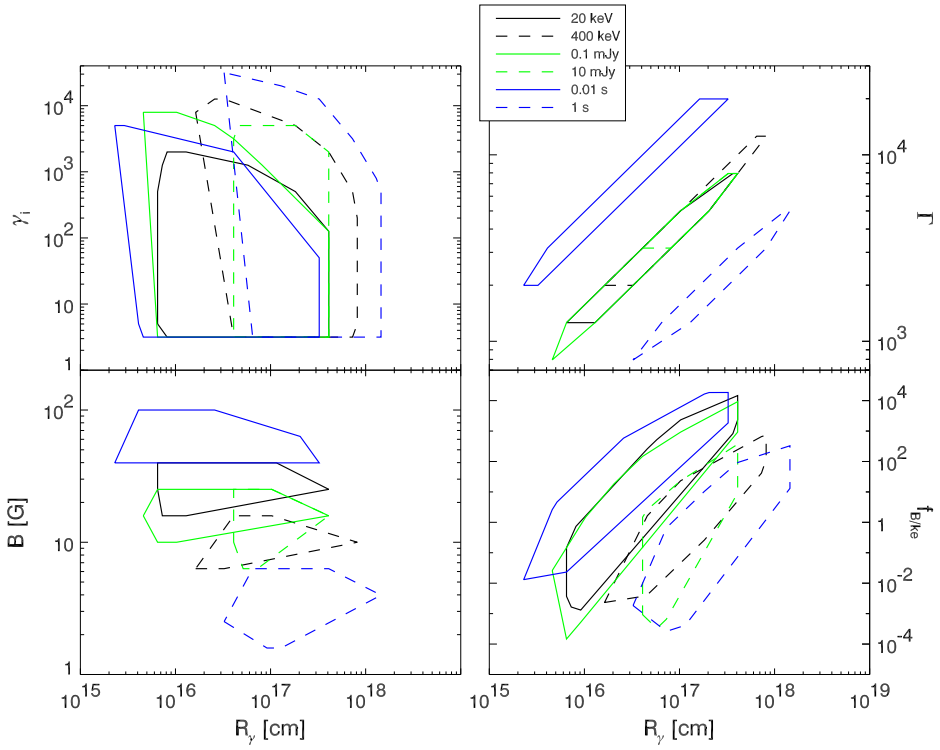

Figure 6.2 Results of numerical calculation for the allowed synchrotron solution space when the spectrum below the peak of νf_ν, at ν_γ, is: $f_\nu \propto \nu^{-(p-1)/2}$ for $\nu < \nu_\gamma$. A point in the 5-D parameter space $(\gamma_i, \Gamma, B, N, \tau)$ is considered an allowed solution for the observed GRB parameters (ν_γ, f_γ, t_γ, α) provided that ν_γ is within a factor 2 of the observed value, the pulse duration (t_γ) & flux at ν_γ (f_γ) are within a factor 1.5 & 3 of the observed value respectively; the larger tolerance on flux is due to larger error in flux calculation. The x-axis shows the distance of the γ-ray source from the center of the explosion. The top left panel is γ_i – the minimum LF of electrons in source comoving frame at the site where they are accelerated (electron distribution function for $\gamma_e > \gamma_i$ is: $dn_e/d\gamma_e \propto \gamma_e^{-2.5}$ i.e. $p = 2.5$). The top right panel shows the bulk LF of the source, the bottom left panel shows the comoving magnetic field in Gauss, and the bottom right panel shows the ratio of energy in the magnetic field and electrons. For all of the numerical calculations we took the burst redshift $z = 1$. Legend shows several different cases of GRBs corresponding to different observed values for ν_γ, f_γ, and t_γ. Only one observational parameter – that noted in the legend – is changed at a time, all the remaining parameters are left unchanged; the base value for the parameters is same as we took for *GRB-*♮, i.e. $\nu_\gamma = 100$ keV, $f_\gamma = 1$mJy, $t_\gamma = 0.1$s, and $t_a = t_\gamma$. For instance, for the 20 keV case, denoted by the solid black line, $\nu_\gamma = 20$keV, and f_γ & t_γ are same as for *GRB-*♮ i.e. 1 mJy and 0.1 s respectively.

ensure $R_\gamma < R_d$ for self consistent solutions. The deceleration radius for GRB-ejecta is calculated using eq. (6.26) and is given by

$$R_d \approx \begin{cases} 2.6\times10^{16}\, E_{53}^{\frac{1}{3}} n_0^{-\frac{1}{3}} \nu_{\gamma_5}^{\frac{3p-19}{48}} f_\gamma^{-\frac{1}{8}} t_\gamma^{\frac{1}{4}} \nu_{i_5}^{\frac{3-p}{16}} t_a^{-\frac{1}{6}} Y^{\frac{1}{8}} (1+Y)^{-\frac{1}{6}} (1+z)^{-\frac{1}{6}} d_{L_{28}}^{-\frac{1}{4}} A_{1p}^{-\frac{1}{8}} \text{cm} \\ \quad s=0 \\ \\ 1.8\times10^{13}\, E_{53} A_*^{-1} \nu_{\gamma_5}^{\frac{3p-19}{16}} f_\gamma^{-\frac{3}{8}} t_\gamma^{\frac{3}{4}} \nu_{i_5}^{\frac{9-3p}{16}} t_a^{-\frac{1}{2}} Y^{\frac{3}{8}} (1+Y)^{-\frac{1}{2}} (1+z)^{-\frac{1}{2}} d_{L_{28}}^{-\frac{3}{4}} A_{1p}^{-\frac{3}{8}} \text{cm} \\ \quad s=2 \end{cases} \tag{6.40}$$

and the ratio of R_γ and R_d is:

$$\frac{R_\gamma}{R_d} \approx \begin{cases} 2.3 E_{53}^{-\frac{1}{3}} n_0^{\frac{1}{3}} \nu_{\gamma_5}^{\frac{19-3p}{12}} f_\gamma^{\frac{1}{2}} \nu_{i_5}^{\frac{p-3}{4}} t_a^{\frac{2}{3}} Y^{-\frac{1}{2}} (1+Y)^{\frac{2}{3}} (1+z)^{-\frac{1}{3}} d_{L_{28}} A_{1p}^{\frac{1}{2}} & s=0 \\ \\ 3.3\times10^3 E_{53}^{-1} A_* \nu_{\gamma_5}^{\frac{19-3p}{8}} f_\gamma^{\frac{3}{4}} t_\gamma^{-\frac{1}{2}} \nu_{i_5}^{\frac{3p-9}{8}} t_a Y^{-\frac{3}{4}} (1+Y) d_{L_{28}}^{\frac{3}{2}} A_{1p}^{\frac{3}{4}} & s=2 \end{cases} \tag{6.41}$$

Substituting in the observable parameters for *GRB-♮* into the above equation and solving for n_0 & A_* such that $R_\gamma/R_d < 1$, we find

$$n_0 < 0.057 E_{53} (t_a/t_\gamma)^{-2} Y^{\frac{3}{2}} (1+Y)^{-2}\ \text{cm}^{-3} \quad s=0 \tag{6.42}$$

$$A_* < 5.5\times10^{-5} E_{53} (t_a/t_\gamma)^{-1} Y^{\frac{3}{4}} (1+Y)^{-1} \quad s=2 \tag{6.43}$$

Note that n_0 & A_* must be very small to ensure that $R_\gamma < R_d$, especially for $Y < 1$ expected of synchrotron solutions. Figure (6.3) shows the results of numerical calculations which confirms these analytical estimates. Moreover, if we want $R_\gamma/R_d \lesssim 0.5$, in order to have a clear separation between internal and external shocks, then $n_0 \lesssim 10^{-2}\text{cm}^{-3}$. Therefore, self-consistent synchrotron solutions with $R_\gamma \lesssim R_d$ require very low density for the circumstellar medium

compared with $n_0 \sim 1$ cm^{-3} obtained from afterglow modeling (Panaitescu and Kumar 2001). The limit on n_0 can be increased by decreasing t_a (see eq. 6.42). Numerical result for the upper limit on n_0 when $t_a = t_\gamma/100$ is shown in fig. 6.3. It confirms the analytical result that $n_0 \sim 1$ cm^{-3} can give $R_\gamma < R_d$ provided that $t_a \ll t_\gamma$. It should be noted that for systems involving shock heating of particles we expect $t_a \sim t_\gamma$ because electrons are accelerated at the shock front and there is no subsequent acceleration as particles travel downstream; in magnetic reconnections or dissipation it is natural to expect $t_a \ll t_\gamma$.

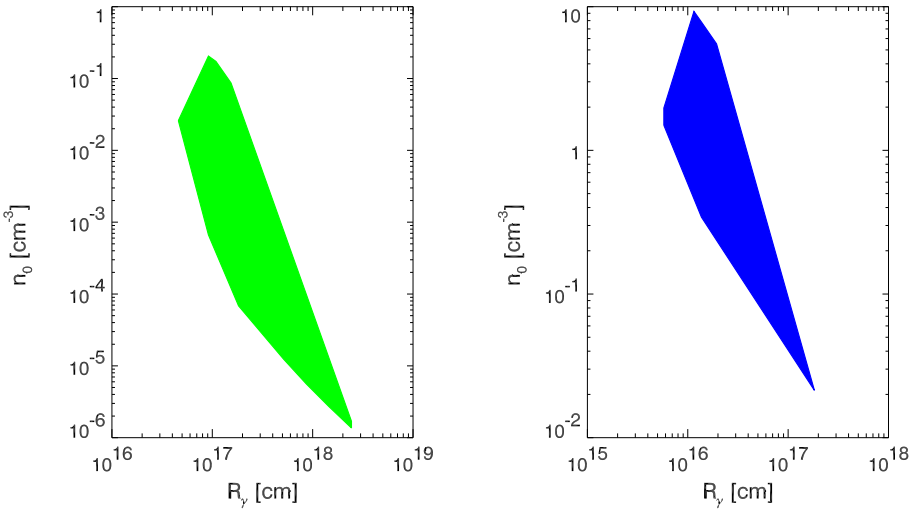

Figure 6.3 *Left panel:* the upper limit to the ISM density (n_0) for synchrotron solutions with $\alpha = -(p-1)/2$ for a burst with $\nu_\gamma = 100$ keV, $f_\gamma = 1$ mJy, $t_\gamma = 1$ s & $t_a = t_\gamma$. *Right panel:* same as the left panel except that $t_a = t_\gamma/100$. Note that by decreasing the amount of time electrons have to radiate away their energy before being re-accelerated (t_a) increases the max(n_0) roughly as t_a^{-1}. The n_0 upper limit decreases when any of the GRB parameters (ν_γ, f_γ, t_γ) is increased; $n_0 \propto f_\gamma^{-1}$.

We now estimate the ratio of energy in $e^{\pm}$ and magnetic field to find out if it is much less than unity or not when $t_a < t_\gamma$ (a small value for $E_\pm/E_B$ results in low efficiency for γ-ray generation). The ratio $E_\pm/E_B$ can be calculated using eqs. (6.28) & (6.29) and is given by

$$\frac{E_\pm}{E_B} \approx 1.5(3-p)\left(\frac{\nu_{\gamma_5}}{\nu_{i_5}}\right)^{p-\frac{5}{2}}\left[\frac{t_a}{t_\gamma}\right] Y(1+Y), \tag{6.44}$$

for $2 < p < 3$ (numerical calculations take $p = 2.5$). For the solution space corresponding to $\alpha = -(p-1)/2$, $0.1 \lesssim \nu_\gamma/\nu_i \lesssim 10^5$ and so $E_\pm > E_B$ even when $t_a/t_\gamma \sim 10^{-2}$. Therefore, small t_a/t_γ solutions are fine from the point of radiative efficiency; the above equation needs to be modified, when $t_a \ll t_\gamma$, to include the total energy input in electrons during a GRB pulse width of t_γ, which will further improve the radiative efficiency when t_a/t_γ is very small.

The reason that these synchrotron solutions have large R_γ is not hard to understand. It requires a certain minimum number of electrons to produce the observed flux of $f_\gamma \sim 1$ mJy at $\nu_\gamma \sim 100$ keV: $N \sim 10^{53}/(B\Gamma)$ – see eq. 6.15. And in order to keep the Compton-Y parameter, $Y \sim \tau\gamma_i\gamma_c$, less ~ 10 — otherwise most of the energy will come out in IC-scattered photons at $\nu \gg 1$ MeV — we must have large R_γ for the source. The solution offered by $t_a \ll t_\gamma$ is also easy to understand. Frequent re-acceleration of charge particles makes it possible to have larger magnetic field while keeping $\nu_c \gtrsim 100$ keV. This decreases the number of particles required to produce the observed flux f_γ, and that in turn makes it possible to have a smaller R_γ.

We conclude that the synchrotron process in a shock heated medium

cannot account for the prompt γ-ray emission of long-duration GRBs with low energy spectrum $f_\nu \propto \nu^{-\frac{p-1}{2}}$. However, synchrotron solutions appear to be viable when $t_a \ll t_\gamma$, i.e. when electrons are accelerated repeatedly, as might occur when magnetic field is dissipated and the energy is deposited in $e^{\pm}$.

6.2.2 Synchrotron solution when the low energy spectrum is $\nu^{\frac{1}{3}}$

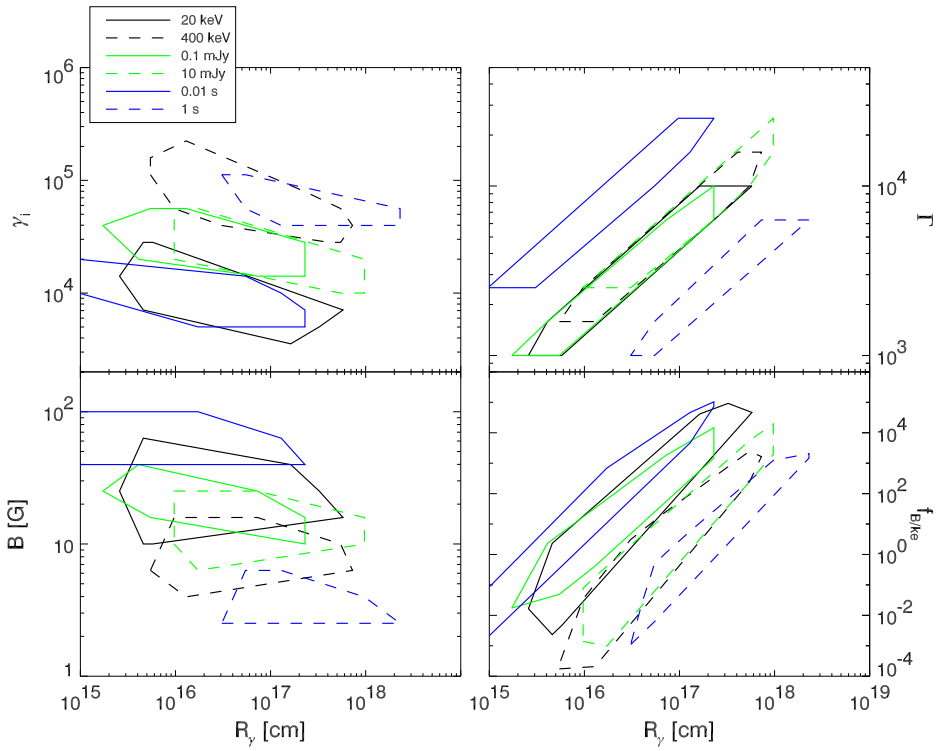

Figure 6.4 Synchrotron solution space when the spectrum below ν_γ, the peak of νf_ν, is $f_\nu \propto \nu^{1/3}$, i.e. $\alpha = 1/3$. See Figure 6.2 caption for details.

This is a special case of $\alpha = -(p-1)/2$ analyzed in the previous

subsection (§6.2.1) when $\gamma_i \sim \gamma_c$; the solutions are a subset of those found in §6.2.1. The analytical solutions for this case, obtained by substituting $\xi = \frac{p}{(p-2)}$ (see eq. 6.7), $\nu_{i_5} \sim \nu_{c_5} = \nu_{\gamma_5}$, and $f_\gamma \sim f_{\nu_p}$, into equations 6.20–6.23 are

$$\Gamma \approx 10^3 \nu_{\gamma_5}^{\frac{5}{16}} f_\gamma^{\frac{3}{16}} t_\gamma^{-\frac{3}{8}} t_a^{\frac{1}{4}} Y^{-\frac{3}{16}} (1+Y)^{\frac{1}{4}} (1+z)^{\frac{1}{4}} d_{L_{28}}^{\frac{3}{8}} \left[\frac{p}{p-2}\right]^{\frac{3}{16}} \quad (6.45)$$

$$\gamma_i \approx 4.7 \times 10^4 \nu_{\gamma_5}^{\frac{9}{16}} f_\gamma^{-\frac{1}{16}} t_\gamma^{\frac{1}{8}} t_a^{\frac{1}{4}} Y^{\frac{1}{16}} (1+Y)^{\frac{1}{4}} (1+z)^{\frac{1}{4}} d_{L_{28}}^{-\frac{1}{8}} \left[\frac{p}{p-2}\right]^{-\frac{1}{16}} \quad (6.46)$$

$$B \approx 4.0 \nu_{\gamma_5}^{-\frac{7}{16}} f_\gamma^{-\frac{1}{16}} t_\gamma^{\frac{1}{8}} t_a^{-\frac{3}{4}} Y^{\frac{1}{16}} (1+Y)^{-\frac{3}{4}} (1+z)^{\frac{1}{4}} d_{L_{28}}^{-\frac{1}{8}} \left[\frac{p}{p-2}\right]^{-\frac{1}{16}} \text{ Gauss} \quad (6.47)$$

$$\tau \approx 3.3 \times 10^{-10} \nu_{\gamma_5}^{-\frac{9}{8}} f_\gamma^{\frac{1}{8}} t_\gamma^{-\frac{1}{4}} t_a^{-\frac{1}{2}} Y^{\frac{7}{8}} (1+Y)^{-\frac{1}{2}} (1+z)^{-\frac{1}{2}} d_{L_{28}}^{\frac{1}{4}} \left[\frac{p}{p-2}\right]^{-\frac{7}{8}}. \quad (6.48)$$

Substituting $f_\gamma = 1$mJy, $\nu_{\gamma_5} = 1$, $t_\gamma = 0.1$s (the observed parameters for *GRB-♮*), & $t_a \sim t_\gamma$, in these equations, we find

$$\Gamma \sim 2.5 \times 10^3 \, Y^{-\frac{3}{16}} (1+Y)^{\frac{1}{4}} \quad (6.49)$$

$$\gamma_i \sim 2 \times 10^4 \, Y^{\frac{1}{16}} (1+Y)^{\frac{1}{4}} \quad (6.50)$$

$$B \sim 18 \, Y^{\frac{1}{16}} (1+Y)^{-\frac{3}{4}} \text{ Gauss} \quad (6.51)$$

$$\tau \sim 6.3 \times 10^{-10} \, Y^{\frac{7}{8}} (1+Y)^{-\frac{1}{2}} \quad (6.52)$$

and indeed, the solutions are a subset of the $\alpha = -(p-1)/2$ solution space – these have smaller τ and larger Γ & γ_i. The distance of the source from the

center of the explosion is:

$$R_\gamma \approx 6.0\times10^{16}\,\nu_{\gamma_5}^{\frac{5}{8}} f_\gamma^{\frac{3}{8}} t_\gamma^{\frac{1}{4}} t_a^{\frac{1}{2}} Y^{-\frac{3}{8}} (1+Y)^{\frac{1}{2}} (1+z)^{-\frac{1}{2}} d_{L_{28}}^{\frac{3}{4}} \left[\frac{p}{p-2}\right]^{\frac{3}{8}} \text{ cm} \quad (6.53)$$

or $R_\gamma \sim 2\times10^{16}\,Y^{-\frac{3}{8}}(1+Y)^{\frac{1}{2}}$ cm for *GRB-♮*. This case has the same problems as $\alpha = -(p-1)/2$ case discussed in §6.2.1 i.e., large R_γ and Γ, and requiring extremely small external density in order that $R_\gamma \lesssim R_d$. Also, the conclusions drawn in §6.2.1 regarding $t_a/t_\gamma \ll 1$ offering a way out of this problem apply here as well.

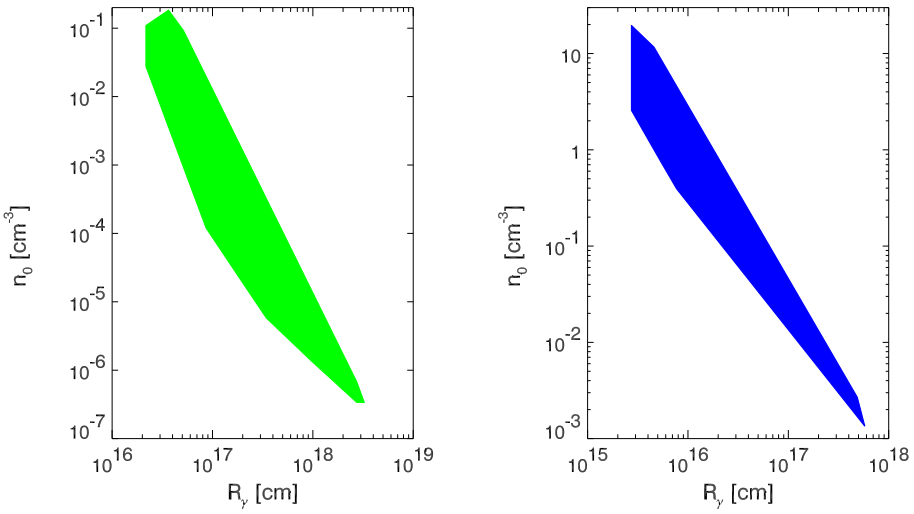

Figure 6.5 *Left panel:* the maximum density of the circum-bust-medium so that $R_\gamma < R_d$ for synchrotron solutions with $\alpha = 1/3$ and for a burst with $\nu_\gamma = 100$ keV, $f_\gamma = 1$ mJy, $t_\gamma = 1$ s & $t_a = t_\gamma$. *Right panel:* is same as the left panel except that $t_a = t_\gamma/100$; note that by decreasing the amount of time electrons have to radiate away their energy before being re-accelerated (t_a) increases the upper limit for n_0 roughly as t_a^{-1}. The n_0 upper limit is weakly dependent on ν_γ, and decreases with increasing t_γ & f_γ being most sensitive to f_γ – $\max(n_0) \overset{\propto}{\sim} f_\gamma$.

The numerical calculation of the hypersurface in 5-D parameter space

allowed by GRB observations – ν_γ, f_γ & t_γ – for *GRB-♮* finds $\gamma_i \gtrsim 10^4$, $\Gamma \gtrsim 10^3$, $200 \lesssim \gamma_i/\Gamma \lesssim 700$, source radius ($R_\gamma$) $10^{16} - 10^{18}$ cm, and B between 1 and 10^2Gauss for the entire solution space (see fig. 6.4) – which is in very good agreement with analytical estimates. For a wide range of values for the three observable parameters we find the GRB source to be located between $\sim 10^{15}$ cm & 10^{18} cm, $\gamma_i \gtrsim 3 \times 10^3$, and $\Gamma \gtrsim 10^3$ (fig. 6.4). In order that $R_\gamma/R_d < 1$, the density of the surrounding medium (n_0) is required to be less than ~ 0.1 cm^{-3} which is much smaller than the value inferred from late time afterglow modeling for long duration GRBs. The density requirement is relaxed if $t_a \ll t_\gamma$ (see fig. 6.5).

In conclusion, the synchrotron process, in a shock heated medium, has serious problems accounting for prompt γ-ray emission for those bursts that have spectrum below the peak frequency (ν_γ) scaling as $f_\nu \propto \nu^{1/3}$ or $\nu^{-(p-1)/2}$. A possible resolution is provided if electrons are more or less continuously accelerated while they are radiating γ-ray photons during the entire time period of a spike in the observed GRB lightcurve; in other words $t_a \ll t_\gamma$. It should be pointed out that $t_a \sim t_\gamma$ in shocks whereas continuous acceleration might be possible in regions of magnetic reconnection/dissipation.

6.2.3 Synchrotron solution when the low energy spectrum is $\nu^{-1/2}$

Substituting $f_{\nu_p} = f_\gamma \, (\nu_{i_5}/\nu_{c_5})^{\frac{1}{2}}$, $\nu_{\gamma_5} = \nu_{i_5}$, and ξ from equation (6.7) for the case where $\nu_c < \nu_i$, into eqs. 6.20–6.23 we find the allowed part of the

5-D parameter space when the spectrum below ν_γ is $f_\nu \propto \nu^{-1/2}$

$$\Gamma \approx 10^3 \nu_{\gamma_5}^{\frac{3}{16}} f_\gamma^{\frac{3}{16}} t_\gamma^{-\frac{3}{8}} \nu_{c_5}^{\frac{1}{8}} t_a^{\frac{1}{4}} Y^{-\frac{3}{16}} (1+Y)^{\frac{1}{4}} (1+z)^{\frac{1}{4}} d_{L_{28}}^{\frac{3}{8}} A_{2p}^{\frac{3}{16}} \quad (6.54)$$

$$\gamma_i \approx 4.7 \times 10^4 \nu_{\gamma_5}^{\frac{7}{16}} f_\gamma^{-\frac{1}{16}} t_\gamma^{\frac{1}{8}} \nu_{c_5}^{\frac{1}{8}} t_a^{\frac{1}{4}} Y^{\frac{1}{16}} (1+Y)^{\frac{1}{4}} (1+z)^{\frac{1}{4}} d_{L_{28}}^{-\frac{1}{8}} A_{2p}^{-\frac{1}{16}} \quad (6.55)$$

$$B \approx 4.0 \nu_{\gamma_5}^{-\frac{1}{16}} f_\gamma^{-\frac{1}{16}} t_\gamma^{\frac{1}{8}} \nu_{c_5}^{-\frac{3}{8}} t_a^{-\frac{3}{4}} Y^{\frac{1}{16}} (1+Y)^{-\frac{3}{4}} (1+z)^{\frac{1}{4}} d_{L_{28}}^{-\frac{1}{8}} A_{2p}^{-\frac{1}{16}} \text{ Gauss} \quad (6.56)$$

$$\tau \approx 3.3 \times 10^{-10} \nu_{\gamma_5}^{-\frac{3}{8}} f_\gamma^{\frac{1}{8}} t_\gamma^{-\frac{1}{4}} \nu_{c_5}^{-\frac{3}{4}} t_a^{-\frac{1}{2}} Y^{\frac{7}{8}} (1+Y)^{-\frac{1}{2}} (1+z)^{-\frac{1}{2}} d_{L_{28}}^{\frac{1}{4}} A_{2p}^{-\frac{7}{8}}, \quad (6.57)$$

where

$$A_{2p} \equiv \frac{p-1}{p-2}. \quad (6.58)$$

For *GRB-♮* — $t_\gamma = 0.1$s, $\nu_\gamma = 100$keV, $f_\gamma = 1$mJy & $t_a = t_\gamma$ — and taking $\nu_{c_5} < 10^{-4}$ (in agreement with the numerical calculation) we find

$$\Gamma \lesssim 720 Y^{-\frac{3}{16}} (1+Y)^{\frac{1}{4}} \quad (6.59)$$

$$\gamma_i \lesssim 6.7 \times 10^4 Y^{\frac{1}{16}} (1+Y)^{\frac{1}{4}} \quad (6.60)$$

$$B \gtrsim 590\, Y^{\frac{1}{16}} (1+Y)^{-\frac{3}{4}} \text{ Gauss} \quad (6.61)$$

$$\tau \gtrsim 8.9 \times 10^{-7} Y^{\frac{7}{8}} (1+Y)^{-\frac{1}{2}}. \quad (6.62)$$

In contrast to the previous two cases considered in §6.2.1 & §6.2.2, $\Gamma < 1000$ in this case. We find the γ-ray source distance, R_γ, to be

$$R_\gamma \approx 6.0 \times 10^{16}\, \nu_{\gamma_5}^{\frac{3}{8}} f_\gamma^{\frac{3}{8}} t_\gamma^{\frac{1}{4}} \nu_{c_5}^{\frac{1}{4}} t_a^{\frac{1}{2}} Y^{-\frac{3}{8}} (1+Y)^{\frac{1}{2}} (1+z)^{-\frac{1}{2}} d_{L_{28}}^{\frac{3}{4}} A_{2p}^{\frac{3}{8}} \text{ cm} \quad (6.63)$$

which is $R_\gamma \sim 2\times10^{15}Y^{-\frac{3}{8}}(1+Y)^{\frac{1}{2}}$ cm for *GRB-*$\natural$. We compare this radius to the deceleration radius, R_d, which is obtained from eq. (6.26) and is given by

$$R_d \approx \begin{cases} 2.6\times10^{16}\, E_{53}^{\frac{1}{3}} n_0^{-\frac{1}{3}} \nu_{\gamma_5}^{-\frac{1}{8}} f_\gamma^{-\frac{1}{8}} t_\gamma^{\frac{1}{4}} \nu_{c_5}^{-\frac{1}{12}} t_a^{-\frac{1}{6}} Y^{\frac{1}{8}} (1+Y)^{-\frac{1}{6}} (1+z)^{-\frac{1}{6}} d_{L_{28}}^{-\frac{1}{4}} A_{2p}^{-\frac{1}{8}} \text{cm} \\ \quad s=0 \\ \\ 1.8\times10^{13}\, E_{53} A_*^{-1} \nu_{\gamma_5}^{-\frac{3}{8}} f_\gamma^{-\frac{3}{8}} t_\gamma^{\frac{3}{4}} \nu_{c_5}^{-\frac{1}{4}} t_a^{-\frac{1}{2}} Y^{\frac{3}{8}} (1+Y)^{-\frac{1}{2}} (1+z)^{\frac{1}{2}} d_{L_{28}}^{-\frac{3}{4}} A_{2p}^{-\frac{3}{8}} \text{cm} \\ \quad s=2 \end{cases} \tag{6.64}$$

and for the ratio $R_\gamma/R_d < 1$, we find that $n_0 \lesssim 8\, E_{53} Y^{\frac{3}{2}}(1+Y)^{-2}$ cm^{-3} and $A_* < 0.014 E_{53} Y^{\frac{3}{4}}(1+Y)^{-1}$ if $\nu_{c_5} \sim 0.1$; the limits on n_0 & A_* are much higher for $\nu_{c_5} \ll 0.1$ and poses no problem for synchrotron solutions in a shock heated source.

If the synchrotron solutions were to arise in a shock heated medium, we can calculate the LF of the shock front wrt the unshocked fluid, Γ_{sh}, using equation 6.11:

$$\Gamma_{sh} \approx 26\, \varepsilon_e^{-1} \nu_{\gamma_5}^{\frac{7}{16}} f_\gamma^{-\frac{1}{16}} t_\gamma^{\frac{1}{8}} \nu_{c_5}^{\frac{1}{8}} t_a^{\frac{1}{4}} Y^{\frac{1}{16}} (1+Y)^{\frac{1}{4}} (1+z)^{\frac{1}{4}} d_{L_{28}}^{-\frac{1}{8}} A_{2p}^{\frac{15}{16}}. \tag{6.65}$$

or $\Gamma_{sh} \lesssim 32 Y^{\frac{1}{16}}(1+Y)^{\frac{1}{4}}$ for *GRB-*$\natural$assuming that electrons receive half of the shock energy and that there are no $e^\pm$ pairs. Note that as long as $\nu_{\gamma_5} \sim 1$, Γ_{sh} is pretty high (~ 20), and it is insensitive to ν_{c_5} (and the other quantities). In order to produce $\Gamma_{sh} \sim 20$ in internal shocks, we need the relative LF of the two colliding shells $\Gamma_{rel} \sim 2\Gamma_{sh}^2 (n_1/n_2)^{\frac{1}{2}}$, where n_1 and n_2 are the comoving densities of the two colliding shells (see appendix A for a discussion of how we calculate Γ_{rel}). For $\Gamma_{rel} \lesssim 5$, so that the ratio of the LFs of the colliding shells

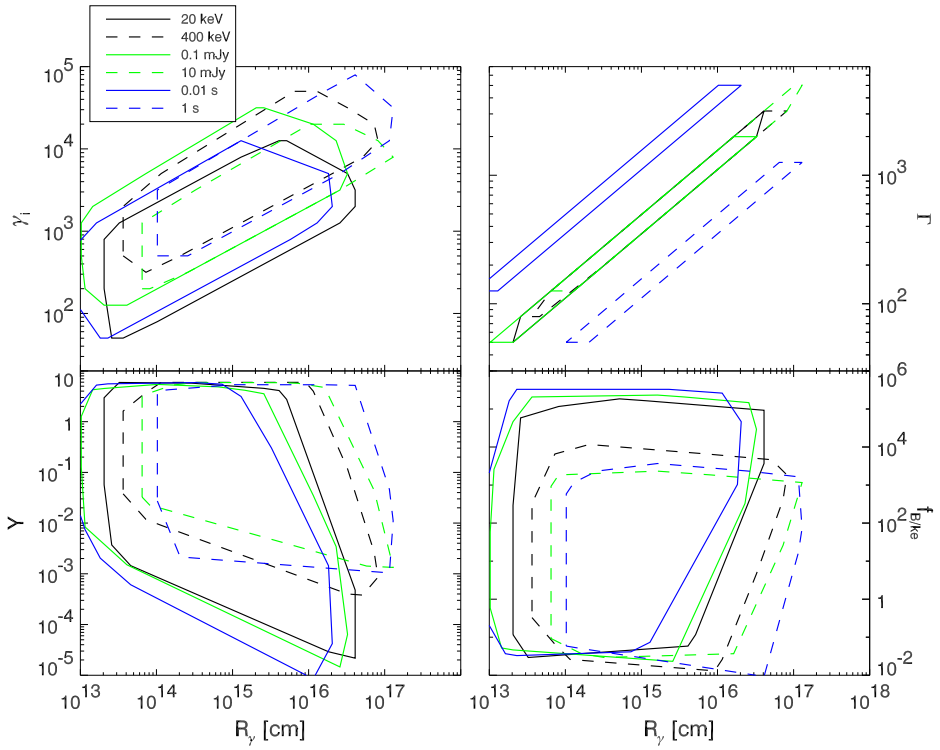

Figure 6.6 Synchrotron solution space when the spectrum below the peak of νf_ν is $f_\nu \propto \nu^{-1/2}$ for $\nu < \nu_\gamma$. γ_i, Γ, Y, and $f_{B/ke}$ are plotted against the distance of the source from the center of explosion (R_γ). The solution spaces for several different values of ν_γ, f_γ, and GRB pulse duration (t_γ) are shown in the four panels. Please see the Figure 6.2 caption for details.

is not larger than 10, $n_1/n_2 \lesssim \sim 10^{-5}$ is required (see appendix A); $\Gamma_{rel} > 5$ is an unlikely situation to be realized in nature.

We calculate the total energy in electrons ($E_\pm$) and magnetic field (E_B) to determine the efficiency for synchrotron radiation — if there is a lot more energy in magnetic field than that in the electrons, the efficiency for γ-ray radiation would be small. The magnetic and electron energies for the case of

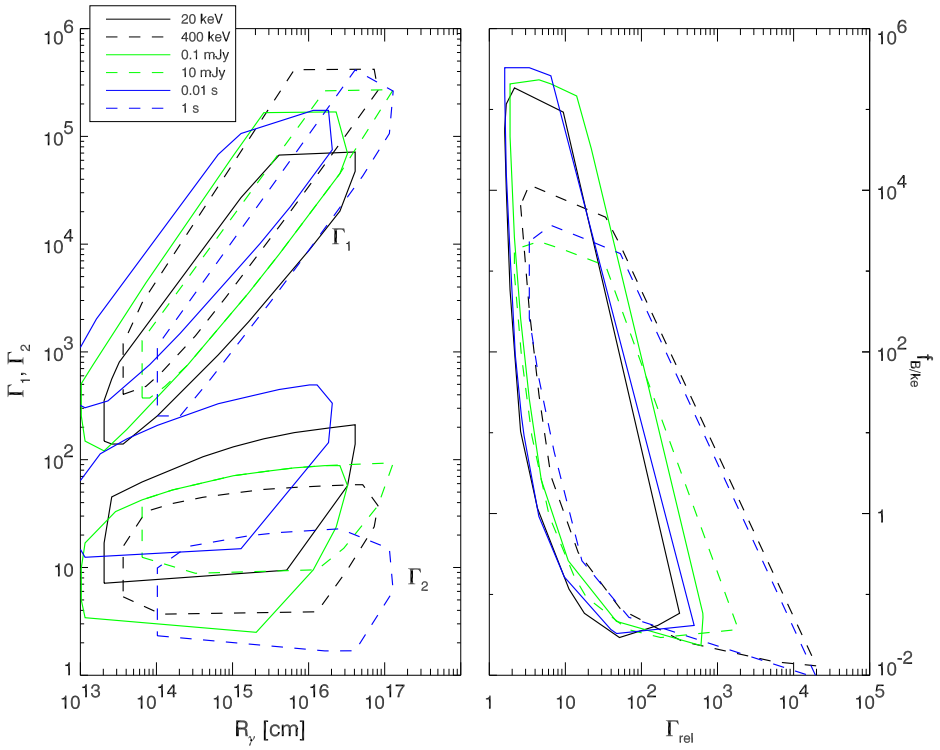

Figure 6.7 This figure, unlike all the previous ones, shows *model dependent* results. For each point in the allowed region of the 5-D parameter space, corresponding to synchrotron solutions for $\alpha = -1/2$ and for given ν_γ, f_γ & t_γ, we calculate parameters for the popular internal shock model for GRBs (see appendix A for details). The *left panel* shows the LFs Γ_1 & Γ_2 of the two colliding shells in the internal shock model as a function of R_γ, the distance from the center where the shells collide. The *right panel* shows $\Gamma_{rel} = \Gamma_1\Gamma_2\,(1 - v_1 v_2)$ vs. $f_{B/ke}$ (the ratio of energy in magnetic field and electrons). Different ν_γ, f_γ and t_γ cases are displayed as described in Figure 6.2. Note that Γ_{rel} is correlated with $f_{B/ke}$; for high Γ_{rel}, $f_{B/ke}$ is small (< 1), and for low Γ_{rel}, $f_{B/ke} \gg 1$. Low Γ_{rel} & $f_{B/ke} \gg 1$ solutions might correspond to a highly magnetized outflow.

$\nu^{-1/2}$ spectrum are obtained from equation (6.10) and the solutions for B, Γ,

γ_i and R_γ derived above, and are given by –

$$E_B = B^2 R_\gamma^3/6 \approx 6.0 \times 10^{50}\, \nu_{\gamma_5} f_\gamma t_\gamma Y^{-1} (1+z)^{-1} d_{L_{28}}^2 A_{2p}\, \mathrm{ergs}, \tag{6.66}$$

and

$$E_\pm = N(p-1) m_e c^2 \gamma_i \Gamma/(p-2) \approx \\ 8.7 \times 10^{50}\, \nu_{\gamma_5} f_\gamma t_a (1+Y)(1+z)^{-1} d_{L_{28}}^2 A_{2p}\, \mathrm{ergs}.$$

The ratio $E_B/E_\pm$ is

$$f_{B/ke} \equiv \frac{E_B}{E_\pm} \approx 0.68 t_\gamma t_a^{-1} Y^{-1} (1+Y)^{-1}. \tag{6.67}$$

For $t_a \ll t_\gamma$ the above expression for the ratio $f_{B/ke}$ would need to be modified to include the total energy deposited in $e^\pm$s as a result of multiple acceleration episodes during a GRB pulse time period of t_γ; for $t_\gamma/t_a \sim 1$ the expression for $f_{B/ke}$ reduces to the familiar form that depends only on the Compton-Y. For $Y \ll 1$ most of the energy is in the magnetic field and for these solutions the radiative efficiency to produce a GRB is very small.

We numerically search the 5-D parameter space subject to the three observational constraints (ν_γ, f_γ, t_γ) and find solutions with 10^{13} cm $< R_\gamma <$ 10^{17} cm, 10 Gauss $< B <$ 10^7Gauss, $100 < \gamma_i < 3 \times 10^4$, $80 < \Gamma < 3000$, and $10^{-3} < Y < 7$ (see fig. 6.6) — all in good agreement with analytical estimates presented above. We find $2 < \Gamma_{sh} < 100$ and $10^{-2} < f_{B/ke} < 10^4$. So it would seem that we have solutions with $f_{B/ke} \sim 1$ and Γ_{sh} of order a few – however it turns out that for $f_{B/ke} \lesssim 10$, $\Gamma_{sh} \gtrsim 5$. For $\Gamma_{sh} \gtrsim 5$, $10^{-5} < \frac{n_1}{n_2} < 0.1$, and the ratio of the LFs of two colliding shells, Γ_{rel}, to produce this Γ_{sh} is greater than 20 (see fig. 6.7) — fluctuations in the LF of the outflow with Γ_{rel} on the order of a few are typically expected in internal shocks.

Numerical solutions for the allowed part of the 5-D space for a range of observable parameters are shown in Figure 6.6. An increase in ν_γ leads to a slight increase of γ_i and R_γ whereas Γ is quite insensitive to it. These behaviors are consistent with our analytical calculations (eqs. 6.54–6.57). The decrease of $f_{B/ke}$ with ν_γ (fig. 6.6) is due to an increase of Y. An increase of f_γ has little effect on γ_i (for the allowed solution space), Γ & Y increase a little, and $f_{B/ke}$ decreases; these parameters have a very weak dependence on f_γ (see eqs. 6.54–6.57). And finally, when t_γ is increased, γ_i and Y increase, and Γ and $f_{B/ke}$ decrease. This is again in agreement with the analytical estimates – $\gamma_i \propto t_\gamma^{\frac{1}{2}}$. The large decrease in Γ with t_γ is due to an increase of Y with t_γ – $\Gamma \propto t_\gamma^{-\frac{1}{8}} Y^{-\frac{3}{16}}$.

We have looked at the variation of Γ_{sh}, Γ_{rel} and $f_{B/ke}$ with ν_γ, f_γ & t_γ. The results are shown in Figure 6.7. The minimum value of Γ_{rel} has a weak dependence on ν_γ, f_γ, and t_γ; Γ_{rel} is between 5 and 20 for $f_{B/ke} \lesssim 10$; $\Gamma_{rel} \sim 5$ solutions are only present when $t_\gamma \lesssim 0.01$s, $f_\gamma \lesssim 0.1$ mJy, or $\nu_\gamma < 20$ keV (note that we only alter one of the three at a time, i.e. for $t_\gamma \sim 0.01$s, $\nu_\gamma \sim 100$ keV and $f_\gamma \sim 1$ mJy). Γ_{rel} may be small enough, then, that the synchrotron mechanism can produce GRBs with $\nu^{-\frac{1}{2}}$ spectra if it has very short pulse duration, small peak frequency, or small flux.

6.2.3.1 X-ray flux during the GRB when $\alpha = -\frac{1}{2}$

So far, we have only considered prompt γ-ray emission due to the synchrotron process. We now calculate emission in other wavelengths, particularly

the X-ray and optical, that should accompany γ-ray photons. In this subsection, and in §6.2.3.2, we relate the solutions we found in §6.2.3 to the internal shock model for GRBs (Rees and Mészáros 1994; see Piran 1999, for complete references) according to which shells of material ejected in the explosion undergo collisions and the resulting shocks convert part of the kinetic energy of the outflow to radiation. Throughout this section we assume that the γ-ray emission is produced in shell '1' which is taken to be the faster of the two shells. The results are essentially identical if we assume that the GRB is produced in the outer, slower, shell, which we shall refer to as shell '2'. The x-ray flux from shell '1', however, is independent of the internal shock model, and is expected to accompany the prompt synchrotron $\nu^{-\frac{1}{2}}$ γ-ray emission.

The x-ray and optical flux from shell '1' lie on the $\nu^{-1/2}$ extrapolation of the γ-ray flux and therefore it is straightforward to calculate these using f_γ and the information that $\nu_c \lesssim 2$eV & $\nu_a \lesssim 5$eV for the entire solution sub-space of the 5-D parameter space. The calculation of emission from shell '2' is more involved and also a bit uncertain. We provide here (and in §6.2.3.2) a lower limit to the x-ray and optical flux from shell '2' for each point in the 5-D space that satisfies the three observational constraints (ν_γ, f_γ, t_γ). The calculation of flux from shell '2' requires the knowledge of the LF of the shock front moving into this shell as well as the ratio of densities (n_1/n_2). The calculation for these quantities is described in appendix A. The synchrotron injection frequency in shell '2', ν_{i_2}, is smaller than that in shell 1 by a factor of $\left(\Gamma_{s_2}-1\right)^2 / \left(\Gamma_{s_1}-1\right)^2$; Γ_{s_1} & Γ_{s_2} are shock front LFs into shell '1' & '2' wrt unshocked gas in shells

'1' & '2' respectively. This factor is approximately $\simeq \frac{n_1}{n_2}$ for $\Gamma_{s_1}, \Gamma_{s_2} \gg 1$, but the approximation breaks down for $\frac{n_1}{n_2} \lesssim 10^{-2}$ (see Figure A.2) since the shock in shell '2' becomes mildly relativistic (we note that this approximation is not used in our numerical calculations). The peak flux of the synchrotron spectrum at $\nu = \min(\nu_{i_2}, \nu_{c_2})$ in shell '2', $f_{\nu_{p_2}}$, is larger than $f_{\nu_{p_1}}$ by a factor of $\left(\frac{n_2}{n_1}\right)^{\frac{1}{2}}$. The magnetic field is assumed to be the same in the two shells, and therefore the difference between the cooling frequencies in the shells is due to different Y-parameters; since synchrotron dominates over SSC here by design, the difference between ν_{c_2} and ν_{c_1} ends up being very small. The shell '2' synchrotron self absorption frequency, ν_{a_2} is larger than that in shell 1 by a factor of $\left(\frac{n_1}{n_2}\right)^{0.2}$, or a factor of a few.

The 1 keV synchrotron and SSC flux from shells '1' and '2' for *GRB-♮* is shown in the top left panel of Figure 6.8. The shell '2' synchrotron flux contributes the most to the prompt x-ray flux, and the shell 1 synchrotron flux contributes a slightly smaller amount. SSC flux from either shell is negligible. There is a weak dependence of x-ray flux on Γ_{rel}. The shell '1' synchrotron flux at 1 keV is about 10 mJy. This is simply the extrapolation of the 100 keV flux back to 1 keV, with a spectral index of $-\frac{1}{2}$ or $\left(\frac{1}{100}\right)^{-\frac{1}{2}}$ 1mJy $\sim$ 10mJy for *GRB-♮*.

Shell '2' synchrotron x-ray flux ranges from 1 to 100 mJy. We expect the flux from shell '2' at 1 keV to be

$$f_{2_x} \sim f_\gamma \frac{f_{\nu_{p_2}}}{f_{\nu_{p_1}}} \left(\frac{1\text{keV}}{\nu_{i_2}}\right)^{-\frac{p}{2}} \left(\frac{\nu_{i_2}}{100\text{keV}}\right)^{-\frac{1}{2}} \sim f_\gamma \left(\frac{n_1}{n_2}\right)^{\frac{1}{4}} \left(\frac{1\text{keV}}{\nu_\gamma}\right)^{-\frac{5}{4}} \text{ mJy} \quad (6.68)$$

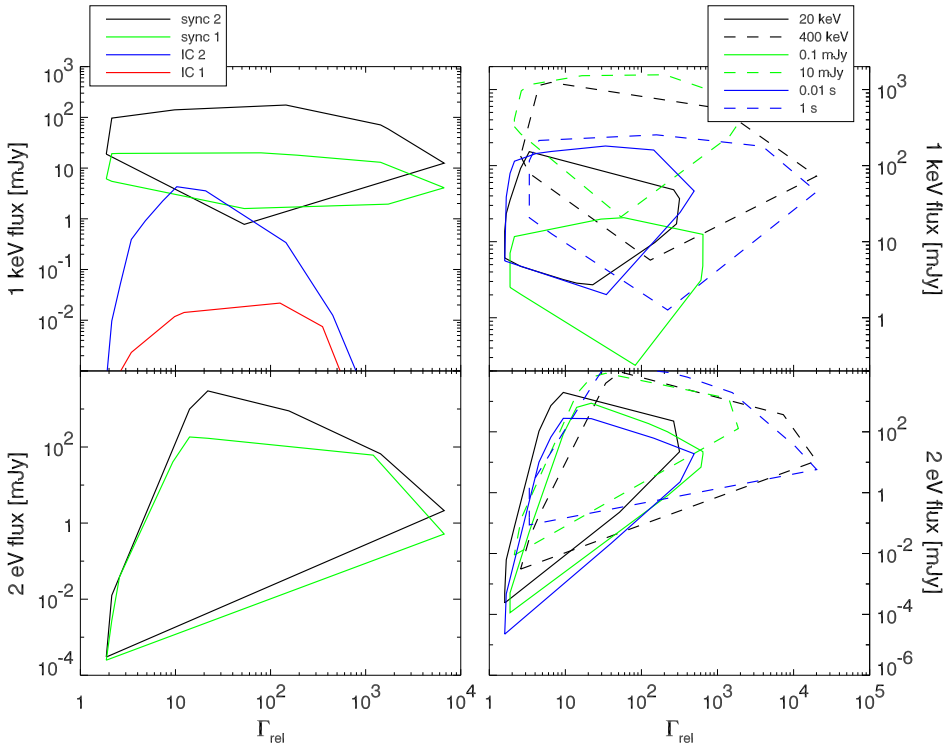

Figure 6.8 Prompt x-ray [1 keV] and optical [2 eV] flux associated with points in the solution sub-space of 5-D parameter space when cast in terms of the internal shock model or two colliding shells; the solutions are for synchrotron radiation with low energy spectrum $f_\nu \propto \nu^{-\frac{1}{2}}$. Top left: contributions of SSC and synchrotron to x-ray flux at 1 keV from shells '1' and '2' (see legend) for *GRB-♮*. Top right: sum of all contributions is shown for the cases that have been described in Figure 6.2. Bottom left: contributions of synchrotron emission from shells '1' and '2' to the optical flux; IC contributions are negligible from either shell. Bottom right: sum of all contributions in the optical, for the same cases as the top right panel. The results shown here assume that the γ-ray flux is produced in shell '1'; production of the GRB in shell '2' does not change the results significantly.

using the above arguments and assuming that $\nu_{i_2} < 1$ keV (valid when $\frac{n_1}{n_2} \lesssim 0.01$ – satisfied by roughly half of the solution points in the 5-D space), $\nu_{c_1} \sim \nu_{c_2}$, and $p = 2.5$. From this equation, we estimate that the flux at 1 keV should

be between $\sim$ 20 and 300 mJy (for $f_{1_\gamma} = 1$ mJy and $\nu_\gamma \sim 100$ keV) – in agreement with the numerical results in Figure 6.8.

The shell '2' SSC flux at 1 keV ranges from 10^{-5} to almost 10 mJy. The SSC peak frequency ($\sim \nu_{i_2}\gamma_{i_2}^2$) ranges from about 100 eV to very high values, so over a large part of the solution space, the expected SSC flux at 1 keV in comparison to the synchrotron 100 keV flux from shell '1' is (assuming that $\nu_{i_2} > \nu_{c_2}$)

$$\frac{f_{2_x}^{ic}}{f_\gamma} \approx \frac{f_{\nu_{p_2}}\tau_2}{f_{\nu_{p_1}}} \left(\frac{1\text{keV}}{\gamma_{c2}^2\nu_{c_2}}\right)^{-\frac{1}{2}} \left(\frac{\nu_{c_1}}{100\text{keV}}\right)^{-\frac{1}{2}} \sim 10 \left(\frac{n_2}{n_1}\right) \tau_1\gamma_{c_2} \tag{6.69}$$

which, after substituting in the solutions for τ and γ_c, is

$$f_{2_x}^{ic} \approx 1.5\times10^{-4} \left(\frac{n_2}{n_1}\right) \nu_{\gamma_5}^{-\frac{7}{16}} f_\gamma^{\frac{17}{16}} t_\gamma^{-\frac{1}{8}} \nu_{c_5}^{-\frac{1}{8}} t_a^{-\frac{1}{4}} Y^{\frac{15}{16}} (1+Y)^{-\frac{1}{4}} (1+z)^{-\frac{1}{4}} d_{L_{28}}^{\frac{1}{8}} A_{2p}^{-\frac{15}{16}} \text{ mJy}; \tag{6.70}$$

with $Y \sim 1$ and $1 < n_2/n_1 < 10^5$, the range for the x-ray flux obtained from the above equation is in agreement with the numerical solutions.

The sum of synchrotron and SSC contributions to flux at 1 keV from both shells for various values of ν_γ, f_γ, and t_γ are shown in the upper right hand panel of Figure 6.8. The 1 keV flux ranges from 0.1 to a few thousand mJy, and is most sensitive to f_γ and ν_γ – in agreement with equation (6.68), $f_{2_x} \propto f_\gamma \nu_\gamma^{\frac{5}{4}}$, since synchrotron emission dominates.

The early 0.2-10 keV x-ray flux as observed by the Swift x-ray telescope ranges from 10^{-12} to 10^{-8} ergs cm^{-2} s^{-1},[6] which corresponds to 1 keV flux of

[6] `http://swift.gsfc.nasa.gov/cgi-bin/swift/grb\_table/grb\_table.py`

about 10^{-4} to a few mJy (assuming $\nu^{-\frac{1}{2}}$ in the x-ray band). These observations are made at roughly 100s after the GRB trigger. The x-ray light curve from the γ-ray source should peak at about the same time as the GRB light curve. After the peak, assuming that the outflow opening angle is greater than $1/\Gamma$, the emission should be dominated by off-axis emission and the light curve should fall off as $t^{-2+\beta}$ (Kumar and Panaitescu 2000), which in this case is $t^{-2.5}$ since $f_\nu \propto \nu^{-1/2}$. Extrapolating the observed 1 keV flux of $\sim 10^{-4}$–1 mJy backwards in time from 100s to 10s, we find the x-ray flux during the GRB to be consistent with values shown in the upper right panel of Figure 6.8.

6.2.3.2 Prompt optical emission when the GRB index $\alpha = -\frac{1}{2}$

In the bottom left panel of Figure 6.8, the R band (2 eV) flux from shell '1' and '2' are plotted against Γ_{rel}. Optical flux from the γ-ray source can be pretty bright during the burst for these solutions ranging from 10^{-3} and 100 mJy (24th to 11th magnitude in the R band). The synchrotron flux is smaller for smaller Γ_{rel} solutions. The SSC makes negligible contribution to the optical flux compared to the synchrotron process, because $\nu_a \gamma_c^2$ is well above the optical.

If we extrapolate the shell '1' 100 keV flux back to 2 eV using the spectral index $\alpha = -\frac{1}{2}$, we expect $f_{1R} \sim 225 \nu_{\gamma_5}^{1/2} f_\gamma \sim 225$mJy for *GRB-ϟ* whereas for most of the solution space the optical flux for shell '1' falls below 10 mJy (fig. 6.8 bottom left panel) — this is because the synchrotron self absorption frequency is larger than the R-band frequency by a factor ~ 10 or

more. The range of shell '2' R-band flux is higher than shell '1' by a factor of $\frac{f_{\nu_{p_2}}}{f_{\nu_{p_1}}} \sim \sqrt{\frac{n_2}{n_1}} \sim 30$.

In the bottom right panel of Figure 6.8, we show the affect of varying ν_γ, f_γ, and t_γ on the prompt optical flux; the total flux – obtained by adding the contributions for the two colliding shells – ranges from 10^{-4} to 10^3 mJy, or R magnitude of 26 to 9. The optical flux increases with ν_γ, f_γ, and t_γ – longer GRB pulses with higher peak frequency and/or flux tend to be brighter in the optical band. Synchrotron self absorption is larger at smaller Γ_{rel}, and that makes the optical flux smallest at the minimum of Γ_{rel}. There are $\Gamma_{rel} \sim 5$ solutions with $f_{B/ke} \sim 1$, that have small enough optical flux to be in accord with the observed upper limits, especially for smaller ν_γ, f_γ, and t_γ. Although $\nu_a > 2$ eV for much of the solution space, the optical light curve should peak at the same time as the GRB light curve, since $\nu_c < 2$ eV. After the peak, the light curve should fall off – if dominated by off-axis emission – as $t^{-2.5}$.

6.2.4 Synchrotron solutions for $f_\nu \propto \nu^{-\frac{p}{2}}$

If the observed spectral index is steep and consistent with $\nu^{-\frac{p}{2}}$ and no break is detected in the observed energy band of 15-150 keV, for instance, then this is a special case of either $\nu^{-\frac{1}{2}}$ or $\nu^{-\frac{(p-1)}{2}}$ low energy spectrum discussed in §6.2.1 & 6.2.3 – with $\nu_{\gamma_5} = \max(\nu_{\gamma_5}, \nu_{c_5}) \lesssim 0.15$. The allowed solution space for this situation should be close to the $\nu_\gamma = 20$ keV case in Figures 6.2 and 6.6; Specifically, $\gamma_i \lesssim 10^3$, $\Gamma > 100$, and $2 \lesssim \Gamma_{rel} \lesssim 200$.

6.3 Synchrotron-self-Compton – SSC – solutions

In this section, we present solutions for the prompt γ-ray emission to be produced via the synchrotron-self-inverse-Compton radiation or the SSC process. The basic approach is same as in section 6.2. We determine the hypersurface in the 5-D parameter space $(\gamma_i, \Gamma, B, N, \tau)$ that has SSC emission consistent with the three observational constraints ν_γ, f_γ & t_γ. Since different cases of low energy spectral index have different ordering for the characteristic synchrotron frequencies (ν_i, ν_c, ν_a), we do not consider a general SSC solution, but describe analytical and numerical solutions for the positive low energy spectral index case i.e., $f_\nu \propto \nu^\alpha$ with $\alpha > 0$ for $\nu < \nu_\gamma$, and the negative index case i.e., $\alpha < 0$, separately in several subsections below.

6.3.1 SSC solutions: Positive low energy spectral index

This section is broken up in two subsections. One dealing with the special case of $f_\nu \propto \nu^{1/3}$ is discussed below. All the other cases of $\alpha > 1/3$ are discussed in §6.3.1.2.

6.3.1.1 SSC solutions: $\alpha \approx +1/3$

The SSC spectrum (νf_ν^{ic}) peaks at $\nu_\gamma \sim 4 \max(\nu_i, \nu_c) \max(\gamma_i, \gamma_c)^2$; where ν_i & ν_c are the injection and cooling frequencies of the underlying synchrotron radiation, γ_i is the minimum LF of electrons in the source comoving frame and γ_c is the LF of electrons that cool on time scale t_a available since last accelerated. For the spectrum below ν_γ to be $\sim \nu^{1/3}$, we must have $\gamma_i \sim \gamma_c$,

and in that case $\nu_\gamma \sim 4\nu_i\gamma_i^2$. The IC flux at ν_γ is $f_\gamma \sim f_{\nu_p}\tau$ (f_{ν_p} is the synchrotron flux at ν_i). The equations for pulse duration t_γ and Compton-Y are same as in §6.2. The equations for $\nu_i \sim \nu_c$, the peak IC frequency ν_γ, the IC flux f_γ at ν_γ, and the Compton Y-parameter are given below –

$$B^2\Gamma\gamma_i \approx 7.7 \times 10^8 (1+z) t_a^{-1} (1+Y)^{-1} \tag{6.71}$$

$$B\gamma_i^4\Gamma \approx 2.3 \times 10^{12} \nu_{\gamma_5} (1+z) \tag{6.72}$$

$$B\Gamma^5\tau^2 \approx 1.6 \times 10^6 f_\gamma t_\gamma^{-2} (1+z) d_{L_{28}}^2 \tag{6.73}$$

$$\tau\gamma_i^2 \approx \frac{3}{4} Y \left(\frac{p-1}{p-2}\right)^{-1} \tag{6.74}$$

We first eliminate τ from equation (6.73) using (6.74) to get

$$B\Gamma^5\gamma_i^{-4} \approx 2.8 \times 10^6 f_\gamma t_\gamma^{-2} (1+z) d_{L_{28}}^2 Y^{-2} \left(\frac{p-1}{p-2}\right)^2. \tag{6.75}$$

Next, we divide equations (6.71) and (6.72) to eliminate Γ:

$$B\gamma_i^{-3} \approx 3.3 \times 10^{-4} t_a^{-1} (1+Y)^{-1} \nu_{\gamma_5}^{-1}, \tag{6.76}$$

divide equations (6.72) and (6.75) to eliminate B:

$$\gamma_i^8\Gamma^{-4} \approx 8.2 \times 10^5 \nu_{\gamma_5} f_\gamma^{-1} t_\gamma^2 d_{L_{28}}^{-2} Y^2 \left(\frac{p-1}{p-2}\right)^{-2}, \tag{6.77}$$

and combine equations (6.71) and (6.75) to obtain:

$$B\Gamma \approx 4.6 \times 10^4 t_a^{-\frac{4}{9}} (1+Y)^{-\frac{4}{9}} f_\gamma^{\frac{1}{9}} t^{-\frac{2}{9}} (1+z)^{\frac{5}{9}} d_{L_{28}}^{\frac{2}{9}} Y^{-\frac{2}{9}} \left(\frac{p-1}{p-2}\right)^{\frac{2}{9}}. \tag{6.78}$$

Equations (6.76) and (6.78) give

$$\Gamma\gamma_i^3 \approx 1.4\times10^8 \nu_{\gamma_5} t_a^{\frac{5}{9}} (1+Y)^{\frac{5}{9}} f_\gamma^{\frac{1}{9}} t_\gamma^{-\frac{2}{9}} (1+z)^{\frac{5}{9}} d_{L_{28}}^{\frac{2}{9}} Y^{-\frac{2}{9}} \left(\frac{p-1}{p-2}\right)^{\frac{2}{9}}, \quad (6.79)$$

and substituting this into equation (6.77), we find the solution for γ_i to be

$$\gamma_i \approx 84 \nu_{\gamma_5}^{\frac{1}{4}} f_\gamma^{-\frac{1}{36}} t_\gamma^{\frac{1}{18}} t_a^{\frac{1}{9}} Y^{\frac{1}{18}} (1+Y)^{\frac{1}{9}} d_{L_{28}}^{-\frac{1}{18}} (1+z)^{\frac{1}{9}} A_{2_p}^{-\frac{1}{18}}. \quad (6.80)$$

Note that the electron LF γ_i has a very weak dependence on the observed quantities as well as the Compton-Y parameter, and therefore $\gamma_i \sim 80$ for the entire SSC solution space. By plugging equation (6.80) back into equations (6.76), (6.77), and (6.74), we find the remaining parameters

$$B \approx 200 \nu_{\gamma_5}^{-\frac{1}{4}} f_\gamma^{-\frac{1}{12}} t_\gamma^{\frac{1}{6}} t_a^{-\frac{2}{3}} Y^{\frac{1}{6}} (1+Y)^{-\frac{2}{3}} d_{L_{28}}^{-\frac{1}{6}} (1+z)^{\frac{1}{3}} A_{2_p}^{-\frac{1}{6}} \text{ Gauss} \quad (6.81)$$

$$\Gamma \approx 240 \nu_{\gamma_5}^{\frac{1}{4}} f_\gamma^{\frac{7}{36}} t_\gamma^{-\frac{7}{18}} t_a^{\frac{2}{9}} Y^{-\frac{7}{18}} (1+Y)^{\frac{2}{9}} d_{L_{28}}^{\frac{7}{18}} (1+z)^{\frac{2}{9}} A_{2_p}^{\frac{7}{18}} \quad (6.82)$$

$$\tau \approx 1.1\times10^{-4} \nu_{\gamma_5}^{-1/2} f_\gamma^{\frac{1}{18}} t_\gamma^{-\frac{1}{9}} t_a^{-\frac{2}{9}} Y^{\frac{8}{9}} (1+Y)^{-\frac{2}{9}} d_{L_{28}}^{\frac{1}{9}} (1+z)^{-\frac{2}{9}} A_{2_p}^{-\frac{8}{9}}. \quad (6.83)$$

All of these parameters are weakly dependent on the three observable quantities viz. ν_{γ_5}, f_γ & t_γ. Substituting the *observed* values for *GRB-♮*, i.e. $\nu_{\gamma_5}=1$, $f_\gamma = 1$ mJy, and $t_a \sim t_\gamma = 0.1$ s, $z=1$, & taking p=3.2, we find that $\gamma_i \sim 58 Y^{\frac{1}{18}}(1+Y)^{\frac{1}{9}}$, $B \sim 1.1\times10^3 Y^{\frac{1}{6}}(1+Y)^{-\frac{2}{3}}$Gauss, $\Gamma \sim 110 Y^{-\frac{7}{18}}(1+Y)^{\frac{2}{9}}$, and $\tau \sim 1.3\times10^{-4} Y^{\frac{8}{9}}(1+Y)^{-\frac{2}{9}}$.

The distance of the γ-ray source from the center of the explosion, R_γ, is given by

$$R_\gamma \approx 3.3\times10^{15}\, \nu_{\gamma_5}^{\frac{1}{2}} f_\gamma^{\frac{7}{18}} t_\gamma^{\frac{2}{9}} t_a^{\frac{4}{9}} Y^{-\frac{7}{9}} (1+Y)^{\frac{4}{9}} (1+z)^{-\frac{5}{9}} d_{L_{28}}^{\frac{7}{9}} A_{2_p}^{\frac{7}{9}} \text{ cm}, \quad (6.84)$$

or $R_\gamma \sim 1.3 \times 10^{15} Y^{-\frac{7}{9}} (1+Y)^{\frac{4}{9}}$cm for *GRB-♮*. This distance is smaller than the deceleration radius for a homogeneous or a wind external medium, unlike the situation when γ-rays are produced via the synchrotron process (see §3).

One constraint that we have not yet considered is that the SSC self absorption frequency, $\nu_a^{ic} \sim 4\nu_a\gamma_i^2$, must be smaller than ∼20 keV otherwise the low energy spectral index, obtained by Band function fit to the BATSE or *Swift*/BAT data, would be steeper than $\alpha = 1/3$ we are considering in this subsection. The expression for ν_a^{ic}, valid for $\nu_a < \nu_i, \nu_c$, is

$$\nu_a^{ic} \sim \frac{1.7 \times 10^{-14} \gamma_i^2 \Gamma^{\frac{6}{5}}}{(1+z)} \left(\frac{f'_p \nu_i^{-\frac{1}{3}}}{2\gamma_i m_e} \right)^{\frac{3}{5}} \tag{6.85}$$

where $f'_p \equiv \sqrt{3} q^3 B\tau / \sigma_T m_e c^2$ is the comoving synchrotron flux. Substituting for γ_i, Γ, B & τ using equations 6.80–6.83 we find

$$\nu_a^{ic} \sim 2.2 \times 10^5 \, \nu_{\gamma_5}^{\frac{1}{10}} f_\gamma^{\frac{1}{6}} t_\gamma^{-\frac{1}{3}} t_a^{-\frac{1}{15}} Y^{\frac{4}{15}} (1+Y)^{-\frac{1}{15}} (1+z)^{-\frac{2}{3}} d_{L_{28}}^{\frac{1}{3}} A_{2_p}^{-\frac{4}{15}} \text{ eV} \tag{6.86}$$

which is very insensitive to *all* of the observed quantities and for a wide range of observables $\nu_a^{ic} \sim 100$ keV which is too large to produce an SSC spectrum with $f_\nu^{ic} \propto \nu^{\frac{1}{3}}$ below the peak.

We now try relaxing one of the constraints we had imposed to simplify the analytical calculation i.e., $\gamma_i \sim \gamma_c$. This approximation was guided by the observational result that the observed spectrum for $\nu > \nu_\gamma$ is almost always $\sim \nu^{-1.5}$ for GRBs with $\alpha \sim 1/3$. This result suggests $\gamma_i \sim \gamma_c$ provided that $p \approx 3$. However, if the electron distribution is steeper, $p \sim 4$, then ν_c

can be much greater than ν_i, and a high energy spectrum of $\nu^{-(p-1)/2} \sim \nu^{-1.5}$ would be consistent with observations. We now investigate this possibility and determine if letting $\nu_c > \nu_i$ would allow for a smaller ν_a^{ic} and hence $\alpha = 1/3$ solutions. Note that the opposite arrangement of frequencies ($\nu_c < \nu_i$) is uninteresting, since the low energy index is -1/2 in this case.

For $\nu_c > \nu_i$ equation (6.71) is modified to read

$$\gamma_i B^2 \Gamma = \frac{7.7 \times 10^8 (1+z)}{\eta_i t_a (1+Y)} \tag{6.87}$$

where $\eta_i \equiv \gamma_c/\gamma_i$. We also need to use the appropriate expression for Y when $\gamma_c \gg \gamma_i$ and $p > 3$ (see eq. 6.6)

$$Y = \frac{4}{3} \frac{(p-1)}{(p-2)(p-3)} \tau \gamma_i^2, \tag{6.88}$$

which apart from a factor $(p-3)$ is same as equation (6.74). We solve the above two equations together with eqs. (6.73) & (6.74) to find that $\nu_a^{ic} \propto \eta_i^{-\frac{1}{15}}$; so ν_a^{ic} does not decrease by much even if we take γ_c to be larger than γ_i by many orders of magnitude, and therefore there are no SSC solutions with low energy spectrum of $\nu^{1/3}$ between $\sim$ 15 keV and 200 keV.

The above analytical calculation is based on a number of approximations for the SSC spectrum and flux. We check the validity of analytical results using numerical calculations and by searching the 5-D parameter space for SSC solutions with low energy spectral index $\alpha \approx 1/3$. It turns out that numerically also we find no solutions — ν_a^{ic} is indeed too high to produce a GRB with a low energy spectrum of $\nu^{1/3}$ in the $\sim$15–200 keV band.

The only other possibility is that the $\alpha \approx 1/3$ index is transitory, i.e. the spectrum is changing continuously from $\alpha \approx 1$ at $\nu \sim 20$ keV to $\alpha \approx -1$ at $\nu = \nu_\gamma$ and that $\alpha \sim 1/3$ is realized at some intermediate frequency. This might, however, pose a problem for those GRBs with $\nu_\gamma \gtrsim 100$keV, since the spectrum would be steeper than $\nu^{1/3}$ near 15 keV and therefore a Band function fit to the spectrum will yield $\alpha > 1/3$.

6.3.1.2 SSC solutions: Spectral index $1/3 < \alpha \leq 1$

The analytical solution for this case is similar to the SSC $\alpha = 1/3$ case analyzed in §6.3.1.1. We take $\gamma_i \sim \gamma_c$ in order that the high energy spectrum is $\propto \nu^{-p/2} \sim \nu^{-1.5}$. The equations we solve are for ν_γ, f_γ, Compton-Y, and $\gamma_i \sim \gamma_c$:

$$B^2\Gamma\gamma_i \approx 7.7 \times 10^8 (1+z) t_a^{-1} (1+Y)^{-1} \tag{6.89}$$

$$B\gamma_i^4\Gamma \approx 2.3 \times 10^{12} \nu_{\gamma_5} (1+z) \eta_a^{-2} \tag{6.90}$$

$$B\Gamma^5\tau^2 \approx 1.6 \times 10^6 f_\gamma t_\gamma^{-2} (1+z) d_{L_{28}}^2 \eta_a^p \tag{6.91}$$

$$\tau\gamma_i^2 \approx \frac{3}{4} Y \left(\frac{p-1}{p-2}\right)^{-1} \tag{6.92}$$

where $\eta_a \equiv \gamma_a/\gamma_i \gtrsim 1$ since $\nu_a \gtrsim \nu_c, \nu_i$. The above equations are solved in the exact same way that we solved them in section 6.3.1.1, and we find that the

solutions are:

$$\gamma_i \approx 84 \nu_{\gamma_5}^{\frac{1}{4}} f_\gamma^{-\frac{1}{36}} t_\gamma^{\frac{1}{18}} t_a^{\frac{1}{9}} Y^{\frac{1}{18}} (1+Y)^{\frac{1}{9}} d_{L_{28}}^{-\frac{1}{18}} (1+z)^{\frac{1}{9}} A_{2p}^{-\frac{1}{18}} \eta_a^{\frac{-(p+18)}{36}} \quad (6.93)$$

$$B \approx 200 \nu_{\gamma_5}^{-\frac{1}{4}} f_\gamma^{-\frac{1}{12}} t_\gamma^{\frac{1}{6}} t_a^{-\frac{2}{3}} Y^{\frac{1}{6}} (1+Y)^{-\frac{2}{3}} d_{L_{28}}^{-\frac{1}{6}} (1+z)^{\frac{1}{3}} A_{2p}^{-\frac{1}{6}} \eta_a^{\frac{6-p}{12}} \text{ Gauss} \quad (6.94)$$

$$\Gamma \approx 240 \nu_{\gamma_5}^{\frac{1}{4}} f_\gamma^{\frac{7}{36}} t_\gamma^{-\frac{7}{18}} t_a^{\frac{2}{9}} Y^{-\frac{7}{18}} (1+Y)^{\frac{2}{9}} d_{L_{28}}^{\frac{7}{18}} (1+z)^{\frac{2}{9}} A_{2p}^{\frac{7}{18}} \eta_a^{\frac{7p-18}{36}} \quad (6.95)$$

$$\tau \approx 1.1 \times 10^{-4} \nu_{\gamma_5}^{-\frac{1}{2}} f_\gamma^{\frac{1}{18}} t_\gamma^{-\frac{1}{9}} t_a^{-\frac{2}{9}} Y^{\frac{8}{9}} (1+Y)^{-\frac{2}{9}} d_{L_{28}}^{\frac{1}{9}} (1+z)^{-\frac{2}{9}} A_{2p}^{-\frac{8}{9}} \eta_a^{\frac{p+18}{18}}. \quad (6.96)$$

For $p = 3.2$, $t_a \sim t_\gamma$, and parameters corresponding to *GRB-♮* we find the following set of inequalities ($\eta_a \gtrsim 1$)

$$\gamma_i \lesssim 58 Y^{\frac{1}{18}} (1+Y)^{\frac{1}{9}} \quad (6.97)$$

$$B \gtrsim 1.1 \times 10^3 \, Y^{\frac{1}{6}} (1+Y)^{-\frac{2}{3}} \text{ Gauss} \quad (6.98)$$

$$\Gamma \gtrsim 110 Y^{-\frac{7}{18}} (1+Y)^{\frac{2}{9}} \quad (6.99)$$

$$\tau \gtrsim 1.3 \times 10^{-4} Y^{\frac{8}{9}} (1+Y)^{-\frac{2}{9}}. \quad (6.100)$$

Or for $Y \sim 10$ we find $\gamma_i \lesssim 100$, $B \lesssim 250$ Gauss, $\Gamma \gtrsim 80$, and $\tau \gtrsim 5.5 \times 10^{-4}$. These analytical results are roughly consistent with numerical determination of the allowed region in 5-D parameter space (see fig. 6.9); we also find $\eta_a \approx 1$ numerically.

The distance of the γ-ray source from the center of the explosion is shown in fig. (6.9) for various GRB parameters and is greater than $\sim 10^{14}$cm for $Y \lesssim 10$. The ratio of magnetic to electron energy is small – $f_{B/ke} < 0.1$ for the entire solution space (fig. 6.9) since $Y \gtrsim 1$.

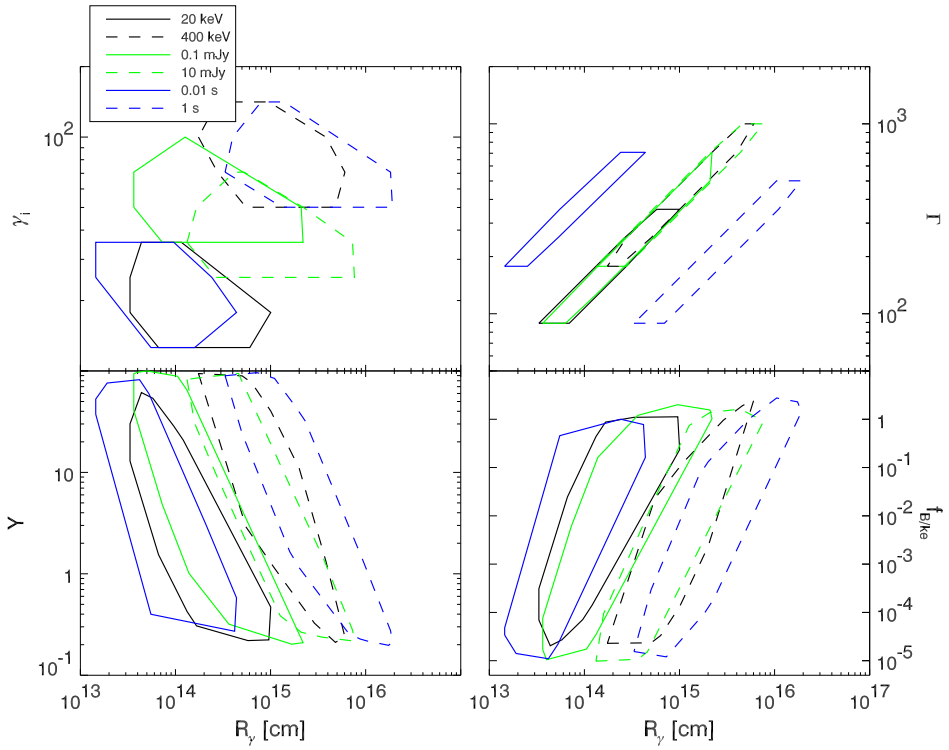

Figure 6.9 The SSC solution space when the low energy spectrum is $f_\nu^{ic} \propto \nu^\alpha$, for $\nu < \nu_\gamma$, with $1/3 < \alpha \leq 1$. The different cases in legend are as described in Figure 6.2.

The SSC solutions we have found can be related to the internal shock model. The relative LF of collision between shells – obtained from γ_i (see eq. 6.11 and appendix A) – is found to be between 2 and 10, which is significantly less than what we were finding for synchrotron solutions. The LFs of shells before collision (assuming that γ-rays are produced in the inner, faster, shell) is $300 \lesssim \Gamma_1 \lesssim 5000$ and $100 \lesssim \Gamma_2 \lesssim 1000$; the ratio $\Gamma_1/\Gamma_2 > 2$ and the efficiency for producing γ-rays is $\gtrsim 10\%$ for the allowed 5-D parameter space for SSC. The

bulk LF of post-shock gas $100 < \Gamma < 1000$ is compatible with late time afterglow modeling.

We now calculate the x-ray and optical emissions accompanying the γ-ray pulse.

6.4.1.2a. X-ray emission for $1/3 < \alpha \leq 1$ SSC solutions

The 1 keV prompt emission from SSC and synchrotron processes is shown in the top two panels of figure 6.10. The contributions of SSC & synchrotron to 1 keV flux is shown separately in the top left panel for *GRB-♮*, and the sum of the two for a variety of GRB parameters can be found in the top right panel.

The x-ray flux can be estimated analytically using the expression for synchrotron flux $f_x = f_{\nu_p}(1\mathrm{keV}/\nu_i)^{-p/2}$, since $\nu_i \sim \nu_c \sim \nu_a$; f_x can also be expressed as $f_x \sim f_\gamma \tau^{-1} \gamma_i^{-p} (25)^{p/2} \nu_{\gamma 5}^{p/2}$, or in terms of observable parameters

$$f_x \sim \frac{9\times10^3}{17^p} \nu_{\gamma 5}^{\frac{p+2}{4}} f_\gamma^{\frac{34+p}{36}} t_\gamma^{\frac{2-p}{18}} t_a^{\frac{2-p}{9}} Y^{-\frac{16+p}{18}} (1+Y)^{\frac{2-p}{9}} d_{L28}^{\frac{p-2}{18}} (1+z)^{\frac{2-p}{9}} A_{2p}^{\frac{16+p}{18}} \eta_a^{\frac{(p-2)(p+18)}{36}} \mathrm{mJy}, \quad (6.101)$$

or $f_x \sim 9 Y^{-\frac{16}{15}} (1+Y)^{-\frac{2}{15}} \mathrm{mJy}$ for *GRB-♮* with $\eta_a > 1$, $p = 3.2$ and $t_a \sim t_\gamma$; this is roughly consistent with the numerically calculated flux shown in fig. 6.10.

In the top right panel of Figure 6.10, the total 1 keV prompt flux is shown for a number of different values of ν_γ, f_γ, and t_γ. The dependence of the x-ray flux on these quantities agree with equation (6.101), which gives $f_x \overset{\propto}{\sim} \nu_\gamma^{\frac{13}{10}} f_\gamma^{\frac{31}{30}} t_\gamma^{-\frac{1}{15}}$ for $p = 3.2$: an increase in ν_γ or f_γ leads to an increase of f_x, and an increase in t_γ has little effect on the x-ray flux (fig. 6.10). The 1 keV flux for all of these cases ranges from 0.01 to 10^3 mJy during the burst; the

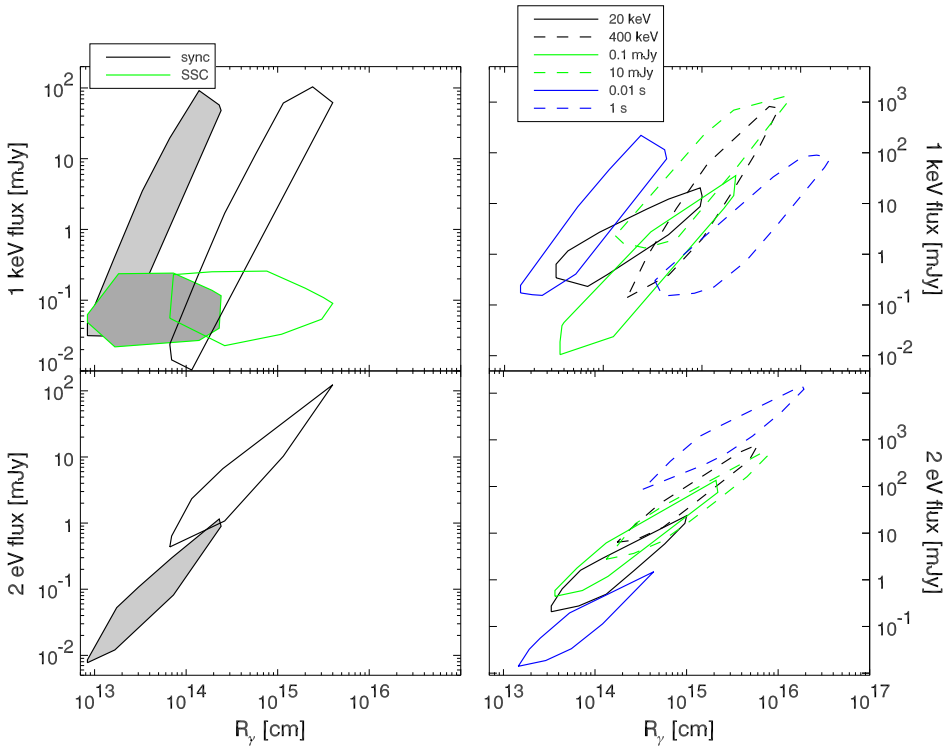

Figure 6.10 X-ray (1 keV) and optical (2eV) synchrotron and SSC flux accompanying the prompt GRB emission for SSC solutions with $1/3 < \alpha \leq 1$. **Right panels:** The sum of SSC and synchrotron contributions for several different sets of ν_γ, f_γ & t_γ as described in Figure 6.8. **Left two panels:** the areas shaded in gray are the x-ray and optical flux for *GRB-♮* (a GRB that has $\nu_\gamma = 100$keV, $f_\gamma = 1$mJy & $t_\gamma = 0.1$s) and with $t_a = t_\gamma/100$, and the unshaded areas are for *GRB-♮* with $t_a = t_\gamma$.

flux at 100s, the time when the x-ray telescope aboard the *Swift* satellite starts looking at the burst, would be smaller by a factor of ~ 10–10^3 depending on GRB pulse duration. So, the x-ray flux accompanying the γ-ray radiation, for the SSC model of GRBs, is consistent with the observed data.

6.4.1.2b. Optical emission for $1/3 < \alpha \leq 1$ SSC solutions

The prompt optical flux accompanying γ-rays, in the SSC model, is shown in the bottom left panel of Figure 6.10. Analytically we find the prompt R-band flux due to the synchrotron component underlying the SSC model to be: $f_R \sim f_{\nu_p} \sim f_\gamma \tau^{-1}$, or

$$f_R \sim 9 \times 10^3 \nu_{\gamma_5}^{\frac{1}{2}} f_\gamma^{\frac{17}{18}} t_\gamma^{\frac{1}{9}} t_a^{\frac{2}{9}} Y^{-\frac{8}{9}} (1+Y)^{\frac{2}{9}} d_{L_{28}}^{-\frac{1}{9}} (1+z)^{\frac{2}{9}} A_{2_p}^{\frac{8}{9}} \eta_a^{\frac{17p-18}{18}} \text{mJy} \qquad (6.102)$$

which for *GRB-♮* reduces to $f_R \sim (8 \times 10^3 \text{ mJy})\ Y^{-\frac{8}{9}}(1+Y)^{\frac{2}{9}}$. There are, however, many numerical solutions corresponding to $Y \gtrsim 10$ for which $f_R \sim 70$ mJy. It turns out that $\nu_a > 2$ eV for the low radius solutions, by up to a factor of 3. If $\nu_i < 2$ eV$< \nu_a$, then the expression for optical flux is

$$f_R \sim 50 \nu_{\gamma_5}^{-\frac{3}{4}} f_\gamma^{\frac{29}{36}} t_\gamma^{\frac{7}{18}} t_a^{\frac{7}{9}} Y^{-\frac{11}{18}} (1+Y)^{\frac{7}{9}} d_{L_{28}}^{-\frac{7}{18}} (1+z)^{\frac{7}{9}} A_{2_p}^{\frac{11}{18}} \eta_a^{-\frac{(7p+126)}{36}} \text{mJy} \qquad (6.103)$$

giving $f_R \lesssim 7 Y^{-\frac{11}{18}} (1+Y)^{\frac{7}{9}}$ mJy for *GRB-♮*.

The optical flux, obtained by numerical calculations, is shown in the bottom right panel of Figure 6.10, for several sets of (ν_γ, f_γ, t_γ). The results are consistent with the dependences found in equations (6.102) or (6.103) when $\nu_a > 2$eV. The reason that the self absorbed f_R increases with ν_γ numerically while equation (6.103) shows a decrease is that $\eta_a \sim \nu_\gamma^{-1/2}$ (confirmed numerically), and the huge dependence of $f_R \propto \eta_a^{4.1}$ gives positive dependence of $f_R \sim \nu_\gamma^{1.3}$. The dependence of optical flux on the duration of the GRB pulse is due to the fact that longer pulses have larger R_γ and $\nu_a < 2$eV. The range of optical flux for SSC solutions is between 0.01 mJy to a few times 10^4 mJy (R

magnitude from 21- to 6-mag). There is an approximately linear relationship between f_R and R_γ. Solutions with R-magnitude of above 9-mag (1 Jy) are most likely ruled out. In particular, this rules out the 1 s pulse duration solutions that have $R_\gamma \gtrsim 2\times10^{15}$cm. If the pulse width were 10 s, the SSC solutions would have prompt optical of between 1 and 4 Jy, or $R\sim7$ mag, which is too bright to have been missed in optical follow up observations. We note that if GRB dissipation radius is $\sim 10^{16}$cm as found in Kumar et al. (2007), then bright optical flux of $R>9$ mag is expected in every GRB produced via SSC. Since this bright optical emission is not seen, this may pose major problems for the SSC process to produce GRBs with positive α.

If, however, electrons are accelerated multiple times during the course of a γ-ray pulse in the GRB light-curve, i.e. $t_a \ll t_\gamma$, the optical flux can be reduced significantly. The dependence $f_R \propto t_a^{2/9}$ (eq. 6.102) itself does not reduce f_R by much, but since $\nu_a \propto t_a^{-\frac{4(p+3)}{9(p+5)}} \sim t_a^{-0.3}$ as well, a smaller t_a gives a larger ν_a and that reduces the optical flux by an additional factor of $\sim t_a^{-0.6}$ and results in $f_R \overset{\propto}{\sim} t_a^{7/9}$; for $t_a = t_\gamma/100$, the optical flux is reduced by a factor of $\sim 10^2$ compared with the case where $t_a \sim t_\gamma$, in agreement with the numerical results found in the lower left hand panel of Figure 6.10. We've numerically searched the whole range of observable parameters and find that the scaling $f_R \overset{\propto}{\sim} t_a^{7/9}$ is valid through the entire solution space, and even the highest optical flux levels of 10 Jy (for the $t_\gamma \sim 1$s case) is reduced below 0.1 Jy, or $R>11$ mag, if $t_a \lesssim t_\gamma/10^2$. Multiple acceleration episodes for electrons is, therefore, a possible way of reducing the excessive optical flux that otherwise necessarily

accompanies SSC solutions for γ-ray emission.

The optical flux should peak at the same time the GRB light curve peaks, since ν_c is on the order of 2 eV. The temporal decay of optical flux in this case is dictated by the curvature or the off-axis emission (Kumar and Panaitescu 2000) — the optical light curve should fall off as $t^{-2-p/2} \sim t^{-3.6}$ as long as ν_a is below the R band. At first glance, it might seem that if $\nu_a > 2$ eV, and the synchrotron spectrum $\propto \nu^{5/2}$ or ν^2 in the optical band, the optical LC would be flat $\sim t^0$ or even rise as $t^{1/2}$. This behavior, however, lasts for a very short time since $(\nu_a/2\text{eV}) \lesssim$ a few, and $\nu_a \propto t^{-1}$ for off-axis emission; once ν_a drops below 2eV the optical flux would start falling off as $\sim t^{-3.6}$. The upper limit of $V \sim 18.5$-mag (0.2 mJy) at 100s for many Swift detected bursts (e.g. Roming et al. 2006) is a lot smaller than the flux expected during the burst for the SSC model. If the pulse occurs at $\sim$ 1s post-trigger then the optical flux at 100s would be smaller than the prompt optical flux by a factor $\sim 10^7$ and that is quite consistent with observational upper limits for almost the entire solution space for the SSC-model.

We emphasize that a bright optical flash ($R \lesssim 14$-mag) concurrent with γ-ray emission is a generic prediction of the SSC-model for GRBs with positive low energy index. Bright, prompt, optical radiation has been reported for a few bursts with positive α – e.g. 990123 (Akerlof et al. 1999; Briggs et al. 1999), 061007 (Golenetskii et al. 2006; Yamaoka et al. 2006), and the second emission episodes of 050401 (Golenetskii et al. 2005) and 050820A (Cummings et al. 2005) – however, if future observations fail to detect prompt optical with

$R \lesssim 14$-mag then that will suggest that one of the assumptions of the model developed in this work has to be abandoned – the most likely possibility, in our view, is to discard the assumption that $t_a \sim t_\gamma$ and that suggests that γ-rays are not generated in a shock heated medium.

6.3.2 SSC solutions for negative low energy spectral index

In this section we consider synchrotron-self-Compton solutions when the spectrum below ν_γ, the peak of νf_ν^{ic}, is $f_\nu^{ic} \propto \nu^\alpha$ with $\alpha < 0$. There are two different class of solutions in this case – those with the underlying seed synchrotron spectrum having $\nu_c < \nu_i$ and vice versa. We treat the two cases separately analytically, but plot the numerical solutions for both cases together in Figure 6.11. We use one vital piece of information gained from the numerical solutions to simplify our analytical calculations: the synchrotron self absorption frequency, ν_a, is larger than $\max(\nu_i, \nu_c)$, and therefore $\nu_\gamma \sim 4\nu_a \max(\gamma_i, \gamma_c)^2$; note that even though $\nu_a > \max(\nu_i, \nu_c)$, the spectral index below ν_γ is negative down to the frequency $\sim \nu_a \min(\gamma_i, \gamma_c)^2 < 10$ keV.

6.3.2.1 $\nu_c < \nu_i$ case

The equations that are solved for this case can be cast in a form very similar to the SSC $\alpha \approx 1/3$ case (considered in §6.3.1.1 by introducing two variables: $\eta_i \equiv \gamma_i/\gamma_c$ and $\eta_a \equiv \gamma_a/\gamma_i$. The equations for ν_c, ν_γ, f_γ, and

Compton-Y expressed in terms of η_i & η_a are:

$$B^2\Gamma\gamma_i \sim 7.7\times10^8\eta_i(1+z)t_a^{-1}(1+Y)^{-1} \tag{6.104}$$

$$B\gamma_i^4\Gamma \sim 2.3\times10^{12}\nu_{\gamma_5}(1+z)\eta_a^{-2} \tag{6.105}$$

$$B\Gamma^5\tau^2 \sim 1.6\times10^6 f_\gamma t_\gamma^{-2}(1+z)d_{L_{28}}^2\eta_a^p\eta_i^2 \tag{6.106}$$

$$\tau\gamma_i^2 \sim 0.75Y\left(\frac{p-1}{p-2}\right)^{-1}\eta_i. \tag{6.107}$$

These equations are solved the same way as outlined in the previous section, and we find the solutions to be:

$$\gamma_i \propto \eta_i^{-\frac{1}{9}}\eta_a^{\frac{-(p+18)}{36}} \tag{6.108}$$

$$B \propto \eta_i^{\frac{2}{3}}\eta_a^{\frac{6-p}{12}} \tag{6.109}$$

$$\Gamma \propto \eta_i^{-\frac{2}{9}}\eta_a^{\frac{7p-18}{36}} \tag{6.110}$$

$$\tau \propto \eta_i^{\frac{11}{9}}\eta_a^{\frac{p+18}{18}}. \tag{6.111}$$

The dependence of B, Γ, γ_i & τ on the observables is same as in equations 6.80-6.83 – the difference is in the dependence on η_a and η_1. The distance of the γ-ray source from the center of the explosion is $R_\gamma \propto t_\gamma\Gamma^2 \propto \eta_i^{-\frac{4}{9}}\eta_a^{\frac{7p-18}{18}}$. We use the constraint that $\nu_a^{ic} \sim 4\nu_a\gamma_c^2 \sim 10^5\nu_{\gamma_5}\eta_i^{-2} < 10$ keV to infer that $\eta_i \gtrsim 3.2$ for these solutions; we numerically find that $\eta_i \gtrsim 10$.

Plugging in the observed values for *GRB-♮* with $p = 2.5$, and using

$\eta_a > 1$ and $\eta_i > 3$, we find the limit on parameters to be

$$\gamma_i \lesssim 50 Y^{\frac{1}{18}} (1+Y)^{\frac{1}{9}} \tag{6.112}$$

$$B \gtrsim 1.2 \times 10^3 \, Y^{\frac{1}{6}} (1+Y)^{-\frac{2}{3}} \text{ Gauss} \tag{6.113}$$

$$\Gamma \lesssim 650 Y^{-\frac{7}{18}} (1+Y)^{\frac{2}{9}} \tag{6.114}$$

$$\tau \gtrsim 3 \times 10^{-4} Y^{\frac{8}{9}} (1+Y)^{-\frac{2}{9}} \tag{6.115}$$

and numerically we find $\gamma_i \lesssim 50$, $B \gtrsim 200$ Gauss, $\Gamma \lesssim 300$, and $\tau \gtrsim 3 \times 10^{-3}$. There is good agreement between the numerical and analytical γ_i and Γ solutions (see fig. 6.11), although analytical and numerical solutions for B, τ & R_γ can differ by a factor of a few due to the difference of a factor of a few in the analytical and numerical value of η_i.

In figure 6.11, we show the numerical solutions for the allowed region in the 5-D space for the SSC-model for a wider range of observables. Note that results for both $\nu_i > \nu_c$ & $\nu_i < \nu_c$ (to be considered analytically in the next subsection) are plotted together in fig. 6.11. The allowed range for electron LF γ_i is 3–200 (fig. 6.11) which is characteristic of mildly relativistic shocks. If we cast the 5-D parameter solutions in terms of colliding shells as described in appendix A, we find the relative LF of collision between shells to be less than a few. For $\Gamma \sim 100$ & $\Gamma_{rel} \sim$ a few, there is little chance of an external forward-shock origin for these SSC photons. However, the 5-D solutions we find appear to be consistent with an internal shock; R_γ is smaller than the

deceleration radius and $f_{B/ke} \lesssim 1$ for the entire SSC solution space.

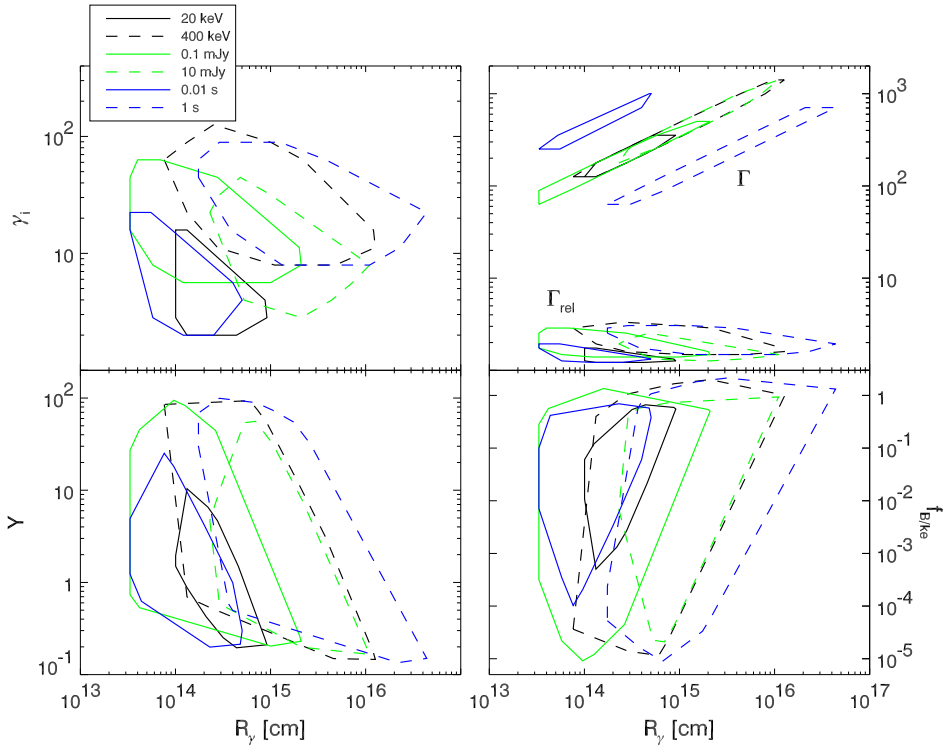

Figure 6.11 Synchrotron-Self-Compton solutions when the spectral index, α, below ν_γ (the peak of νf_ν^{ic}) is less than 0. There are two branches of the solutions both of which are shown in the figure. For one of these branches $\nu_c < \nu_i$, and for the other $\nu_c > \nu_i$; γ-ray sources corresponding to the $\nu_c < \nu_i$ branch lie at a smaller distance from the center of explosion (R_γ) than the other branch. Allowed regions for the 5-D parameter space is shown for a number of different sets of GRB observable parameters (see figure 6.2 caption for details). The top right panel shows the LF of the γ-ray source (one of the five basic parameters we use to describe the source) as well as the Γ_{rel} – the relative LF of collision of two shells obtained by mapping the 5-D parameter solution to internal shocks (see appendix A).

The dependence of the solution space on ν_γ, f_γ, and t_γ is in agreement with analytical estimates; for example, we have verified the analyti-

cal dependence, $\gamma_i \propto \nu_\gamma^{\frac{1}{4}} f_\gamma^{-\frac{1}{36}} t_\gamma^{\frac{1}{6}}$ (for $t_a = t_\gamma$), given in equation (6.108), and $\Gamma \propto \nu_\gamma^{\frac{1}{4}} f_\gamma^{\frac{7}{36}} t_\gamma^{-\frac{1}{6}}$ (eq. 6.110). We find that SSC can produce a wide variety of GRBs with the low energy spectral index $\alpha \sim -1/2$ without requiring extreme parameter values.

In order for these solutions to remain viable, the prompt optical and x-ray flux needs to be in accord with observations and/or upper limits. We next look at the prompt x-ray and optical emission from these solutions.

6.4.2.1a. Prompt x-ray emission for SSC solutions with $\alpha \leq -1/2$

In the top two panels of Figure 6.12, we've plotted the synchrotron and SSC contributions to the x-ray (1 keV) flux accompanying the γ-ray emission during the burst. In the top left panel, we see that the 1 keV flux ranges from 0.1 to over 100 mJy for *GRB-♮* and much of it is due to the underlying synchrotron emission.

There are at least a few solutions for each value of ν_γ, f_γ & t_γ we have considered with x-ray flux less than 10 mJy (fig. 6.12) with the exception of the $f_\gamma \sim 10$ mJy case. The high end of this range of x-ray flux is above the value typically observed by *Swift* at 100 seconds following the burst (10^{-4} to a few mJy); but we know from early x-ray observations that this flux is initially falling off very steeply, $\sim t^{-3}$, and therefore x-ray flux of $\sim 10^3$ mJy during the burst, $t_\gamma \lesssim$10s, would be less than 1 mJy at 100s, or within the observed flux range of the x-ray telescope aboard *Swift*.

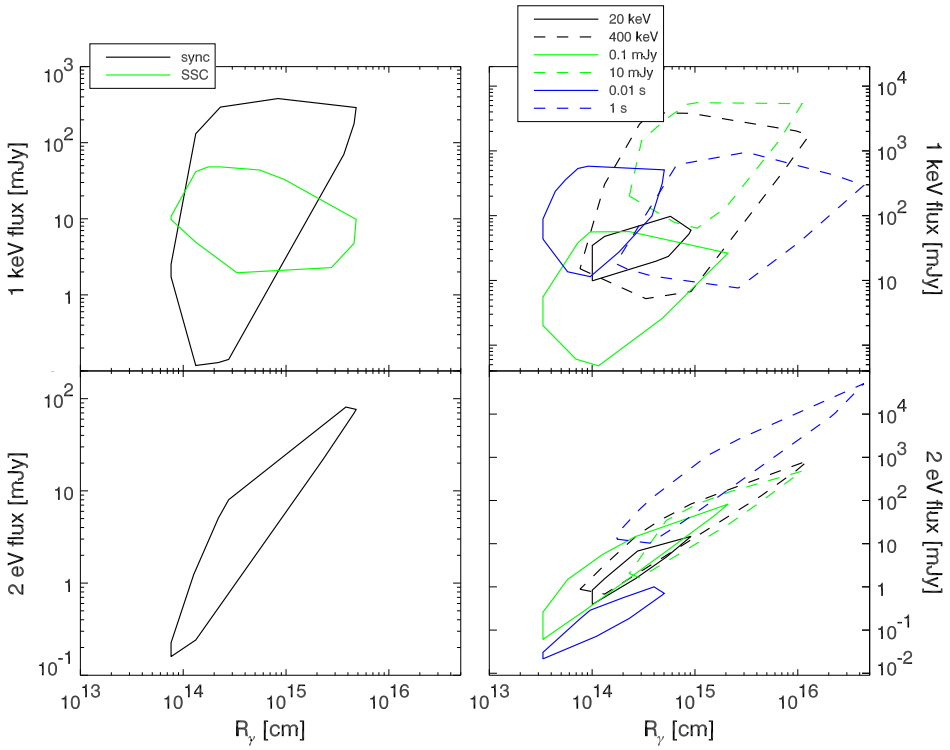

Figure 6.12 X-ray (1 keV) and optical flux simultaneous with the GRB emission for the SSC solutions with $\alpha < 0$ are plotted against the γ-ray emission radius. The top left panel shows the synchrotron & SSC contributions to the 1 keV flux for *GRB*-♮, and the bottom left panel shows the optical (2 eV) flux associated with *GRB*-♮-SSC solutions. The right panels show the 1 keV flux (top right) and 2 eV flux (bottom right) by summing up contributions of synchrotron and SSC for various sets of observed parameters for GRBs as described in the caption for fig. 6.2.

We expect the x-ray flux to be

$$f_x = f_{\nu_p} \left(\frac{1\text{keV}}{\nu_i} \right)^{-\frac{p}{2}} \left(\frac{\nu_i}{\nu_c} \right)^{-\frac{1}{2}}, \tag{6.116}$$

(since synchrotron dominates). In terms of the observable quantities the flux

is

$$f_x \approx \frac{9\times10^3}{17^p}\nu_{\gamma_5}^{\frac{p+2}{4}} f_\gamma^{\frac{34+p}{36}} t_\gamma^{\frac{2-p}{18}} t_a^{\frac{2-p}{9}} Y^{-\frac{16+p}{18}}(1+Y)^{\frac{2-p}{9}} \times d_{L_{28}}^{\frac{p-2}{18}}(1+z)^{\frac{2-p}{9}} A_{2p}^{\frac{16+p}{18}} \eta_a^{\frac{(p-2)(p+18)}{36}} \eta_i^{\frac{p-2}{9}} \text{ mJy}, \quad (6.117)$$

so for $p = 2.5$ and $t_a \sim t_\gamma$, $f_x \propto \nu_\gamma^{\frac{9}{8}} f_\gamma^{\frac{73}{72}} t_\gamma^{-\frac{1}{12}}$. This analytical formula is in good agreement with numerical solutions shown in fig. 6.12.

The upper limit to the synchrotron flux can be understood from the limit we place on the synchrotron 10 keV flux. We restrict synchrotron flux at 10 keV to be less than the 10 keV SSC flux, in order that the GRB spectrum is SSC dominated. The 1 keV synchrotron flux is then $< f_\gamma(10\text{keV}/\nu_\gamma)^{(p-1)/2} \sim$ 55 mJy for *GRB-♮*, in agreement with Figure 6.12.

6.4.2.1b. Prompt optical emission for SSC solutions with $\alpha \leq -1/2$

In the bottom two panels of Figure 6.12, we plot the optical emission accompanying the γ-ray radiation for the SSC solutions. In the optical (2 eV), we look only at the synchrotron emission, since the SSC flux is highly suppressed as $\nu_a^{ic} \gg 2$eV. The optical flux is between 0.2 and 100 mJy, or between $R \sim$ 18 and 11 mags for *GRB-♮* (fig. 6.12). For the range of ν_γ, f_γ, and t_γ we have considered, we find the optical flux to be between 0.02 mJy and 50 Jy, or $R \sim$ 20 to 4 mags (bottom right panel of fig. 6.12). Observational limits on R band flux, 100s after the burst, are $\gtrsim$18.5 mag, or $\lesssim$0.2 mJy, for approximately half of Swift bursts (Roming et al. 2006). For small values of ν_γ, f_γ, and t_γ there is no problem satisfying this upper limit, but large ν_γ, f_γ, or t_γ might exceed the observed optical flux limit. Since the prompt optical flux falls off very rapidly

with time as $t^{-(4+p)/2}$, for $t > t_\gamma$, SSC solutions with hundreds of mJy optical flux during the burst are consistent with the upper limit of $\sim$ 18mag at 100s. The solutions with optical flux greater than 100 mJy or so, however, can be ruled out, since prompt optical flux this bright is very rare.

Analytically, the R-band flux, dominated by synchrotron photons, is

$$f_R \approx \left(\frac{2\mathrm{eV}}{\nu_a}\right)^{\frac{5}{2}} \left(\frac{\nu_a}{\nu_i}\right)^{-\frac{p}{2}} \left(\frac{\nu_i}{\nu_c}\right)^{-\frac{1}{2}} f_{\nu_p}, \tag{6.118}$$

provided that $\nu_a > 2\mathrm{eV}$, and $\nu_c < \nu_i < \nu_a$. In terms of the observed quantities the flux is given by

$$f_R \sim 2 \times 10^3 \, \nu_{\gamma_5}^{-\frac{3}{4}} f_\gamma^{\frac{29}{36}} t_\gamma^{\frac{7}{18}} t_a^{\frac{7}{9}} Y^{-\frac{11}{18}} (1+Y)^{\frac{7}{9}} d_{L_{28}}^{-\frac{7}{18}} (1+z)^{\frac{7}{9}} A_{2p}^{\frac{11}{18}} \eta_a^{-\frac{7(p+18)}{36}} \eta_i^{-\frac{7}{9}} \, \mathrm{mJy}. \tag{6.119}$$

If we assume that $t_a \sim t_\gamma$, we find $f_R \propto \nu_\gamma^{-\frac{3}{4}} f_\gamma^{\frac{29}{36}} t_\gamma^{\frac{7}{6}}$. This agrees with what we find numerically for f_γ and t_γ, but not ν_γ. Numerically, f_R increases with ν_γ, while this expression shows a decrease. This difference is caused by the sensitivity of $f_R \sim \eta_a^{-4}$ – numerically we find that $\eta_a \propto \nu_\gamma^{-1/2}$, changing the above dependence on ν_γ to be $f_R \sim \nu_\gamma^{\frac{5}{4}}$, in accord with results shown in Figure 6.12.

For *GRB-ϟ*, $f_R \lesssim 120 Y^{-\frac{11}{18}} (1+Y)^{\frac{7}{9}}$ mJy. This estimation for f_R is larger by a factor $\sim$ 10 than what we find numerically (see fig. 6.12). This factor of 10 difference is due to the fact that $\gamma_c \sim 1$ for many of these solutions. When $\gamma_c < 2$, we have a population of electrons that don't radiate synchrotron emission and we need to reduce the number of radiating particles. This is done by using $\nu_c \propto (\gamma_c - 1)^2$. Since $f_R \propto \nu_c^{\frac{1}{2}}$, the correct value of f_R, is a factor of

$\gamma_c/(\gamma_c-1)$ smaller than the crude analytical estimate above. The smallest value of γ_c that we find numerically is 1.08, and therefore the analytical expression for f_R overestimates the true flux, calculated numerically, by a factor of about ~ 14. This indeed reconciles the analytical and numerical results.

The R-band flux increases with increasing t_γ. This is because increasing the pulse duration increases the radius at which the GRB emission is produced, and the synchrotron self absorption frequency is smaller at larger radii, and therefore brighter optical flux is observed. Thus, a prediction of the SSC model is that brighter optical flux accompanies wider GRB pulses — very spiky light curves (with short variability time scale) will have small optical flux that can escape detection, but those with wide pulses should have bright early optical afterglows. If a pulse duration were to be 10 s, we should expect prompt optical flux of 100 mJy or larger (R-band magnitude smaller than 11^{th}). If this optical emission is not detected, it will point to one of the assumptions in our model for the SSC-emission being violated – most likely $t_a \not\sim t_\gamma$, i.e. electrons are not accelerated just once, but multiple times, during the course of a pulse duration of t_γ.

6.3.2.2 $\nu_i < \nu_c$ case

Analytically this case is very similar to the case of $\nu_c < \nu_i$ discussed in §6.3.2.1. We require this time that $\gamma_i/\gamma_c = \eta_i < 1$ and η_a is still > 1. Since the ratio $\gamma_a/\gamma_c = \eta_a\eta_i$, we will see that some of the solutions can be expressed in terms of $\eta_a\eta_i$ instead of using η_i and η_a separately.

The equations that we are solving for, in this case are

$$B^2\Gamma\gamma_i \sim 7.7\times10^8\eta_i(1+z)t_a^{-1}(1+Y)^{-1} \tag{6.120}$$

$$B\gamma_i^4\Gamma \sim 2.3\times10^{12}\nu_{\gamma_5}(1+z)\eta_a^{-2}\eta_i^2 \tag{6.121}$$

$$B\Gamma^5\tau^2 \sim 1.6\times10^6 f_\gamma t_\gamma^{-2}(1+z)d_{L28}^2\eta_a^p\eta_i^{2-p} \tag{6.122}$$

$$\tau\gamma_i^2 \sim 0.75Y\left(\frac{p-1}{(p-2)(3-p)}\right)^{-1}\eta_i^{3-p}. \tag{6.123}$$

These equations are almost identical to the SSC $\nu^{\frac{1}{3}}$ case of §6.3.1.1, with exception of the dependence on the variables η_i and η_a and a slight change in the Y expression with an additional factor of $(3-p)$. These equations are solved same way as outlined in §6.3.1.1. We find that the solutions have the following dependence on η_i and η_a:

$$\gamma_i \propto \eta_a^{\frac{-(p+18)}{36}}\eta_i^{\frac{18-p}{36}} \tag{6.124}$$

$$B \propto (\eta_i\eta_a)^{\frac{6-p}{12}} \tag{6.125}$$

$$\Gamma \propto (\eta_i\eta_a)^{\frac{7p-18}{36}} \tag{6.126}$$

$$\tau \propto \eta_i^{\frac{36-17p}{18}}\eta_a^{\frac{p+18}{18}}. \tag{6.127}$$

The rest of the dependence on ν_γ, f_γ & t_γ is same as in equations 6.108–6.111. The distance of γ-ray source $R_\gamma \propto \Gamma^2 \propto (\eta_i\eta_a)^{\frac{7p-18}{18}}$. We constrain η_i by requiring $\nu_a^{ic} \sim 4\nu_a\gamma_i^2 \sim \nu_\gamma\eta_i^2 \lesssim 10$ keV, which suggests that $\eta_i \lesssim 0.3$, in accord with the numerical calculation.

Numerically, we find $\gamma_i \lesssim 20$, $B \lesssim 2 \times 10^3$ Gauss, $\Gamma \lesssim 10^3$, and $\tau \gtrsim 10^{-3}$ for *GRB-♮* (fig. 6.11). The γ-ray source radius $R_\gamma \lesssim 2 \times 10^{15} Y^{-\frac{7}{9}} (1+Y)^{\frac{4}{9}}$ cm is in good agreement with $R_\gamma \lesssim 5 \times 10^{15}$cm obtained by numerical calculations. Note that R_γ for this case is a factor of a few higher than the $\nu_c < \nu_i$ case discussed in §6.3.2.1.

The numerical results for the allowed region of 5-D space, for $\nu_c > \nu_i$, are also shown in Figure 6.11. The solutions corresponding to $\nu_i > \nu_c$ are those at larger radius – the right hand side of each solution contour, or bubble, shown in the figure. These solutions have smaller γ_i, larger Γ, smaller B & τ, and a little bit smaller Y. Since these solutions too seem viable for shock models, we explore below the x-ray and optical flux accompanying γ-ray emission.

6.4.2.2a. Prompt X-ray and optical flux

The analytical expression for the x-ray flux is almost identical to that found for the $\nu_c < \nu_i$ case (eq. 6.117) – the only difference is in the dependence on η_a and η_i. We find that –

$$f_x \propto (\eta_i \eta_a)^{\frac{(p-2)(p+18)}{36}} , \tag{6.128}$$

and the lower limit on the x-ray flux is $\sim 50 Y^{-\frac{37}{36}} (1+Y)^{-\frac{1}{18}}$mJy; this is in agreement with numerical results shown in fig. (6.12).

The R-band flux, dominated by synchrotron emission, is

$$f_R \sim \left(\frac{2\text{eV}}{\nu_a}\right)^2 \left(\frac{\nu_a}{\nu_c}\right)^{-\frac{p}{2}} \left(\frac{\nu_c}{\nu_i}\right)^{-\frac{p-1}{2}} f_{\nu_p} \tag{6.129}$$

which is, in terms of the observed quantities, given by

$$f_R \sim 3\times 10^3\, \nu_{\gamma_5}^{-\frac{1}{2}} f_\gamma^{\frac{5}{6}} t_\gamma^{\frac{1}{3}} t_a^{\frac{2}{3}} Y^{-\frac{2}{3}} (1+Y)^{\frac{2}{3}} d_{L_{28}}^{-\frac{1}{3}} (1+z)^{\frac{2}{3}} A_{1p}^{\frac{2}{3}} (\eta_a\eta_i)^{-\frac{p+18}{6}} \text{ mJy} \quad (6.130)$$

with the value of $f_R \lesssim 1700$ mJy for *GRB-♮*. This is higher than the numerical results that give $f_R \lesssim 200$ due to the sensitivity of f_R on $\eta_a\eta_i \gtrsim 2$. If we assume that $t_a \sim t_\gamma$, as has been done numerically, we find $f_R \propto \nu_\gamma^{-\frac{1}{2}} f_\gamma^{\frac{5}{6}} t_\gamma$. Numerically we find that f_R increases with ν_γ, f_γ, and t_γ, and is most sensitive to t_γ. The increase of f_R with ν_γ is again due to the high sensitivity on $\eta_a\eta_i$ which numerically we find is $\propto \nu_\gamma^{-1/2}$.

We note that the optical flux for this case ($\nu_i < \nu_c$) is larger than when $\nu_c < \nu_i$ – 10^2– 10^3mJy – since R_γ is larger for these solutions. For $t_a/t_\gamma = 10^{-2}$ f_R is reduced by a factor of ~ 50. This brings the highest flux for the $t_\gamma \sim 1$ s solutions down to about 140 mJy – still a bit bright, but there are many other solutions for this case that have flux smaller than about 10 mJy, and probably in accord with observations and upper limits. Thus, bright optical flux is a generic prediction of the SSC model for γ-ray generation whether the low energy spectral index is positive or negative; the optical is particularly bright for $\alpha > 0$. This is a problem for the SSC model if $R_\gamma \sim 10^{16}$ cm, as found in Kumar et al. (2007), as the brightest optical flux is produced at the larger R_γ. One of the, possibly only, ways to avoid bright, prompt, optical emission is if $t_a \ll t_\gamma$.

6.4 GeV photon signal for synchrotron and SSC solutions

Detection of GeV photons by the Gamma Ray Large Area Space Telescope (GLAST) (McEnery and GLAST Mission Team 2006) will be a useful piece of evidence to use to determine if GRBs are produced by synchrotron or SSC emission mechanisms. The IC scattering of γ-ray photons produced by synchrotron will peak above the GLAST band, $\gg 100$ GeV, while the second IC scattered SSC photons will peak at ~ 1 GeV.

For the synchrotron cases $\alpha = 1/3$ and $-(p-1)/2$, $\max(\gamma_i, \gamma_c) \sim 10^4$ and $\tau \lesssim 10^{-6}$, giving the peak of IC scattered flux νf_ν at $\nu_G \sim \nu_\gamma \max(\gamma_i, \gamma_c)^2 \sim 10^4$ GeV and flux $\nu f_\nu \sim \tau f_\gamma \nu_G \sim 10^{-7}$ erg s^{-1} cm^{-2}. We need to ensure that such high energy photons can escape the source region and are not converted to electron-positron pairs. This effect is incorporated in our numerical calculations and is discussed below; moreover, $\nu_G < \max(\gamma_i, \gamma_c)\Gamma m_e c^2/(1+z)$.

The SSC $\alpha > 0$ solutions have $\gamma_i \sim \gamma_c \lesssim 10^2$ and $\tau \gtrsim 10^{-4}$ giving the second scattering peak of $\nu_G \sim 4\nu_\gamma \gamma_i^2 \sim 1$ GeV and the flux $\nu f_\nu \sim 10^{-7}$ erg s^{-1} cm^{-2}. The SSC $\alpha < 0$ solutions have very similar ν_G and νf_ν. The SSC signals are well above the GLAST threshold,[7] so we expect to see a GeV signal from GRBs produced by the SSC process. The synchrotron flux, however, might be below the GLAST threshold. The spectral shape will also be different – ν_G peaks well above the GLAST band for the synchrotron case, while SSC should

[7] `http://www-glast.slac.stanford.edu/software/IS/glast_lat_performance.htm`

peak at the low end of the GLAST band.

Using analytical results for the synchrotron $\alpha = 1/3$ case (Equations 6.45–6.48), we find that the IC scattered signal peaks at

$$\begin{aligned}&\nu_G^s \sim \gamma_i \Gamma m_e c^2/(1+z) \sim \\ &2\times 10^4 \nu_{\gamma_5}^{\frac{1}{4}} f_\gamma^{\frac{1}{8}} t_\gamma^{-\frac{1}{4}} t_a^{\frac{1}{2}} Y^{-\frac{1}{8}} (1+Y)^{\frac{1}{2}} d_{L_{28}}^{\frac{1}{4}} (1+z)^{-\frac{1}{2}} \left[\tfrac{p}{p-2}\right]^{\frac{1}{8}} \text{GeV};\end{aligned} \tag{6.131}$$

This is due to the Klein-Nishina reduction to cross-section above electron rest frame photon energy of $m_e c^2$.

The frequency above which the high energy spectrum is attenuated due to $\gamma\gamma \rightarrow e^- e^+$ is $\nu_\pm \sim (\Gamma m_e c^2)^2/\nu_{\tau\sim 1}$, where $\nu_{\tau\sim 1}$ is the frequency of the synchrotron photon at which the optical depth to pair production with $nu_\pm$ photons is 1. The optical depth to pair production is $\tau_{\gamma\gamma} \sim \sigma_T n'_{\nu'} R_\gamma/\Gamma$, where $n'_{\nu'} \sim L_{iso}(\nu)/4\pi\Gamma c R_\gamma^2$ is the comoving number density of photons between ν' and $2\nu'$, R_γ/Γ is the comoving shell width, and $L_{iso}(\nu)$ is the observed isotropic luminosity per unit frequency. To find $\nu_{\tau\sim 1}$, we set $\tau_{\gamma\gamma} \sim 1$ and solve the equation using the observed γ-ray spectrum; $\nu_\pm$ is calculated from Γ & $\nu_{\tau\sim 1}$. In terms of the observable parameters for the synchrotron $\alpha = 1/3$ case, we find

$$\nu_\pm \sim 4\times 10^3 \nu_{\gamma_5}^{\frac{1}{4}} f_\gamma^{\frac{1}{4}} t_\gamma^{-1} t_a Y^{-\frac{3}{4}} (1+Y) d_{L_{28}}^{\frac{1}{2}} (1+z)^{\frac{1}{2}} \left[\frac{p}{p-2}\right]^{\frac{3}{4}} \text{GeV} \tag{6.132}$$

where we have assumed that the synchrotron GRB spectrum is $L_{iso}(\nu) \propto \nu^{-2}$ for $\nu > \nu_\gamma$. Since $\nu_\pm < \nu_G^s$ (calculated above), and the spectrum falls off very steeply above $\nu_\pm$, the IC spectrum will peak at $\nu_\pm$ for many of the synchrotron solutions.

The flux at ν_G^s, with appropriate Klein-Nishina cross section, is

$$[\nu f_\nu]^s \sim 8 \times 10^{-10} \nu_{\gamma_5}^{-\frac{3}{2}} f_\gamma^{\frac{3}{2}} t_\gamma^{-1} Y^{\frac{1}{2}} d_{L_{28}} (1+z)^{-2} \left[\frac{p}{p-2}\right]^{-\frac{1}{2}} \text{ erg s}^{-1}\text{cm}^{-2}. \quad (6.133)$$

This flux is probably just at the GLAST threshold for detection. If $\nu_\pm < \nu_G^s$, the νf_ν spectrum peaks at $\nu_\pm$, and the flux at this frequency will be smaller than that in equation 6.133. The results are very similar for the $\alpha = -(p-1)/2$ case, since the $\alpha = 1/3$ case is a subset of the $\alpha = -(p-1)/2$ solutions with $\gamma_i \sim \gamma_c$.

For the SSC case, using the $\alpha > 0$ analytical results in Equations 6.93 – 6.96, the 2^{nd} IC peak is

$$\nu_G^{ic} \sim 3\nu_{\gamma_5}^{\frac{3}{2}} f_\gamma^{-\frac{1}{18}} t_\gamma^{\frac{1}{9}} t_a^{\frac{2}{9}} Y^{\frac{1}{9}} (1+Y)^{\frac{2}{9}} d_{L_{28}}^{-\frac{1}{9}} (1+z)^{\frac{2}{9}} A_{2_p}^{-\frac{1}{9}} \eta_a^{-\frac{p+18}{18}} \text{ GeV} \quad (6.134)$$

and the flux at this peak is

$$[\nu f_\nu]^{ic} \sim 7 \times 10^{-7} \nu_{\gamma_5} f_\gamma Y A_{2_p}^{-1} \text{ erg s}^{-1}\text{cm}^{-2}. \quad (6.135)$$

ν_G is smaller than $\nu_\pm$ for the majority of the SSC solution space, so the 2nd inverse Compton scattering spectrum will indeed peak at ν_G. For the SSC $\alpha < 0$ case, the expressions are very similar – the only difference is the dependence on η_a, η_i, and p:

$$\nu_G^{ic} \sim 3\nu_{\gamma_5}^{\frac{3}{2}} f_\gamma^{-\frac{1}{18}} t_\gamma^{\frac{1}{9}} t_a^{\frac{2}{9}} Y^{\frac{1}{9}} (1+Y)^{\frac{2}{9}} d_{L_{28}}^{-\frac{1}{9}} (1+z)^{\frac{2}{9}} A_{1_p}^{-\frac{1}{9}} \eta_a^{-\frac{p+18}{18}} \eta_i^{\frac{18-p}{18}} \text{ GeV} \quad (6.136)$$

and the flux at this peak is

$$[\nu f_\nu]^{ic} \sim 7 \times 10^{-7} \nu_{\gamma_5} f_\gamma Y \eta_i^{3-p} A_{1_p}^{-1} \text{ erg s}^{-1}\text{cm}^{-2}. \quad (6.137)$$

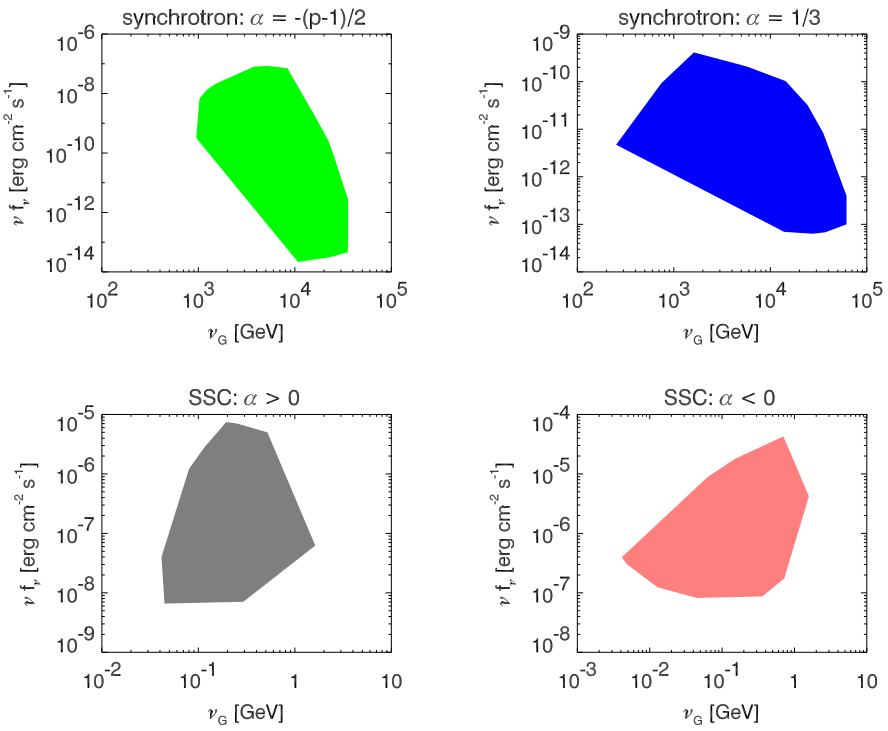

Figure 6.13 Numerical results for the IC scattering of prompt γ-ray photons in the source. The four panels show the peak of IC spectrum (ν_G) and the flux (νf_ν) at the peak when the γ-ray emission is produced via the synchrotron process (top two panels) and via the SSC process (bottom two panels) for $\alpha > 0$ & $\alpha < 0$ cases; for all of these cases we took the underlying γ-ray spectrum with $\nu_\gamma = 100$keV & $f_\gamma = 0.1$mJy. The IC signal for many of the synchrotron solutions are affected by photon-photon pair production, and that is included in these numerical calculations; the effect of pair production is very small in the SSC cases. The Klein-Nishina cross-section has been used in these calculations, and it significantly affects the IC peak flux when γ-rays are generated via the synchrotron process.

We show numerical results for ν_G and νf_ν for 4 cases in Figure 6.13 – the two synchrotron cases of $\alpha = -(p-1)/2$ and $1/3$ and the SSC cases of $\alpha < 0$ and > 0. These numerical results are in rough agreement with our analytical

estimates.

In summary, IC scattering of prompt γ-ray photons, when the GRB emission is produced via the synchrotron process, gives rise to a spectrum that peaks at $\sim$ TeV, the flux is of order 10^{-9} erg cm^{-2} s^{-1} (Figure 6.13), the spectrum below the peak is between $\nu^{1/3}$ or $\nu^{-(p-1)/2}$, and the spectrum above the peak is expected to be sharply cutoff due to pair production. On the other hand, if the GRB emission is produced via the SSC process then the spectrum of 2^{nd} IC scattered photons should peak at $\sim$ 1 GeV, with a flux of $\sim 10^{-6}$ erg cm^{-2} s^{-1} (Figure 6.13), and the spectrum above the peak should be $f_\nu \propto \nu^{-1.5}$. This signal should be detected by GLAST. If GRBs are not detected in the GLAST band, that would suggest that GRB prompt emission is not generated via the SSC process. We note that the GLAST band flux cannot be reduced in the case of repeated acceleration of electrons during a single GRB pulse.

6.5 Comparison with prior work on γ-ray generation mechanism

We provide a brief comparison with published work on γ-ray generation in the internal shock model (Rees and Mészáros 1994; Paczynski and Xu 1994; Papathanassiou and Mészáros 1996; Mészáros and Rees 1997b; Sari and Piran 1997b) and the formalism/results of this chapter. There is a fairly extensive literature on this topic and this is not the place to provide a general review. What we wish to do is to describe the main difference between

previous approaches and the work presented here.

We should note that γ-ray generation in the external shock model has also been looked at by a number of people eg. Rees and Mészáros (1992); Mészáros and Rees (1993a); Piran et al. (1993); Dermer et al. (1999); Dermer and Mitman (1999); McMahon et al. (2004); Ramirez-Ruiz and Granot (2006); the issue of variability in external shocks is discussed in Sari and Piran (1997a); Dermer and Mitman (1999); Nakar and Granot (2006). We don't have anything particularly enlightening to say regarding the external shock model that has not already been mentioned by one of these authors; the general problem with shocks is discussed in §6.2 & §6.3.

The main difference between previous works and our approach is that previous works considered the forward problem i.e., starting with a parameterization of the properties of colliding shells and resulting shocks the emergent radiation field was calculated, whereas our approach is to start with the minimum number of physical parameters needed (five) to calculate the observed flux and spectrum – at one instant in time or for one pulse in a multi-pulse GRB lightcurve – and determine these using the observed data. For synchrotron & IC radiations the parameters needed are γ_i, Γ, B, N, and τ, which are determined by the observational data ν_γ, f_γ, t_γ, and α for a pulse in GRB LC. The 5 parameters in turn are used to provide constraint on the nature of GRB source. The *old forward approach* is wedded to a particular model – either internal or external shock – whereas the method used in this work is relatively model independent.

The parameters of the internal shock model can be mapped into the five parameters (γ_i, Γ, B, N, τ) in a straightforward manner – this in fact is done implicitly in all the *forward approach* papers in order to calculate the emergent radiation. The converse of this is not true, however, since the internal shock model has more than 5 independent parameters (appendix A describes how to go from the five parameters to providing a limit on some of the internal shock parameters such as the initial LFs of colliding shells and their comoving densities).

Papathanassiou and Mészáros (1996) and Sari and Piran (1997b) carried out a fairly detailed analysis of prompt emission in the internal shock model. These authors addressed a set of questions such as the ability of synchrotron/SSC in internal shocks to produce a spectral peak near 100 keV, the observed flux in the γ-ray band, and short time scale variability. Papathanassiou and Mészáros (1996) and Sari and Piran (1997b) realized that the cooling time scale for electrons (compared to the dynamical time) for internal shocks is short and although Sari and Piran (1997b) don't explicitly say, their work applies to GRBs with $\alpha = -1/2$. Papathanassiou and Mészáros (1996) look at composite synchrotron/SSC spectra, however there are many free parameters and little comparison to observed properties of GRBs. Had these authors investigated the self-consistency of synchrotron internal-shock model for the case of $\alpha = 1/3$, they would have discovered the problem reported in this chapter using their *forward modeling* approach.

Ghisellini et al. (2000) did in fact worry about synchrotron solutions

when $\alpha > 0$ and concluded that it is impossible to account for it in shock based models (this is paraphrasing their actual wordings). They pointed out that electron cooling time, during prompt emission, is much smaller than the dynamical time [as was reported in Papathanassiou and Mészáros (1996) and Sari and Piran (1997b)] and therefore the GRB spectrum below the peak should be always $\nu^{-1/2}$ if the radiation is produced via synchrotron process. Ghisellini et al. (2000) considered the possibility that a lower strength magnetic field would avoid the excessive cooling of electrons, and rejected it based on the argument that IC emission would dominate in this case i.e., $Y \gg 1$, and that IC spectrum too would be falling of as $\nu^{-1/2}$ or steeper due to IC cooling. We find that a smaller magnetic field can avoid excessive cooling, so that $\alpha = 1/3$, and at the same time Compton $Y \sim 1$. The reason for these different conclusions is that we don't impose any restriction on the source distance that *forward calculations* based on internal shocks do. The most serious problem with synchrotron $\alpha = 1/3$ case is that $R_\gamma > R_d$ unless $n_0 \ll 1$ cm^{-3} (see §6.2.2).

Ghisellini et al. (2000) correctly pointed out that re-acceleration of electrons, in shock based models, would not work because it requires too much energy; one has a continuous stream of electrons crossing the shock front – and to accelerate all of these electrons to their original energy distribution, so that $\alpha = 1/3$, while they are rapidly losing energy to radiation will indeed require much more energy than is available in the shock. The re-acceleration invoked in this work is not shock based. It in fact requires abandoning shock models and

considering a scenario where particles are NOT being added to the "system" – the source for γ-ray photons – continuously (as in shock based models) but where the source has a fixed number of particles that are being continuously accelerated; there is no excessive energy problem in this scenario.

6.6 Discussion

In this chapter we have investigated the generation of γ-rays in gamma-ray bursts via synchrotron or synchrotron-self-inverse-Compton (SSC) emissions in a relativistic outflow. The SSC radiation from a relativistic source can be fully described by a set of 5 parameters (γ_i, Γ, B, N, τ); see table 6.1 for definition of symbols used in the chapter. For each possible low energy spectral index, we have analytically and numerically determined the region of the 5-D parameter space that is consistent with a set of GRB observations – ν_γ, f_γ, & t_γ. For these allowed regions – or *solution* sub-space – we calculate the x-ray and optical fluxes that should be seen concurrent with the γ-ray radiation to further narrow down the properties of γ-ray sources. The set of five parameters also allows us to determine the distance of the source from the center of explosion (R_γ).

We find that if γ-ray emission were to be produced via the synchrotron process, the required set of parameters and burst radius have extreme values that are not internally consistent and are in conflict with afterglow data. In particular, when the low energy spectrum is $f_\nu \propto \nu^{1/3}$ or $\nu^{-\frac{p-1}{2}}$, the Lorentz factor of the source is required to be larger than $\sim 10^3$, in disagreement with

afterglow modeling, and the source distance (R_γ) is larger than the deceleration radius even when the density of the medium is as small as ~ 0.1 cm^{-3}. The requirement on the magnetic field strength is also very stringent; the comoving field strength is required to lie in a very narrow range of about $\sim$ 10–30 Gauss in order to explain the radiation for a typical burst as synchrotron emission. Allowing for the possibility of multiple electron acceleration episodes, i.e. $t_a \ll t_\gamma$, alleviates the problem of large R_γ & Γ; in this scenario the synchrotron process could account for the prompt γ-ray radiation for GRBs (see §6.2.1 & 6.2.2).

The reason that synchrotron solutions with $\alpha = -(p-1)/2$ & $1/3$ require large R_γ & Γ is easy to understand. The number of electrons needed to produce the observed flux via the synchrotron process is $\sim 10^{53} f_\gamma/(B\Gamma)$. And in order to keep the Compton-Y parameter ($Y \sim \tau\gamma_i\gamma_c$) less than ~ 10 — otherwise most of the energy will come out in IC-scattered photons at $\nu \gg 1$ GeV — the source must have small τ or large R_γ. Moreover, since $t_\gamma \sim R_\gamma/(4c\Gamma^2)$, large R_γ solutions also have large Γ for a given GRB pulse width of t_γ. The reason that $t_a \ll t_\gamma$ offers a way out of this problem is also easy to understand. Frequent re-acceleration of charge particles makes it possible to have larger magnetic field while keeping $\nu_c \gtrsim 100$ keV. This decreases the number of particles required to produce the observed flux (f_γ), and that in turn makes it possible to have a smaller R_γ.

For $f_\nu \propto \nu^{-1/2}$, the allowed region of the 5-D parameter space for the synchrotron process is quite reasonable. However, interpreting these solutions

in terms of the internal shock model requires the ratio of LFs of the two colliding shells to be rather large ($\gtrsim 10-20$) when the ratio of magnetic energy to electron energy is $\lesssim 10$, i.e. if we want the energy fraction in electrons to be not too small – otherwise γ-ray production would be very inefficient (see §6.2.3).

The SSC process provides viable solutions for the prompt emission of a large fraction of GRBs. We have considered almost all different possibilities of the low energy spectrum for GRBs: $f_\nu^{ic} \propto \nu^\alpha$ below the peak of νf_ν^{ic} with $-1 \lesssim \alpha \leq 1$. The solution space (a hypersurface in the 5-D parameter space) is quite large for $\alpha < 0$ and $0.5 \lesssim \alpha \leq 1$. However, there are no SSC solutions when $\alpha \sim 1/3$; the reason is that the synchrotron characteristic and cooling frequencies should be equal ($\nu_i \sim \nu_c$) in order that $\alpha = 1/3$, and in that case the synchrotron-self-absorption frequency is shown to be roughly equal to ν_i as well (see §6.3.1.1), and therefore the low energy spectral index is ~ 1 and NOT $\sim 1/3$ as desired.

The SSC solution space for $\alpha < 0$ and $0.5 \lesssim \alpha \leq 1$ has source LF of order 100, the minimum electron energy $\lesssim 10^2 m_e c^2$ (characteristic of mildly relativistic shocks), and $10^{14} \lesssim R_\gamma \lesssim 10^{16}$cm is smaller than the deceleration radius. These solutions are accompanied by bright optical synchrotron flux of ~ 10 mJy (14^{th} mag) to several hundred mJy – brightest for bursts with $\alpha \sim 1$ and those bursts with large pulse duration on the order of $\gtrsim$1s. Moreover, the optical flux is correlated with R_γ – the flux is larger for larger R_γ – and for $R_\gamma \gtrsim 2 \times 10^{15}$ (cf. Kumar et al. 2007), the optical flux is $\gtrsim$100mJy ($< 12^{th}$ mag).

Bright optical flux contemporaneous with γ-rays is a prediction of the SSC model that future observations should be able to test. We note that the large optical flux accompanying γ-rays can be reduced only if each radiating electron is accelerated numerous times ($\gtrsim$100) in time period of order the duration of a pulse in the GRB lightcurve, i.e. $t_a \lesssim t_\gamma/10^2$. GRB models based on converting kinetic energy to radiation via shocks have $t_a \sim t_\gamma$, where particles are accelerated at the shock-front and not down-stream, but continuous particle acceleration might work for some alternate scenarios such as magnetic field reconnection/dissipation.

There have, in fact, been simultaneous optical and γ-ray observations for a few bursts that show bright optical flares. For example, GRB 041219a, which probably had $\alpha \sim -0.5$, was observed in both the optical and IR simultaneously with the γ-rays (Vestrand et al. 2005; Blake et al. 2005). The optical flux peaked at 13.7 magnitude at approximately the same time as the first main pulse of the GRB lightcurve; the optical emission is within the range of flux expected for the SSC model. The IR measurements in Blake et al. (2005) show evidence of rapid variability with the last spikes in the GRB light curve, giving support to the idea of a common source of the γ-ray and optical flux. GRB 990123 had a positive α and the peak optical flux during the burst was $\sim$ 1Jy (Akerlof et al. 1999) – again in agreement with the expectation of the SSC model. However, the optical lightcurve for GRB 990123 was not correlated with the γ-ray lightcurve, and therefore the optical emission might have had a different origin and is widely ascribed to the reverse-shock heated GRB ejecta

(Sari and Piran 1999).

To summarize our main conclusions, we find that the synchrotron process has serious difficulty accounting for the prompt emission in GRBs. The SSC offers reasonable solutions for all GRBs except those with spectral index of $\sim 1/3$ below the peak. SSC solutions predict very bright optical emission (> 10mJy or 14-mag) accompanying γ-ray lightcurves. If future prompt optical observations fail to find bright optical emission then that will point to a problem with the SSC model. In that case, the assumption that $t_a \sim t_\gamma$ will have to be dropped. The assumption of one shot acceleration of electrons i.e., $t_a \sim t_\gamma$, is motivated by shock based physics for GRBs and will have to be replaced with an alternate scenario in which all electrons that radiate in the γ-ray band are accelerated continuously throughout the duration of a γ-ray pulse. In that scenario synchrotron solutions can also become a viable possibility, particularly when $\alpha \sim 1/3$ – a case that otherwise cannot be explained by the SSC mechanism.

Appendices

Appendix A

Determination of the relative Lorentz factor of colliding shells

We consider shocks as being produced by collision of two shells, as shown in Figure A.1. Internal shocks are produced by a collision between fast ejecta catching up with slower ejecta (Rees and Mészáros 1994; Paczynski and Xu 1994) which in the discrete version is modeled as the collision between two homogeneous shells moving with LFs Γ_1 and Γ_2 (Γ_1 is LF of the faster, inner shell). The external shock is produced by a collision between a stationary circum-stellar medium ($\Gamma_2 = 1$) and the ejecta from the burst.

This appendix is devoted to describing the method we use to place a lower limit to the relative LF of the colliding shells from Γ_{sh}, the LF of the shock front in the γ-ray producing shell, which is directly related to γ_i (one of the 5 parameters) via equation (6.11), and by varying the ratio of densities in the inner and outer shells (n_1/n_2) subject to the condition that the efficiency for γ-ray production is not less than $\sim$10%.

The LF of unshocked inner shell, which is moving faster and lies a bit closer to the center of explosion than the outer shell, can be determined from

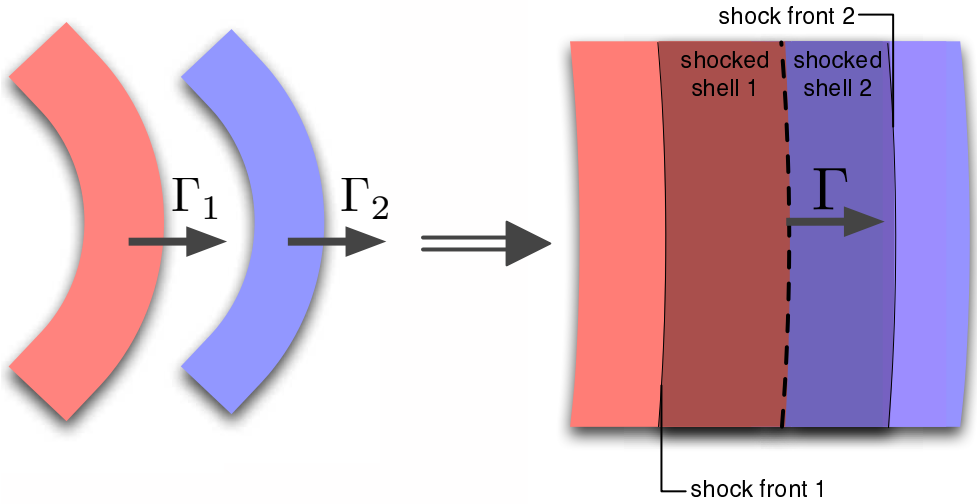

Figure A.1 Pictorial representation of our two shell model.

the addition of LFs Γ_{sh} and Γ –

$$\Gamma_1 = \Gamma_{sh}\Gamma(1 + v_{sh}v), \tag{A.1}$$

provided that the γ-ray emission we observe is produced in the inner shell when it is shock heated (v & v_{sh} are speeds corresponding to LFs Γ – the LF of the γ-ray source – & Γ_{sh}). On the other hand if it is the outer shell that produces the observed γ-ray emission then its LF factor, before it was shocked, is given by

$$\Gamma_2 = \Gamma_{sh}\Gamma(1 - v_{sh}v). \tag{A.2}$$

The LF of the shell that does not contribute significantly to the observed γ-ray emission cannot be determined uniquely. The problem is that in the absence of any observed emission that can be identified with this shell we

cannot say anything directly about the LF of the shock front moving into this shell. However, we can still constrain its LF by requiring that the comoving density of this shell is such that the efficiency for thermal energy produced in the collision is no less than ∼10% (most GRBs for which we have good afterglow data and we can determine the kinetic energy of the ejecta show that the efficiency for converting kinetic energy to γ-rays is about 10% or more).

The efficiency of γ-ray production is used to constrain n_1/n_2, and that in turn provides a lower limit for the relative LF Γ_{rel}. The fraction of kinetic energy converted to thermal energy when two shells of mass m_1 and m_2 collide with a relative LF of Γ_{rel} is (Kumar 1999; Piran 1999)

$$f_r = 1 - \left[1 + \frac{2(m_2/m_1)(\Gamma_{rel} - 1)}{[1 + m_2/m_1]^2}\right]^{-1/2} \tag{A.3}$$

For equal mass shells a $\Gamma_{rel} = 1.5$ collision converts 10% of the kinetic energy of shells to thermal energy, and for $\Gamma_{rel} > 5$ the conversion efficiency is more than 40%. We need, however, to figure out the fraction of energy produced in a collision that is radiated in the typical γ-ray observing band of 15–400 keV during the time interval t_γ, in two shells that are not of equal mass.

The ratio of the mass of the two shells is the mass swept up by the two shocks in the time equal to the shock transit time for the shell that produces the observed γ-ray emission. This is given by

$$\frac{m_1}{m_2} = \frac{n_1(4\Gamma_{s_1} + 3)v_{ss_1}}{n_2(4\Gamma_{s_2} + 3)v_{ss_2}}. \tag{A.4}$$

where n_1 and n_2 are the densities of shell 1 & 2, Γ_{s_1} and Γ_{s_2} are the shock LFs in the frame of each unshocked shell (if the GRB emission is predominantly from shell 1, then $\Gamma_{s_1} = \Gamma_{sh}$), and v_{ss_1} and v_{ss_2} are the speeds of the shock fronts with respect to each unshocked shell.

The shock front speeds are determined from the following cubic equation obtained from the continuity of energy, momentum and particle number fluxes across the shock front (Landau and Lifshitz 1959):

$$\Gamma_{ss}^3 + \left(1 - \frac{2}{\alpha}\right)\Gamma_{su}\Gamma_{ss}^2 - \left(1 - \frac{1}{\alpha^2}\right)\Gamma_{ss} - \Gamma_{su}\left(1 - \frac{1}{\alpha}\right)^2 = 0. \tag{A.5}$$

where Γ_{su} & Γ_{ss} are the LF of the shock front wrt to the unshocked and shocked fluid respectively, and α depends on the equation of state of the shocked gas and is approximated by

$$\alpha = \frac{4\Gamma_0 + 1}{\Gamma_0 + 1}, \tag{A.6}$$

which provides a smooth interpolation between the sub-relativistic value for $\alpha = 5/2$ and the highly relativistic value of 4.

The shock LF wrt the unshocked fluid in the shell not dominating the GRB emission (Γ_{s_2}, if we assume that the GRB is being produced in shell 1) can be determined from the condition of pressure balance across the surface of discontinuity separating the shocked fluids in the two shells-

$$n_1(4\Gamma_{s_1} + 3)(\Gamma_{s_1} - 1) = n_2(4\Gamma_{s_2} + 3)(\Gamma_{s_2} - 1). \tag{A.7}$$

For a given density ratio n_1/n_2 and Γ_{s_1} we can solve the above equation to determine Γ_{s_2}, which in turn is used to determine shock front speed wrt the

unshocked fluid for the outer/inner shell using

$$\Gamma_{s_2} = \Gamma_{ss_2}\Gamma_{su_2}\left[1 - v_{ss_2}v_{su_2}\right], \tag{A.8}$$

and the cubic equation A.5 for Γ_{ss_2}. These pieces together give us m_1/m_2 and Γ_{rel}, which are used to calculate f_r – the fraction of the kinetic energy of the two shells converted to thermal energy in shell collision (eq. A3).

The ratio of the internal energy of the shocked gas in these two shells is

$$\frac{E_1}{E_2} = \frac{n_1(4\Gamma_{s_1}+3)(\Gamma_{s_1}-1)v_{ss_1}}{n_2(4\Gamma_{s_2}+3)(\Gamma_{s_2}-1)v_{ss_2}}. \tag{A.9}$$

The fraction of the total internal energy of the shocked gas in shell '1' is then $f_1 = \frac{E_1}{E_2}/\left(\frac{E_1}{E_2}+1\right)$. We assume that the majority of this energy is indeed being radiated in the GRB band. For shell '2', $f_2 = 1 - f_1$, and we find the fraction of the total radiation contributing to the GRB band, f_{GRB}; f_{GRB} is found from the ratio $\nu_{i_1} f_{\nu_2}(\nu_{i_1})/\nu_{i_2} f_{\nu_2}(\nu_{i_2})$, where $\nu_{i_1}/\nu_{i_2} = (\gamma_{i_1}/\gamma_{i_2})^2$ (assuming that the magnetic field is equal in both shells). The radiation efficiency in the GRB band for the shell collision is then $f_R\,(f_1 + f_2 f_{GRB})$.

When considering synchrotron radiation as the primary source of emission in the γ-ray band we need to take into account the energy fraction that is lost to very high energy photons ($\nu \gg 200$ keV) produced via the inverse-Compton process. The fraction of energy radiated via the synchrotron emission is $1/(1+Y)$, therefore, the total efficiency for energy production in shell collisions must be larger than the desired 10% by a factor of $1+Y$ – this effectively restricts solutions to $Y \lesssim 10$. $Y \gtrsim 0.1$ if inverse-Compton emission is the

main source for the observed γ-ray emission and also Y must not be greater than $\sim 10^3$ otherwise most of the radiative energy will be in the 2nd inverse-Compton photons of much higher energy. In the same sense, we need to make sure the ratio of magnetic energy to that in electrons is $\lesssim$1, in order for the electrons to radiate efficiently.

For highly relativistic forward and reverse shocks $v_{ss_1} \approx v_{ss_2} \approx 1/3$, $\Gamma_{s_2} \approx \Gamma_{s_1}(n_1/n_2)^{1/2}$, $\Gamma_{rel} \approx \Gamma_{s_1}\Gamma_{s_2}$, $m_1/m_2 \approx (n_1/n_2)^{1/2}$, and the ratio of the characteristic synchrotron frequency in shell 1 to shell 2 (assuming the same magnetic field strength) is $\sim n_2/n_1$. We note that the assumption of highly relativistic shocks is not valid for many solutions we find for the prompt γ-ray emissions, and that all the results reported in paper are obtained by numerically solving the appropriate equations. The numerically solved relationships of the ratio of the masses and injection frequencies in the two shells are shown in Figure A.2, and compared to the analytical estimates for highly relativistic shocks.

In summary, for a given $\Gamma_{sh}(\gamma_i)$ we vary n_1/n_2 and determine the mass ratio and the relative LF of the shell collision (Γ_{rel}) so that the gamma-ray production efficiency is above a certain desired value (10%). All of the numerical results we show for Γ_{rel} were calculated using these steps. Using our upper limit on Γ_2, we also calculate the expected emission from the shell 2 in the x-ray and optical bands, and include this in our analysis.

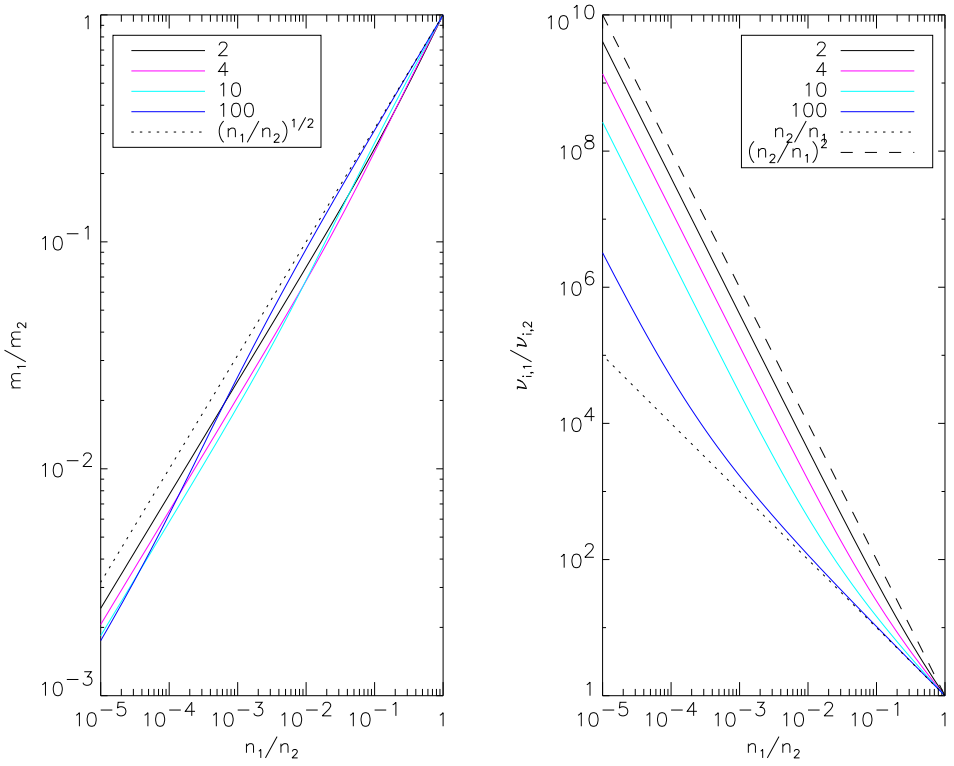

Figure A.2 Left panel: Dependence of the ratio of the two shell masses, m_1/m_2, on the ratio of densities, n_1/n_2. The colored lines show the relation for different relative Lorentz factor, Γ_{rel}, as shown in the legends. The dotted and dashed lines show the applicable dependence on the density ratio. For high Γ_{rel} and $n_1/n_2 > 0.01$, $m_1/m_2 \propto (n_1/n_2)^{1/2}$, however the deviation from this relation for small Γ_{rel} and n_1/n_2 is small – about a factor of 2. Right panel: Dependence of the ratio of synchrotron injection frequencies (ν_i) in the two shells on n_1/n_2. For high Γ_{rel} and $n_1/n_2 > 0.01$, $\nu_{i,1}/\nu_{i,2} \propto n_2/n_1$. At low Γ_{rel} and small n_1/n_2, the ratio of injection frequencies in the two shells significantly deviates from this, and for mildly relativistic Γ_{rel}, can be better approximated by $\nu_{i,1}/\nu_{i,2} \propto (n_2/n_1)^2$, shown by the the dashed line.

Appendix B

Jitter radiation process and GRBs

A radiation mechanism, called jitter radiation, has been suggested by Medvedev (2000) as the process for γ-ray emission for those cases where the low energy spectrum rises more steeply than $\nu^{1/3}$ expected of the synchrotron radiation (such spectra are said to lie "above the line of death" because a non-self-absorbed synchrotron spectrum cannot have this steep of a rise). The jitter radiation is produced when the coherence length scale for magnetic field is short and electron trajectory is perturbed before it has traveled a distance of a Larmor radius. This is an attractive idea for explaining a class of GRBs lying above the line of death, and we explore its applicability to GRBs in this appendix.

The peak jitter frequency in lab frame (as seen by an observer at rest in the host galaxy) is:

$$\nu_j = \sqrt{16\pi q^2 \Gamma_{sh} n_e/(m_e \bar{\gamma}_e)}\gamma_p^2 \Gamma, \tag{B.1}$$

where q is electron charge, Γ is the bulk Lorentz factor (LF) of the source, $\gamma_p = \min\{\gamma_i, \gamma_c\}$, γ_c is the thermal LF of electrons that cool on a dynamical time, γ_i is the minimum thermal LF of electrons behind the shock front (note that $\gamma_i = \varepsilon_e(m_p/m_e)\Gamma_{sh}(p-2)/(p-1)$; where Γ_{sh} is the LF of the shock front

wrt the unshocked shell), n_e is the comoving electron density in the unshocked shell, and $\bar{\gamma}_e \sim 3 - 4$ is the initial effective thermal Lorentz factor of the streaming electrons.

In order to get the gamma-ray burst spectrum below the peak to be proportional to $\sim \nu^1$, we want $\nu_j \sim 10^5$ eV (the peak of the GRB spectrum is of order 100 keV). Therefore, from the above equation we find the following condition on comoving electron density in the unshocked shell:

$$n_e \approx \frac{4 \times 10^{28}}{\Gamma^2 \gamma_p^4} (\bar{\gamma}_e / \Gamma_{sh}) \tag{B.2}$$

or the optical depth of the source to Thomson scattering is:

$$\tau \approx 4 n_e \Gamma_{sh} R_\gamma \sigma_T / \Gamma \approx \frac{10^{16} \bar{\gamma}_e t_\gamma}{\Gamma \gamma_p^4} \tag{B.3}$$

where R_γ is the distance of the source from the center of the explosion, and $t_\gamma \approx R_\gamma / (4\Gamma^2 c)$ is the GRB variability time scale.

For internal shock Γ_{sh} is of order a few, and therefore, $\gamma_i \approx 10^3$. In this case we find the optical depth of the source to be

$$\tau \approx \frac{10^4 \bar{\gamma}_e t_\gamma}{\Gamma}. \tag{B.4}$$

Or $\tau \sim 1$ for $t_\gamma \sim 10^{-2}$ sec, and $\Gamma \sim 10^3$. The next step is to estimate the LF of cooling electrons (γ_c), which can be shown to be:

$$\gamma_c \approx \frac{6\pi m_e c (1+z)}{\sigma_T B^2 t_\gamma \Gamma (1+Y)}, \tag{B.5}$$

where B is the magnetic field in the source co-moving frame, and Y is the Compton-Y-parameter; $Y \approx \tau \gamma_c \gamma_i$ (for $p \approx 2$).

If γ_c is not much less than γ_i then Y is very large (of order a million), and most of the radiation energy will come out as SSC photons at $> 10^2$ GeV. And moreover, electrons cool very rapidly resulting in the synchrotron cooling frequency (ν_c) to be much less than 100 keV, and therefore the spectrum below the peak will be $\nu^{-1/2}$ and not $\propto \nu^1$. Even if we take γ_c to be order unity, we still run into similar problems.

We, therefore, do not include the jitter process in our analysis of GRB prompt radiation mechanism.

Bibliography

C. Akerlof, R. Balsano, S. Barthelemy, J. Bloch, P. Butterworth, D. Casperson, T. Cline, S. Fletcher, F. Frontera, G. Gisler, J. Heise, J. Hills, R. Kehoe, B. Lee, S. Marshall, T. McKay, R. Miller, L. Piro, W. Priedhorsky, J. Szymanski, and J. Wren. Observation of contemporaneous optical radiation from a gamma-ray burst. *Nature*, 398:400–402, 1999.

C. Akerlof, R. Balsano, S. Barthelmy, J. Bloch, P. Butterworth, D. Casperson, T. Cline, S. Fletcher, F. Frontera, G. Gisler, J. Heise, J. Hills, K. Hurley, R. Kehoe, B. Lee, S. Marshall, T. McKay, A. Pawl, L. Piro, J. Szymanski, and J. Wren. Prompt Optical Observations of Gamma-Ray Bursts. *ApJ*, 532:L25–L28, March 2000a.

C. Akerlof, R. Balsano, S. Barthelmy, J. Bloch, P. Butterworth, D. Casperson, T. Cline, S. Fletcher, F. Frontera, G. Gisler, J. Heise, J. Hills, K. Hurley, R. Kehoe, B. Lee, S. Marshall, T. McKay, A. Pawl, L. Piro, J. Szymanski, and J. Wren. Prompt Optical Observations of Gamma-Ray Bursts. *ApJ*, 532:L25–L28, March 2000b.

C. W. Akerlof, R. L. Kehoe, T. A. McKay, E. S. Rykoff, D. A. Smith, D. E. Casperson, K. E. McGowan, W. T. Vestrand, P. R. Wozniak, J. A. Wren, M. C. B. Ashley, M. A. Phillips, S. L. Marshall, H. W. Epps, and J. A.

Schier. The ROTSE-III Robotic Telescope System. *PASP*, 115:132–140, January 2003.

L. Amati, F. Frontera, M. Tavani, J. J. M. in't Zand, A. Antonelli, E. Costa, M. Feroci, C. Guidorzi, J. Heise, N. Masetti, E. Montanari, L. Nicastro, E. Palazzi, E. Pian, L. Piro, and P. Soffitta. Intrinsic spectra and energetics of BeppoSAX Gamma-Ray Bursts with known redshifts. *A&A*, 390:81–89, July 2002.

D. Band, J. Matteson, L. Ford, B. Schaefer, D. Palmer, B. Teegarden, T. Cline, M. Briggs, W. Paciesas, G. Pendleton, G. Fishman, C. Kouveliotou, C. Meegan, R. Wilson, and P. Lestrade. BATSE observations of gamma-ray burst spectra. I - Spectral diversity. *ApJ*, 413:281–292, August 1993.

S. D. Barthelmy, P. Butterworth, T. L. Cline, N. Gehrels, G. J. Fishman, C. Kouveliotou, and C. A. Meegan. BACODINE, the Real-Time BATSE Gamma-Ray Burst Coordinates Distribution Network. *Ap&SS*, 231:235–238, September 1995.

S. D. Barthelmy, J. K. Cannizzo, N. Gehrels, G. Cusumano, V. Mangano, P. T. O'Brien, S. Vaughan, B. Zhang, D. N. Burrows, S. Campana, G. Chincarini, M. R. Goad, C. Kouveliotou, P. Kumar, P. Mészáros, J. A. Nousek, J. P. Osborne, A. Panaitescu, J. N. Reeves, T. Sakamoto, G. Tagliaferri, and R. A. M. J. Wijers. Discovery of an Afterglow Extension of the Prompt Phase of Two Gamma-Ray Bursts Observed by Swift. *ApJ*, 635:L133–L136, December 2005. doi: 10.1086/499432.

A. M. Beloborodov. On the Efficiency of Internal Shocks in Gamma-Ray Bursts. *ApJ*, 539:L25–L28, August 2000.

E. Berger, S. R. Kulkarni, D. B. Fox, A. M. Soderberg, F. A. Harrison, E. Nakar, D. D. Kelson, M. D. Gladders, J. S. Mulchaey, A. Oemler, A. Dressler, S. B. Cenko, P. A. Price, B. P. Schmidt, D. A. Frail, N. Morrell, S. Gonzalez, W. Krzeminski, R. Sari, A. Gal-Yam, D.-S. Moon, B. E. Penprase, R. Jayawardhana, A. Scholz, J. Rich, B. A. Peterson, G. Anderson, R. McNaught, T. Minezaki, Y. Yoshii, L. L. Cowie, and K. Pimbblet. Afterglows, Redshifts, and Properties of Swift Gamma-Ray Bursts. *ApJ*, 634: 501–508, November 2005. doi: 10.1086/491667.

C. H. Blake, J. S. Bloom, D. L. Starr, E. E. Falco, M. Skrutskie, E. E. Fenimore, G. Duchêne, A. Szentgyorgyi, S. Hornstein, J. X. Prochaska, C. McCabe, A. Ghez, Q. Konopacky, K. Stapelfeldt, K. Hurley, R. Campbell, M. Kassis, F. Chaffee, N. Gehrels, S. Barthelmy, J. R. Cummings, D. Hullinger, H. A. Krimm, C. B. Markwardt, D. Palmer, A. Parsons, K. McLean, and J. Tueller. An infrared flash contemporaneous with the γ-rays of GRB 041219a. *Nature*, 435:181–184, May 2005. doi: 10.1038/nature03520.

M. S. Briggs, D. L. Band, R. M. Kippen, R. D. Preece, C. Kouveliotou, J. van Paradijs, G. H. Share, R. J. Murphy, S. M. Matz, A. Connors, C. Winkler, M. L. McConnell, J. M. Ryan, O. R. Williams, C. A. Young, B. Dingus, J. R. Catelli, and R. A. M. J. Wijers. Observations of GRB 990123 by the Compton Gamma Ray Observatory. *ApJ*, 524:82–91, October 1999.

A. E. Broderick. Supernovae in helium star-compact object binaries: a possible γ-ray burst mechanism. *MNRAS*, 361:955–964, August 2005. doi: 10.1111/j.1365-2966.2005.09220.x.

D. N. Burrows, P. Romano, A. Falcone, S. Kobayashi, B. Zhang, A. Moretti, P. T. O'Brien, M. R. Goad, S. Campana, K. L. Page, L. Angelini, S. Barthelmy, A. P. Beardmore, M. Capalbi, G. Chincarini, J. Cummings, G. Cusumano, D. Fox, P. Giommi, J. E. Hill, J. A. Kennea, H. Krimm, V. Mangano, F. Marshall, P. Mészáros, D. C. Morris, J. A. Nousek, J. P. Osborne, C. Pagani, M. Perri, G. Tagliaferri, A. A. Wells, S. Woosley, and N. Gehrels. Bright X-ray Flares in Gamma-Ray Burst Afterglows. *Science*, 309:1833–1835, September 2005. doi: 10.1126/science.1116168.

A. J. Castro-Tirado, T. J. Mateo, A. d. Ugarte, M. Jlinek, P. Kubnek, R. Hudec, S. Vitek, P. Pta, and J. . Bern. GRB 030115, simultaneous observations by BOOTES-1. *GCN Circulars*, 1826:1–+, 2003.

G. Chincarini, A. Moretti, P. Romano, S. Covino, G. Tagliaferri, S. Campana, M. Goad, S. Kobayashi, B. Zhang, L. Angelini, P. Banat, S. Barthelmy, A. P. Beardmore, P. T. Boyd, A. Breeveld, D. N. Burrows, M. Capalbi, M. M. Chester, G. Cusumano, E. E. Fenimore, N. Gehrels, P. Giommi, J. E. Hill, D. Hinshaw, S. T. Holland, J. A. Kennea, H. A. Krimm, V. La Parola, V. Mangano, F. E. Marshall, K. O. Mason, J. A. Nousek, P. T. O'Brien, J. P. Osborne, M. Perri, P. Mészáros, P. W. A. Roming, T. Sakamoto, P. Schady, M. Still, and A. A. Wells. Prompt and afterglow early X-ray phases in the

comoving frame. Evidence for Universal properties? *ArXiv Astrophysics e-prints*, June 2005.

E. Costa, F. Frontera, J. Heise, M. Feroci, J. in 't Zand, F. Fiore, M. N. Cinti, D. dal Fiume, L. Nicastro, M. Orlandini, E. Palazzi, M. Rapisarda, G. Zavattini, R. Jager, A. Parmar, A. Owens, S. Molendi, G. Cusumano, M. C. Maccarone, S. Giarrusso, A. Coletta, L. A. Antonelli, P. Giommi, J. M. Muller, L. Piro, and R. C. Butler. Discovery of an X-ray afterglow associated with the gamma-ray burst of 28 February 1997. *Nature*, 387: 783–785, 1997.

J. Cummings, L. Barbier, S. Barthelmy, D. Hullinger, E. Fenimore, N. Gehrels, H. Krimm, C. Markwardt, D. Palmer, A. Parsons, T. Sakamoto, G. Sato, and J. Tueller. GRB 050820A BAT observations of second, larger episode of emission. 3858:1–+, 2005.

M. Della Valle, D. Malesani, S. Benetti, V. Testa, M. Hamuy, L. A. Antonelli, G. Chincarini, G. Cocozza, S. Covino, P. D'Avanzo, D. Fugazza, G. Ghisellini, R. Gilmozzi, D. Lazzati, E. Mason, P. Mazzali, and L. Stella. Evidence for supernova signatures in the spectrum of the late-time bump of the optical afterglow of GRB 021211. *A&A*, 406:L33–L37, July 2003. doi: 10.1051/0004-6361:20030855.

M. Della Valle, D. Malesani, J. S. Bloom, S. Benetti, G. Chincarini, P. D'Avanzo, R. J. Foley, S. Covino, A. Melandri, S. Piranomonte, G. Tagliaferri, L. Stella, R. Gilmozzi, L. A. Antonelli, S. Campana, H.-W. Chen,

P. Filliatre, F. Fiore, D. Fugazza, N. Gehrels, K. Hurley, I. F. Mirabel, L. J. Pellizza, L. Piro, and J. X. Prochaska. Hypernova Signatures in the Late Rebrightening of GRB 050525A. *ApJ*, 642:L103–L106, May 2006. doi: 10.1086/504636.

C. D. Dermer and K. E. Mitman. Short-Timescale Variability in the External Shock Model of Gamma-Ray Bursts. *ApJ*, 513:L5–L8, March 1999. doi: 10.1086/311898.

C. D. Dermer, J. Chiang, and M. Böttcher. Fireball Loading and the Blast-Wave Model of Gamma-Ray Bursts. *ApJ*, 513:656–668, March 1999. doi: 10.1086/306871.

Y. Fan and T. Piran. Gamma-ray burst efficiency and possible physical processes shaping the early afterglow. *MNRAS*, 369:197–206, June 2006. doi: 10.1111/j.1365-2966.2006.10280.x.

Y.-Z. Fan, Z.-G. Dai, Y.-F. Huang, and T. Lu. Optical Flash of GRB 990123: Constraints on the Physical Parameters of the Reverse Shock. *Chinese Journal of Astronomy and Astrophysics*, 2:449–453, October 2002.

E. E. Fenimore, E. Ramirez-Ruiz, and B. Wu. GRB 990123: Evidence that the Gamma Rays Come from a Central Engine. *ApJ*, 518:L73–L76, June 1999.

G. J. Fishman and C. A. Meegan. Gamma-Ray Bursts. *ARA&A*, 33:415–458, 1995.

D. A. Frail, S. R. Kulkarni, S. R. Nicastro, M. Feroci, and G. B. Taylor. The radio afterglow from the gamma-ray burst of 8 May 1997. *Nature*, 389: 261–263, 1997.

D. A. Frail, S. R. Kulkarni, R. Sari, S. G. Djorgovski, J. S. Bloom, T. J. Galama, D. E. Reichart, E. Berger, F. A. Harrison, P. A. Price, S. A. Yost, A. Diercks, R. W. Goodrich, and F. Chaffee. Beaming in Gamma-Ray Bursts: Evidence for a Standard Energy Reservoir. *ApJ*, 562:L55–L58, November 2001.

A. Gal-Yam, D. B. Fox, P. A. Price, E. O. Ofek, M. R. Davis, D. C. Leonard, A. M. Soderberg, B. P. Schmidt, K. M. Lewis, B. A. Peterson, S. R. Kulkarni, E. Berger, S. B. Cenko, R. Sari, K. Sharon, D. Frail, D.-S. Moon, P. J. Brown, A. Cucchiara, F. Harrison, T. Piran, S. E. Persson, P. J. McCarthy, B. E. Penprase, R. A. Chevalier, and A. I. MacFadyen. A novel explosive process is required for the γ-ray burst GRB 060614. *Nature*, 444:1053–1055, December 2006. doi: 10.1038/nature05373.

T. Galama, P. J. Groot, J. Vanparadijs, C. Kouveliotou, C. R. Robinson, G. J. Fishman, C. A. Meegan, K. C. Sahu, M. Livio, L. Petro, F. D. Macchetto, J. Heise, J. Int Zand, R. G. Strom, J. Telting, R. G. M. Rutten, M. Pettini, N. Tanvir, and J. Bloom. The Decay of Optical Emission from the gamma-Ray Burst GRB970228. *Nature*, 387:479–+, May 1997.

T. J. Galama and R. A. M. J. Wijers. High Column Densities and Low Ex-

tinctions of Gamma-Ray Bursts: Evidence for Hypernovae and Dust Destruction. *ApJ*, 549:L209–L213, March 2001. doi: 10.1086/319162.

N. Gehrels, G. Chincarini, P. Giommi, K. O. Mason, J. A. Nousek, A. A. Wells, N. E. White, S. D. Barthelmy, D. N. Burrows, L. R. Cominsky, K. C. Hurley, F. E. Marshall, P. Mészáros, P. W. A. Roming, L. Angelini, L. M. Barbier, T. Belloni, S. Campana, P. A. Caraveo, M. M. Chester, O. Citterio, T. L. Cline, M. S. Cropper, J. R. Cummings, A. J. Dean, E. D. Feigelson, E. E. Fenimore, D. A. Frail, A. S. Fruchter, G. P. Garmire, K. Gendreau, G. Ghisellini, J. Greiner, J. E. Hill, S. D. Hunsberger, H. A. Krimm, S. R. Kulkarni, P. Kumar, F. Lebrun, N. M. Lloyd-Ronning, C. B. Markwardt, B. J. Mattson, R. F. Mushotzky, J. P. Norris, J. Osborne, B. Paczynski, D. M. Palmer, H.-S. Park, A. M. Parsons, J. Paul, M. J. Rees, C. S. Reynolds, J. E. Rhoads, T. P. Sasseen, B. E. Schaefer, A. T. Short, A. P. Smale, I. A. Smith, L. Stella, G. Tagliaferri, T. Takahashi, M. Tashiro, L. K. Townsley, J. Tueller, M. J. L. Turner, M. Vietri, W. Voges, M. J. Ward, R. Willingale, F. M. Zerbi, and W. W. Zhang. The Swift Gamma-Ray Burst Mission. *ApJ*, 611:1005–1020, August 2004. doi: 10.1086/422091.

N. Gehrels, C. L. Sarazin, P. T. O'Brien, B. Zhang, L. Barbier, S. D. Barthelmy, A. Blustin, D. N. Burrows, J. Cannizzo, J. R. Cummings, M. Goad, S. T. Holland, C. P. Hurkett, J. A. Kennea, A. Levan, C. B. Markwardt, K. O. Mason, P. Mészáros, M. Page, D. M. Palmer, E. Rol, T. Sakamoto, R. Willingale, L. Angelini, A. Beardmore, P. T. Boyd,

A. Breeveld, S. Campana, M. M. Chester, G. Chincarini, L. R. Cominsky, G. Cusumano, M. de Pasquale, E. E. Fenimore, P. Giommi, C. Gronwall, D. Grupe, J. E. Hill, D. Hinshaw, J. Hjorth, D. Hullinger, K. C. Hurley, S. Klose, S. Kobayashi, C. Kouveliotou, H. A. Krimm, V. Mangano, F. E. Marshall, K. McGowan, A. Moretti, R. F. Mushotzky, K. Nakazawa, J. P. Norris, J. A. Nousek, J. P. Osborne, K. Page, A. M. Parsons, S. Patel, M. Perri, T. Poole, P. Romano, P. W. A. Roming, S. Rosen, G. Sato, P. Schady, A. P. Smale, J. Sollerman, R. Starling, M. Still, M. Suzuki, G. Tagliaferri, T. Takahashi, M. Tashiro, J. Tueller, A. A. Wells, N. E. White, and R. A. M. J. Wijers. A short γ-ray burst apparently associated with an elliptical galaxy at redshift z = 0.225. *Nature*, 437:851–854, October 2005. doi: 10.1038/nature04142.

N. Gehrels, J. K. Cannizzo, and J. P. Norris. Gamma-ray bursts in the Swift era. *New Journal of Physics*, 9:37–+, February 2007. doi: 10.1088/1367-2630/9/2/037.

G. Ghisellini, A. Celotti, and D. Lazzati. Constraints on the emission mechanisms of gamma-ray bursts. *MNRAS*, 313:L1–L5, March 2000.

M. R. Goad, G. Tagliaferri, K. L. Page, A. Moretti, J. P. Osborne, S. Kobayashi, P. Kumar, P. I. Mészáros, G. Chincarini, T. Sakamoto, B. Zhang, S. D. Barthelmy, A. P. Beardmore, D. N. Burrows, S. Campana, M. Capalbi, L. Cominsky, G. Cusumano, N. Gehrels, P. Giommi, O. Godet, J. E. Hill, J. A. Kennea, H. Krimm, V. La Parola, V. Mangano, T. Mi-

neo, D. C. Morris, K. Mukerjee, J. A. Nousek, P. T. O'Brien, C. Pagani, M. Perri, P. Romano, and A. A. Wells. Swift observations of the prompt X-ray emission and afterglow from GRB050126 and GRB050219A. *A&A*, 449:89–100, April 2006. doi: 10.1051/0004-6361:20054457.

S. Golenetskii, R. Aptekar, E. Mazets, V. Pal'shin, D. Frederiks, and T. Cline. Konus-Wind observation of GRB 050401. 3179:1–+, 2005.

S. Golenetskii, R. Aptekar, E. Mazets, V. Pal'shin, D. Frederiks, and T. Cline. Konus-Wind observation of GRB 061007. 5722:1–+, 2006.

J. Goodman. Radio scintillation of gamma-ray-burst afterglows. *New Astronomy*, 2:449–460, November 1997. doi: 10.1016/S1384-1076(97)00031-6.

J. Granot, T. Piran, and R. Sari. Images and Spectra from the Interior of a Relativistic Fireball. *ApJ*, 513:679–689, March 1999. doi: 10.1086/306884.

J. Heise, J. in't Zand, R. M. Kippen, and P. M. Woods. X-Ray Flashes and X-Ray Rich Gamma Ray Bursts. In E. Costa, F. Frontera, and J. Hjorth, editors, *Gamma-ray Bursts in the Afterglow Era*, pages 16–+, 2001. doi: 10.1007/10853853_4.

J. Hjorth, D. Watson, J. P. U. Fynbo, P. A. Price, B. L. Jensen, U. G. Jorgensen, D. Kubas, J. Gorosabel, P. Jakobsson, J. Sollerman, K. Pedersen, and C. Kouveliotou. The optical afterglow of the short γ-ray burst GRB 050709. *Nature*, 437:859–861, October 2005. doi: 10.1038/nature04174.

K. Hurley, T. Cline, E. Mazets, R. Aptekar, S. Golenetskii, D. Frederiks, D. Frail, S. Kulkarni, J. Trombka, T. McClanahan, R. Starr, and J. Goldsten. Interplanetary Network Localization of GRB 991208 and the Discovery of its Afterglow. *ApJ*, 534:L23–L25, May 2000.

R. Jimenez, D. Band, and T. Piran. Energetics of Gamma-Ray Bursts. *ApJ*, 561:171–177, November 2001.

J. I. Katz. Low-frequency spectra of gamma-ray bursts. *ApJ*, 432:L107–L109, September 1994.

J. I. Katz. Yet Another Model of Gamma-Ray Bursts. *ApJ*, 490:633–+, December 1997. doi: 10.1086/304896.

R. Kehoe, C. Akerlof, R. Balsano, S. Barthelmy, J. Bloch, P. Butterworth, D. Casperson, T. Cline, S. Fletcher, G. Gisler, K. Hurley, M. Kippen, B. Lee, S. Marshall, T. McKay, E. Rykoff, D. Smith, T. Vestrand, and J. Wren. A Search for Early Optical Emission from Short- and Long-Duration Gamma-Ray Bursts. *ApJ*, 554:L159–L162, June 2001.

R. W. Klebesadel, I. B. Strong, and R. A. Olson. Observations of Gamma-Ray Bursts of Cosmic Origin. *ApJ*, 182:L85+, June 1973.

S. Kobayashi. Light Curves of Gamma-Ray Burst Optical Flashes. *ApJ*, 545: 807–812, December 2000.

S. Kobayashi, T. Piran, and R. Sari. Hydrodynamics of a Relativistic Fireball: The Complete Evolution. *ApJ*, 513:669–678, March 1999.

S. Kobayashi, B. Zhang, P. Mészáros, and D. Burrows. Inverse Compton X-Ray Flare from Gamma-Ray Burst Reverse Shock. *ApJ*, 655:391–395, January 2007. doi: 10.1086/510198.

C. Kouveliotou, C. A. Meegan, G. J. Fishman, N. P. Bhat, M. S. Briggs, T. M. Koshut, W. S. Paciesas, and G. N. Pendleton. Identification of two classes of gamma-ray bursts. *ApJ*, 413:L101–L104, August 1993.

P. Kumar. Gamma-Ray Burst Energetics. *ApJ*, 523:L113–L116, October 1999.

P. Kumar and A. Panaitescu. A unified treatment of the gamma-ray burst 021211 and its afterglow. *MNRAS*, 346:905–914, December 2003.

P. Kumar and A. Panaitescu. Afterglow Emission from Naked Gamma-Ray Bursts. *ApJ*, 541:L51–L54, October 2000.

P. Kumar, E. McMahon, S. D. Barthelmy, D. Burrows, N. Gehrels, M. Goad, J. Nousek, and G. Tagliaferri. A unified picture for gamma-ray burst prompt and X-ray afterglow emissions. *MNRAS*, 367:L52–L56, March 2006. doi: 10.1111/j.1745-3933.2006.00138.x.

P. Kumar, E. McMahon, A. Panaitescu, R. Willingale, P. O'Brien, D. Burrows, J. Cummings, N. Gehrels, S. Holland, S. B. Pandey, D. vanden Berk, and S. Zane. The nature of the outflow in gamma-ray bursts. *MNRAS*, 376: L57–L61, March 2007. doi: 10.1111/j.1365-2966.2007.00286.x.

L. D. Landau and E. M. Lifshitz. *Course of Theoretical Physics: Fluid Mechanics*, volume 6. Pergamon Press, 1959.

D. Lazzati and M. C. Begelman. Thick Fireballs and the Steep Decay in the Early X-Ray Afterglow of Gamma-Ray Bursts. *ApJ*, 641:972–977, April 2006. doi: 10.1086/500502.

D. Lazzati, G. Ghisellini, A. Celotti, and M. J. Rees. Compton-dragged Gamma-Ray Bursts Associated with Supernovae. *ApJ*, 529:L17–L20, January 2000. doi: 10.1086/312452.

W. Li, A. V. Filippenko, R. Chornock, and S. Jha. The Early Light Curve of the Optical Afterglow of GRB 021211. *ApJ*, 586:L9–L12, March 2003a. doi: 10.1086/374684.

Z. Li, Z. G. Dai, T. Lu, and L. M. Song. Pair Loading in Gamma-Ray Burst Fireballs and Prompt Emission from Pair-rich Reverse Shocks. *ApJ*, 599: 380–386, December 2003b. doi: 10.1086/379231.

Y. Lithwick and R. Sari. Lower Limits on Lorentz Factors in Gamma-Ray Bursts. *ApJ*, 555:540–545, July 2001.

M. Lyutikov. Did Swift measure gamma-ray burst prompt emission radii? *MNRAS*, 369:L5–L8, June 2006. doi: 10.1111/j.1745-3933.2006.00161.x.

M. Lyutikov and R. Blandford. Gamma Ray Bursts as Electromagnetic Outflows. *ArXiv Astrophysics e-prints*, December 2003.

P. Mészáros. Theories of Gamma-Ray Bursts. *ARA&A*, 40:137–169, 2002.

P. Mészáros. Gamma-ray bursts. *Reports of Progress in Physics*, 69:2259–2322, 2006.

P. Mészáros and M. J. Rees. Gamma-Ray Bursts: Multiwaveband Spectral Predictions for Blast Wave Models. *ApJ*, 418:L59+, December 1993a.

P. Mészáros and M. J. Rees. Relativistic fireballs and their impact on external matter - Models for cosmological gamma-ray bursts. *ApJ*, 405:278–284, March 1993b.

P. Mészáros and M. J. Rees. Poynting Jets from Black Holes and Cosmological Gamma-Ray Bursts. *ApJ*, 482:L29+, June 1997a.

P. Mészáros and M. J. Rees. Optical and Long-Wavelength Afterglow from Gamma-Ray Bursts. *ApJ*, 476:232–+, February 1997b. doi: 10.1086/303625.

P. Mészáros, P. Laguna, and M. J. Rees. Gasdynamics of relativistically expanding gamma-ray burst sources - Kinematics, energetics, magnetic fields, and efficiency. *ApJ*, 415:181–190, September 1993.

P. Mészáros, M. J. Rees, and H. Papathanassiou. Spectral properties of blast-wave models of gamma-ray burst sources. *ApJ*, 432:181–193, September 1994.

D. Malesani, G. Tagliaferri, G. Chincarini, S. Covino, M. Della Valle, D. Fugazza, P. A. Mazzali, F. M. Zerbi, P. D'Avanzo, S. Kalogerakos, A. Simoncelli, L. A. Antonelli, L. Burderi, S. Campana, A. Cucchiara, F. Fiore,

G. Ghirlanda, P. Goldoni, D. Götz, S. Mereghetti, I. F. Mirabel, P. Romano, L. Stella, T. Minezaki, Y. Yoshii, and K. Nomoto. SN 2003lw and GRB 031203: A Bright Supernova for a Faint Gamma-Ray Burst. *ApJ*, 609: L5–L8, July 2004. doi: 10.1086/422684.

T. Matheson, P. M. Garnavich, K. Z. Stanek, D. Bersier, S. T. Holland, K. Krisciunas, N. Caldwell, P. Berlind, J. S. Bloom, M. Bolte, A. Z. Bonanos, M. J. I. Brown, W. R. Brown, M. L. Calkins, P. Challis, R. Chornock, L. Echevarria, D. J. Eisenstein, M. E. Everett, A. V. Filippenko, K. Flint, R. J. Foley, D. L. Freedman, M. Hamuy, P. Harding, N. P. Hathi, M. Hicken, C. Hoopes, C. Impey, B. T. Jannuzi, R. A. Jansen, S. Jha, J. Kaluzny, S. Kannappan, R. P. Kirshner, D. W. Latham, J. C. Lee, D. C. Leonard, W. Li, K. L. Luhman, P. Martini, H. Mathis, J. Maza, S. T. Megeath, L. R. Miller, D. Minniti, E. W. Olszewski, M. Papenkova, M. M. Phillips, B. Pindor, D. D. Sasselov, R. Schild, H. Schweiker, T. Spahr, J. Thomas-Osip, I. Thompson, D. Weisz, R. Windhorst, and D. Zaritsky. Photometry and Spectroscopy of GRB 030329 and Its Associated Supernova 2003dh: The First Two Months. *ApJ*, 599:394–407, December 2003.

Mazets. Personal communication.

E. P. Mazets, S. V. Golenetskii, V. N. Ilinskii, I. A. Gurian, and T. V. Kharitonova. Investigations of diffuse cosmic gamma radiation in the range 28 keV-4.1 MeV. *ZhETF Pis ma Redaktsiiu*, 20:77–80, July 1974.

J. McEnery and GLAST Mission Team. The Gamma-ray Large Area Space Telescope and Gamma-Ray Bursts. In S. S. Holt, N. Gehrels, and J. A. Nousek, editors, *Gamma-Ray Bursts in the Swift Era*, volume 836 of *American Institute of Physics Conference Series*, pages 660–663, May 2006.

E. McMahon, P. Kumar, and A. Panaitescu. Prompt γ-ray and early afterglow emission in the external shock model. *MNRAS*, 354:915–923, November 2004. doi: 10.1111/j.1365-2966.2004.08245.x.

E. McMahon, P. Kumar, and T. Piran. Reverse shock emission as a probe of gamma-ray burst ejecta. *MNRAS*, 366:575–585, February 2006. doi: 10.1111/j.1365-2966.2005.09884.x.

M. V. Medvedev. Theory of "Jitter" Radiation from Small-Scale Random Magnetic Fields and Prompt Emission from Gamma-Ray Burst Shocks. *ApJ*, 540:704–714, September 2000.

M. V. Medvedev and A. Loeb. Generation of Magnetic Fields in the Relativistic Shock of Gamma-Ray Burst Sources. *ApJ*, 526:697–706, December 1999.

M. R. Metzger, S. G. Djorgovski, S. R. Kulkarni, C. C. Steidel, K. L. Adelberger, D. A. Frail, E. Costa, and F. Frontera. Spectral constraints on the redshift of the optical counterpart to the gamma-ray burst of 8 May 1997. *Nature*, 387:878–880, 1997.

C. G. Mundell, A. Melandri, C. Guidorzi, S. Kobayashi, I. A. Steele, D. Malesani, L. Amati, P. D'Avanzo, D. F. Bersier, A. Gomboc, E. Rol, M. F. Bode,

D. Carter, C. J. Mottram, A. Monfardini, R. J. Smith, S. Malhotra, J. Wang, N. Bannister, P. T. O'Brien, and N. R. Tanvir. The Remarkable Afterglow of GRB 061007: Implications for Optical Flashes and GRB Fireballs. *ApJ*, 660:489–495, May 2007. doi: 10.1086/512605.

E. Nakar and J. Granot. Smooth Light Curves from a Bumpy Ride: Relativistic Blast Wave Encounters a Density Jump. *ArXiv Astrophysics e-prints*, June 2006.

E. Nakar and T. Piran. Early afterglow emission from a reverse shock as a diagnostic tool for gamma-ray burst outflows. *MNRAS*, 353:647–653, September 2004. doi: 10.1111/j.1365-2966.2004.08099.x.

E. Nakar, A. Gal-Yam, T. Piran, and D. B. Fox. The Distances of Short-Hard Gamma-Ray Bursts and the Soft Gamma-Ray Repeater Connection. *ApJ*, 640:849–853, April 2006. doi: 10.1086/498229.

L. Nicastro, L. Amati, L. A. Antonelli, E. Costa, G. Cusumano, M. Feroci, F. Frontera, E. Palazzi, E. Pian, and L. Piro. The X-ray afterglow of GRB 980519. *A&AS*, 138:437–438, September 1999.

J. A. Nousek, C. Kouveliotou, D. Grupe, K. L. Page, J. Granot, E. Ramirez-Ruiz, S. K. Patel, D. N. Burrows, V. Mangano, S. Barthelmy, A. P. Beardmore, S. Campana, M. Capalbi, G. Chincarini, G. Cusumano, A. D. Falcone, N. Gehrels, P. Giommi, M. R. Goad, O. Godet, C. P. Hurkett, J. A. Kennea, A. Moretti, P. T. O'Brien, J. P. Osborne, P. Romano, G. Tagliaferri,

and A. A. Wells. Evidence for a Canonical Gamma-Ray Burst Afterglow Light Curve in the Swift XRT Data. *ApJ*, 642:389–400, May 2006. doi: 10.1086/500724.

P. T. O'Brien, R. Willingale, J. Osborne, M. R. Goad, K. L. Page, S. Vaughan, E. Rol, A. Beardmore, O. Godet, C. P. Hurkett, A. Wells, B. Zhang, S. Kobayashi, D. N. Burrows, J. A. Nousek, J. A. Kennea, A. Falcone, D. Grupe, N. Gehrels, S. Barthelmy, J. Cannizzo, J. Cummings, J. E. Hill, H. Krimm, G. Chincarini, G. Tagliaferri, S. Campana, A. Moretti, P. Giommi, M. Perri, V. Mangano, and V. LaParola. The Early X-Ray Emission from GRBs. *ApJ*, 647:1213–1237, August 2006. doi: 10.1086/505457.

B. Paczynski and J. E. Rhoads. Radio Transients from Gamma-Ray Bursters. *ApJ*, 418:L5+, November 1993. doi: 10.1086/187102.

B. Paczynski and G. Xu. Neutrino bursts from gamma-ray bursts. *ApJ*, 427: 708–713, June 1994. doi: 10.1086/174178.

A. Panaitescu and P. Kumar. Jet Energy and Other Parameters for the Afterglows of GRB 980703, GRB 990123, GRB 990510, and GRB 991216 Determined from Modeling of Multifrequency Data. *ApJ*, 554:667–677, June 2001.

A. Panaitescu and P. Kumar. Properties of Relativistic Jets in Gamma-Ray Burst Afterglows. *ApJ*, 571:779–789, June 2002.

A. Panaitescu and P. Kumar. Analysis of two scenarios for the early optical emission of the gamma-ray burst afterglows 990123 and 021211. *MNRAS*, 353:511–522, September 2004. doi: 10.1111/j.1365-2966.2004.08083.x.

A. Panaitescu and P. Mészáros. Simulations of Gamma-Ray Bursts from External Shocks: Time Variability and Spectral Correlations. *ApJ*, 492:683–+, January 1998.

A. Panaitescu and P. Mészáros. Gamma-Ray Bursts from Upscattered Self-absorbed Synchrotron Emission. *ApJ*, 544:L17–L21, November 2000.

A. Panaitescu, M. Spada, and P. Mészáros. Power Density Spectra of Gamma-Ray Bursts in the Internal Shock Model. *ApJ*, 522:L105–L108, September 1999.

A. Panaitescu, P. Mészáros, D. Burrows, J. Nousek, N. Gehrels, P. O'Brien, and R. Willingale. Evidence for chromatic X-ray light-curve breaks in Swift gamma-ray burst afterglows and their theoretical implications. *MNRAS*, 369:2059–2064, July 2006. doi: 10.1111/j.1365-2966.2006.10453.x.

H. Papathanassiou and P. Mészáros. Spectra of Unsteady Wind Models of Gamma-Ray Bursts. *ApJ*, 471:L91+, November 1996. doi: 10.1086/310343.

E. Pian, P. A. Mazzali, N. Masetti, P. Ferrero, S. Klose, E. Palazzi, E. Ramirez-Ruiz, S. E. Woosley, C. Kouveliotou, J. Deng, A. V. Filippenko, R. J. Foley, J. P. U. Fynbo, D. A. Kann, W. Li, J. Hjorth, K. Nomoto, F. Patat, D. N. Sauer, J. Sollerman, P. M. Vreeswijk, E. W. Guenther, A. Levan,

P. O'Brien, N. R. Tanvir, R. A. M. J. Wijers, C. Dumas, O. Hainaut, D. S. Wong, D. Baade, L. Wang, L. Amati, E. Cappellaro, A. J. Castro-Tirado, S. Ellison, F. Frontera, A. S. Fruchter, J. Greiner, K. Kawabata, C. Ledoux, K. Maeda, P. Moller, L. Nicastro, E. Rol, and R. Starling. An optical supernova associated with the X-ray flash XRF 060218. *Nature*, 442:1011–1013, August 2006. doi: 10.1038/nature05082.

T. Piran. The physics of gamma-ray bursts. *Reviews of Modern Physics*, 76: 1143–1210, January 2005. doi: 10.1103/RevModPhys.76.1143.

T. Piran. The implications of the Compton (GRO) observations for cosmological gamma-ray bursts. *ApJ*, 389:L45–L48, April 1992. doi: 10.1086/186345.

T. Piran. Gamma-ray bursts and the fireball model. *Phys. Rep.*, 314:575–+, 1999.

T. Piran, A. Shemi, and R. Narayan. Hydrodynamics of Relativistic Fireballs. *MNRAS*, 263:861–+, August 1993.

L. Piro, L. Scarsi, and R. C. Butler. SAX: the wideband mission for x-ray astronomy. In S. Fineschi, editor, *Proc. SPIE Vol. 2517, p. 169-181, X-Ray and EUV/FUV Spectroscopy and Polarimetry, Silvano Fineschi; Ed.*, volume 2517 of *Presented at the Society of Photo-Optical Instrumentation Engineers (SPIE) Conference*, pages 169–181, October 1995.

R. D. Preece, M. S. Briggs, R. S. Mallozzi, G. N. Pendleton, W. S. Paciesas, and D. L. Band. The BATSE Gamma-Ray Burst Spectral Catalog. I. High

Time Resolution Spectroscopy of Bright Bursts Using High Energy Resolution Data. *ApJS*, 126:19–36, January 2000.

R. Quimby, E. McMahon, and J. Murphy. GRBlog: A Database for Gamma-Ray Bursts. *ArXiv Astrophysics e-prints*, December 2003.

E. Ramirez-Ruiz and J. Granot. A Simple Test of the External Shock Model for the Prompt Emission in Gamma-Ray Bursts. *ArXiv Astrophysics e-prints*, August 2006.

M. J. Rees and P. Mészáros. Unsteady outflow models for cosmological gamma-ray bursts. *ApJ*, 430:L93–L96, August 1994.

M. J. Rees and P. Mészáros. Relativistic fireballs - Energy conversion and time-scales. *MNRAS*, 258:41P–43P, September 1992.

J. E. Rhoads. The Dynamics and Light Curves of Beamed Gamma-Ray Burst Afterglows. *ApJ*, 525:737–749, November 1999.

P. Romano, M. Perri, A. Beardmore, V. Mangano, D. N. Burrows, J. E. Hill, B. Zhang, and N. Gehrels. GRB 050219: Prompt X-ray position. *GCN Circulars*, 3036:1–+, 2005.

P. W. A. Roming, P. Schady, D. B. Fox, B. Zhang, E. Liang, K. O. Mason, E. Rol, D. N. Burrows, A. J. Blustin, P. T. Boyd, P. Brown, S. T. Holland, K. McGowan, W. B. Landsman, K. L. Page, J. E. Rhoads, S. R. Rosen, D. Vanden Berk, S. D. Barthelmy, A. A. Breeveld, A. Cucchiara,

M. De Pasquale, E. E. Fenimore, N. Gehrels, C. Gronwall, D. Grupe, M. R. Goad, M. Ivanushkina, C. James, J. A. Kennea, S. Kobayashi, V. Mangano, P. Mészáros, A. N. Morgan, J. A. Nousek, J. P. Osborne, D. M. Palmer, T. Poole, M. D. Still, G. Tagliaferri, and S. Zane. Very Early Optical Afterglows of Gamma-Ray Bursts: Evidence for Relative Paucity of Detection. *ApJ*, 652:1416–1422, December 2006. doi: 10.1086/508481.

George B. Rybicki and Alan P. Lightman. *Radiative Processes in Astrophysics*. Wiley-Interscience, 1979.

F. Ryde. Is Thermal Emission in Gamma-Ray Bursts Ubiquitous? *ApJ*, 625: L95–L98, June 2005. doi: 10.1086/431239.

E. Rykoff, B. Schaefer, and R. Quimby. GRB 050319: Detection of Possible Optical Counterpart. *GCN Circulars*, 3116:1–+, 2005.

R. Sari and T. Piran. Predictions for the Very Early Afterglow and the Optical Flash. *ApJ*, 520:641–649, August 1999.

R. Sari and T. Piran. Variability in Gamma-Ray Bursts: A Clue. *ApJ*, 485: 270–+, August 1997a. doi: 10.1086/304428.

R. Sari and T. Piran. Cosmological gamma-ray bursts: internal versus external shocks. *MNRAS*, 287:110–116, May 1997b.

R. Sari, T. Piran, and R. Narayan. Spectra and Light Curves of Gamma-Ray Burst Afterglows. *ApJ*, 497:L17+, April 1998.

R. Sari, T. Piran, and J. P. Halpern. Jets in Gamma-Ray Bursts. *ApJ*, 519: L17–L20, July 1999. doi: 10.1086/312109.

G. Sato, R. Yamazaki, K. Ioka, T. Sakamoto, T. Takahashi, K. Nakazawa, T. Nakamura, K. Toma, D. Hullinger, M. Tashiro, A. M. Parsons, H. A. Krimm, S. D. Barthelmy, N. Gehrels, D. N. Burrows, P. T. O'Brien, J. P. Osborne, G. Chincarini, and D. Q. Lamb. Swift Discovery of Gamma-Ray Bursts without a Jet Break Feature in Their X-Ray Afterglows. *ApJ*, 657: 359–366, March 2007. doi: 10.1086/510610.

P. Schady, M. Ivanushkina, T. Poole, C. Gronwall, A. Blustin, P. Brown, S. Rosen, K. McGowan, M. D. Pasquale, P. Boyd, S. Holland, M. Still, W. Landsman, S. Hunsberger, A. Breeveld, P. Roming, K. Mason, H. Huckle, P. Broos, T. Kennedy, P. Smith, B. Hancock, S. Koch, M. Carter, J. Racusin, E. Fenimore, B. Zhang, J. Nousek, and N. Gehrels. GRB 050219a: No Swift UVOT Detection of Afterglow Emission. *GCN Circulars*, 3039:1–+, 2005.

D. A. Smith, A. Levine, H. Bradt, K. Hurley, M. Feroci, P. Butterworth, S. Golenetskii, G. Pendleton, and S. Phengchamnan. X-Ray Light Curves of Gamma-Ray Bursts Detected with the All-Sky Monitor on RXTE. *ApJS*, 141:415–428, August 2002.

D. A. Smith, C. W. Akerlof, and R. Quimby. XRF 030723: Re-analysis of ROTSE-III early images. *GCN Circulars*, 2338:1–+, 2003.

I. A. Smith, R. P. J. Tilanus, N. Tanvir, V. E. Barnard, G. H. Moriarty-Schieven, D. A. Frail, R. A. M. J. Wijers, P. Vreeswijk, E. Rol, and C. Kouveliotou. SCUBA sub-millimeter observations of gamma-ray bursts. IV. GRB 021004, 021211, 030115, 030226, 041006. *A&A*, 439:987–996, September 2005. doi: 10.1051/0004-6361:20053107.

A. M. Soderberg and E. Ramirez-Ruiz. Was GRB 990123 a unique optical flash? *MNRAS*, 330:L24–L28, February 2002.

A. M. Soderberg, E. Berger, M. Kasliwal, D. A. Frail, P. A. Price, B. P. Schmidt, S. R. Kulkarni, D. B. Fox, S. B. Cenko, A. Gal-Yam, E. Nakar, and K. C. Roth. The Afterglow, Energetics, and Host Galaxy of the Short-Hard Gamma-Ray Burst 051221a. *ApJ*, 650:261–271, October 2006. doi: 10.1086/506429.

M. Spada, A. Panaitescu, and P. Mészáros. Analysis of Temporal Features of Gamma-Ray Bursts in the Internal Shock Model. *ApJ*, 537:824–832, July 2000.

H. C. Spruit, F. Daigne, and G. Drenkhahn. Large scale magnetic fields and their dissipation in GRB fireballs. *A&A*, 369:694–705, April 2001. doi: 10.1051/0004-6361:20010131.

K. Z. Stanek, T. Matheson, P. M. Garnavich, P. Martini, P. Berlind, N. Caldwell, P. Challis, W. R. Brown, R. Schild, K. Krisciunas, M. L. Calkins, J. C. Lee, N. Hathi, R. A. Jansen, R. Windhorst, L. Echevarria, D. J. Eisenstein,

B. Pindor, E. W. Olszewski, P. Harding, S. T. Holland, and D. Bersier. Spectroscopic Discovery of the Supernova 2003dh Associated with GRB 030329. *ApJ*, 591:L17–L20, July 2003.

G. Tagliaferri, M. Goad, G. Chincarini, A. Moretti, S. Campana, D. N. Burrows, M. Perri, S. D. Barthelmy, N. Gehrels, H. Krimm, T. Sakamoto, P. Kumar, P. I. Mészáros, S. Kobayashi, B. Zhang, L. Angelini, P. Banat, A. P. Beardmore, M. Capalbi, S. Covino, G. Cusumano, P. Giommi, O. Godet, J. E. Hill, J. A. Kennea, V. Mangano, D. C. Morris, J. A. Nousek, P. T. O'Brien, J. P. Osborne, C. Pagani, K. L. Page, P. Romano, L. Stella, and A. Wells. An unexpectedly rapid decline in the X-ray afterglow emission of long γ-ray bursts. *Nature*, 436:985–988, August 2005. doi: 10.1038/nature03934.

G. B. Taylor, D. A. Frail, A. J. Beasley, and S. R. Kulkarni. Position and parallax of the γ-ray burst of 8 May 1997. *Nature*, 389:263–265, September 1997. doi: 10.1038/38456.

C. Thompson. A Model of Gamma-Ray Bursts. *MNRAS*, 270:480–+, October 1994.

V. V. Usov. Millisecond pulsars with extremely strong magnetic fields as a cosmological source of gamma-ray bursts. *Nature*, 357:472–474, June 1992. doi: 10.1038/357472a0.

V. V. Usov. On the Nature of Nonthermal Radiation from Cosmological Gamma-Ray Bursters. *MNRAS*, 267:1035–+, April 1994.

J. van Paradijs, P. J. Groot, T. Galama, C. Kouveliotou, R. G. Strom, J. Telting, R. G. M. Rutten, G. J. Fishman, C. A. Meegan, M. Pettini, N. Tanvir, J. Bloom, H. Pedersen, H. U. Nordgaard-Nielsen, M. Linden-Vornle, J. Melnick, G. van der Steene, M. Bremer, R. Naber, J. Heise, J. in 't Zand, E. Costa, M. Feroci, L. Piro, F. Frontera, G. Zavattini, L. Nicastro, E. Palazzi, K. Bennet, L. Hanlon, and A. Parmar. Transient optical emission from the error box of the gamma-ray burst of 28 February 1997. *Nature*, 386:686–689, 1997.

W. T. Vestrand, P. R. Wozniak, J. A. Wren, E. E. Fenimore, T. Sakamoto, R. R. White, D. Casperson, H. Davis, S. Evans, M. Galassi, K. E. McGowan, J. A. Schier, J. W. Asa, S. D. Barthelmy, J. R. Cummings, N. Gehrels, D. Hullinger, H. A. Krimm, C. B. Markwardt, K. McLean, D. Palmer, A. Parsons, and J. Tueller. A link between prompt optical and prompt γ-ray emission in γ-ray bursts. *Nature*, 435:178–180, May 2005. doi: 10.1038/nature03515.

N. Vlahakis and A. Königl. Magnetohydrodynamics of Gamma-Ray Burst Outflows. *ApJ*, 563:L129–L132, December 2001. doi: 10.1086/338652.

D. Watson, J. P. U. Fynbo, C. C. Thöne, and J. Sollerman. No supernovae detected in two long-duration Gamma-Ray Bursts. *ArXiv Astrophysics e-prints*, March 2007.

E. Waxman, S. R. Kulkarni, and D. A. Frail. Implications of the Radio Af-

terglow from the Gamma-Ray Burst of 1997 May 8. *ApJ*, 497:288–+, April 1998. doi: 10.1086/305467.

J. C. Wheeler, I. Yi, P. Höflich, and L. Wang. Asymmetric Supernovae, Pulsars, Magnetars, and Gamma-Ray Bursts. *ApJ*, 537:810–823, July 2000. doi: 10.1086/309055.

J. C. Wheeler, D. L. Meier, and J. R. Wilson. Asymmetric Supernovae from Magnetocentrifugal Jets. *ApJ*, 568:807–819, April 2002. doi: 10.1086/338953.

R. A. M. J. Wijers and T. J. Galama. Physical Parameters of GRB 970508 and GRB 971214 from Their Afterglow Synchrotron Emission. *ApJ*, 523: 177–186, September 1999.

R. Willingale, P. T. O'Brien, J. P. Osborne, O. Godet, K. L. Page, M. R. Goad, D. N. Burrows, B. Zhang, E. Rol, N. Gehrels, and G. Chincarini. Testing the standard fireball model of GRBs using late X-ray afterglows measured by Swift. *ArXiv Astrophysics e-prints*, December 2006.

S. E. Woosley and J. S. Bloom. The Supernova Gamma-Ray Burst Connection. *ARA&A*, 44:507–556, September 2006. doi: 10.1146/annurev.astro.43.072103.150558PDF:http://arjournals.annualreviews.org/doi/pdf/10.1146/annurev.astro.43.072103.150558.

K. Yamaoka, S. Sugita, M. Ohno, T. Takahashi, T. Asano, T. Uehara, Y. Fukazawa, Y. Terada, M. Suzuki, T. Tamagawa, M. Tashiro, K. Abe,

K. Onda, Y. Sato, M. Suzuki, Y. Urata, T. Enoto, R. Miyawaki, K. Kokubun, K. Makishima, K. Nakazawa, T. Takahashi, and S. Hong. GRB 061007: Suzaku/WAM observation of the prompt emission. 5724: 1–+, 2006.

S. A. Yost, H. F. Swan, E. S. Rykoff, F. Aharonian, C. W. Akerlof, A. Alday, M. C. B. Ashley, S. Barthelmy, D. Burrows, D. L. Depoy, R. J. Dufour, J. D. Eastman, R. D. Forgey, N. Gehrels, E. Göğüş, T. Güver, J. P. Halpern, L. C. Hardin, D. Horns, Ü. Kiziloglu, H. A. Krimm, S. Lepine, E. P. Liang, J. L. Marshall, T. A. McKay, T. Mineo, N. Mirabal, M. Özel, A. Phillips, J. L. Prieto, R. M. Quimby, P. Romano, G. Rowell, W. Rujopakarn, B. E. Schaefer, J. M. Silverman, R. Siverd, M. Skinner, D. A. Smith, I. A. Smith, S. Tonnesen, E. Troja, W. T. Vestrand, J. C. Wheeler, J. Wren, F. Yuan, and B. Zhang. Exploring Broadband GRB Behavior during γ-Ray Emission. *ApJ*, 657:925–941, March 2007. doi: 10.1086/510896.

B. Zhang. Gamma-Ray Bursts in the Swift Era. *Chinese Journal of Astronomy and Astrophysics*, 7:1–50, February 2007. doi: 10.1088/1009-9271/7/1/01.

B. Zhang and S. Kobayashi. Gamma-Ray Burst Early Afterglows: Reverse Shock Emission from an Arbitrarily Magnetized Ejecta. *ApJ*, 628:315–334, July 2005. doi: 10.1086/429787.

B. Zhang, S. Kobayashi, and P. Mészáros. Gamma-Ray Burst Early Optical Afterglows: Implications for the Initial Lorentz Factor and the Central Engine. *ApJ*, 595:950–954, October 2003.

B. Zhang, Y. Z. Fan, J. Dyks, S. Kobayashi, P. Mészáros, D. N. Burrows, J. A. Nousek, and N. Gehrels. Physical Processes Shaping Gamma-Ray Burst X-Ray Afterglow Light Curves: Theoretical Implications from the Swift X-Ray Telescope Observations. *ApJ*, 642:354–370, May 2006. doi: 10.1086/500723.

Vita

Erin Malia McMahon was born on July 15, 1980, in Bremerton, Washington to Michael and Joanne McMahon. She grew up in St. Leonard, Maryland and attended Calvert High School. She received her B.S. in Physics, graduating summa cum laude, from the University of Tennessee, Knoxville, in May 2002. In August 2002, Erin moved to Austin, Texas to attend graduate school in the Department of Astronomy at the University of Texas, Austin. She received her M.A. in Astronomy in 2004. Following the completion of her dissertation, she plans on taking a position with the Space Department at John's Hopkins University Applied Physics Lab in Laurel, Maryland.

Permanent address: 106 Sylvan St
Hutto, Texas 78634

This dissertation was typeset with LaTeX[†] by the author.

[†]LaTeX is a document preparation system developed by Leslie Lamport as a special version of Donald Knuth's TeX Program.